Activity-dependent Integration and Plasticity of New Neurons During Postnatal Neurogenesis.

By

Chia-Wei Lin

B.S. Life Sciences
National Yang-Ming University, Taiwan (2000)

SUBMITTED TO THE DEPARTMENT OF BRAIN AND COGNITIVE SCIENCES IN PARTIAL FULFULLMENT OF THE REQUIRMENTS FOR THE DEGREE OF

DOCTOR OF PHILOSOPHY IN NEUROSCIENCE
AT THE
MASSACHUSETTS INSTITUTE OF TECHNOLOGY

June 2010

Signature of Author: _____
Department of Brain and Cognitive Sciences
May 19, 2010

Certified by: _____
Carlos Lois, M.D. Ph.D.
Assistant Professor of Brain and Cognitive Sciences
Thesis Supervisor

Accepted by: _____
Earl Miller, Ph.D.
Picower Professor of Neuroscience
Chairman, Committee for Graduate Students

Activity-dependent Integration and Plasticity of New Neurons During Postnatal Neurogenesis.

By

Chia-Wei Lin

Submitted to the Department of Brain and Cognitive Sciences on May 19, 2010 in Partial Fulfillment of the Requirements for the Degree of Doctor of Philosophy in Neuroscience

ABSTRACT

Most neurons are born during the embryonic period to become the building blocks for a variety of brain circuits. However, two brain regions only start to assemble during the postnatal period. Both brain areas, olfactory bulb and dentate gyrus, mainly accommodate the integration of new neurons during the postnatal period, and continuously receive new neurons throughout animals' life. In this thesis, I used the rat olfactory bulb (OB) as a model system to address two important issues regarding the integration and plasticity of new neurons generated during the postnatal period.

The first feature of postnatal neurogenesis is that when new neurons arrive and integrate into an adult OB, only half of neurons can ultimately survive. However, what form of activity pattern determines the survival of new neurons remains unclear. Using NaChBac sodium channels to selectively alter the intrinsic excitability of new neurons *in vivo*, this manipulation reveals that neuronal survival critically depends on the level of membrane depolarization.

Once neurons integrate and survive in the brain circuits, neurons have the capability of monitoring their activity level and adaptively maintain their membrane excitability within the operational range. How they achieve the long-term stability of membrane excitability remains unclear. By altering the resting membrane potential of individual neurons *in vivo*, OB granule neurons are found to use a subthreshold parameter, resting membrane potential, to guide the compensatory changes of intrinsic ion channels and synaptic receptors.

In summary, studies from this thesis have revealed the cellular mechanisms underlying neuronal survival in an *in vivo* brain circuit. I also uncover a novel form of homeostatic computation by which granule neurons preferentially use the subthreshold membrane potential response rather than spiking rates as a set point.

Thesis Supervisor: Carlos Lois

Title: Assistant Professor of Brain and Cognitive Sciences

TABLE OF CONTENTS

Acknowledgements

My graduate life at MIT is just like what I always tried to figure out in my research: a new neuron strives to find an avenue to integrate into a seemingly harsh adult brain circuits.

My interest at science did not originate until my freshman year. Like most of people, I was not born to become a scientist and did not learn analytical skills and electrophysiology on my own. I could not have finished my thesis without the training from my previous mentor. Before MIT, my college mentor, Dr. Tsung-Yu Chen now as full professor at UC Davis, has already shaped my scientific thinking and influenced my research styles profoundly. He literally taught me everything about electrophysiology and biophysics when he first went back to Taiwan from Brandeis after finishing his postdoctoral training with Christopher Miller. Back in 1997, when I was still a sophomore, Tsung-Yu had a small lab consisting of only two students, including a master student and me as an UROP. It was quite remarkable for Tsung-Yu to spend his time teaching me, and allowed me to stay in the lab for almost 12 to 14 hours a day until 3 a.m. In retrospect, I believe, this was how I got interested at science seriously.

It was a dramatic turn and whole new experience when I first came to MIT. Everything worked very differently here. The more lab space, the larger research resource, and the greater diversity really makes MIT an excellent educational place. I chose Neuroscience as my Ph.D. study because I would like to learn and discover the basic principles behind neural computation. It was my advisor, Carlos Lois, who first brought the research of adult neurogenesis to my attention because the function of massive production of new neurons in adult brains still remained unclear. In addition, the new genetic techniques being developed

in his lab, such as retroviruses and enhancer traps for producing transgenic rodents, were really one of his kinds. Throughout my graduate study, I learned invaluable lessons from Carlos, especially on how to convey exciting scientific ideas to general audience. Things in basic science can be complex but at the same time, it should be made simple to make a big impact on knowledge of science. One invaluable gift Carlos has also given to me is an education book *Writing Well* written by Mark Tredinnick. This book changed the way I used to think about writing and has helped my writing ever since. Finally, the best thing about Carlos is that once he gets excited about ideas, he will test the idea even on his own if he is free from administrative burden. Carlos really fits the ideal type of group leaders as recently discussed in David Hubel's viewpoint that appeared in October 29 2009 issue of Neuron.

I am deeply indebted to my thesis committee members because they have made constructive comments on improving my thesis and have helped strengthen my research rigor along the way. Professor Yasunori Hayashi has always been one of my favorite science audiences since my first year at MIT. We always chatted about science and life during the coffee hours and he was always available for discussing my thesis progress and giving helpful advice. Professor Weifeng Xu has been extremely helpful on my thesis research. Especially, I learned a lot from Weifeng in terms of future career choices. My committee chair, Professor Michale Fee, is one of inspirational teachers at MIT I have ever met. I learned the critical thinking and computational concepts from his computational neuroscience class. I have applied this newly acquired computational skill to develop the homeostasis project and formulate the computational model for the research project that appears in ***Chapter 6***.

The graduate school is not just a great place for research but also a place for meeting people who share strong scientific zeal. Benjamin Scott has always been the best person for me to

talk to in terms of sciences and lives. The scientific debate with Ben was always not an easy fight because we have very different philosophy about presenting research. Nevertheless, I always enjoyed the intellectual stimulation during the conversation, which significantly helps my rhetoric skills when engaging in a scientific argument. Wolfgang Kelsch, now in Germany, was the previous postdoctoral fellow and has been my best collaborator in Carlos' lab. He helped me on initiating the first experiments when I first joined the lab. His hardworking and tenacious attitude toward the research is his trademark. Sanjay Magavi, also the previous postdoctoral fellow, showed me a lot of surgical techniques in the beginning of my research. In particular, it has been extremely useful for me to know the alternative career paths from Sanjay who now works in the pharmaceutical sector.

I deeply believe that a good scientist is shaped not only by nature but also largely by nurture. Because of my fantastic UROP experience in Taiwan, mentoring UROPs also brought me the excitement of teaching. My first MIT undergraduate Alice Ainsworth, now a medical student at UCSF, has contributed significantly to the neuronal survival project. The second comes Dimitri Porcelli, who just entered his sophomore year at MIT. He has participated in the homeostatic plasticity projects and facilitated the investigation. Both are diligent and talented. There are also other lab members, Marie, Masayoshi, Ni, Garrett, Shuyin, Tarciso, and Yarden who have collectively made the lab a wonderful and diverse place for graduate studies and have directly or indirectly facilitated my research.

I would like to thank my girlfriend, Nan-Wei who has always surprised me by showing me completely opposite perspectives. She used to be a material scientist. Now, she has been learning exponentially to become a top Ph.D. student and a new-generation engineer at MIT Media Lab. Her transition in research interest from material sciences to electrical engineering

completely changed my prejudice about the difference between science and engineering. Because of this experience, I also got interested at electrical engineering and took engineering courses as a minor to fulfill my Ph.D. degree requirement. The things I have learned from engineering departments turned out to be intellectually challenging and extremely useful for both my thesis projects and future works. Finally, I would like to express my highest gratitude to my mother, Pao-Kuei, for her single-handedly raising me up when my beloved father, Kuo-Tai, died of liver cancer in my fifth grade. It was difficult for her to give advice about academic career to me because I am the first family member that actually has obtained the degree higher than high school. Although she did not quite understand my research, she always seemed interested and showed her unlimited support about my career choice.

What could best describe my graduate life? You could say that it is just like another adventure of a new neuron trying to strive in the adult brain. However, unlike the neurons whose fates are predetermined, my future adventure and identity will be of less certainty, less stereotype and hopefully more excitement.

Chapter One

Introduction

Unlike most of brain circuits that form during the embryonic period, two brain regions, olfactory bulb (OB) and dentate gyrus (DG), start to assemble by continuously recruiting new neurons during the postnatal period (Lledo et al., 2006; Zhao et al., 2008). The life-long production of new neurons offers excellent opportunities for exploring the mechanisms underlying new neurons' integration into a functioning brain circuit. It also holds the promise that knowledge gained from studying adult neurogenesis can be ultimately applied to mend neurological disorders. In this thesis, I will focus on one specific type of neurons, known as granule cells (GCs), in the rodent OB, and use the OB circuit as a model system to introduce and study important questions regarding postnatal neurogenesis.

The olfactory bulb circuit: The relay center of smell inputs

Olfaction is critical to the survival of animals. A street rat has to differentiate the odor of restaurant A that always has leftover food from the odor of restaurant B whose kitchen is always immaculate. By doing so, a rat can strategically allocate its energy searching for food and survive in a city by remembering reliable food source.

How is olfactory information processed in a rat brain? The inhaled odorant first arrive inside the nostril of a rat (Figure 1A). Once dissolved in the mucous of olfactory epithelium (OE), the odorant finds its receptor expressed on olfactory sensory neurons (OSN), which triggers the downstream G-protein-coupled signaling pathway to elicit electrical impulses in OSNs

(Buck, 2000; Imai and Sakano, 2007; Mombaerts, 2004). The electrical impulses then propagate down the OSNs' long axons that eventually merge at the glomerulus within the OB (Figure 1). Each glomerulus is a highly organized neuronal structure because it receives axons whose cell bodies express the identical odorant receptors (Buck, 2000; Imai and Sakano, 2007; Mombaerts, 2004). Within the glomerulus, sensory-input-triggered impulses depolarize the OSNs' axons, induce calcium influx, and evoke neurotransmitter releases to open the postsynaptic receptors on the primary dendrites of principal neurons (Figures 1B). Unlike most sensory inputs such as somatosensory and auditory signals that need to transit via the thalamus before reaching destined cortical regions, the odorant signal reaches the olfactory cortex via the OB, the relay center for processing smell (Kay and Sherman, 2007; Shepherd, 2004).

Key Neuronal Elements within the OB

The OB consists of various types of neurons, which organize in distinct neuroanatomical layers (Figure 1B). There are two types of major principal neurons in the OB, which is anatomically defined based on the distribution of their cell bodies and dendrites (Shepherd, 2004). One type is called mitral cell that preferentially positions its cell body on the border between the external plexiform layer (EPL) and granular cell layer (Gr) (Figure 1B). Because of this orderly arrangement, a dense array of mitral cell bodies creates a distinct anatomical structure called mitral cell layer (MCL), which is recognizable under the light microscope. The other type of principal neurons is called tufted cell, the cell body of which is loosely distributed within the EPL that encompasses the dendrites from both excitatory principal and inhibitory GCs (Figure 1B). Despite different anatomical distribution of mitral and tufted cells (M/T), both types of principal neurons have been shown to share similar structural

moiety and identical computation principle that underlies olfactory signal processing within the OB (Christie et al., 2001; Shepherd, 2004).

Once OB mitral cells get sufficient excitatory inputs, an action potential is initiated and will be transmitted in two directions (Egger and Urban, 2006). One is known as ***feed-forward excitation***, which describes the direction of signal flow in which electrical impulses of mitral cells can transmit via axons to the excitatory pyramidal neurons located in the olfactory cortex (Figure 2). From there, the information will be further processed and decoded (Shepherd, 2004). Owing to the scope and focus of the thesis, the neuroanatomy and neural computation within olfactory cortex will be ignored in this introduction. The second way of transmission is known as the ***feedback inhibition*** where the excitation of mitral cells can trigger the excitatory neurotransmitter release from their secondary dendrites to excite the reciprocal GCs (Figure 2A), thereby receiving feedback inhibition (Chen et al., 2000; Isaacson, 2001; Schoppa et al., 1998).

Dendrodentric synapses: communication between principal and granule cells

Granule cells (GCs) are the most abundant neurons in the OB (Lledo et al., 2006; Shepherd, 2004). They are inhibitory neurons without axons; therefore their sole output to their synaptic partners is via their dendrites by releasing inhibitory GABAergic vesicles (Shepherd, 2004). GCs communicate with mitral cells mainly via dendrodendritic synapses (Figure 2A). Namely, mitral cells release excitatory glutamatergic vesicles from their secondary dendrites onto the apical dendrites of granule neurons (Shepherd, 2004). In return, GCs' inhibitory output activates GABAergic receptors located on the secondary dendrites of mitral cells, thereby hyperpolarizing the membrane potential and dampening mitral cells' excitability

(Chen et al., 2000). This reciprocal synaptic connection forms the basis of dendrodendritic signaling (Shepherd, 2004). Besides the dendrodendrtic synapses, mitral cells also send axons to target the proximal dendrites of granule neurons via conventional axo-dendritic synapses (Figure 2A) (Schoppa, 2006). This synaptic connection has been shown to be a powerful input source that can critically gate the cell-wide membrane excitability of GCs (Balu et al., 2007; Halabisky and Strowbridge, 2003). Several well-established microcircuits exist in the OB, historically with a predominant emphasis on the interaction between the mitral cells and GCs (Halabisky and Strowbridge, 2003; Schoppa and Urban, 2003; Shepherd, 2004). Although there are other types of local interneurons, their functions within the OB circuit were less characterized (Pressler and Strowbridge, 2006). The existence of dendrodendritic synapses offers important cellular substrates for two specific forms of neural computation (Egger and Urban, 2006; Shepherd, 2004). One is ***dendrodendritic inhibition (recurrent inhibition)*** that activation of mitral cells excites the GCs whose inhibitory outputs, with a time delay, reciprocally influences the spiking probability of imposing mitral cells (Figure 2A). This negative feedback inhibition presumably can dampen the excitability of mitral cells, thus fine-tuning their firing rates within the operational range (Jahr and Nicoll, 1980; Margrie et al., 2001; Shepherd, 2004). The other is ***lateral inhibition*** that mitral cells' activity, via a granule cell's inhibition, can indirectly influence the activity of other mitral cells (Arevian et al., 2008; Schoppa and Westbrook, 1999, 2001). This neural computation requires the anatomical arrangement that a single GC connects with multiple mitral cells (Figure 2B). The lateral inhibition potentially provides neural substrates for contrasting multiple incoming odorant signals (Egger and Urban, 2006; Shepherd, 2004). For example, two different principal neurons receive sensory signals via their primary dendrites

from two glomeruli, A and B, respectively. Because each glomerulus only accommodates OSNs' axons whose cell bodies express the same odorant receptors, each mitral cell also encodes the signals for each odorant (Buck, 2000; Imai and Sakano, 2007; Mombaerts, 2004; Schoppa and Westbrook, 2001). Depending on the extent of excitation of mitral cells and the degree of lateral inhibition feedback from GCs, the output of each mitral cell consequently depends on other mitral cell's excitability level (Arevian et al., 2008). The lateral inhibition has hence been proposed to subserve the function for contrasting simultaneously arriving odorants and sharpening odorant signals (Abraham et al., 2010; Yokoi et al., 1995).

Postnatal neurogenesis of granule neurons: life-long addition of local interneurons

Although GCs are essential building blocks underlying various neural computations in the OB, they do not come into existence in the OB circuit at once during the embryonic period. Instead, GCs are continuously produced throughout animal's life (Lledo et al., 2006; Zhao et al., 2008). This life-long production of GCs differs from other OB neuronal types such as mitral cells that are only generated during the embryonic period. OB GCs are born from stem cell niches abutting the subventricular zones (SVZ) where several types of stem cells reside (Kriegstein and Alvarez-Buylla, 2009; Lois and Alvarez-Buylla, 1994). There are two major stem precursors discovered so far along the lateral ventricles, **astrocytic self-renewing GFAP$^+$ cells** and **transiently amplifying Mash1$^+$ cells** (Figure 3A) (Doetsch et al., 1999; Kriegstein and Alvarez-Buylla, 2009). Mash1$^+$ stem cells are normally produced from quiescent GFAP$^+$ cells but can be induced by injury such as stroke from the other cell type known as CD133$^+$ ependymal cells (Duan et al., 2008). Mash1$^+$ stem cells also directly give rise to neuroblasts that are destined to become either OB GCs or periglomerular cells (PGCs), the other type of interneurons also being continually produced in adult animals

(Duan et al., 2008). Because Mash1$^+$ stem cells constantly undergo nuclear division, they are highly accessible to genetic manipulation using retrovirus-based viral particles that only infect actively dividing cells (Carleton et al., 2003; Kelsch et al., 2008; Kelsch et al., 2007). From the SVZ, it takes new neurons/neuroblasts about one week to travel long distance, via rostral migratory stream (RMS), to reach the OB located in the frontal brain region (Figure 3) (Lois and Alvarez-Buylla, 1994). In adult rats, the length of RMS can be up to 3 to 6 mm long. During their migration, those new neurons/neuroblasts have distinct cellular morphologies named leading and trailing processes, and move in a chain-like fashion in the RMS ensheathed by astrocytes (Lois et al., 1996). Once they reach the OB, they change their migration mode from tangential to radial movement, leave the OB's RMS, and enter the GC layer (Lois and Alvarez-Buylla, 1994; Lois et al., 1996). In the GC layer, new neurons spend about 1 week positioning their cell bodies, growing and extending their dendrites into EPL, and developing first synapses with mitral cells, thereby completing the initial step of maturation (Figure 3B) (Carleton et al., 2003). By the second week after their birth, they have already possessed the dendritic morphology similar to a mature GC (Kelsch et al., 2007; Petreanu and Alvarez-Buylla, 2002; Whitman and Greer, 2007).

Determinants for shaping dendritic patterns of GCs

How neurons obtain their dendritic patterns in a brain circuit has been a long-standing question, which also applies to the formation of dendritic pattern in new GCs. For example, once new neurons enter the granule cell layer (Gr) and start to establish their dendritic territory, the dendrites need to navigate through different neuronal layers such as Gr and EPL layers before making connections with their synaptic partners in EPL (Figure 4). Within the EPL, GCs' dendrites interact with secondary dendrites from either mitral or tufted cells. It is

still unclear how new GCs choose their synaptic targets, mitral versus tufted cells. Two models can potentially account for the dendritic development of GCs (Figure 4). The first is ***contact-and-establish model*** (Figure 4A). This model assumes that new GCs establish their dendritic patterns in a probabilistic manner and once their newly grown dendrites meet with dendrites of mitral/tufted cells, they establish connections by forming dendrodendritic synapses. Because mitral cells mainly position their secondary dendrites in the deep EPL, they presumably encounter newly incoming dendrites from young GCs more often than tufted cells whose dendritic territory is in the superficial EPL. This simple model predicts that the synaptic organization of EPL will start from the deep EPL and complete in the superficial EPL, in an inside-out manner.

The alternative model that can account for the dendritic targeting of GCs is inspired by the experiments showing that genetic programs can confer individual neurons specific receptors and complimentary ligands (or tags) for synaptic matching, thus establishing specific connection (Figure 3). This model, known as ***chemoaffinity/genetic predetermination model***, underlies the specialization of cerebral organization as a result of targeted projection of axons from one brain area to another (Sperry, 1963). It has been postulated that individual GCs, at birth, may already possess intrinsic factors that confer them special identity (or tags) for establishing predetermined cell fates or dendritic contacts with either principal cells (M/T cells). Indeed, the fates of adult-generated neurons, either GCs or PGCs, are exclusively determined by the identities of stem cells found at distinct locations of the SVZ (Merkle et al., 2007). This genetics-based principle may also underlie the dendritic targeting of OB GCs. To test this hypothesis, the experimental designs will be introduced in ***Chapter 2*** and its result was already published (Kelsch et al., 2007).

Critical period for granule cells' survival

Once new GCs migrate into the granule cell layer, they spend two weeks developing their dendritic branches, spines and acquire a mature neuron-like morphology by the second week after their birth (Figure 3B). Nevertheless, only fifty percent of neurons can survive and integrate into the OB circuit after this stage, which marks the beginning of critical period for survival (Figure 3B). By using BrdU or ^{3}H-thymidine-labeling method that only labeled actively dividing cells, the critical period of new GCs' survival was first discovered in between 2nd and 4th week after neurons' birth (Petreanu and Alvarez-Buylla, 2002; Winner et al., 2002). Sensory inputs have been known to influence the survival of new neurons because nostril occlusion decreased the survival of new neurons specifically during the critical period (Petreanu and Alvarez-Buylla, 2002; Yamaguchi and Mori, 2005). It was further shown that sensory deprivation, performed either before or after the critical period, did not affect GCs' survival, suggesting a sensitive time period for determining new neurons' integration (Yamaguchi and Mori, 2005). Those experiments imply that neurons' survival might depend on special sensory-input-mediated activity patterns to either promote the survival mechanisms or stop the apoptosis/death program of new neurons (Petreanu and Alvarez-Buylla, 2002; Winner et al., 2002; Yamaguchi and Mori, 2005). Several laboratories have documented that certain behavioral paradigms paired with olfactory discrimination can enhance the survival of new GCs (Alonso et al., 2006; Breton-Provencher et al., 2009; Mouret et al., 2008). On the contrary, repeated and daily exposure of multiple odorants to mice do not enhance their survival chances (Magavi et al., 2005). Taken together, those experiments suggest that neuronal survival in adult animals could be a complex cellular

process, which depends on the source, timing, or patterns of neuronal activity mediated by sensory experience (Kirn et al., 1994; Wilbrecht et al., 2002).

The mechanism for survival: performance hypothesis

The mechanism of survival has been the persistent interest of adult neurogenesis research because addition of new neurons has been found to promote the cognitive functions of animals (Lledo et al., 2008; Zhao et al., 2008). The earliest work regarding the functions of adult neurogenesis came from the interesting observation that the singing repertoire of canary highly correlated with the seasonal alteration of neuronal numbers in their high-vocal centers (HVC) that controls the song output (Kirn et al., 1994; Nottebohm, 2004). It is believed that the change of neuronal number, hence structure, enables the plasticity of singing behaviors of canary (Nottebohm, 2004). It was later found that ablation of adult-generated neurons in zebra finches with irradiation also impaired singing plasticity, suggesting an involvement of adult neurogenesis in learning (Nottebohm, 2004; Scharff et al., 2000). Similarly, this hypothesis has been examined on other animal species such as rodents, and the results have so far been confirmative (Breton-Provencher et al., 2009; Clelland et al., 2009; Mouret et al., 2009). Because adult neurogenesis positively contributes to animals' learning, this has led to the popular hypothesis that new neurons may be selected for survival based on their beneficial contribution to the brain circuit (Kee et al., 2007; Wilbrecht et al., 2002; Wilbrecht and Kirn, 2004). Since the timing of action potential in neurons are highly relevant to the signal processing that underlies the sensory computation, the precise timing and patterns of action potential of new neurons could be a critical survival determinant during their integration (Wilbrecht et al., 2002). Despites the preponderance of this performance-survival hypothesis, there is no experiment available to directly test it. In ***Chapter 5***, I will introduce

the experimental design that genetically and selectively altered the firing patterns of new GCs and discussed its results and implication in terms of survival regulation of GCs (Lin et al., 2010).

Life after integration: Activity-dependent maintenance of membrane excitability

Once surviving in the brain circuits, new neurons not only continually remodel their dendritic morphology but also gradually fine-tune their electrical membrane properties (Carleton et al., 2003; Spitzer, 2006). Eventually new neurons reach a developmental stage with a characteristic membrane excitability that is considered both stable and mature (Carleton et al., 2003). Furthermore, this "characteristic membrane excitability" can be used to classify functionally distinct types of neurons (Nelson et al., 2006; Parra et al., 1998) because each neuronal type has its own unique subcellular distribution of ion channels and synaptic receptors. This electrical diversity confers a repertoire of biophysical properties tailored for each unique neural computation (Lai and Jan, 2006; Nusser, 2009; Spruston, 2008). It is believed that genetic programs initially determine the membrane properties of neurons and activity can further fine-tune their electrical behaviors (Katz and Shatz, 1996; Spitzer, 2006). For instance, rhythmically spiking neurons from a lobster fire action potentials in a bursting pattern *in vivo* (Turrigiano et al., 1994). However, once cultured in an *in vitro* environment that is deprived of natural input activity, neurons first stop firing action potentials, but gradually remodeled their ion channels and synaptic receptors over time to restore their bursting firing patterns (Turrigiano et al., 1994). This electrical remodeling has a tendency to restore neurons' characteristic activity patterns and hence is generally referred to as homeostatic plasticity (Davis, 2006; Davis and Bezprozvanny, 2001; Turrigiano et al., 1998; Turrigiano and Nelson, 2004).

The cellular sensors for homeostatic plasticity: firing rates

Neurons have the capability to maintain their excitability level within the operational range in the face of activity changes (Burrone and Murthy, 2003; Davis, 2006; Marder and Goaillard, 2006). What cellular parameters do neurons use to monitor and thereby maintain their membrane excitability? It has been believed that neurons can monitor their spontaneous firing rates such that deviation from this ***characteristic/target*** firing range can trigger adjustment of membrane ion channels and synaptic receptors, thereby stably maintaining the target firing rates (Ibata et al., 2008; Turrigiano, 2008). This negative-feedback system that aims to restore the target firing rates has been observed robustly in neurons such as lobster neurons as mentioned above (Turrigiano et al., 1994). It also operates in mammalian neurons including cortical neurons whose visual input was deprived by eyelid suture, dopaminergic striatal neurons whose spontaneous spiking activity was suppressed by TTX (Chan et al., 2007), and purkinje neurons whose voltage-gated sodium channels (Nav1.6) were genetically eliminated (Swensen and Bean, 2005). Therefore, spontaneously and rhythmically firing neurons are believed to update the binary-like firing rate information to monitor their excitability level and use it as a set point (Marder and Goaillard, 2006; Turrigiano, 2008).

Revisit the firing rate-homeostasis hypothesis

Although those experiments favor the roles of spontaneous firing rates as a set point, a thorough examination of each published literature questions its interpretation and general application. ***First***, previous studies mainly investigated the spontaneously spiking neurons that have a high firing rate, ~ 1Hz (Burrone et al., 2002; Turrigiano, 2008). The change of firing rate presumably can be a sensitive measure for monitoring the activity change in

rhythmically spiking neurons. However, there are other neurons that rarely spike *in vivo* or only moderately spike given with sufficient sensory-related inputs relevant to behaviors (Fino et al., 2009; Hahnloser et al., 2002; Shoham et al., 2006). It is unclear how sparsely spiking neurons can use very infrequent signals to reliably monitor and achieve their long-term stable membrane excitability. ***Second***, the published literature that advocated the firing rate as a target activity often used studies that the firing rate was in fact not a constant (Desai et al., 1999; Maffei and Turrigiano, 2008). In those studies, the firing rates were not the fixed parameters during the entire experiments, and greatly deviated from control values. In some cases, neurons that have undergone sensory deprivation or have experienced reduced activity became paradoxically hyperactive by displaying much higher firing rates than controls (Hausser and Monsivais, 2003; Nelson et al., 2003; Saghatelyan et al., 2005). ***Third***, previous studies use either sensory deprivation, pharmacological or genetic intervention to study the questions of homeostasis (Desai et al., 1999; Maffei and Turrigiano, 2008; Paradis et al., 2001; Turrigiano et al., 1994). However, those experimental procedures not only alter the single neuron's activity but also drastically alter the circuit activity or structure, it is unclear whether the compensated changes came from cell-autonomous mechanisms within individual neurons or the combined effects from the neuron itself and the surrounding circuits (Burrone et al., 2002; Hartman et al., 2006). Taken together, the most parsimonious explanation for those experiments is that neurons can sense the change of firing rates but do not necessarily use it as a homeostatic set point.

Searching cellular mechanisms for homeostatic regulation

Previous studies have mostly focused on firing rates to explore and understand homeostatic plasticity because calcium influx has been thought to be the messenger for mediating this

process (Davis, 2006; Ibata et al., 2008; Turrigiano, 2008). Because high-threshold-activated L-type calcium channels only significantly open above the spike threshold, the action potential-dependent calcium influx has remained the most plausible candidate for homeostatic regulation (Bean, 2007; Ibata et al., 2008). However, this conventional viewpoint is biased because neurons not only allow influx of calcium during the action potential but also spontaneously bring in significant concentration of calcium at rest in the absence of spikes (Figure 5) (Castro and Urban, 2009; Magee et al., 1996; Manita and Ross, 2009). There are several types of calcium-conducting ion channels capable of operating in the absence of action potentials, including NMDA and AMPA receptors, low-threshold L-type, T-type calcium channels, and ryanodine receptors, to just name a few (Egger, 2007; Lin et al., 2007; Magee et al., 1996; Manita and Ross, 2009). Moreover, synaptic inputs often bombard neurons by depolarizing or hyperpolarizing the membrane potential without reaching the spike threshold (Figure 5), which is known as subthreshold membrane potential fluctuation (Marder, 2006). The fluctuations of subthreshold membrane potentials constantly open and close those calcium-conducting ion channels, thus presumably providing mechanistic substrate for dynamically modulating basal calcium level (Alle and Geiger, 2008; Manita and Ross, 2009). Although the functions of the subthreshold membrane potential fluctuation remain relatively unexplored, intracellular signaling events that happen below the spike threshold may influence homeostatic computation.

Functions of resting membrane potential

Although the resting membrane potential (RMP) has been conventionally thought as a passive cellular parameter, cumulative evidence suggests that it can underscore specific types of neuronal computation. The RMP at subthreshold can determine or modulate the release

probability of synaptic vesicles from axons of invertebrate and mammalian neurons (Alle and Geiger, 2008; Manor et al., 1997; Marder, 2006; Shu et al., 2006) and from dendrites of OB mitral and periglomerular cells (Castro and Urban, 2009; Murphy et al., 2005). The subthreshold membrane potential also controls the spontaneous calcium release from intracellular calcium stores via IP_3 and ryanodine receptors, in the dendrites of pyramidal neurons (Magee et al., 1996; Manita and Ross, 2009). Furthermore, the daily variation of RMP, rather than firing rates, has also recently been reported to underlie the circadian electrical behaviors of neurons in the suprachiasmatic nuclei (SCN), the brain region that controls the circadian rhythm of animals (Belle et al., 2009). Thus, the subthreshold RMP is the basis of several important neuronal functions and may subserve other functions left to be discovered. In ***Chapter 6***, I specifically altered the RMP of individual new GCs *in vivo* and found a novel form of homeostatic regulation that mainly uses subthreshold membrane potential fluctuations, instead of firing rates, as a set point.

Figures

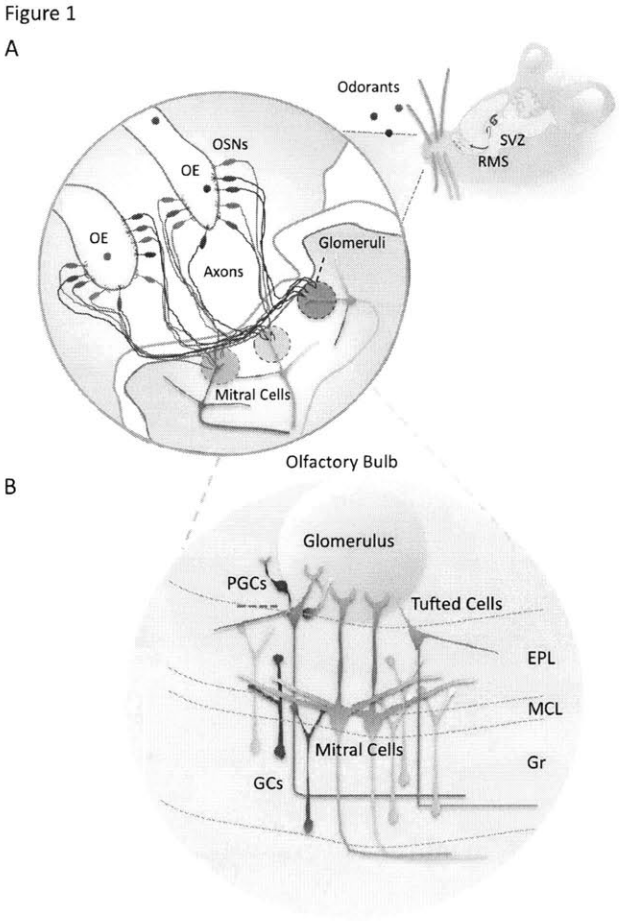

Figure 1. Synaptic organization of olfactory pathways

(A) Odorants enter the rat nostrils, get dissolved in the mucus of olfactory epithelium (OE), and bind to cognate receptors expressed by olfactory sensory neurons (OSNs). Inside the OE, odorants trigger downstream signal transduction in OSNs and initiate action potentials. OSNs expressing the same olfactory receptors (ORs) will converge their axons into the same glomerulus.

(B) An olfactory bulb circuit contains various types of neurons and only well-established neuronal types are shown in this cartoon. Two principal neurons, mitral/tufted cells, receive sensory inputs within the glomerulus from the OSNs, and send their impulses to olfactory cortex via axons or to local granule cells (GCs) via their secondary dendrites. Like GCs, periglomerular cells (PGCs) are also continuously produced in adult animals and are primarily located around/within the glomerulus.

Figure 2

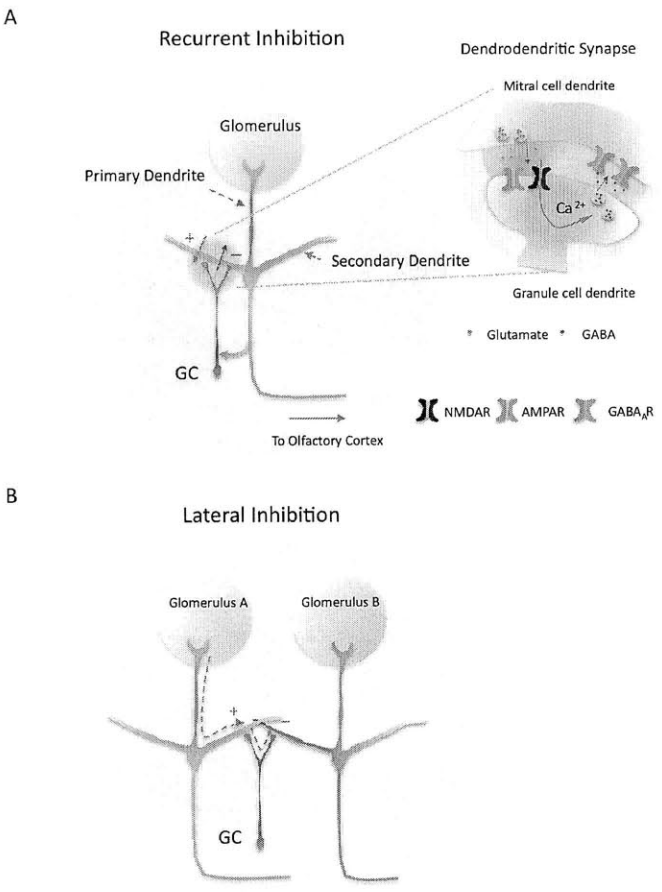

Figure 2. Interaction between mitral and granule cells allows for two types of neural computation.

(A) GCs and mitral cells interact reciprocally via their dendrodendritic synapses. Once mitral cells get sufficiently depolarized, synaptic vesicles are released from their secondary dendrites, which open both AMPARs and NMDARs on the apical dendrites of GCs and produce membrane potential depolarization. The membrane depolarization in GCs activates voltage-sensitive calcium channels, elevate influx of calcium, and trigger inhibitory output from GCs.

(B) The lateral inhibition occurs if a single GC interacts with multiple mitral cells. The cell-wide excitation of GC by one mitral cell can trigger lateral inhibition onto the other mitral cell, which theoretically can further enhance salient signals.

Figure 3

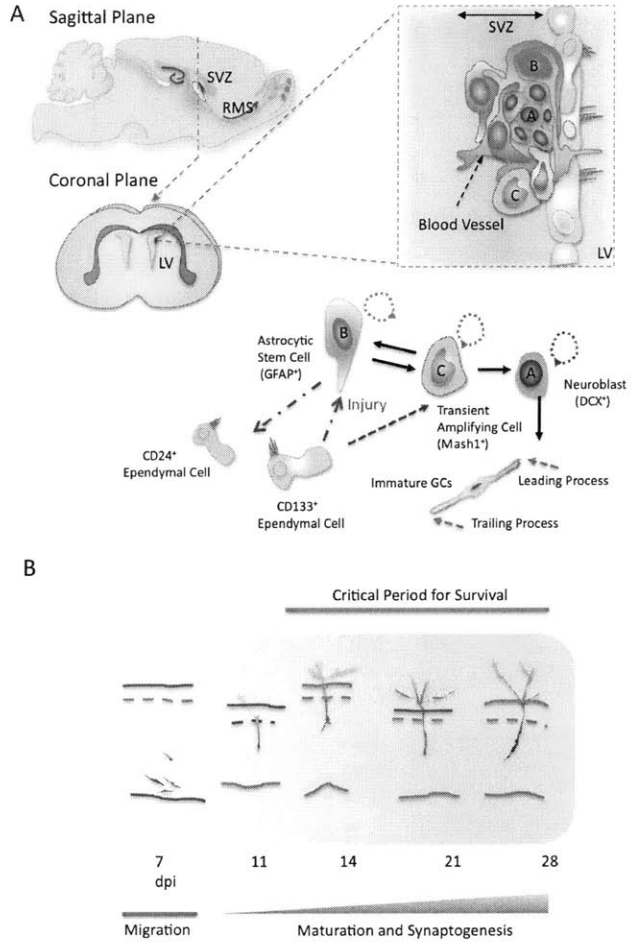

Figure 3. The origins, production and maturation of postnatal-born GCs

(A) Two types of neural stem cells are found to reside in the niche along the lateral ventricles, including type B mother stem cells and transiently amplifying type C stem cells. Type C stem cells give rise to neuroblasts, the immature migrating neurons. Neuroblasts migrate tangentially in the rostral migratory stream (RMS) and move towards the OB located in the anterior of forebrain where they settle, differentiate and become mature.

(B) GCs develop stereotypically during their development. It takes about 7 days for migrating neuroblasts to reach a rat OB. There, new neurons will take another 7 days to fully develop their dendrites. However, after the second week of their integration, new neurons undergo a survival selection process that only half of neurons would ultimately survive in an adult circuit. This is called the critical period for survival, which happens at times between 14 and 28 days after new neurons' birth.

Figure 4

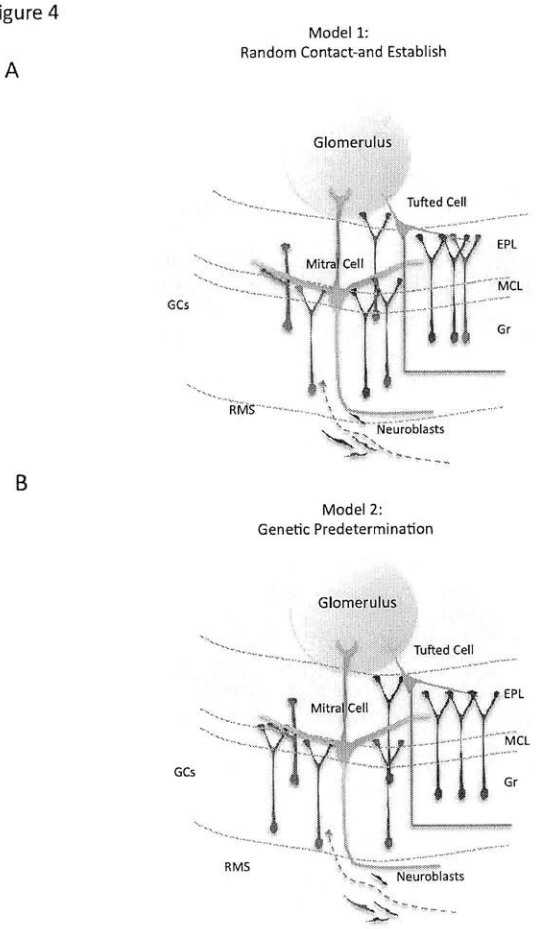

Figure 4. Two models account for dendritic targeting of GCs

(A) Contact-and-establish model posits that the dendritic targeting of GCs is a stochastic event such that once the dendrites of GCs meet with dendrites of mitral cells; they interact and form synaptic connection. This model predicts that OB develops in an inside-out fashion because the dendrites from the inner external plexiform layer (EPL) would have higher chances to encounter with newly growing dendrites from new GCs.

(B) Genetic predetermination model: new neurons may carry intrinsic genetic factors that pair their synaptic connection to their cognate mitral cells' dendrites.

Figure 5

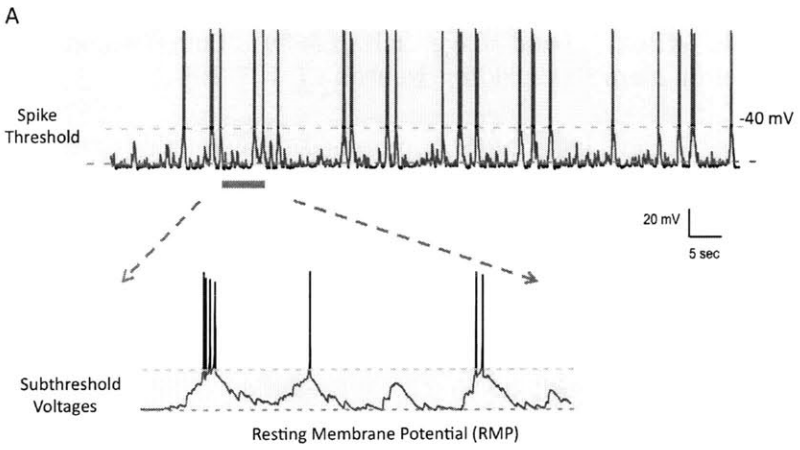

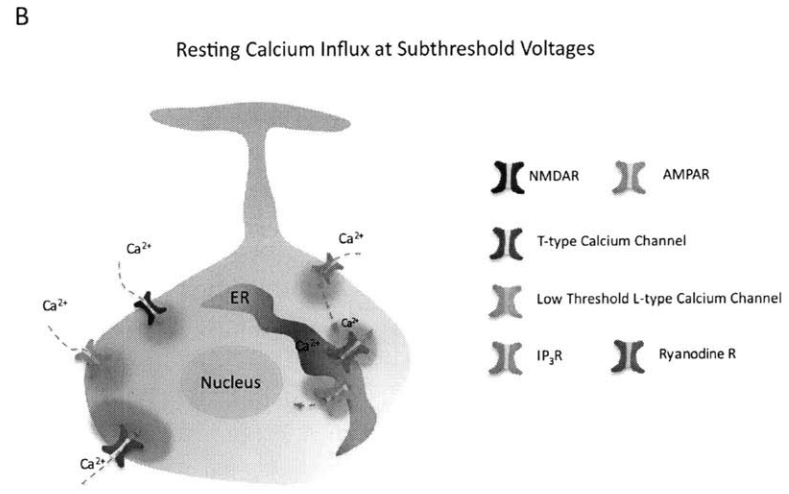

Figure 5. Subthreshold membrane potential fluctuation can mediate significant influx of Ca^{2+}

(A) Neurons receive synaptic inputs that constantly depolarize their membrane potential in the subthreshold voltages.

(B) Several types of Ca^{2+}-conducting ion channels can contribute to influx of Ca^{2+} near the resting membrane potential (RMP).

References

Abraham, N.M., Egger, V., Shimshek, D.R., Renden, R., Fukunaga, I., Sprengel, R., Seeburg, P.H., Klugmann, M., Margrie, T.W., Schaefer, A.T., and Kuner, T. (2010). Synaptic inhibition in the olfactory bulb accelerates odor discrimination in mice. Neuron *65*, 399-411.

Aimone, J.B., Wiles, J., and Gage, F.H. (2009). Computational influence of adult neurogenesis on memory encoding. Neuron *61*, 187-202.

Alle, H., and Geiger, J.R. (2006). Combined analog and action potential coding in hippocampal mossy fibers. Science *311*, 1290-1293.

Alle, H., and Geiger, J.R. (2008). Analog signalling in mammalian cortical axons. Curr Opin Neurobiol *18*, 314-320.

Alle, H., Roth, A., and Geiger, J.R. (2009). Energy-efficient action potentials in hippocampal mossy fibers. Science *325*, 1405-1408.

Alonso, M., Viollet, C., Gabellec, M.M., Meas-Yedid, V., Olivo-Marin, J.C., and Lledo, P.M. (2006). Olfactory discrimination learning increases the survival of adult-born neurons in the olfactory bulb. J Neurosci *26*, 10508-10513.

Altman, J. (1962). Are new neurons formed in the brains of adult mammals? Science (New York, N.Y *135*, 1127-1128.

Arevian, A.C., Kapoor, V., and Urban, N.N. (2008). Activity-dependent gating of lateral inhibition in the mouse olfactory bulb. Nat Neurosci *11*, 80-87.

Balu, R., Pressler, R.T., and Strowbridge, B.W. (2007). Multiple modes of synaptic excitation of olfactory bulb granule cells. J Neurosci *27*, 5621-5632.

Batista-Brito, R., Close, J., Machold, R., and Fishell, G. (2008). The distinct temporal origins of olfactory bulb interneuron subtypes. J Neurosci *28*, 3966-3975.

Bean, B.P. (2007). The action potential in mammalian central neurons. Nat Rev Neurosci *8*, 451-465.

Belle, M.D., Diekman, C.O., Forger, D.B., and Piggins, H.D. (2009). Daily electrical silencing in the mammalian circadian clock. Science *326*, 281-284.

Bernard, C., Anderson, A., Becker, A., Poolos, N.P., Beck, H., and Johnston, D. (2004). Acquired dendritic channelopathy in temporal lobe epilepsy. Science *305*, 532-535.

Bischofberger, J. (2007). Young and excitable: new neurons in memory networks. Nature neuroscience *10*, 273-275.

Breton-Provencher, V., Lemasson, M., Peralta, M.R., 3rd, and Saghatelyan, A. (2009). Interneurons produced in adulthood are required for the normal functioning of the olfactory bulb network and for the execution of selected olfactory behaviors. J Neurosci *29*, 15245-15257.

Brickley, S.G., Revilla, V., Cull-Candy, S.G., Wisden, W., and Farrant, M. (2001). Adaptive regulation of neuronal excitability by a voltage-independent potassium conductance. Nature *409*, 88-92.

Brunjes, P.C. (1994). Unilateral naris closure and olfactory system development. Brain Res Brain Res Rev *19*, 146-160.

Buck, L.B. (2000). The molecular architecture of odor and pheromone sensing in mammals. Cell *100*, 611-618.

Burrone, J., and Murthy, V.N. (2003). Synaptic gain control and homeostasis. Curr Opin Neurobiol *13*, 560-567.

Burrone, J., O'Byrne, M., and Murthy, V.N. (2002). Multiple forms of synaptic plasticity triggered by selective suppression of activity in individual neurons. Nature *420*, 414-418.

Cang, J., and Isaacson, J.S. (2003). In vivo whole-cell recording of odor-evoked synaptic transmission in the rat olfactory bulb. J Neurosci *23*, 4108-4116.

Carleton, A., Petreanu, L.T., Lansford, R., Alvarez-Buylla, A., and Lledo, P.M. (2003). Becoming a new neuron in the adult olfactory bulb. Nat Neurosci *6*, 507-518.

Castro, J.B., and Urban, N.N. (2009). Subthreshold glutamate release from mitral cell dendrites. J Neurosci *29*, 7023-7030.

Chan, C.S., Guzman, J.N., Ilijic, E., Mercer, J.N., Rick, C., Tkatch, T., Meredith, G.E., and Surmeier, D.J. (2007). 'Rejuvenation' protects neurons in mouse models of Parkinson's disease. Nature *447*, 1081-1086.

Chen, K., Aradi, I., Thon, N., Eghbal-Ahmadi, M., Baram, T.Z., and Soltesz, I. (2001). Persistently modified h-channels after complex febrile seizures convert the seizure-induced enhancement of inhibition to hyperexcitability. Nat Med *7*, 331-337.

Chen, W.R., Xiong, W., and Shepherd, G.M. (2000). Analysis of relations between NMDA receptors and GABA release at olfactory bulb reciprocal synapses. Neuron *25*, 625-633.
Christie, J.M., Schoppa, N.E., and Westbrook, G.L. (2001). Tufted cell dendrodendritic inhibition in the olfactory bulb is dependent on NMDA receptor activity. J Neurophysiol *85*, 169-173.

Clelland, C.D., Choi, M., Romberg, C., Clemenson, G.D., Jr., Fragniere, A., Tyers, P., Jessberger, S., Saksida, L.M., Barker, R.A., Gage, F.H., and Bussey, T.J. (2009). A functional role for adult hippocampal neurogenesis in spatial pattern separation. Science *325*, 210-213.

Copenhagen, D. (2001). Is the retina going digital? Neuron *30*, 303-305.

Davis, G.W. (2006). Homeostatic control of neural activity: from phenomenology to molecular design. Annu Rev Neurosci *29*, 307-323.

Davis, G.W., and Bezprozvanny, I. (2001). Maintaining the stability of neural function: a homeostatic hypothesis. Annu Rev Physiol *63*, 847-869.

Desai, N.S., Rutherford, L.C., and Turrigiano, G.G. (1999). Plasticity in the intrinsic excitability of cortical pyramidal neurons. Nat Neurosci *2*, 515-520.

Doetsch, F., Caille, I., Lim, D.A., Garcia-Verdugo, J.M., and Alvarez-Buylla, A. (1999). Subventricular zone astrocytes are neural stem cells in the adult mammalian brain. Cell *97*, 703-716.

Duan, X., Kang, E., Liu, C.Y., Ming, G.L., and Song, H. (2008). Development of neural stem cell in the adult brain. Curr Opin Neurobiol *18*, 108-115.

Egger, V., Svoboda, K., and Mainen, Z.F. (2003). Mechanisms of lateral inhibition in the olfactory bulb: efficiency and modulation of spike-evoked calcium influx into granule cells. J Neurosci *23*, 7551-7558.

Egger, V., and Urban, N.N. (2006). Dynamic connectivity in the mitral cell-granule cell microcircuit. Semin Cell Dev Biol *17*, 424-432.

Fino, E., Deniau, J.M., and Venance, L. (2009). Brief subthreshold events can act as Hebbian signals for long-term plasticity. PLoS One *4*, e6557.

Frazier-Cierpial, L.L., and Brunjes, P.C. (1989). Early postnatal differentiation of granule cell dendrites in the olfactory bulbs of normal and unilaterally odor-deprived rats. Brain research *47*, 129-136.

Ge, S., Yang, C.H., Hsu, K.S., Ming, G.L., and Song, H. (2007). A critical period for enhanced synaptic plasticity in newly generated neurons of the adult brain. Neuron *54*, 559-566.

Goldstein, S.A., Bockenhauer, D., O'Kelly, I., and Zilberberg, N. (2001). Potassium leak channels and the KCNK family of two-P-domain subunits. Nat Rev Neurosci *2*, 175-184.
Gray, N.W., Weimer, R.M., Bureau, I., and Svoboda, K. (2006).

Rapid redistribution of synaptic PSD-95 in the neocortex in vivo. PLoS biology *4*, e370.

Hack, M.A., Saghatelyan, A., de Chevigny, A., Pfeifer, A., Ashery-Padan, R., Lledo, P.M., and Gotz, M. (2005). Neuronal fate determinants of adult olfactory bulb neurogenesis. Nature neuroscience *8*, 865-872.

Hahnloser, R.H., Kozhevnikov, A.A., and Fee, M.S. (2002). An ultra-sparse code underlies the generation of neural sequences in a songbird. Nature *419*, 65-70.

Halabisky, B., and Strowbridge, B.W. (2003). Gamma-frequency excitatory input to granule cells facilitates dendrodendritic inhibition in the rat olfactory Bulb. J Neurophysiol *90*, 644-654.

Hartman, K.N., Pal, S.K., Burrone, J., and Murthy, V.N. (2006). Activity-dependent regulation of inhibitory synaptic transmission in hippocampal neurons. Nat Neurosci *9*, 642-649.

Hausser, M., and Monsivais, P. (2003). Less means more: inhibition of spontaneous firing triggers persistent increases in excitability. Neuron *40*, 449-451.

Hille, B. (2001). Ion channels of excitable membranes (Sunderland ,MA Sinauer Associates).

Hoffman, D.A., Magee, J.C., Colbert, C.M., and Johnston, D. (1997). K+ channel regulation of signal propagation in dendrites of hippocampal pyramidal neurons. Nature *387*, 869-875.

Ibata, K., Sun, Q., and Turrigiano, G.G. (2008). Rapid synaptic scaling induced by changes in postsynaptic firing. Neuron *57*, 819-826.

Imai, T., and Sakano, H. (2007). Roles of odorant receptors in projecting axons in the mouse olfactory system. Curr Opin Neurobiol *17*, 507-515.

Inoue, T., and Strowbridge, B.W. (2008). Transient activity induces a long-lasting increase in the excitability of olfactory bulb interneurons. J Neurophysiol *99*, 187-199.
Isaacson, J.S. (2001).

Mechanisms governing dendritic gamma-aminobutyric acid (GABA) release in the rat olfactory bulb. Proc Natl Acad Sci U S A *98*, 337-342.

Jahr, C.E., and Nicoll, R.A. (1980). Dendrodendritic inhibition: demonstration with intracellular recording. Science *207*, 1473-1475.

Katz, L.C., and Shatz, C.J. (1996). Synaptic activity and the construction of cortical circuits. Science *274*, 1133-1138.

Kay, L.M., and Sherman, S.M. (2007). An argument for an olfactory thalamus. Trends Neurosci *30*, 47-53.

Kee, N., Teixeira, C.M., Wang, A.H., and Frankland, P.W. (2007). Preferential incorporation of adult-generated granule cells into spatial memory networks in the dentate gyrus. Nat Neurosci *10*, 355-362.

Kelsch, W., Lin, C.W., and Lois, C. (2008). Sequential development of synapses in dendritic domains during adult neurogenesis. Proceedings of the National Academy of Sciences of the United States of America *105*, 16803-16808.

Kelsch, W., Mosley, C.P., Lin, C.W., and Lois, C. (2007). Distinct mammalian precursors are committed to generate neurons with defined dendritic projection patterns. PLoS Biol *5*, e300.

Kirn, J., O'Loughlin, B., Kasparian, S., and Nottebohm, F. (1994). Cell death and neuronal recruitment in the high vocal center of adult male canaries are temporally related to changes in song. Proc Natl Acad Sci U S A *91*, 7844-7848.

Kollo, M., Holderith, N., Antal, M., and Nusser, Z. (2008). Unique clustering of A-type potassium channels on different cell types of the main olfactory bulb. Eur J Neurosci *27*, 1686-1699.

Kriegstein, A., and Alvarez-Buylla, A. (2009). The glial nature of embryonic and adult neural stem cells. Annu Rev Neurosci *32*, 149-184.

Lai, H.C., and Jan, L.Y. (2006). The distribution and targeting of neuronal voltage-gated ion channels. Nat Rev Neurosci *7*, 548-562.

Leslie, K.R., Nelson, S.B., and Turrigiano, G.G. (2001). Postsynaptic depolarization scales quantal amplitude in cortical pyramidal neurons. J Neurosci *21*, RC170.

Li, Z., and Murthy, V.N. (2001). Visualizing postendocytic traffic of synaptic vesicles at hippocampal synapses. Neuron *31*, 593-605.

Lin, C.W., Sim, S., Ainsworth, A., Okada, M., Kelsch, W., and Lois, C. (2010). Genetically increased cell-intrinsic excitability enhances neuronal integration into adult brain circuits. Neuron *65*, 32-39.

Livneh, Y., Feinstein, N., Klein, M., and Mizrahi, A. (2009). Sensory input enhances synaptogenesis of adult-born neurons. J Neurosci *29*, 86-97.

Lledo, P.M., Alonso, M., and Grubb, M.S. (2006). Adult neurogenesis and functional plasticity in neuronal circuits. Nat Rev Neurosci *7*, 179-193.

Lledo, P.M., Merkle, F.T., and Alvarez-Buylla, A. (2008). Origin and function of olfactory bulb interneuron diversity. Trends Neurosci *31*, 392-400.

Lledo, P.M., and Saghatelyan, A. (2005). Integrating new neurons into the adult olfactory bulb: joining the network, life-death decisions, and the effects of sensory experience. Trends in neurosciences *28*, 248-254.

Lois, C., and Alvarez-Buylla, A. (1993). Proliferating subventricular zone cells in the adult mammalian forebrain can differentiate into neurons and glia. Proceedings of the National Academy of Sciences of the United States of America *90*, 2074-2077.

Lois, C., and Alvarez-Buylla, A. (1994). Long-distance neuronal migration in the adult mammalian brain. Science *264*, 1145-1148.

Lois, C., Garcia-Verdugo, J.M., and Alvarez-Buylla, A. (1996). Chain migration of neuronal precursors. Science *271*, 978-981.

Luan, H., Lemon, W.C., Peabody, N.C., Pohl, J.B., Zelensky, P.K., Wang, D., Nitabach, M.N., Holmes, T.C., and White, B.H. (2006). Functional dissection of a neuronal network required for cuticle tanning and wing expansion in Drosophila. J Neurosci *26*, 573-584.

Luskin, M.B. (1993). Restricted proliferation and migration of postnatally generated neurons derived from the forebrain subventricular zone. Neuron *11*, 173-189.

Maffei, A., and Turrigiano, G.G. (2008). Multiple modes of network homeostasis in visual cortical layer 2/3. J Neurosci *28*, 4377-4384.

Magavi, S.S., Mitchell, B.D., Szentirmai, O., Carter, B.S., and Macklis, J.D. (2005). Adult-born and preexisting olfactory granule neurons undergo distinct experience-dependent modifications of their olfactory responses in vivo. J Neurosci *25*, 10729-10739.

Magee, J.C., Avery, R.B., Christie, B.R., and Johnston, D. (1996). Dihydropyridine-sensitive, voltage-gated Ca2+ channels contribute to the resting intracellular Ca2+ concentration of hippocampal CA1 pyramidal neurons. J Neurophysiol *76*, 3460-3470.

Manita, S., and Ross, W.N. (2009). Synaptic activation and membrane potential changes modulate the frequency of spontaneous elementary Ca2+ release events in the dendrites of pyramidal neurons. J Neurosci *29*, 7833-7845.

Manor, Y., Nadim, F., Abbott, L.F., and Marder, E. (1997). Temporal dynamics of graded synaptic transmission in the lobster stomatogastric ganglion. J Neurosci *17*, 5610-5621.
Marder, E. (2006). Neurobiology: extending influence. Nature *441*, 702-703.

Marder, E., and Goaillard, J.M. (2006). Variability, compensation and homeostasis in neuron and network function. Nat Rev Neurosci *7*, 563-574.

Margrie, T.W., Sakmann, B., and Urban, N.N. (2001). Action potential propagation in mitral cell lateral dendrites is decremental and controls recurrent and lateral inhibition in the mammalian olfactory bulb. Proc Natl Acad Sci U S A *98*, 319-324.

Merkle, F.T., Mirzadeh, Z., and Alvarez-Buylla, A. (2007). Mosaic organization of neural stem cells in the adult brain. Science (New York, N.Y *317*, 381-384.

Meyer, M.P., and Smith, S.J. (2006). Evidence from in vivo imaging that synaptogenesis guides the growth and branching of axonal arbors by two distinct mechanisms. J Neurosci *26*, 3604-3614.

Mombaerts, P. (2004). Odorant receptor gene choice in olfactory sensory neurons: the one receptor-one neuron hypothesis revisited. Curr Opin Neurobiol *14*, 31-36.

Mori, K. (1987). Membrane and synaptic properties of identified neurons in the olfactory bulb. Prog Neurobiol *29*, 275-320.

Mouret, A., Gheusi, G., Gabellec, M.M., de Chaumont, F., Olivo-Marin, J.C., and Lledo, P.M. (2008). Learning and survival of newly generated neurons: when time matters. J Neurosci *28*, 11511-11516.

Mouret, A., Lepousez, G., Gras, J., Gabellec, M.M., and Lledo, P.M. (2009). Turnover of newborn olfactory bulb neurons optimizes olfaction. J Neurosci *29*, 12302-12314.

Murphy, G.J., Darcy, D.P., and Isaacson, J.S. (2005). Intraglomerular inhibition: signaling mechanisms of an olfactory microcircuit. Nat Neurosci *8*, 354-364.

Nelson, A.B., Krispel, C.M., Sekirnjak, C., and du Lac, S. (2003). Long-lasting increases in intrinsic excitability triggered by inhibition. Neuron *40*, 609-620.

Nelson, S.B., Hempel, C., and Sugino, K. (2006). Probing the transcriptome of neuronal cell types. Curr Opin Neurobiol *16*, 571-576.

Nelson, S.B., and Turrigiano, G.G. (2008). Strength through diversity. Neuron *60*, 477-482.

Niell, C.M., Meyer, M.P., and Smith, S.J. (2004). In vivo imaging of synapse formation on a growing dendritic arbor. Nature neuroscience *7*, 254-260.

Nissant, A., Bardy, C., Katagiri, H., Murray, K., and Lledo, P.M. (2009). Adult neurogenesis promotes synaptic plasticity in the olfactory bulb. Nature neuroscience.

Nitabach, M.N., Wu, Y., Sheeba, V., Lemon, W.C., Strumbos, J., Zelensky, P.K., White, B.H., and Holmes, T.C. (2006). Electrical hyperexcitation of lateral ventral pacemaker neurons desynchronizes downstream circadian oscillators in the fly circadian circuit and induces multiple behavioral periods. J Neurosci *26*, 479-489.

Nottebohm, F. (2002). Why are some neurons replaced in adult brain? J Neurosci *22*, 624-628.

Nottebohm, F. (2004). The road we travelled: discovery, choreography, and significance of brain replaceable neurons. Ann N Y Acad Sci *1016*, 628-658.

Nusser, Z. (2009). Variability in the subcellular distribution of ion channels increases neuronal diversity. Trends Neurosci *32*, 267-274.

Panama, B.K., and Lopatin, A.N. (2006). Differential polyamine sensitivity in inwardly rectifying Kir2 potassium channels. J Physiol *571*, 287-302.

Paradis, S., Sweeney, S.T., and Davis, G.W. (2001). Homeostatic control of presynaptic release is triggered by postsynaptic membrane depolarization. Neuron *30*, 737-749.

Parra, P., Gulyas, A.I., and Miles, R. (1998). How many subtypes of inhibitory cells in the hippocampus? Neuron *20*, 983-993.

Petreanu, L., and Alvarez-Buylla, A. (2002). Maturation and death of adult-born olfactory bulb granule neurons: role of olfaction. J Neurosci *22*, 6106-6113.

Preisig-Muller, R., Schlichthorl, G., Goerge, T., Heinen, S., Bruggemann, A., Rajan, S., Derst, C., Veh, R.W., and Daut, J. (2002).

Heteromerization of Kir2.x potassium channels contributes to the phenotype of Andersen's syndrome. Proc Natl Acad Sci U S A *99*, 7774-7779.

Pressler, R.T., Inoue, T., and Strowbridge, B.W. (2007). Muscarinic receptor activation modulates granule cell excitability and potentiates inhibition onto mitral cells in the rat olfactory bulb. J Neurosci *27*, 10969-10981.

Pressler, R.T., and Strowbridge, B.W. (2006). Blanes cells mediate persistent feedforward inhibition onto granule cells in the olfactory bulb. Neuron *49*, 889-904.

Ren, D., Navarro, B., Xu, H., Yue, L., Shi, Q., and Clapham, D.E. (2001). A prokaryotic voltage-gated sodium channel. Science (New York, N.Y *294*, 2372-2375.

Saghatelyan, A., Roux, P., Migliore, M., Rochefort, C., Desmaisons, D., Charneau, P., Shepherd, G.M., and Lledo, P.M. (2005). Activity-dependent adjustments of the inhibitory network in the olfactory bulb following early postnatal deprivation. Neuron *46*, 103-116.

Scharff, C., Kirn, J.R., Grossman, M., Macklis, J.D., and Nottebohm, F. (2000). Targeted neuronal death affects neuronal replacement and vocal behavior in adult songbirds. Neuron *25*, 481-492.

Schmidt-Hieber, C., Jonas, P., and Bischofberger, J. (2004). Enhanced synaptic plasticity in newly generated granule cells of the adult hippocampus. Nature *429*, 184-187.

Schoppa, N.E. (2006). Synchronization of olfactory bulb mitral cells by precisely timed inhibitory inputs. Neuron *49*, 271-283.

Schoppa, N.E., Kinzie, J.M., Sahara, Y., Segerson, T.P., and Westbrook, G.L. (1998). Dendrodendritic inhibition in the olfactory bulb is driven by NMDA receptors. J Neurosci *18*, 6790-6802.

Schoppa, N.E., and Urban, N.N. (2003). Dendritic processing within olfactory bulb circuits. Trends Neurosci *26*, 501-506.

Schoppa, N.E., and Westbrook, G.L. (1999). Regulation of synaptic timing in the olfactory bulb by an A-type potassium current. Nat Neurosci *2*, 1106-1113.

Schoppa, N.E., and Westbrook, G.L. (2001). Glomerulus-specific synchronization of mitral cells in the olfactory bulb. Neuron *31*, 639-651.

Sheng, M. (2001). Molecular organization of the postsynaptic specialization. Proceedings of the National Academy of Sciences of the United States of America *98*, 7058-7061.

Shepherd, G.M. (2004). The synaptic organization of the brain, 5th ed. edn (Oxford: Oxford University Press).

Shoham, S., O'Connor, D.H., and Segev, R. (2006). How silent is the brain: is there a "dark matter" problem in neuroscience? J Comp Physiol A Neuroethol Sens Neural Behav Physiol *192*, 777-784.

Shu, Y., Hasenstaub, A., Duque, A., Yu, Y., and McCormick, D.A. (2006). Modulation of intracortical synaptic potentials by presynaptic somatic membrane potential. Nature *441*, 761-765.

Sperry, R.W. (1963). Chemoaffinity in the Orderly Growth of Nerve Fiber Patterns and Connections. Proc Natl Acad Sci U S A *50*, 703-710.

Spitzer, N.C. (2006). Electrical activity in early neuronal development. Nature *444*, 707-712.

Spruston, N. (2008). Pyramidal neurons: dendritic structure and synaptic integration. Nat Rev Neurosci *9*, 206-221.

Sudhof, T.C., and Jahn, R. (1991). Proteins of synaptic vesicles involved in exocytosis and membrane recycling. Neuron *6*, 665-677.

Swensen, A.M., and Bean, B.P. (2005). Robustness of burst firing in dissociated purkinje neurons with acute or long-term reductions in sodium conductance. J Neurosci *25*, 3509-3520.

Taglialatela, M., Ficker, E., Wible, B.A., and Brown, A.M. (1995). C-terminus determinants for Mg2+ and polyamine block of the inward rectifier K+ channel IRK1. EMBO J *14*, 5532-5541.

Turrigiano, G., Abbott, L.F., and Marder, E. (1994). Activity-dependent changes in the intrinsic properties of cultured neurons. Science *264*, 974-977.

Turrigiano, G.G. (2008). The self-tuning neuron: synaptic scaling of excitatory synapses. Cell *135*, 422-435.

Turrigiano, G.G., Leslie, K.R., Desai, N.S., Rutherford, L.C., and Nelson, S.B. (1998). Activity-dependent scaling of quantal amplitude in neocortical neurons. Nature *391*, 892-896.

Turrigiano, G.G., and Nelson, S.B. (2004). Homeostatic plasticity in the developing nervous system. Nat Rev Neurosci *5*, 97-107.

Wellis, D.P., and Scott, J.W. (1990). Intracellular responses of identified rat olfactory bulb interneurons to electrical and odor stimulation. J Neurophysiol *64*, 932-947.

Whitman, M.C., and Greer, C.A. (2007). Synaptic integration of adult-generated olfactory bulb granule cells: basal axodendritic centrifugal input precedes apical dendrodendritic local circuits. J Neurosci *27*, 9951-9961.

Wilbrecht, L., Crionas, A., and Nottebohm, F. (2002). Experience affects recruitment of new neurons but not adult neuron number. J Neurosci *22*, 825-831.

Wilbrecht, L., and Kirn, J.R. (2004). Neuron addition and loss in the song system: regulation and function. Ann N Y Acad Sci *1016*, 659-683.

Winner, B., Cooper-Kuhn, C.M., Aigner, R., Winkler, J., and Kuhn, H.G. (2002). Long-term survival and cell death of newly generated neurons in the adult rat olfactory bulb. Eur J Neurosci *16*, 1681-1689.

Yamaguchi, M., and Mori, K. (2005). Critical period for sensory experience-dependent survival of newly generated granule cells in the adult mouse olfactory bulb. Proceedings of the National Academy of Sciences of the United States of America *102*, 9697-9702.

Yang, J., Jan, Y.N., and Jan, L.Y. (1995). Control of rectification and permeation by residues in two distinct domains in an inward rectifier K+ channel. Neuron *14*, 1047-1054.

Yokoi, M., Mori, K., and Nakanishi, S. (1995). Refinement of odor molecule tuning by dendrodendritic synaptic inhibition in the olfactory bulb. Proc Natl Acad Sci U S A *92*, 3371-3375.

Yue, L., Navarro, B., Ren, D., Ramos, A., and Clapham, D.E. (2002). The cation selectivity filter of the bacterial sodium channel, NaChBac. J Gen Physiol *120*, 845-853.

Zhang, W., and Linden, D.J. (2003). The other side of the engram: experience-driven changes in neuronal intrinsic excitability. Nat Rev Neurosci *4*, 885-900.

Zhao, C., Deng, W., and Gage, F.H. (2008). Mechanisms and functional implications of adult neurogenesis. Cell *132*, 645-660.

Chapter Two

Distinct Mammalian Precursors Are Committed to Generate Neurons with Defined Dendritic Projection Patterns

Wolfgang Kelsch[1,2], Colleen P. Mosley[3], Chia-Wei Lin[1,2], Carlos Lois[1,2,3]

[1] *Picower Institute for Learning and Memory, Massachusetts Institute of Technology, Cambridge, Massachusetts, United States of America,*

[2] *Department of Brain and Cognitive Sciences, Massachusetts Institute of Technology, Cambridge, Massachusetts, United States of America,*

[3] *Department of Biology, Massachusetts Institute of Technology, Cambridge, Massachusetts, United States of America*

This paper was published in *PLoS Biology* 2007. Nov 13; 5(11): e300

Note: I developed the acute-slice recordings of OB GCs and performed whole-cell patch clamp recordings to examine the possibility that GCs of distinct dendritic projection patterns might have different electrical membrane properties. However, recording result suggests that GCs of different projection patterns share identical repertoires of ion channels, which give rise to similar firing patterns. The result was presented in ***Figure 4***.

Abstract

The mechanisms that regulate how dendrites target different neurons to establish connections with specific cell types remain largely unknown. In particular, the formation of cell-type–specific connectivity during postnatal neurogenesis could be either determined by the local environment of the mature neuronal circuit or by cell-autonomous properties of the immature neurons, already determined by their precursors. Using retroviral fate mapping, we studied the lamina-specific dendritic

targeting of one neuronal type as defined by its morphology and intrinsic somatic electrical properties in neonatal and adult neurogenesis. Fate mapping revealed the existence of two separate populations of neuronal precursors that gave rise to the same neuronal type with two distinct patterns of dendritic targeting—innervating either a deep or superficial lamina, where they connect to different types of principal neurons. Furthermore, heterochronic and heterotopic transplantation demonstrated that these precursors were largely restricted to generate neurons with a predetermined pattern of dendritic targeting that was independent of the host environment. Our results demonstrate that, at least in the neonatal and adult mammalian brain, the pattern of dendritic targeting of a given neuron is a cell-autonomous property of their precursors.

Introduction

Dendrites are the major source of synaptic input for neurons. Thus, the specific computation that a neuron can accomplish is largely determined by the synaptic partners that contact its dendrites. In many regions of the central nervous system, including the cortex, spinal cord, retina, and olfactory bulb [1–4], neurons that share a common morphology and similar microenvironment have dendrites that target synaptic partners in different laminae. Although significant advances have been made in understanding the mechanisms that control axonal pathfinding during development [5,6], relatively less is known about the regulation of dendritic connectivity [7–9]. In recent years, some of the cellular mechanisms involved in dendritic growth into specific laminae have been characterized [4,7,9–11]. In addition, some cell-adhesion molecules involved in the formation of cell type–specific dendritic connectivity

have been identified [8]. However, it remains unknown whether lamina-specific targeting is a cell-autonomous property of immature neurons, or alternatively, determined by the cellular environment in which the neurons differentiate. How lamina-specific dendritic targeting is specified is a particularly interesting question for neurons generated in the neonatal or adult period, because these new neurons have to integrate into a functioning, mature neuronal circuit.

In this study, we examined the regulation of differential dendritic targeting of one neuronal type, the granule cell (GC) neuron of the olfactory bulb. GCs are axonless inhibitory interneurons that are continuously incorporated into the olfactory bulb throughout life [12,13]. GCs form dendro-dendritic synapses with the two types of projection neurons of the bulb, the mitral and the tufted cells (Figure 1A). GCs have distinct patterns of dendritic targeting—innervating either a deep or superficial lamina, where they connect to either mitral or tufted cells, respectively [14–16].

How is the lamina-specific dendritic targeting regulated in GCs? Throughout postnatal life, GCs are generated from neuronal precursors that proliferate in the subventricular zone (SVZ) and give rise to neuroblasts that migrate through the rostral migratory stream (RMS) into the olfactory bulb [12,13]. One possible scenario is that local cues within the olfactory bulb regulate the lamina-specific dendritic targeting of immature GCs at the time of their differentiation. Another possibility is that immature GCs are already committed to specific patterns of dendritic arborization at the moment of their birth in the SVZ, before they reach the bulb. To investigate these possibilities, we performed retroviral fate-mapping and

transplantation experiments to test whether different populations of precursors give rise to GCs with lamina-specific dendritic arborizations. We discovered that the SVZ contained distinct populations of neuronal precursors committed to generate GCs with dendritic targeting to specific laminae. Furthermore, these precursors were largely restricted in their developmental potential with respect to dendritic targeting even when challenged with a SVZ microenvironment that normally generated GCs with dendrites that targeted the other lamina. Our results demonstrate that, in the neonatal and adult mammalian brain, the pattern of dendritic targeting of a given neuron can be a cell-intrinsic property that is already determined at the time of its birth. These findings have important implications both for assembly of neuronal circuits, and for the potential uses of adult neuronal stem cells in cell replacement therapies.

Results

Distinct Populations of Neonatal SVZ Precursors Gave Rise to GCs with Lamina-Specific Dendritic Targeting

In the neonatal brain, precursors in the SVZ give rise to GCs that integrate into the olfactory bulb. Most GCs have an apical dendrite that branches either in the deep or the superficial lamina of the external plexiform layer (EPL) (Figure 1A). To investigate whether precursors along the entire length of the neonatal SVZ have a similar developmental potential to give rise to GCs with a specific pattern of dendritic targeting, we used retroviral fate mapping to label precursors located in either one region of the anterior or posterior SVZ (aSVZ and pSVZ, respectively) of neonatal rats (Figures 1B and S1D). Oncoretroviruses have a half-life

of only 6 h [17] and infect only actively dividing cells. Since the transient amplifying cell population is the most abundant actively dividing cell type in the SVZ, and the direct precursor to immature GCs, oncoretroviral infection is very effective for birth dating a single cohort of immature neurons [18]. Indeed, after infecting SVZ precursors with oncoretroviral vectors, we detected a single wave of labeled precursors that reached the olfactory bulb together. At 14 and 21 days postinfection (d.p.i.), only 4.8% (n = 1,218) and 1.3% (n = 780), respectively, of the total number of retrovirally labeled cells were still found in the RMS of the olfactory bulb.

An oncoretroviral vector expressing green fluorescent protein (GFP) was stereotactically injected into the aSVZ or the pSVZ, and the morphology of GFP-positive (GFP^+) GCs in the olfactory bulb was assessed 28 d.p.i., when they had acquired a mature neuronal morphology (Figure 2). We observed that the apical dendrite of GCs generated in the aSVZ of neonatal animals branched predominantly in the superficial lamina of the EPL, whereas the branches of the apical dendrite of GCs generated in the pSVZ of neonatal animals were mostly confined to the deep lamina of the EPL (Figure 2). This result was found to be independent of the strain or sex of the animals (see Materials and Methods and Figure S1A). Furthermore, we confirmed that the lamina-specific targeting and position of the initial dendritic branch point of new GCs was observed at all stages of their maturation (Figures 1C and 2).

To quantify these findings, we measured the position of the initial branch point of the apical dendrite of GFP^+ GCs from each precursor population (n = 250 for each time point after injection and each site of injection). To determine the position of the initial dendritic branch point, the width of the EPL was assigned percentages, with 0% being the mitral cell layer (MCL), and 100% being the border between the EPL and glomerular layer (GL) (Figure 1B).

The EPL was then divided into 10% steps, and the position of the initial branch point of the apical dendrite was assessed using this scale. The cumulative distribution of the initial branch-point positions revealed that the dendrites of GCs generated from neonatal aSVZ precursors branched superficially, with a median initial branch point approximately halfway through the EPL (50.1% of EPL, median for all time points, n = 1,000; Figure 1C). In contrast, neonatal pSVZ precursors gave rise to GCs with apical dendrites that branched in the deep EPL, with a median branch point close to the MCL (2% of EPL, median for all time points, n = 500; Figure 1C). The distribution of the initial dendritic branching point was significantly different for neonatal-generated GCs from the aSVZ and pSVZ ($p < 0.0001$; n = 1,000 and 500, respectively). It is important to note that retroviral injection into the aSVZ is also likely to label some of the precursors that originate in other parts of the SVZ (e.g., pSVZ), but that proliferate in the aSVZ while they migrate through it on their way towards the olfactory bulb. However, after injecting into the aSVZ, the number of transit-proliferating cells that originated from the pSVZ was less than 5% (n = 500). As shown in Figure 1C, the cumulative distribution of the initial branching point for the pSVZ cells was very steep close to the MCL, whereas that of the aSVZ cells was nearly flat in this same region. In summary, fate-mapping experiments demonstrate the existence of at least two distinct precursor populations in the neonatal SVZ, each committed to generate GCs with specific patterns of dendritic targeting in the olfactory bulb.

Adult SVZ Precursors Continue to Generate GCs with Lamina-Specific Dendritic Targeting

Because new GCs continue to be added into the olfactory bulb throughout life, we also investigated whether distinct GC precursor populations persisted into adulthood. Similar to

our previous experiments, we observed that oncoretroviral infection of the adult aSVZ led to the efficient labeling of a single cohort of immature GCs in the olfactory bulb. At 14 and 21 d after retroviral labeling of precursors in adult rats, only 8.7% (n = 922) and 0.8% (n = 615), respectively, of the total number of cells labeled were still found migrating in the RMS of the olfactory bulb.

Retroviral fate mapping revealed that GCs generated from precursors located in the aSVZ of adult animals had apical dendrites that branched predominantly in the deep lamina of the EPL (Figure 2). Quantification of this result indicated that the dendrites of GCs born from adult aSVZ precursors had a median branch-point position close to the MCL (4.5% of EPL, median for all time points, n = 1,000; Figure 1C), similar to the dendritic branching pattern of GCs born from neonatal pSVZ precursors. The distribution of the initial dendritic branching point was significantly different for neonatal- and adult-generated GCs from the aSVZ ($p <$ 0.0001; n = 1,000, respectively). Again, this result was found to be independent of the strain or sex of the animals (see Materials and Methods and Figure S1A). Furthermore, as discussed for the neonatal animals, we confirmed that the lamina-specific targeting and position of the initial dendritic branch point of new GCs was observed at different stages of their maturation (Figures 1C and 2C). Interestingly, the normalized soma position of GCs from adult aSVZ was between that of GCs from neonatal aSVZ and pSVZ (Figure 1D) when compared at the same age (postnatal day [P]69–70).

We also investigated the fate of actively dividing precursors in the pSVZ and in the sector of the RMS rostral to the SVZ in adult animals. The dividing precursors in these two regions both gave rise mainly to GCs with deep dendritic targeting even though both regions also contained some GCs with superficial dendritic targeting (see Figure S1B). This observation

suggested that superficially branching GCs are still generated in the adult. However, using the retroviral labeling technique described in this study, we could not detect a SVZ region in the adult animal that exclusively contained actively dividing precursors committed to the generation of superficially branching GCs. Two recent studies [19,20] observed that generation of superficial GCs peaks in the neonatal period and decreases thereafter, consistent with our findings that precursors labeled in the different regions of the adult RMS and SVZ mainly gave rise to deep-targeting GCs. Taken together, these findings indicate that distinct populations of precursors in the SVZ gave rise to GCs that target either the deep or superficial EPL.

Dendritic Morphology and Synaptic Contacts of GCs Derived from Different SVZ Precursor Populations

In our initial experiments, we quantified the position of the initial branch point of the apical dendrite as a surrogate measure of lamina-specific dendritic targeting. To obtain a more comprehensive view of the dendritic targeting of new GCs generated from different SVZ precursor populations, we reconstructed the dendritic arbors of retrovirally labeled GFP^+ GCs, selecting cells that displayed complete dendrites without apparent truncation due to tissue sectioning (Figure 2; n = 10 GCs for each time point and condition). Most GCs generated from neonatal pSVZ and adult aSVZ precursors had fine dendritic branches that ended in the deep lamina of the EPL, whereas GCs generated from neonatal aSVZ had fine dendritic branches that were located in the superficial EPL (Figure 2). GC reconstructions indicated that their dendritic arbors were largely confined to specific laminae, thereby

suggesting that these GCs establish synaptic contacts in specific laminae. An alternative possibility is that GC synapses are not uniformly distributed throughout the dendritic arbor, and that the lamina-specific elaboration of the terminal fine dendritic branches did not reflect lamina-specific innervation. To further investigate these possibilities, we quantified the distribution of spine protrusions studding the branches of the apical dendritic arbor of GCs in the EPL using single-cell GC reconstructions (n = 10 GCs for each time point and condition). Dendritic spines are the major sites of excitatory synaptic transmission in the mammalian brain [21] and are thought to be morphological correlates of synapses. In GCs of the olfactory bulb, dendritic spines are the primary sites of both the inputs and outputs of dendro-dendritic synapses to and from mitral and tufted cells [16]. Few spines were found along the primary apical dendrite prior to the initial dendritic branching point. We found that neonatal pSVZ and adult aSVZ precursors generated GCs with spine protrusions confined to the deep lamina of the EPL (Figure 3), consistent with their pattern of dendritic arborization. Furthermore, neonatal aSVZ generated GCs with spine protrusions confined to the superficial lamina of the EPL (Figure 3).

To further investigate the distribution of synaptic contacts in GC dendritic arbors, we also labeled the postsynaptic sites of glutamatergic synaptic inputs into GCs by expressing a genetic marker, PSD-95 fused to GFP, in GCs using an oncoretroviral vector. PSD-95 is a major scaffolding component of the postsynaptic density at excitatory synapses [22]. When GFP-tagged PSD95 is expressed in neurons, it clusters at the postsynaptic densities of glutamatergic synapses [23–25]. We found that the distribution of postsynaptic sites in GCs generated from precursors in the neonatal aSVZ and adult aSVZ, as labeled using PSD-

95:GFP, was very similar to that described above for spine protrusions (see Figure S2 and Text S1). Thus, two independent methods indicate that distinct neuronal precursors in the postnatal SVZ generate GCs with lamina-specific patterns of synaptic innervation.

Deep and Superficial GCs Share Intrinsic Somatic Electrical Properties

GCs with deep and superficial branching dendrites labeled by retroviral infections shared similar cell morphology (Figure 2). We explored whether GCs with deep or superficial dendritic targeting may also share intrinsic somatic electrical properties that provide a useful criterion towards neuronal type classification [26–28]. Towards this aim, we performed targeted whole-cell recordings in acute slice preparations from GFP^+ neurons with either superficial or deep dendritic targeting (21–23 d.p.i.) that were labeled in the aSVZ or pSVZ, respectively, in neonatal animals (Figure 4). Both deep and superficial neurons had similar delayed firing patterns (Figure 4A) and afterdepolarizations (Figure 4B). In addition, cells with either deep or superficial dendrites had I_A currents that were abolished by exposure to 10 mM of 4-aminopyridine (unpublished data) and similar membrane properties (Figure 4C). The membrane capacitance of deep branching cells was larger than that of the superficial cells, most likely due to their differences in membrane surface. In summary, these data confirm that the new neurons with deep and superficial dendritic targeting not only shared a common morphology, but both also had similar intrinsic somatic electrical properties typical for GCs [29–32]. Thus, these observations suggest that distinct precursors in the SVZ are committed to giving rise to a single neuronal type with two alternative patterns of dendritic targeting.

Fate Determination of GC Precursors

The factors regulating the lamina-specific targeting of GCs in the olfactory bulb are currently unknown. Our results raised the possibility that different populations of SVZ precursors may be committed to generate GCs with a particular pattern of dendritic targeting. Alternatively, local cues in the SVZ or olfactory bulb may control the developmental program of GC precursors or migrating GCs with respect to dendritic targeting. To investigate these possibilities, we performed heterochronic and heterotopic transplantations of different SVZ regions to examine whether their progeny adopt a different fate when challenged with new environments. In transplantation experiments, we isolated explants from three different sources, the neonatal aSVZ or pSVZ and adult aSVZ of GFP^+ transgenic donor rats [33], and stereotactically injected them into the neonatal aSVZ or pSVZ and adult aSVZ of wild-type host rats (Figure 5A). The dendritic targeting of GFP^+ GCs in the olfactory bulb was assessed 35 d post-transplantation to allow for their full maturation (Figure 5) (n = 200–731 neurons from 6–16 host hemispheres, per experiment).

In order to validate that precursors in the SVZ retain their endogenous ability to generate GCs with lamina-specific dendritic targeting, we first performed isochronic, isotopic transplantation experiments in which the aSVZ from neonatal donors was grafted into the aSVZ of neonatal hosts. GCs derived from these transplanted precursors extended dendrites that targeted the superficial lamina of the EPL (Figure 5B and 5C), confirming the results of our retroviral fate-mapping experiments (Figure 1D and 1E). Similarly, isochronic, isotopic transplantation of either pSVZ of neonatal donors into the pSVZ of neonatal hosts or of the aSVZ of adult donors into the aSVZ of adult hosts resulted in GFP^+ GCs whose dendrites targeted the deep lamina of the EPL (Figure 5B and 5C). These data demonstrate that the transplantation procedure itself did not perturb the endogenous developmental potential of

GC precursors with respect to lamina-specific dendritic targeting.

We then tested whether heterochronic and heterotopic transplantation of distinct SVZ regions can give rise to GCs with different dendritic targeting when exposed to a different environment. After heterochronic transplantation of precursors from adult aSVZ donors to neonatal aSVZ hosts as well as heterotopic transplantation from neonatal pSVZ to neonatal aSVZ, GFP^+ GCs largely maintained their deep initial branching point (Figure 5C). After transplantation of precursors from neonatal aSVZ to adult aSVZ or to neonatal pSVZ, the GCs largely maintained their fate and had a superficial initial dendritic branching point (Figure 5C). We only observed a small increase in the number of GFP^+ GCs that had a deeper initial dendritic branching point compared to isochronic and isotopic transplantation from the neonatal aSVZ donors.

To quantify these observations, we counted the number of neurons whose initial branching point occurred below or above the midpoint of the EPL. We then calculated the ratio of cells that branched below the EPL midpoint threshold to the total number of GFP^+ GCs. We measured this ratio for GCs derived from the same donor grafted heterochronically or isochronically, and then calculated the change in the ratio of GCs that initially branched below the EPL midpoint, and expressed it as a percentage.

When neonatal aSVZ was transplanted into adult aSVZ, we observed a small increase (17.1%, Mann-Whitney test: $p < 0.05\%$) of GCs that branched below the EPL midpoint, when compared to isochronic transplantation (neonatal aSVZ to neonatal aSVZ) from the same donor. Heterotopic transplantation from neonatal aSVZ to neonatal pSVZ resulted in 15.8% change ($p = 0.13$; not statistically significant) of GCs that branched below the EPL

midpoint (Figure 5C). When we transplanted neonatal pSVZ into neonatal aSVZ, we observed a very small change (4%, not statistically significant) of GCs that branched above the EPL midpoint (Figure 5C). The small change observed in the population of GC precursors from the neonatal aSVZ after transplantation could be due to some partial phenotypic plasticity of these neonatal progenitors, or alternatively, to the transplantation procedure used in these experiments (see Discussion). Finally, heterochronic transplantation of adult aSVZ into neonatal aSVZ host did not induce a change (0.4%, not statistically significant) in GCs that branched below the EPL midpoint, when compared to isochronic transplantation (adult aSVZ to adult aSVZ) from the same donor (Figure 5C). In summary, even though some small changes can occur when the precursors are challenged with a new environment, the vast majority of new GCs derived from the different SVZ regions maintained their pattern of dendritic targeting.

In order to obtain a more complete picture of the lamina-specific targeting of the apical dendritic arbor of transplant-derived GCs, we reconstructed the morphology of representative GFP^+ GCs, as described above (Figure 6, n = 10 cells per condition). Neuronal reconstructions revealed that precursors that generate GCs with deep dendritic targeting in their native environment still gave rise to GCs with targeting of the deep lamina after heterochronic or heterotopic transplantation (Figure 6). The same observation applied to precursors that generate GCs with superficial dendritic targeting when challenged with a different proliferative environment (Figure 6). Finally, to confirm that the lamina-specific dendritic targeting reflects a lamina-specific distribution of synapses in these GCs, we determined the distribution of spines within the dendritic arbors of transplant-derived GCs. Similar to our previous findings, the distribution of dendritic spines reflected the lamina-

specific dendritic targeting of transplanted GCs (Figure 7). Thus, our transplantation experiments indicate that precursors in the neonatal and adult animals appeared to be committed to generate GCs with a specific pattern of dendrite branching that was not modified by exposure to a brain environment that normally generated GCs with opposite dendritic targeting.

Discussion

In this study, we investigated lamina-specific dendritic targeting of neurons generated in neonatal and adult rats. In particular, we tested whether local factors determine the dendritic targeting or, alternatively, whether a cell-intrinsic program is conferred onto the neuron from its precursor. To investigate these possibilities, we performed retroviral fate mapping and reconstructions of GCs generated in postnatal life in different regions of the SVZ. Our results indicate that at least two separate populations of precursors exist in the SVZ and give rise to GCs that target either the deep or the superficial lamina. Therefore, distinct precursors can produce one type of neuron, as defined by its morphology and intrinsic electric properties, but exhibiting different dendritic targeting. We performed heterochronic and heterotopic transplantations of different SVZ regions and observed that the majority of new GCs maintained their fate of targeting a specific lamina even when their precursors were grafted into SVZ environment that normally generated GCs with dendritic targeting of the opposite principal neuron lamina. Our results demonstrate that, in the mammalian brain, the pattern of dendritic targeting of a given neuron can be a cell-intrinsic property determined at the time of its birth. These findings have important implications, both for understanding the assembly of

brain circuits during development and for the potential uses of adult neuronal stem cells in cell replacement therapies.

One Type of Neuron with Two Different Patterns of Dendritic Targeting

Our findings indicate that the connectivity of one type of neuron as defined by its morphology and intrinsic somatic electrical properties in the same brain region, the GCs of the olfactory bulb, can in fact be determined by the particular population of neuronal precursor from which they derive. This observation suggests that neuronal precursors in the mammalian brain may be committed to produce neurons that are tailored to perform specific functions in a given neuronal microcircuit from as early as the time of their birth.

Our finding that lamina-specific dendritic targeting can be an intrinsic property of an immature neuron determined by the identity of its precursor has important implications for the logic of neuronal circuit assembly. In particular, GCs in the olfactory bulb that target the superficial lamina of the EPL are believed to establish synapses with tufted cells [16,34], whereas GCs that target the deep lamina are connected to mitral cells, and these two microcircuits are believed to serve different functions. The tufted-GC circuit is thought to be an intrabulbar association microcircuit [34] that may be important for low-threshold perception of odorants [35]. In contrast, the mitral-GC circuit is thought to mediate lateral inhibition and to participate in odor discrimination [36]. Thus, GCs that participate in specific microcircuits may be committed to their function already at the time of their birth from distinct populations of neuronal precursors.

To validate whether the neurons we labeled indeed constitute the same neuronal type with different dendritic targeting as suggested by their similar morphology, we measured their

intrinsic somatic electrical properties, a useful feature for classification of neurons [26–28]. Indeed, labeled neurons with either deep or superficial dendritic targeting had similar intrinsic somatic electrical properties. This observation further suggests that one neuronal type (GC in the olfactory bulb) can exhibit two alternative patterns of dendritic targeting. This observation does not, however, preclude that minor differences may exist between GCs with deep and superficial dendritic targeting, such as differential expression of neurotransmitter receptor subunits [37]. In summary, our results suggest that distinct precursors can generate "tailor-made" neurons with different dendritic targeting connected to specific microcircuits. In addition, within one neuronal type, cells with alternative patterns of dendritic targeting may have subtle functional differences, such as differential expression of neurotransmitter receptors or ion channels, specific for their function in separate microcircuits.

Mechanisms That Determine Dendritic Connectivity

Our findings also provide important insights into the developmental processes by which dendritic patterning is established in the mammalian brain. Particularly in comparison to axonal targeting, the mechanisms that regulate dendritic connectivity and allow neurons to establish proper contacts with their synaptic partners are not well understood [3]. Existing models for dendritic targeting can be divided into two major camps: outgrowth followed by pruning, or directed growth. For instance, in the mammalian retina, the dendritic arbor of retinal ganglion cells initially ramifies broadly, but as development proceeds, part of the dendritic branches are eliminated, such that the dendrites are ultimately segregated into two different laminae [7]. Additionally, a large body of work suggests that the refinement and stabilization of dendritic arbors may also be dependent on experience, a mechanism that

would allow the maturing brain to adapt to a changing environment in postnatal life [4,10,11]. In other cases, the growth of dendrites can be targeted to specific laminae or layers in a directed manner. This mode of directed dendritic targeting has recently been demonstrated in the *Drosophila* olfactory system [38] and in the vertebrate retina [9]. For instance, in vivo imaging of zebrafish retinal development revealed that the dendrites of distinct classes of neurons directly grow to and innervate a specific lamina during their development [9].

How are such programs of dendritic development specified and implemented? Our experiments indicate that, in the mammalian olfactory bulb, the lamina-specific dendritic targeting of GC neurons is an intrinsic property determined by the precursor from which it arises. Our findings are compatible with both modes of dendrite growth described above. In one scenario, new neurons may directly extend their dendrites into the specific EPL lamina where they will form synaptic contacts. Alternatively, dendrites may initially grow in an exuberant manner through both laminae, but they will only form contacts with one type of principal neuron in either lamina, as determined by their precursors, and prune the rest of their dendritic arbors. Finally, after these lamina-specific dendritic contacts have been established, neuronal activity-dependent mechanisms then may play a role in the fine sculpting of GC dendritic arborization.

Fate Restriction of Neuronal Precursors

The mechanisms that regulate the generation of neuronal diversity in the vertebrate nervous system have been investigated extensively. Various studies have shown that both the spatial and temporal origins of precursors determine the neurotransmitter phenotype, firing

properties, calcium binding protein expression, and position of the cell body in different layers [28,39–43]. In particular for interneurons, distinct precursors defined by their expression of transcription factors give rise to specific types of interneurons for different brain regions [42]. Such specialization of precursors to produce different cell types persists throughout life in the SVZ for periglomerular and GC neurons [44–47]. While this work was under review, a study was published [48] demonstrating that the SVZ of postnatal animals has a mosaic organization, with different zones containing precursors committed to generate different types of periglomerular and granule neurons, as revealed by the presence of a set of immunocytochemical markers and the position of their cell bodies in the olfactory bulb. Our study advances previous observations [44,48] by demonstrating that the location of the dendrites and synapses of granule neurons is an intrinsic property of the cell, and by showing that there exist distinct precursors committed to generate neurons with dendritic targeting to specific laminae. Furthermore, we demonstrate that dendritic targeting is determined in the precursor cells in the lateral ventricle, before the progeny from these precursor cells have reached their target in the olfactory bulb. The hypothesis of the protomap, as originally proposed for the developing cortex, stated that the progenitors in the brain ventricles already contain the information [49,50] that specifies the identity of the neuronal cell types of the progeny that they will give rise to, their final destination in the different cortical layers, and the features specific to the different functional areas of the cortex. Our observations extend the protomap hypothesis by showing that the pattern of dendrite arborization can also be a feature already determined in the brain ventricles, before the progeny of the neuronal stem cells have reached their target. Furthermore, heterochronic as well as heterotopic transplantations of precursors confirmed that the fate of the dendritic targeting of a new

neuron was maintained for the large majority of donor-derived GCs independent of the host environment in which their precursors had been grafted. These observations suggest that the connectivity of a neuron can be a cell-autonomous characteristic, determined by an intrinsic program in neonatal and adult neuronal stem cells.

Interestingly, we observed a small population of new GCs (<17%) derived from the neonatal aSVZ that displayed dendritic targeting to the opposite lamina both after heterochronic (into adult aSVZ) and heterotopic (into neonatal pSVZ) transplantation. In contrast, GCs derived after heterochronic and heterotopic transplantation of neonatal pSVZ and adult aSVZ donor tissue did not change their fate of dendritic targeting when challenged with a new SVZ environment. Several reasons could account for the small change of dendritic targeting after heterochronic or heterotopic transplantation from neonatal aSVZ donor tissue. First, a small population of aSVZ precursors could be reprogrammed to generate GCs with deep dendritic targeting after transplantation. Second, cells from the pSVZ, which migrate through the aSVZ, may be induced to proliferate and expand when transplanted, and this phenomenon could increase the number of GCs with deep dendritic targeting after transplanting the aSVZ. Third, a previously quiescent stem cell present in the neonatal aSVZ may be activated when exposed to a SVZ environment that generates GCs with deep dendritic targeting. Our experiments cannot currently distinguish between these and other possibilities, since the aSVZ tissue that is transplanted contains neuronal precursors at different stages of commitment, including rarely dividing stem cells, transient amplifying cells, and immature migrating neurons. In addition, by transplanting explants of tissues into a new SVZ environment, it is possible that donor cells surrounding the neuronal precursors could preserve the status of the donor niche, thus preventing the full reprogramming of the grafted

progenitors. Nevertheless, our findings indicate that the precursors in the SVZ are committed to generate GCs with a prespecified pattern of dendrite targeting before they reach their target.

In recent years, there has been a surge in interest in the possibility of using different types of stem cells for cell replacement therapies aimed at correcting neurological disorders caused by neuronal loss, such as stroke and Parkinson, Huntington and Alzheimer diseases [51,52]. Our observations indicate that distinct neuronal stem cells are committed to generate not only a single neuronal type, but also cells with a prespecified pattern of dendritic targeting. Understanding the program by which neuronal stem cells specify how a neuron will target its dendrites towards a given synaptic partner could help to achieve neuronal replacement with cell type–specific connectivity. Further, the potential uses of endogenous adult neuronal stem cells/precursors for neuronal repair could be hindered by their lack of phenotypic plasticity as revealed by this and other recent studies [44–47]. Thus, the determination of cell type–specific dendritic connectivity by separate neuronal precursors may have important implications, both for the potential uses of adult neuronal stem cells in cell replacement therapies and for understanding the assembly of brain circuits during development.

Materials and Methods

Generation of retroviral vectors.

We used an oncoretroviral vector derived from the Moloney sarcoma virus expressing GFP under the control of the Rous sarcoma virus promoter (MolRG). Recombinant virus was

prepared and stored as described [33]. The viral titer was 10^6–10^7 infectious units/μl.

Stereotactic injections.

Animal care and procedures were approved by the local animal welfare committee. Neonatal (P5) and adult (>P56) Sprague-Dawley, Wistar Kyoto, and Lewis rats of either sex were anesthetized by hypothermia (neonatal rats) and with ketamine/xylazine (adult rats). In initial experiments, we injected P3 to P8 animals in the aSVZ and pSVZ. Between P3 to P8, we observed a superficial and deep branching population of GCs for aSVZ and pSVZ, respectively. For consistency, further experiments were performed at P5 for neonatal rats. Stereotactic injections were performed with a glass capillary with a tip diameter of 3–5 μm, and a volume of 0.1–0.5 μl of viral vector stock was injected. The following stereotactic coordinates (relative to bregma in millimeters) were used for neonatal animals: aSVZ: anterior 0.9, lateral ±2.1, ventral 2.1; pSVZ: posterior 0.6, lateral ±2.7, ventral 2.6; and for adult rats: aSVZ: anterior 1.2, lateral ±1.6 ventral 3.1; aRMS: anterior 2.8 lateral ±1.1, ventral 5.4; pRMS anterior 2.3, lateral ±1.4, ventral 4.5; pSVZ: posterior 2.7, lateral ±4.5, ventral 3.4. For neonatal sites of viral infection, see also Figure S1D. After surgery, animals were monitored for 24 h. Quantification of morphology of GCs was only performed at 14 d.p.i. and later time points in order to avoid including immature neurons that could still be migrating or had not yet acquired a mature morphology. After 14 d.p.i., most GCs from different origins (adult or newborn, aSVZ or pSVZ) had acquired a mature neuronal morphology (see Results). Infecting dividing precursors in the RMS within the adult olfactory bulb did not give rise to GFP^+ GCs (n = 6 hemispheres injected; unpublished data), most likely due to the low level of proliferation in his region [20,53].

Transplantation experiments.

FUGW$^+$ transgenic rats [33] were bred on a Sprague-Dawley background. The aSVZ or pSVZ of neonatal and adult GFP$^+$ rats was dissected (same regions as in Figure S1D), cut in small pieces, and then stereotactically transplanted into the aSVZ or pSVZ of either neonatal or adult wild-type Sprague-Dawley rats with the stereotactic coordinates described above.

Tissue preparation and immunohistochemistry.

Rats were killed with ketamine/xylazine at the indicated time points for retroviral fate mapping or 35 d post-transplantation and perfused intracardially with 3% paraformaldehyde. After 24 h post-fixation in 3% paraformaldehyde at 4 °C, brains were cut into 50-μm coronal sections on a vibratome. Tissue sections were incubated with rabbit polyclonal anti-GFP antibody (1:3,000; Chemicon) in blocking solution containing phosphate buffered saline (PBS), bovine serum albumin, and 0.3% TritonX100 overnight at 4 °C, washed several times with PBS, and incubated with secondary anti-rabbit Alexa488 or Alexa555 conjugated antibody (1:750; Molecular Probes) for 2 h at room temperature. Tissue sections were washed in PBS and counterstained with Hoescht 33258 (Molecular Probes).

Light microscopy, stereology, and neuronal reconstructions.

For stereological analysis and neuronal reconstructions, we used a Neurolucida system coupled to an inverted Olympus fluorescent microscope with a motorized X-Y-Z stage. For stereological analysis of the position of the soma and the initial branching point of the apical dendrite, we first determined the position of the soma and then traced the apical dendrite to its first branching point. All neurons of a tissue section that were not truncated before their

initial dendritic branching were counted. For each time point, 250 neurons were traced from nine to 26 different olfactory bulb sections (n = 250 neurons for each time point from four to eight injected hemispheres from more than three animals) depending on the density of GFP^+ GCs. For transplantation experiments, 200–731 neurons were traced. In initial experiments, we determined the distribution of the soma and the initial branching of the apical dendrite in serial sections throughout the anterior-posterior axes of the bulb. As we did not find any regional differences for the position of the soma and of the initial dendritic branching (unpublished data), we used sections from the central parts of the bulb for further analysis because they gave the highest yield of GFP^+ GCs. In addition, we did not observe any differences in the soma distribution and the position of the initial dendritic branching point for animals of either sex, therefore data from both sexes were pooled. Host hemispheres differed in their density of GFP^+ GCs. The distribution of deep and superficial GCs did not, however, differ regardless of the cell density in the same transplantation condition. For each tissue section, we traced the borders of the different layers based on the nuclear counterstaining with Hoechst 33258 (see also Figure 2). Based on these borders, we divided the granule cell layer (GCL) in percentages: 0% being the border between the RMS and GCL, and 100% being the MCL. For our analysis, dividing the internal plexiform layer (IPL) and the GCL did not prove useful because many of the GC somata were located in the level of the IPL or around the MCL. Based on these borders, we divided the EPL in percentages: 0% being the MCL and 100% being the border between the EPL and the GL. For further analysis, the GCL and the EPL were divided in 10% steps, and the position of the somata and of the initial branching of the apical dendrite was plotted as a cumulative distribution. We calculated the differences in percentages of the ratio of GCs that initially branched below

50% (40%) of EPL. The lower threshold (40%) of EPL gave similar results (±3.4%) to the 50% threshold. GCs for single-cell reconstructions were selected based on the typical position of the soma and on the initial branching of the apical dendrite as found for the respective population. Ten GCs for each time point or transplantation condition without apparent truncation due to tissue sectioning were then reconstructed. Of these GCs, we marked spine protrusions manually with a 40× lens while continuously adapting the *z*-axis. All spine-like protrusions were counted that emerged from the dendrites and had a thickness and morphology that would make them appear as spine- or filapodia-like structures. The distribution of spines of the apical dendrite for each GC was attributed to percentage ranges in the EPL (as defined above, here 20% steps) and then the distribution of spines in the EPL for ten GCs was averaged for each time point or transplantation condition. Statistical significance ($p < 0.05$) was determined with a nonparametric Mann-Whitney test for unpaired samples.

Electrophysiological recordings.

Rat pups were bilaterally injected with 1 μl of oncoretroviral vector expressing GFP in aSVZ and pSVZ in neonatal rats. At 21 to 23 d.p.i., animals were anesthetized with isofluorane, and brains were rapidly removed. The 350-μm horizontal olfactory bulb slices were cut with a Leica vibratome in cutting solution containing (in mM): 212 sucrose, 3 KCl, 1.25 NaH_2PO_4, 26 $NaHCO_3$, 7 $MgCl_2$, 0.5 $CaCl_2$, 10 glucose, 310 mOsm, (pH 7.3). Slices were recovered for 30 min at 32 °C with recording solution containing (in mM): 125 NaCl, 2.5 KCl, 1.25 NaH_2PO_4, 26 $NaHCO_3$, 1 $MgCl_2$, 2 $CaCl_2$, 20 glucose, 310 mOsm, (pH 7.3) and continuously bubbled with carbogen. After recovery, slices were kept at room temperature.

Targeted whole-cell recordings were performed on GFP^+ nontruncated CGs with a MultiClamp700B amlpifier (Axon Instruments) and pipette solution containing (in mM): 2 NaCl, 4 KCI, 130 K-gluconate, 10 HEPES, 0.2 EGTA, 4 ATP-Mg, 0.3 GFP-Tris, 14 phosphocreatine, 0.02Alexa555 hydrazide, 292 mOsm, and pH 7.25. Pipette resistance was 6-9 MW. Access resistance was 12-30 MW, which was not compensated and regularly monitored during recordings. Liquid junction potential was not corrected. Data were acquired and analyzed with the pClamp9 software (Axon Instruments). Neurons were considered to have *I* current if in a voltage ramp (10 mV steps for 400ms), the peak-to-plateau ratio was > 2. After recordings, the tissue was fixed and the neurons were reconstructed. Recordings from the correct GCs were confirmed by co-localization of Alexa555 flourescence with GFP^+ GCS.

Reference

1. Sanes JR, Yamagata M (1999) Formation of lamina-specific synaptic connections. Curr Opin Neurobiol 9: 79–87.
2. McAllister AK (2000) Cellular and molecular mechanisms of dendrite growth. Cereb Cortex 10: 963–973.
3. Jan YN, Jan LY (2003) The control of dendrite development. Neuron 40: 229–242.
4. Wong RO, Ghosh A (2002) Activity-dependent regulation of dendritic growth and patterning. Nat Rev Neurosci 3: 803–812.
5. Tessier-Lavigne M, Goodman CS (1996) The molecular biology of axon guidance. Science 274: 1123–1133.
6. Luo L, O'Leary DD (2005) Axon retraction and degeneration in development and disease. Annu Rev Neurosci 28: 127–156.
7. Wang GY, Liets LC, Chalupa LM (2001) Unique functional properties of on and off pathways in the developing mammalian retina. J Neurosci 21: 4310–4317.
8. Yamagata M, Weiner JA, Sanes JR (2002) Sidekicks: synaptic adhesion molecules that promote lamina-specific connectivity in the retina. Cell 110: 649–660.
9. Mumm JS, Williams PR, Godinho L, Koerber A, Pittman AJ, et al. (2006) In vivo imaging reveals dendritic targeting of laminated afferents by zebrafish retinal ganglion cells. Neuron 52: 609–621.
10. Katz LC, Shatz CJ (1996) Synaptic activity and the construction of cortical circuits. Science 274: 1133–1138.
11. Lee WC, Huang H, Feng G, Sanes JR, Brown EN, et al. (2006) Dynamic remodeling of dendritic arbors in GABAergic interneurons of adult visual cortex. PLoS Biol 4: e29
12. Lois C, Alvarez-Buylla A (1993) Proliferating subventricular zone cells in the adult mammalian forebrain can differentiate into neurons and glia. Proc Natl Acad Sci U S A 90: 2074–2077.
13. Luskin MB (1993) Restricted proliferation and migration of postnatally generated neurons derived from the forebrain subventricular zone. Neuron 11: 173–189.

14. Mori K, Kishi K, Ojima H (1983) Distribution of dendrites of mitral, displaced mitral, tufted, and granule cells in the rabbit olfactory bulb. J Comp Neurol 219: 339–355.

15. Orona E, Scott JW, Rainer EC (1983) Different granule cell populations innervate superficial and deep regions of the external plexiform layer in rat olfactory bulb. J Comp Neurol 217: 227–237.

16. Shepherd GM, Chen WR, Greer CA (2004) Olfactory bulb. Shepherd GM, editor. New York: Oxford University Press. pp. 165–216.

17. Andreadis ST, Brott D, Fuller AO, Palsson BO (1997) Moloney murine leukemia virus-derived retroviral vectors decay intracellularly with a half-life in the range of 5.5 to 7.5 hours. J Virol 71: 7541–7548.

18. Sanes JR (1989) Analysing cell lineage with a recombinant retrovirus. Trends Neurosci 12: 21–28.

19. Imamura F, Nagao H, Naritsuka H, Murata Y, Taniguchi H, et al. (2006) A leucine-rich repeat membrane protein, 5T4, is expressed by a subtype of granule cells with dendritic arbors in specific strata of the mouse olfactory bulb. J Comp Neurol 495: 754–768.

20. Lemasson M, Saghatelyan A, Olivo-Marin JC, Lledo PM (2005) Neonatal and adult neurogenesis provide two distinct populations of newborn neurons to the mouse olfactory bulb. J Neurosci 25: 6816–6825.

21. Nimchinsky EA, Sabatini BL, Svoboda K (2002) Structure and function of dendritic spines. Annu Rev Physiol 64: 313–353.

22. Sheng M (2001) Molecular organization of the postsynaptic specialization. Proc Natl Acad Sci U S A 98: 7058–7061.

23. Ebihara T, Kawabata I, Usui S, Sobue K, Okabe S (2003) Synchronized formation and remodeling of postsynaptic densities: long-term visualization of hippocampal neurons expressing postsynaptic density proteins tagged with green fluorescent protein. J Neurosci 23: 2170–2181.

24. Rao A, Kim E, Sheng M, Craig AM (1998) Heterogeneity in the molecular composition of excitatory postsynaptic sites during development of hippocampal neurons in culture. J Neurosci 18: 1217–1229.

25. Washbourne P, Bennett JE, McAllister AK (2002) Rapid recruitment of NMDA receptor transport packets to nascent synapses. Nat Neurosci 5: 751–759.
26. Sugino K, Hempel CM, Miller MN, Hattox AM, Shapiro P, et al. (2006) Molecular taxonomy of major neuronal classes in the adult mouse forebrain. Nat Neurosci 9: 99–107.
27. Markram H, Toledo-Rodriguez M, Wang Y, Gupta A, Silberberg G, et al. (2004) Interneurons of the neocortical inhibitory system. Nat Rev Neurosci 5: 793–807.
28. Butt SJ, Fuccillo M, Nery S, Noctor S, Kriegstein A, et al. (2005) The temporal and spatial origins of cortical interneurons predict their physiological subtype. Neuron 48: 591–604.
29. Carleton A, Petreanu LT, Lansford R, Alvarez-Buylla A, Lledo PM (2003) Becoming a new neuron in the adult olfactory bulb. Nat Neurosci 6: 507–518.
30. Egger V, Svoboda K, Mainen ZF (2003) Mechanisms of lateral inhibition in the olfactory bulb: efficiency and modulation of spike-evoked calcium influx into granule cells. J Neurosci 23: 7551–7558.
31. Schoppa NE, Westbrook GL (1999) Regulation of synaptic timing in the olfactory bulb by an A-type potassium current. Nat Neurosci 2: 1106–1113.
32. Schoppa NE, Kinzie JM, Sahara Y, Segerson TP, Westbrook GL (1998) Dendrodendritic inhibition in the olfactory bulb is driven by NMDA receptors. J Neurosci 18: 6790–6802.
33. Lois C, Hong EJ, Pease S, Brown EJ, Baltimore D (2002) Germline transmission and tissue-specific expression of transgenes delivered by lentiviral vectors. Science 295: 868–872.
34. Liu WL, Shipley MT (1994) Intrabulbar associational system in the rat olfactory bulb comprises cholecystokinin-containing tufted cells that synapse onto the dendrites of GABAergic granule cells. J Comp Neurol 346: 541–558.
35. Nagayama S, Takahashi YK, Yoshihara Y, Mori K (2004) Mitral and tufted cells differ in the decoding manner of odor maps in the rat olfactory bulb. J Neurophysiol 91: 2532–2540.
36. Laurent G (1999) A systems perspective on early olfactory coding. Science 286: 723–

728.

37. Heinbockel T, Hamilton KA, Ennis M (2007) Group I metabotropic glutamate receptors are differentially expressed by two populations of olfactory bulb granule cells. J Neurophysiol 97: 3136–3141.

38. Komiyama T, Luo L (2006) Development of wiring specificity in the olfactory system. Curr Opin Neurobiol 16: 67–73.

39. Valcanis H, Tan SS (2003) Layer specification of transplanted interneurons in developing mouse neocortex. J Neurosci 23: 5113–5122.

40. McConnell SK (1995) Constructing the cerebral cortex: neurogenesis and fate determination. Neuron 15: 761–768.

41. Levitt P (2004) Neuroscience. Sealing cortical cell fate. Science 303: 48–49.

42. Flames N, Marin O (2005) Developmental mechanisms underlying the generation of cortical interneuron diversity. Neuron 46: 377–381.

43. Angevine JB Jr, Sidman RL (1961) Autoradiographic study of cell migration during histogenesis of cerebral cortex in the mouse. Nature 192: 766–768.

44. De Marchis S, Bovetti S, Carletti B, Hsieh YC, Garzotto D, et al. (2007) Generation of distinct types of periglomerular olfactory bulb interneurons during development and in adult mice: implication for intrinsic properties of the subventricular zone progenitor population. J Neurosci 27: 657–664.

45. Kohwi M, Petryniak MA, Long JE, Ekker M, Obata K, et al. (2007) A subpopulation of olfactory bulb GABAergic interneurons is derived from Emx1- and Dlx5/6-expressing progenitors. J Neurosci 27: 6878–6891.

46. Kohwi M, Osumi N, Rubenstein JL, Alvarez-Buylla A (2005) Pax6 is required for making specific subpopulations of granule and periglomerular neurons in the olfactory bulb. J Neurosci 25: 6997–7003.

47. Hack MA, Saghatelyan A, de Chevigny A, Pfeifer A, Ashery-Padan R, et al. (2005) Neuronal fate determinants of adult olfactory bulb neurogenesis. Nat Neurosci 8: 865–872.

48. Merkle FT, Mirzadeh Z, Alvarez-Buylla A (2007) Mosaic organization of neural stem cells in the adult brain. Science 317: 381–384.

49. Mallamaci A, Stoykova A (2006) Gene networks controlling early cerebral cortex arealization. Eur J Neurosci 23: 847–856.

50. Rakic P (1988) Specification of cerebral cortical areas. Science 241: 170–176.

51. Lindvall O, Kokaia Z, Martinez-Serrano A (2004) Stem cell therapy for human neurodegenerative disorders-how to make it work. Nat Med 10(Supp)l): S42–S50.

52. Lie DC, Song H, Colamarino SA, Ming GL, Gage FH (2004) Neurogenesis in the adult brain: new strategies for central nervous system diseases. Annu Rev Pharmacol Toxicol 44: 399–421.

53. Corotto FS, Henegar JA, Maruniak JA (1993) Neurogenesis persists in the subependymal layer of the adult mouse brain. Neurosci Lett 149: 111–114.

Figure1

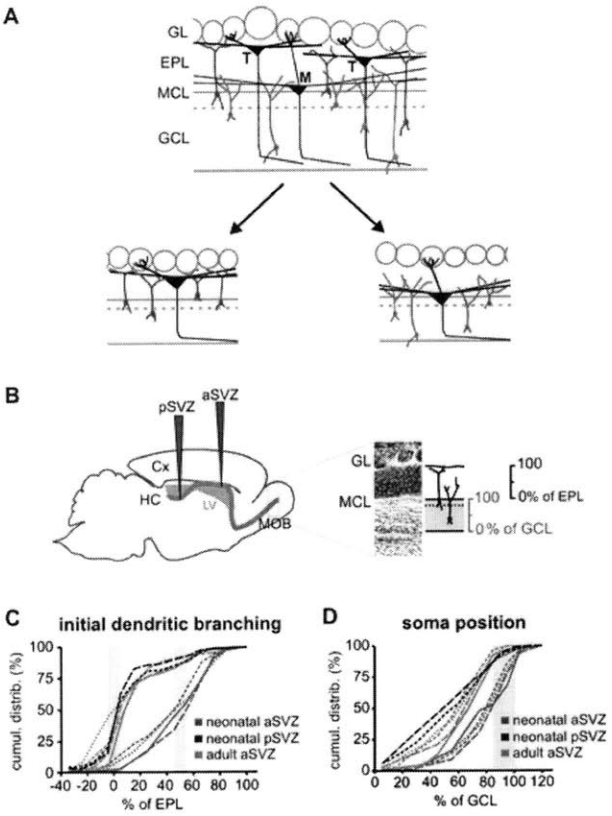

Figure 1. Distinct Precursors Gave Rise to Separate Populations of GCs with Initial Branching of the Apical Dendrite in Different Laminae of the EPL

(A) GCs extend apical dendrites towards the EPL where they form synapses with the dendrites of mitral (M) and tufted (T) cells. The dendrites of one subpopulation of GCs (blue) initially branch near the MCL, whereas the dendrites of the other population of GCs (red) first branch in the superficial lamina of the EPL. Mitral cells (M) extend their lateral dendrites in the deep lamina of the EPL, whereas (middle) tufted cells (T) soma are located in the superficial lamina of the EPL, and extend their dendrites in the superficial EPL. GL, glomerular layer.

(B) Sites for labeling of GC precursors in the aSVZ and pSVZ with a retroviral vector expressing GFP. For quantification of the position of the soma and of the initial branching of the apical dendrite, the GCL and the EPL were divided in percentages, with 0% being the deep and 100% being the superficial border.

(C) Cumulative distribution of initial branching points of the GC apical dendrite. A total of 50% of GCs originating in the anterior aSVZ of neonatal animals initially branched after passing 50% through the EPL. In contrast, over half the GCs derived from the pSVZ of neonatal animals, and GCs derived from the adult aSVZ, branched before they have projected through 10% of the EPL. Different time points were analyzed for aSVZ at 14 (dotted line [···]), 28 (short-dashed line [- - -]), 56 (long-dashed line [– – –]), and 112 d.p.i. (solid line [—]), and for pSVZ at 35 (short-dashed line [- - -]) and 63 d.p.i. (long-dashed line [– – –]).

(D) Cumulative distribution of the soma position in the GCL of GCs generated from the different SVZ precursor populations shown in (C). Same labeling as in (C).

Figure 2

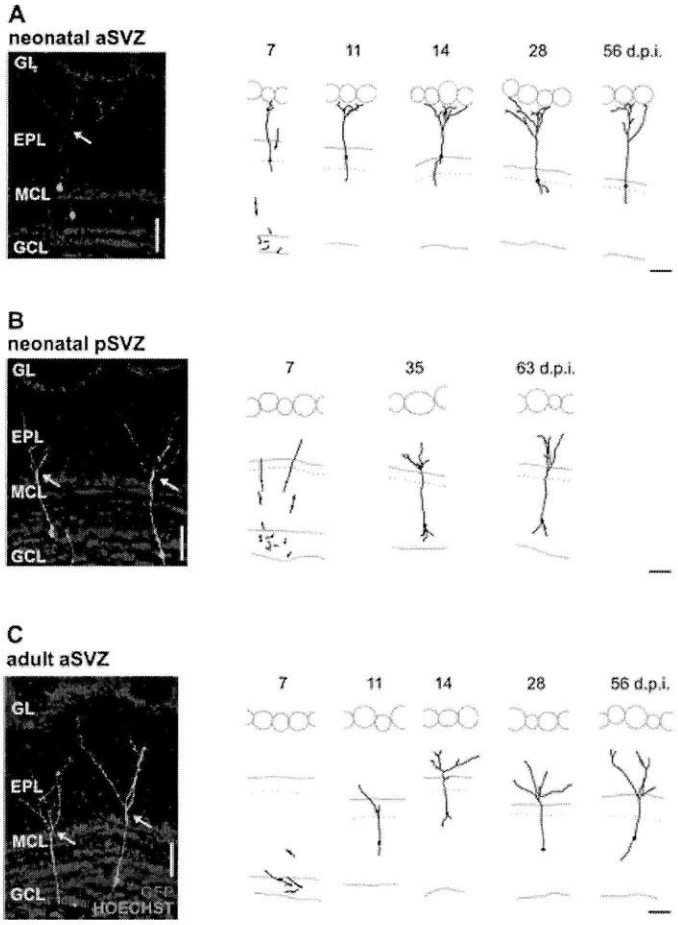

Figure 2. GC Reconstructions Revealed Lamina-Specific Dendritic Targeting

(A) Different types of GCs were generated from distinct precursors in the SVZ labeled with a GFP (green) expressing retrovirus. Hoechst 33258 (blue) revealed the anatomical layers. Precursors infected in the aSVZ of neonatal rats gave rise to GCs whose first dendritic branching point (arrow) was in the superficial EPL.

(B) Infection of precursors in the pSVZ of neonatal rats generated GCs whose first dendritic branching point was the deep EPL (arrow).

(C) Precursors that were infected in the aSVZ of adult rats generated GCs with apical dendrites that branched in the deep layers of the EPL (arrow).

The morphological characteristics of newly generated GCs were established soon after their differentiation and maintained throughout maturity. Time course of GC maturation in the olfactory bulb for precursors from neonatal aSVZ (A), neonatal pSVZ (B), and adult aSVZ (C) at different time points (in d.p.i.) is shown. All bars indicate 100 μm.

Figure 3

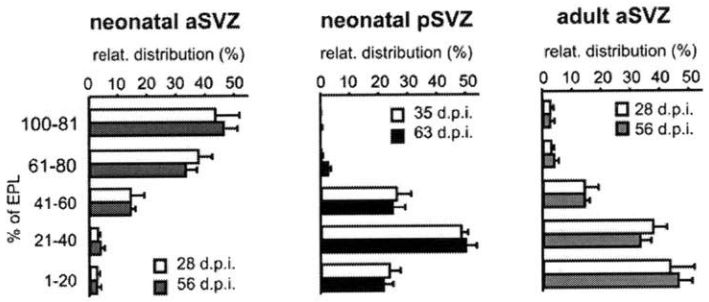

Figure 3. GC Spines in the EPL Were Confined to a Specific Lamina

The relative distribution of spines for GCs generated in newborn animals (that were reconstructed in Figure 2.) is plotted at different time points (in d.p.i.). Precursors in neonatal animals from the aSVZ gave rise to GCs with spines confined to the superficial lamina of the EPL, whereas those from the neonatal pSVZ and adult aSVZ gave rise to GCs with spines in the deep lamina.

Figure 4

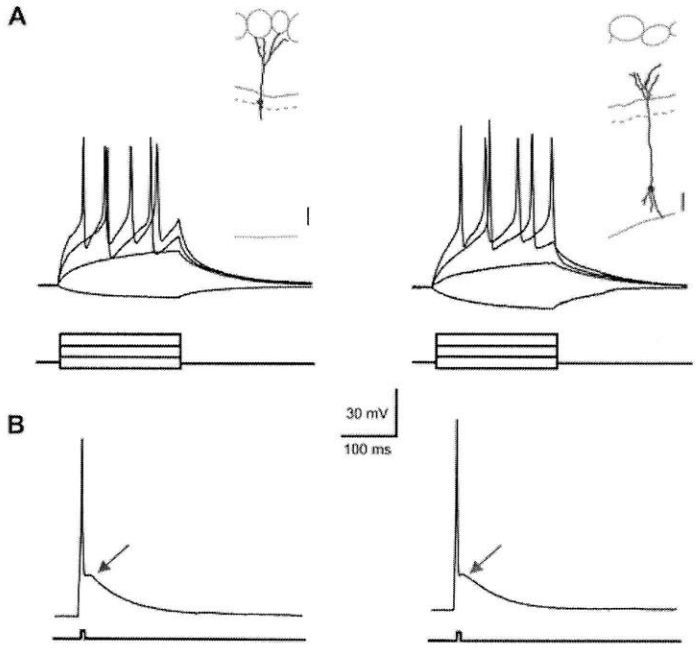

C

	τ_m(ms)	C_m(pF)	R_{IN}(MΩ)	V_{Rest}(mV)	AP_T(mV)	ISI dev(ms)	I_A
Sup. GCs (n= 9)	41.2 ± 3.8	14.9 ± 0.9	735.0 ± 111	-68.8 ± 1.9	-28.0 ± 1.0	43.7 ± 2.1	9/9
Deep GCs (n= 7)	49.4 ± 6.9	24.2 ± 1.7 *	663.5 ± 78	-66.6 ± 2.6	-27.5 ± 1.14	49.4 ± 6.9	7/7

Figure 4. Deep and Superficial Dendritic Targeting GCs Intrinsic Somatic Electrical Properties

(A) Targeted whole-cell recordings of GFP^+ GCs (labeled either in the neonatal aSVZ or pSVZ) were performed (21–23 d.p.i.) and reconstructed after recordings. Both superficial (left panel) and deep (right panel) targeting GCs had a delayed firing pattern (200-ms current injection in 0.1-nA increments).
(B) Both superficial (left panel) and deep (right panel) targeting GCs displayed an afterdepolarization current following a single spike (5-ms current injection in 0.4-nA increments).
(C) The table summarizes passive and active membrane properties determined from superficial and deep targeting GCs. All determined parameters except membrane capacitance were similar for GCs with either deep or superficial dendritic targeting. τ_m is the membrane constant in milliseconds, C_m the membrane capacitance in picofarads, R_{IN} the input resistance in megaohms, V_{rest} the resting membrane potential in millivolts, AP_T the action potential threshold in millivolts, ISI, the interspike interval in millivolts, and I_A is the I_A current.

Figure 5

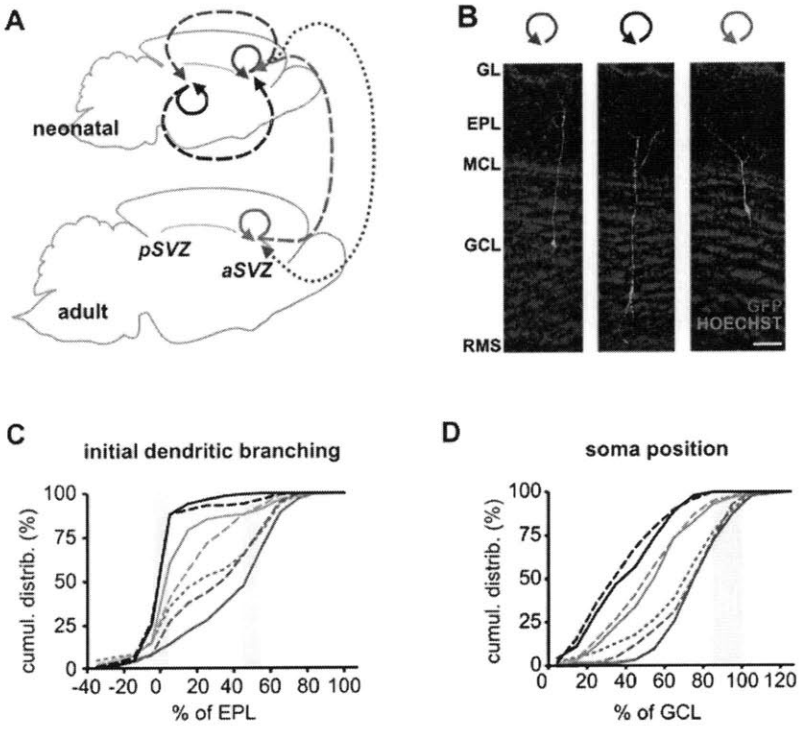

Figure 5. Transplantations of Distinct SVZ Regions Revealed Determination of Initial Dendritic Branching Patterns of GCs in Their Precursors

(A) The diagram shows the different transplantation conditions from aSVZ and pSVZ donor tissue of neonatal and adult animals.

(B) GCs detected 35 d post-transplantation after isochronic, isotopic transplantation of aSVZ of neonatal GFP^+ rats to neonatal host aSVZ (left), pSVZ of neonatal GFP^+ rats to neonatal host pSVZ (middle), and aSVZ of adult GFP^+ rats to adult host aSVZ (right). The bar indicates 100 μm.

(C) Cumulative distribution of initial branching point of the apical dendrite in the EPL of GCs generated from transplanted SVZ regions as described in (A) (same labeling as in [A] for the different transplantation conditions).

(D) Cumulative distribution of the soma position in the GCL of GCs generated from transplantations shown in (C).

Figure 6

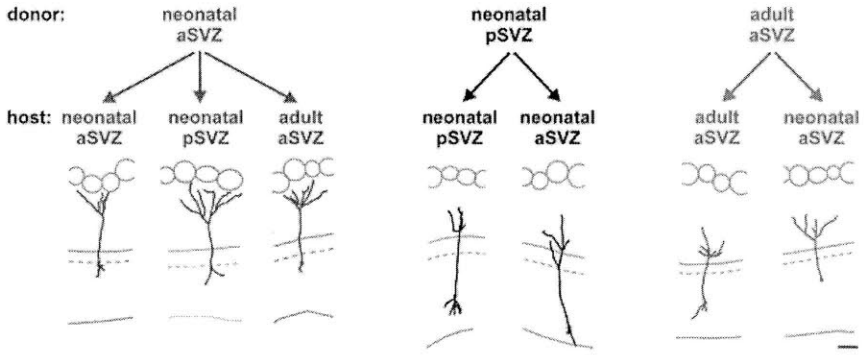

Figure 6. Reconstructions of Transplanted GCs Revealed That They Maintained Their Lamina-Specific Dendritic Targeting after Transplantation

GC reconstructions revealed that the new GCs maintained their lamina-specific dendritic targeting after the different transplantation conditions indicated. The bar indicates 100 μm.

Figure 7

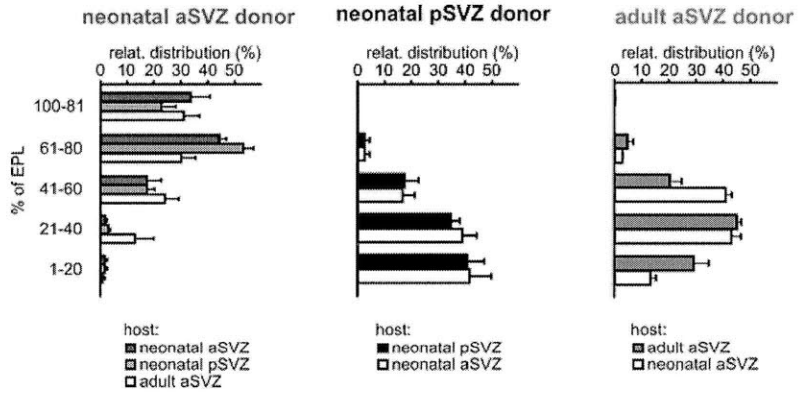

Figure 7. Lamina-Specific Distribution of GC Spines in the EPL Is Maintained after Transplantation

Relative distribution of GC spines in the EPL from aSVZ or pSVZ of neonatal, and aSVZ of adult donors (for the neurons reconstructed in Figure 6.).

Chapter Three

Sequential Development of Synapses in Dendritic Domains during Adult Neurogenesis

Wolfgang Kelsch[*,†], Chia-Wei Lin[*,†], and Carlos Lois[*,†,‡,§]

[*] *Picower Institute for Learning and Memory, Massachusetts Institute of Technology, Cambridge, Massachusetts, United States of America,*

[†] *Department of Brain and Cognitive Sciences, Massachusetts Institute of Technology, Cambridge, Massachusetts, United States of America,*

[‡] *Department of Biology, Massachusetts Institute of Technology, Cambridge, Massachusetts, United States of America*

This paper was published in Proc Natl Acad Sci U S A. 2008 Oct 28;105(43):16803-8

Note: I used whole-cell patch clamp recordings in combination with focal electrical stimulation to study the properties of synaptic inputs of GCs. I found that kinetics of synaptic receptors varied according to dendritic locations. The synapses in the proximal and basal dendrites contain fast-decaying AMPARs whereas those in the distal dendrites contain AMPAR-like receptors with slow decaying kinetics. This implies that GCs might have compartmentalized expression of synaptic receptors of different classes. The result was presented in **supplementary Figure 1**.

Abstract

During the process of integration into brain circuits, new neurons develop both input and output synapses with their appropriate targets. The vast majority of neurons in the mammalian brain is generated before birth and integrate into immature circuits while these are being assembled. In contrast, adult-generated neurons face an additional challenge as they integrate into a mature, fully functional circuit. Here, we examined

how synapses of a single neuronal type, the granule cell in the olfactory bulb, develop during their integration into the immature circuit of the newborn and the fully mature circuit of the adult rat. We used a genetic method to label pre and postsynaptic sites in granule neurons and observed a stereotypical development of synapses in specific dendritic domains. In adult-generated neurons, synapses appeared sequentially in different dendritic domains with glutamatergic input synapses that developed first at the proximal dendritic domain, followed several days later by the development of input-output synapses in the distal domain and additional input synapses in the basal domain. In contrast, for neurons generated in neonatal animals, input and input-output synapses appeared simultaneously in the proximal and distal domains, respectively, followed by the later appearance of input synapses to the basal domain. The sequential formation of synapses in adult-born neurons, with input synapses appearing before output synapses, may represent a cellular mechanism to minimize the disruption caused by the integration of new neurons into a mature circuit in the adult brain.

Introduction

Integration of new neurons continues throughout life in the adult mammalian olfactory bulb (OB) (1, 2). During the process of integration into brain circuits, new neurons develop both input and output synapses with their appropriate targets. Whereas the majority of neurons in the olfactory bulb integrate into an immature circuit while it is being assembled, neurons generated in adulthood face an additional challenge as they integrate into a mature, fully functional circuit. In particular, the formation of synapses by a new neuron in a functioning circuit may interfere with circuit operation and, thus, it could result in maladaptive behaviors.

Additionally, it is still not known whether new neurons integrating into the neonatal and adult olfactory system have the same or different functions in the circuit and, therefore, adult- and neonatal-generated neurons could employ different modes of integration. To compare how new neurons are added to neonatal and adult circuits, we examined the pattern of synapse development of a single neuronal type, the granule cell (GC) in the olfactory bulb, during its integration into the immature circuit of the newborn and the mature circuit of the adult rat.

The majority of neurons added to the OB of adult rats are GC neurons. GCs are axonless inhibitory interneurons that have both a basal dendrite and an apical dendrite (Fig. 1A). The apical dendrite can be divided into an unbranched segment emerging from the soma followed by a branched segment (distal domain). The basal dendrite (basal domain) and unbranched apical dendrite receive axo-dendritic glutamatergic input from axon collaterals of the OB's projection neurons and from the olfactory cortices (3–6). The distal domain of the apical dendrite has bidirectional dendro-dendritic synapses present in spines where input and output synapses are colocalized and functionally coupled. These bidirectional synapses receive glutamatergic input synapses from the lateral dendrites of the OB's projection neurons and release GABA back onto these projection neurons (7). These dendro-dendritic synapses in the distal domain are the exclusive output of GCs, and are responsible for local inhibition of the projection neurons in the olfactory bulb (7–9). Activation of axo-dendritic input sites in the basal domain and the unbranched apical dendrite is thought to globally excite the GCs, thus facilitating recurrent dendro-dendritic inhibition in the distal domain (8, 9).

To visualize the development and distribution of input and output synaptic sites in entire GCs, we labeled their progenitors with genetic markers localized specifically to synapses. To

visualize glutamatergic input synapses, we expressed a PSD-95:GFP fusion protein. PSD-95 is a scaffolding protein that localizes to the postsynaptic density of glutamatergic synapses (10) and has been extensively used as a postsynaptic marker of glutamatergic synapses (11–14). PSD-95 is present in virtually all GC glutamatergic synapses, where it is restricted to clusters in the postsynaptic density (15), is already highly expressed at birth (16), and appears early during assembly of the postsynaptic density (15). To label presynaptic synapses (output synapses), we used a synaptophysin:GFP fusion protein. Synaptophysin:GFP was the first synaptic vesicle protein to be cloned and has been extensively used to study the distribution and density of presynaptic sites in neurons both in vitro and in vivo (17–22).

We labeled progenitors for GC neurons with these genetic markers to visualize their synapse development, and observed that in adult-generated neurons, PSD-95:GFP-positive clusters (PSD^+C) developed initially at high density in the proximal 15% of the unbranched apical dendrite. We therefore defined the proximal 15% of the unbranched apical dendrite as the proximal domain. In contrast, PSD^+Cs in the basal domain only developed later together with PSD^+Cs in the distal domain. The late development of PSD^+Cs in the distal domain was tightly coupled to the development of output synapses as labeled by synaptophysin:GFP^+ clusters (Syp^+C) in the same domain. In contrast, neonatal-generated GCs developed PSD^+Cs and Syp^+Cs in the distal domain simultaneously to PSD^+Cs in the proximal and before those in the basal domain. These observations revealed that new GCs in an adult brain environment follow a pattern of integration that differs from that during the initial circuit assembly when most GCs are generated. The sequential formation of synapses in adult-born neurons, with proximal input synapses appearing before output synapses, may represent a cellular

adaptation to minimize the disruption caused by the integration of new neurons into a functioning circuit.

Results

Development of Glutamatergic Synaptic Input Sites.

The aim of the present study was to examine the development of glutamatergic input and inhibitory output synapses of new GCs in the OB of newborn and adult animals. In some types of neurons, glutamatergic synaptic input is exclusively found in dendritic spines (23). However, spine counting was not appropriate to determine the distribution of glutamatergic synapses in GCs as their spines are frequently branched (Fig. 1B) (24), and some of their glutamatergic synapses are directly located in the dendritic shaft, not associated with spines (24). To visualize the development and distribution of glutamatergic synapses we genetically labeled postsynaptic densities with a GFP-tagged PSD-95 construct (PSD-95:GFP).

We first determined whether PSD-95:GFP delivered to progenitor cells with retroviruses was an appropriate method to label for postsynaptic sites. Indeed, PSD-95:GFP-positive clusters ($PSD^{+}Cs$) were restricted to synapses and overlapped with endogenous PSD-95 expression (supporting information (SI) Fig. S1 C and D). In addition, retroviral expression of PSD-95:GFP did not change the strength and number of glutamatergic synapses in cultured neurons (SI Text, Fig. S1 E–G).

All dendritic domains of GCs born in adulthood (including the basal, proximal and distal domain) received functional glutamatergic synaptic input (SI Text, Fig. S1 A and B) (4, 25), and distal glutamatergic input synapses are colocalized with GABAergic output synapses in

the distal domain with a 1:1 stoichiometry (7, 24, 26). $PSD^{+}Cs$ in GCs were in tight apposition to the presynaptic marker bassoon in vivo (Fig. 1C), indicating that $PSD^{+}Cs$ indeed revealed postsynaptic sites of synapses. To attribute $PSD^{+}Cs$ to a particular GC, we took advantage of the presence of low levels of diffuse PSD-95:GFP protein in the cytoplasm not detectable by its endogenous fluorescence (Fig. 1D). This diffuse PSD-95:GFP protein could be visualized by amplifying its signal with antibodies raised against GFP (coupled to a red fluorophore to distinguish it from the intrinsic green fluorescence of $PSD^{+}Cs$) and allowed us to attribute $PSD^{+}Cs$ to a dendritic arbor belonging to a particular GC.

In adult animals, almost no $PSD^{+}Cs$ were detected at 10 days post infection (d.p.i.) when most GCs had just completed their migration and started to extend their dendritic arbors (Fig. 2A). $PSD^{+}Cs$ started to appear in the proximal dendritic domain ≈14 d.p.i. after the initial formation of the dendritic tree (Fig. 2B). These $PSD^{+}Cs$ at the proximal domain reached their final density at 17 d.p.i., when few $PSD^{+}Cs$ had appeared at the basal or distal domains. At the basal and distal domains $PSD^{+}Cs$ reached their final density only at a later time point (28 d.p.i.; Fig. 2B). We quantified the density of $PSD^{+}Cs$ in the different dendritic domains of new GCs (Fig. 3A) and observed that $PSD^{+}Cs$ at the proximal domain indeed developed first, followed by $PSD^{+}Cs$ at the basal and distal domains (for statistical analysis see SI Text). The $PSD^{+}Cs$ first detected at 14 d.p.i. are likely to represent true synapses, as these $PSD^{+}Cs$ were contacted by the presynaptic marker bassoon (Fig. S2C). In 94% of our GC sample (n = 151), the density of $PSD^{+}Cs$ in the proximal domain was several fold higher than the density in the entire unbranched apical dendrite throughout maturation (Fig. 3A). Maturation of synapses over time was paralleled by an increase in the mean fluorescent area of $PSD^{+}Cs$ (Fig. S2B). Four weeks after the birth of the new neurons, the density of $PSD^{+}Cs$ stabilized and revealed

no significant changes in the dendritic domains between 28 and 56 d.p.i. We did not quantify PSD^+Cs at the soma as their presence and density was highly variable (data not shown).

Whereas adult-generated GCs integrate into a mature, functioning circuit, GCs generated in the neonatal period integrate into a circuit that is still developing. To investigate whether the appearance of synapses in new GCs differs between neonatal and adult animals, we examined the development of PSD^+Cs in neonatal-generated GCs (Figs. 2C and 3C). PSD^+Cs appeared in neonatal-generated GCs ≈10–14 d.p.i., after they had extended their dendritic arbors. In contrast to the situation described for adult neurogenesis, neonatal-generated GCs acquired glutamatergic synapses simultaneously in the proximal and distal domains of their apical dendrite followed by later development of glutamatergic synapses to the basal domain (Figs. 2C and 3C; for statistical analysis see SI Text).

The distal dendritic domain of GCs can either branch deep and superficial in the external plexiform layer where GCs then contact different types of projection neurons (7, 27). However, the sequential development of PSD^+Cs was the same for deep and superficial GCs in adult-born neurons (SI Text, Fig. 3 vs. Fig. S2). Similarly, we observed that both deep and superficial GCs generated in newborn animals had a synchronous synaptic development of proximal axo-dendritic and distal dendro-dendritic input (SI Text, Fig. 3 vs. Fig. S2).

In summary, in adult-generated GCs, the proximal axo-dendritic input domain developed first, and was followed by the appearance of PSD^+Cs in the distal dendro-dendritic and basal domains (Fig. 3B). In contrast, GCs generated in the neonatal period developed PSD^+Cs first in their proximal and distal domains (Fig. 3D), and later in the basal domain.

Development of Synaptic Output Sites in New GCs.

We wondered whether the delayed development of PSD^+Cs in the distal domain of adult generated GCs compared with those generated in the neonatal period was paralleled by a delayed development of the distal output synapses. Ultrastructural studies of dendro-dendritic synapses of GCs have revealed that the glutamatergic input synapses and GABAergic output synapses exist in tight spatial coupling with a 1:1 stoichiometry in spines of the distal domain (26). During embryonic development, the mitral-to-GC input synapse develops first, followed within a day by the GC-to-mitral cell output synapse (26). We investigated the development of the presynaptic output sites in GCs by using synaptophysin:GFP as a genetic marker for the presynaptic vesicle release machinery. The only output synapses of GCs are located in their dendro-dendritic synapses and, as expected, synaptophysin:GFP positive clusters (Syp^+Cs) were only found in the distal domain of GCs (Fig. 4 and Fig. S3C).

To examine the development of output synapses in GCs we used retroviruses encoding synaptophysin:GFP and followed the procedures described for PSD^+Cs. We observed that the development of Syp^+Cs in the distal domain was delayed in adult-generated GCs when compared with neonatal-generated GCs (compare Fig. 4 A and D). Similar to our observations for the development of PSD^+Cs in the distal domain of adult-generated GCs (compare Fig. 3A), we observed that Syp^+Cs in the distal domain were sparse at 17 d.p.i. and reached their final density only at 28 d.p.i. (Fig. 4B, for statistical analysis see SI Text). In contrast, neonatal-generated GCs developed Syp^+Cs in the distal domain from early on (14 d.p.i.) (Fig. 4E) as described above for PSD^+Cs (compare Fig. 3C, for statistical analysis, see SI Text). This observation was independent of whether GCs had deep or superficial dendrites

(SI Text; Fig. S3).

In summary, the development of $Syp^{+}Cs$, as markers for presynaptic output sites, closely paralleled the maturation of $PSD^{+}Cs$ as markers of postsynaptic input sites in the distal domain (compare Fig. 3 B and D to Fig. 4 C and F). These observations reveal that the development of dendro-dendritic synapses is delayed compared with the input synapses at the proximal domain of adult-generated GCs, but not in neonatal-generated GCs.

Discussion

We observed that adult-generated GCs in the mammalian OB develop their presynaptic and postsynaptic sites sequentially in different dendritic domains. In particular, comparing the proximal dendritic domain to the distal domain revealed significant differences in the appearance of synapses. The development of glutamatergic synaptic sites at the proximal domain preceded the development of dendro-dendritic input and output synapses in the distal domain by several days. This observation suggests that adult-generated neurons integrate into the olfactory circuits by first developing input synapses that can control their global excitation before developing distal input-output synapses that mediate recurrent inhibition within the bulb, that is, the new neurons "listen" before they "speak."

A recent study on murine adult-generated GCs based on immunocytochemical staining also suggested a delayed development of the distal dendritic domain (28). However, this study did not provide any quantification of the dynamics of synaptic maturation and did not detect any special pattern of synaptic development in the proximal domain. Our method, based on genetic labeling of presynaptic and postsynaptic sites, allowed us both to quantify the

dynamics of synaptic maturation in complete cells and to measure the density of synaptic sites. Our measurements reveal a unidentified pattern of synapse development in adult-born neurons, with a low density of synapses in the basal and distal domains at a time when the proximal domain already contains a high density of input synapses.

Different Properties of Adult- and Neonatal-generated Neurons.

All dendritic domains of GCs receive input synapses that are glutamatergic and therefore excitatory, while the output synapses are GABAergic and therefore inhibitory. The basal and proximal domain receive axo-dendritic glutamatergic input whereas the distal domain receives dendro-dendritic glutamatergic input and releases GABA with its recurrent output synapse (see also above). Axo-dendritic input synapses originating either from axon collaterals of OB's projection neurons or from centrifugal projections of the olfactory cortex (5, 29) were first formed on the proximal domain of GCs born in adulthood. Axo-dendritic input can evoke action potentials (8, 9) that then spread throughout dendrites to cause Ca^{2+} influx in the spines of GCs (30). This global excitation can then facilitate the release of GABA at the dendro-dendritic synapses in the distal domain, thus mediating inhibition of the OB projection neurons (8, 9). This latter consequence, however, only happens after the dendro-dendritic synapses of the GCs' distal domain are in place and thus enable the new neurons to shape odor discrimination (31). This order, in which the axo-dendritic synapses on the proximal domain are formed first, followed by formation of the dendro-dendritic synapses in the distal domain, ensures that control of global excitation precedes the origination of the inhibitory synaptic output signals that constitute the main task of the OB's GCs. The sequential acquisition of proximal axo-dendritic input, before the dendro-dendritic input and output, could provide a unique form of plasticity for adult-generated GCs, not

present during initial circuit assembly. In line with the different timing in the appearance of axo-dendritic input in the proximal domain compared with the distal dendro-dendritic synapses, adult- and neonatal-generated neurons also differ in the time course in which they start generating action potentials. Neonatal-generated neurons can fire fast action potentials around the time when they finish migrating whereas most adult-generated GCs only develop the ability to spike two weeks after they are born (our unpublished observations in rats) (32) at the time when proximal synapses develop, but before distal synapses emerge. Thus, in adult-generated neurons, the input to the proximal domain, which appears around the time when the neuron gained the ability to fire action potentials, could control the global activity of the new neuron before its dendro-dendritic input-output synapses mature in the distal domain. This observation suggests that adult-generated GCs may integrate silently in the circuit as they will only develop output synapses after they acquired many other functions, like their proximal input synapses and the ability to spike. In contrast, input synapses, as well as the ability to spike, appeared simultaneously to output synapses in neonatal-generated GCs, suggesting that no 'silent' mode of integration is required. It is interesting to note that for neurons born both in neonatal and adult animals, axo-dendritic glutamatergic synapses developed in all cases in two steps, first in the proximal and later in the basal domain. The development of axo-dendritic input in two steps may provide additional excitatory drive to tune their activity. Future studies will reveal whether basal and proximal axo-dendritic input comes from different sources (e.g., centrifugal cortical projections vs. local axon collaterals from OB's projection neurons) and serves different functions.

In addition, the timing of the appearance of glutamatergic input into the proximal dendritic domain could be important to regulate both the integration and survival of new neurons into

the circuits of the olfactory bulb. Whereas most of the postmigratory new neurons added into the bulb of newborns survive (33), only half of these neurons generated in the adult stably integrate and survive (33, 34). Interestingly, the peak of adult-generated GC death (33, 34) occurs between the time when glutamatergic synapses first appear in the proximal domain and when these new neurons reach their final density of distal input-output synapses. The main period of cell death thus precedes the development of output synapses in adult-generated neurons. This again suggests that the initial steps of integration of adult-generated neurons into the circuit occur "silently" before output synapses have appeared. Thus, neonatal- and adult-generated GCs use different strategies for their integration into the olfactory circuit. Additionally, these different strategies of integration could satisfy the demands of olfactory processing which change from neonatal to adult life (35).

Influence of Brain Maturation on Synapse Formation by New Neurons.

The different patterns of synapse development in neonatal- and adult-generated neurons could either be because of different intrinsic properties of the new neurons or to differences in the maturation of the brain circuit into which the new neurons integrate. It is possible that postnatal changes in the structure or function of axon terminals ending at GCs may result in different patterns of synaptic appearance in new GCs, and thus, could explain why axo-dendritic input does not develop before distal dendro-dendritic synapses in neonatal-generated GCs. However, axon terminals from the olfactory cortex ending at the GCs are already functional one week after birth (4, 36), thus preceding the maturation of the neonatal-generated GCs that we studied. In addition, excitatory synapses in the proximal domain preceded those formed on the basal domain even though these two domains both receive axo-dendritic inputs. This observation again suggests that the sequential acquisition of axo-

dendritic input to specific dendritic domains in newly generated GCs cannot be solely explained by the maturational state of the brain. Future experiments exposing new GCs generated in newborn and adult animals to different environments by heterochronic transplantation might elucidate the respective contributions of brain maturation and cell-intrinsic properties for the specific patterns of synaptic development.

Minimizing the Disruption of Brain Function Caused by the Integration of New Neurons in Sequential Steps.

Sequential development of synapses in adult-generated GCs may represent a cellular mechanism to minimize the potential disruption caused by the integration of new neurons into a functioning circuit. Whereas the proximal axo-dendritic input is thought to control the global excitability of GCs, the distal domain contains the only output synapses of these neurons. Thus, the pattern of sequential synaptic development in the adult olfactory bulb may allow control of the new neuron's activity before it can influence the performance of other cells. Interestingly, adult neurogenesis also occurs in motor systems (37). Sequential "silent" integration of new neurons followed by output activation could provide a mechanism by which the brain can recruit new neurons with minimal disruption of existing functions. The sequential incorporation of afferent control and synaptic output could be a key component of successful neuronal integration during adulthood. If our interpretation is correct, then this input-output relation may have to be approached carefully when using neuronal replacement to treat neurological disorders.

Materials and Methods

Generation of Retroviral Vectors. We replaced the ubiquitin-C promoter region of FUGW, a self-inactivating lentiviral vector derived from HIV-1, with a regulatory sequence −570 to −93 bp from the transcription start site of the human synapsin gene to produce a construct called HsynGW. The cDNA of PSD-95:GFP was a fusion protein with GFP at the C terminus (38). PSD-95:GFP was amplified by PCR and inserted into HsynGW replacing GFP (called HsynPSD95g). Recombinant HsynPSD95g virus was prepared and stored as described (39). To visualize spine morphology we used an oncoretroviral vector derived from Moloney Leukemia virus with an internal promoter derived from the LTR from the Rous Sarcoma Virus (RSV) driving palmitoylated GFP (called MRSVPalmG). To visualize glutamatergic postsynaptic clusters or presynaptic release sites, we generated a vector called MRSVPSD95g or MRSVSypg by replacing the palmitoylated GFP from MRSVPalmG with the ORF of PSD95:GFP or Synaptophysin:GFP, respectively.

Stereotaxic Injections. All animal procedures were approved by the local Animal Welfare Committee. Stereotactic injections of retroviral vectors were performed into the subventricular zone of SD rats of either sex (Charles River) (for details see SI Text).

Tissue Processing and Immunohistochemistry. For each time point after viral infection, three rats were given an overdose of ketamine/xylazine and perfused transcardially with PBS at 37°C for 30 s followed by 3 min of 3% PFA. Fifty-μm thick coronal slices were cut and incubated in primary rabbit anti-GFP (1:4.000, Chemicon) or anti-bassoon (1:750) antibodies at 4°C overnight, and Alexa-555 secondary antibodies (1:750, Molecular Probes) diluted in blocking for 2 h at RT.

Confocal Microscopy. Confocal image stacks were acquired by using an Olympus Fluoview

confocal microscope (60× oil-immersion lens (NA, 1.4), Olympus) (pixel size, 0.23 × 0.23 μm), and with z-step 0.25 μm. A typical image stack consisted of approx. 80–150 image planes each of 1024 × 1024 pixels. For each stack, laser intensity and detector sensitivity were set to the same values determined in initial experiments.

Image Processing and Quantification. After acquisition, maximal intensity projections were prepared for each image stack by using the MetaMorph analysis software (Universal Imaging). No filtering was generally necessary. For the projection images the threshold was set so that any possible diffuse GFP fluorescence at the dendritic shaft was below this threshold. The number of PSD-95:GFP$^+$ clusters (PSD$^+$C) in a region of interest was counted by using the integrated morphometry analysis function of the MetaMorph software. The length of the respective segment of the dendritic arbor was then measured and the density of PSD$^+$Cs was determined. All datasets were manually supervised to prevent the inclusion of unspecific green fluorescence. The total number of PSD$^+$Cs analyzed was 48,657. Dendritic length was not corrected for shrinkage because of tissue processing and 2D projection (estimated error up to 15%). To determine whether the late appearance of PSD$^+$Cs at the basal and distal domains was because of setting a threshold for PSD$^+$Cs, we reanalyzed data with a lower threshold. With a lower threshold, the absolute PSD$^+$C density was slightly higher, but the pattern of PSD$^+$C development persisted (Fig. S4B), and was therefore not because of differences in PSD$^+$Cs area in the respective dendritic domain. Syp$^+$Cs were analyzed with the same procedure as described for PSD$^+$Cs (total number of Syp$^+$Cs analyzed 15,389). Each data point (e.g., superficial dendritic branching, adult-born, basal domain, 14 d.p.i.) contained normally distributed PSD$^+$C densities from 14 cells. The first time point that we examined for statistical analysis was 14 d.p.i. We used a three-way ANOVA followed by

a two-way ANOVA and then tested simple effects by using ANOVA.

Acknowledgments

We thank Timothy Gardner for critically reading the manuscript, Kevin Allen and Alexey Ponomarenko for help with the statistic analysis, and the Sheng lab for helpful suggestions and reagents. This work was supported by the David and Lucille Packard Foundation (C.L.).

References

1. Luskin MB (1993) Restricted proliferation and migration of postnatally generated neurons derived from the forebrain subventricular zone. Neuron 11:173–189.

2. Lois C, Alvarez-Buylla A (1993) Proliferating subventricular zone cells in the adult mammalian forebrain can differentiate into neurons and glia. Proc Natl Acad Sci USA 90:2074–2077.

3. Mori K, Kishi K, Ojima H (1983) Distribution of dendrites of mitral, displaced mitral, tufted, and granule cells in the rabbit olfactory bulb. J Comp Neurol 219:339–355.

4. Balu R, Pressler RT, Strowbridge BW (2007) Multiple modes of synaptic excitation of olfactory bulb granule cells. J Neurosci 27:5621–5632.

5. Luskin MB, Price JL (1983) The topographic organization of associational fibers of the olfactory system in the rat, including centrifugal fibers to the olfactory bulb. J Comp Neurol 216:264–291.

6. Davis BJ, Macrides F (1981) The organization of centrifugal projections from the anterior olfactory nucleus, ventral hippocampal rudiment, and piriform cortex to the main olfactory bulb in the hamster: An autoradiographic study. J Comp Neurol 203:475–493.

7. Mori K (1987) Membrane and synaptic properties of identified neurons in the olfactory bulb. Prog Neurobiol 29:275–320.

8. Chen WR, Xiong W, Shepherd GM (2000) Analysis of relations between NMDA receptors and GABA release at olfactory bulb reciprocal synapses. Neuron 25:625–633.

9. Halabisky B, Strowbridge BW (2003) Gamma-frequency excitatory input to granule cells facilitates dendrodendritic inhibition in the rat olfactory Bulb. J Neurophysiol 90:644–654.

10. Sheng M (2001) Molecular organization of the postsynaptic specialization. Proc Natl Acad Sci USA 98:7058–7061.

11. Niell CM, Meyer MP, Smith SJ (2004) In vivo imaging of synapse formation on a growing dendritic arbor. Nat Neurosci 7:254–260.

12. Ebihara T, Kawabata I, Usui S, Sobue K, Okabe S (2003) Synchronized formation and remodeling of postsynaptic densities: Long-term visualization of hippocampal neurons expressing postsynaptic density proteins tagged with green fluorescent protein. J Neurosci 23:2170–2181.

13. Washbourne P, Bennett JE, McAllister AK (2002) Rapid recruitment of NMDA receptor transport packets to nascent synapses. Nat Neurosci 5:751–759.

14. Gray NW, Weimer RM, Bureau I, Svoboda K (2006) Rapid redistribution of synaptic PSD-95 in the neocortex in vivo. PLoS Biol 4:e370.

15. Sassoe-Pognetto M, et al. (2003) Organization of postsynaptic density proteins and glutamate receptors in axodendritic and dendrodendritic synapses of the rat olfactory bulb. J Comp Neurol 463:237–248.

16. Shu F, et al. (2001) Developmental changes in PSD-95 and Narp mRNAs in the rat olfactory bulb. Brain Res Dev Brain Res 132:91–95.

17. Nakata T, Terada S, Hirokawa N (1998) Visualization of the dynamics of synaptic vesicle and plasma membrane proteins in living axons. J Cell Biol 140:659–674.

18. Pennuto M, Bonanomi D, Benfenati F, Valtorta F (2003) Synaptophysin I controls the targeting of VAMP2/synaptobrevin II to synaptic vesicles. Mol Biol Cell 14:4909–4919.

19. Li Z, Murthy VN (2001) Visualizing postendocytic traffic of synaptic vesicles at hippocampal synapses. Neuron 31:593–605.

20. Kaether C, Skehel P, Dotti CG (2000) Axonal membrane proteins are transported in distinct carriers: A two-color video microscopy study in cultured hippocampal neurons. Mol Biol Cell 11:1213–1224.

21. Meyer MP, Smith SJ (2006) Evidence from in vivo imaging that synaptogenesis guides the growth and branching of axonal arbors by two distinct mechanisms. J Neurosci 26:3604–3614.

22. Valtorta F, Pennuto M, Bonanomi D, Benfenati F (2004) Synaptophysin: Leading actor or walk-on role in synaptic vesicle exocytosis? Bioessays 26:445–453.

23. Nimchinsky EA, Sabatini BL, Svoboda K (2002) Structure and function of dendritic

spines. Annu Rev Physiol 64:313–353.

24. Woolf TB, Shepherd GM, Greer CA (1991) Serial reconstructions of granule cell spines in the mammalian olfactory bulb. Synapse 7:181–192.

25. Schoppa NE (2006) AMPA/kainate receptors drive rapid output and precise synchrony in olfactory bulb granule cells. J Neurosci 26:12996–13006.

26. Hinds JW (1970) Reciprocal and serial dendrodendritic synapses in the glomerular layer of the rat olfactory bulb. Brain Res 17:530–534.

27. Kelsch W, Mosley CP, Lin CW, Lois C (2007) Distinct mammalian precursors are committed to generate neurons with defined dendritic projection patterns. PloS Biol 5:e300.

28. Whitman MC, Greer CA (2007) Synaptic integration of adult-generated olfactory bulb granule cells: Basal axodendritic centrifugal input precedes apical dendrodendritic local circuits. J Neurosci 27:9951–9961.

29. Kishi K, Mori K, Ojima H (1984) Distribution of local axon collaterals of mitral, displaced mitral, and tufted cells in the rabbit olfactory bulb. J Comp Neurol 225:511–526.

30. Egger V, Svoboda K, Mainen ZF (2003) Mechanisms of lateral inhibition in the olfactory bulb: Efficiency and modulation of spike-evoked calcium influx into granule cells. J Neurosci 23:7551–7558.

31. Laurent G (1999) A systems perspective on early olfactory coding. Science 286:723–728.

32. Carleton A, Petreanu LT, Lansford R, Alvarez-Buylla A, Lledo PM (2003) Becoming a new neuron in the adult olfactory bulb. Nat Neurosci 6:507–518.

33. Lemasson M, Saghatelyan A, Olivo-Marin JC, Lledo PM (2005) Neonatal and adult neurogenesis provide two distinct populations of newborn neurons to the mouse olfactory bulb. J Neurosci 25:6816–6825.

34. Petreanu L, Alvarez-Buylla A (2002) Maturation and death of adult-born olfactory bulb granule neurons: Role of olfaction. J Neurosci 22:6106–6113.

35. Moriceau S, Sullivan RM (2006) Maternal presence serves as a switch between learning fear and attraction in infancy. Nat Neurosci 9:1004–1006.

36. Schwob JE, Price JL (1984) The development of lamination of afferent fibers to the olfactory cortex in rats, with additional observations in the adult. J Comp Neurol 223:203–222.

37. Nottebohm F (1989) From bird song to neurogenesis. Sci Am 260:74–79.

38. Hsueh YP, Sheng M (1999) Requirement of N-terminal cysteines of PSD-95 for PSD-95 multimerization and ternary complex formation, but not for binding to potassium channel Kv1.4. J Biol Chem 274:532–536.

39. Lois C, Hong EJ, Pease S, Brown EJ, Baltimore D (2002) Germline transmission and tissue-specific expression of transgenes delivered by lentiviral vectors. Science 295:868–872.

Figure 1

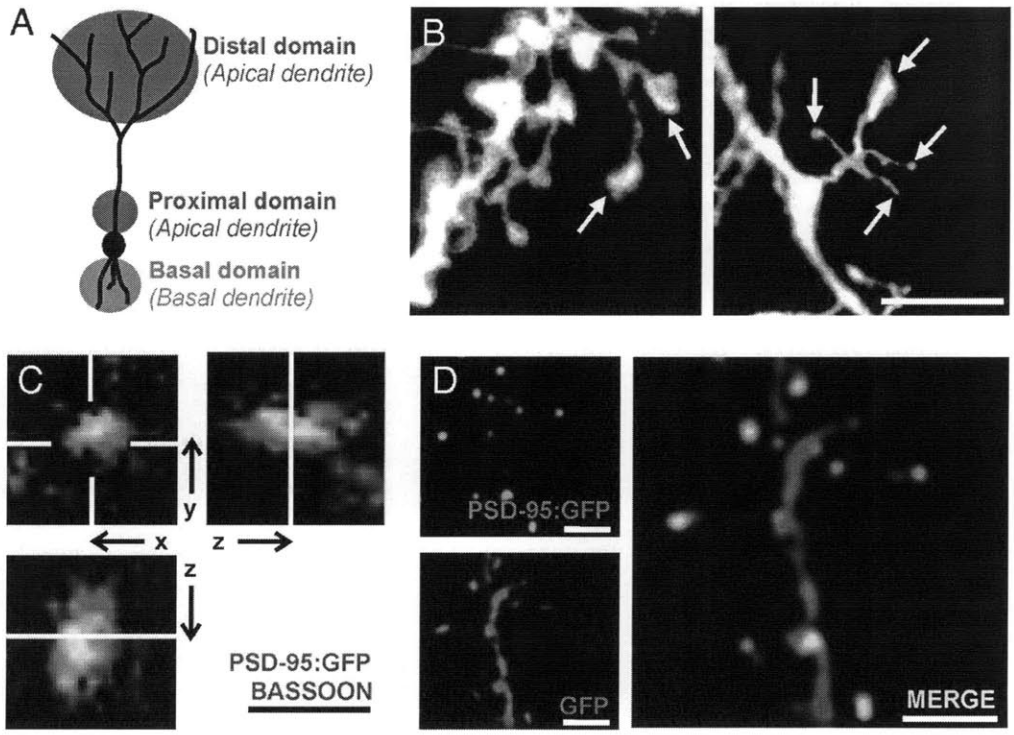

Fig. 1. Glutamatergic input to dendritic domains and PSD-95:GFP positive clusters (PSD^+Cs) in vivo. (A) GCs have different dendritic domains: a basal domain (= basal dendrite) and different domains in the apical dendrite. The apical dendrite divides into an unbranched segment emerging from the soma followed by a more distal branched segment (= distal domain). Because we observed a high density of glutamatergic input synapses in the proximal 15% of the unbranched apical dendrite, we defined it as the proximal domain. (B) Branched spines with several spine heads and filopodia-like protrusions in a GFP labeled adult-generated GC 28 d.p.i. (Scale bar, 5 μm.) (C) Confocal 3D image shows a PSD^+C in a new GC that is contacted by the presynaptic marker, bassoon (bar, 1 μm.) (D) In GCs expressing PSD-95:GFP, PSD^+C could be detected by direct intrinsic fluorescence as green clusters. The dendritic morphology of the GC was revealed by amplification the low levels of PSD-95:GFP in the cytoplasm (that could not be detected by intrinsic fluorescence) with immunofluorescence against GFP (red). The merged images of PSD^+C (intrinsic fluorescence in green) and dendritic morphology (immunofluorescence against GFP in red) allowed attributing PSD^+Cs to specific dendritic domains of identified GCs (Scale bar, 5 μm.)

Figure 2

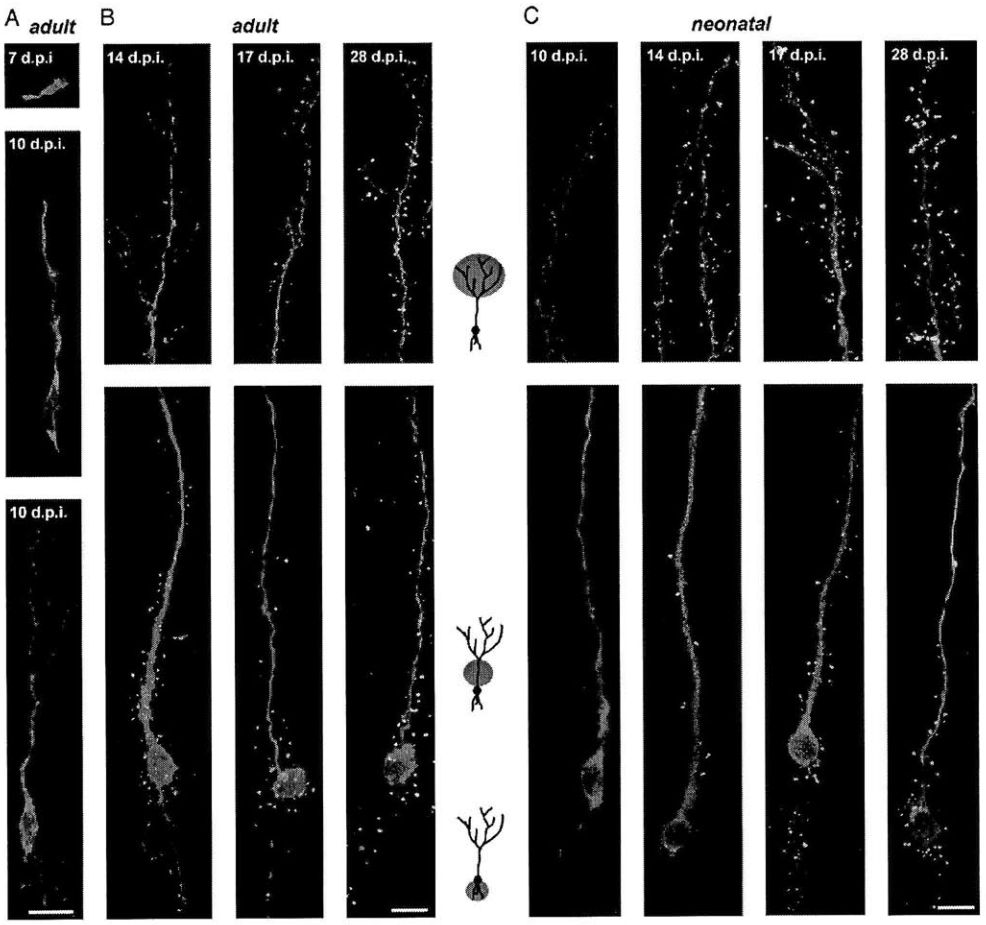

Fig. 2. Development of PSD$^+$Cs during maturation of adult- and neonatal-generated GCs. (A) In adult-generated superficial GCs, no PSD$^+$Cs were detectable during migration (7 d.p.i.) and the initial extension of the dendritic arbor (10 d.p.i.) (Scale bar, 10 μm.) B and C show the development of PSD$^+$Cs at different d.p.i. The Upper row shows the distal domain and the Lower row the basal domain and the unbranched segment of the apical dendrite with the proximal domain of a GC. (B) Only at later time points (14, 17, and 28 d.p.i.) PSD$^+$Cs developed during maturation of adult-generated GCs. PSD$^+$Cs were first observed in high density in the proximal domain followed by PSD$^+$Cs at the distal domain (Scale bar, 10 μm.) (C) In neonatal-generated superficial GCs PSD$^+$Cs developed simultaneously in the proximal and distal domains during maturation of neonatal-generated GCs at 10, 14, 17, 28 d.p.i. (Scale bar, 10 μm.)

Figure 3

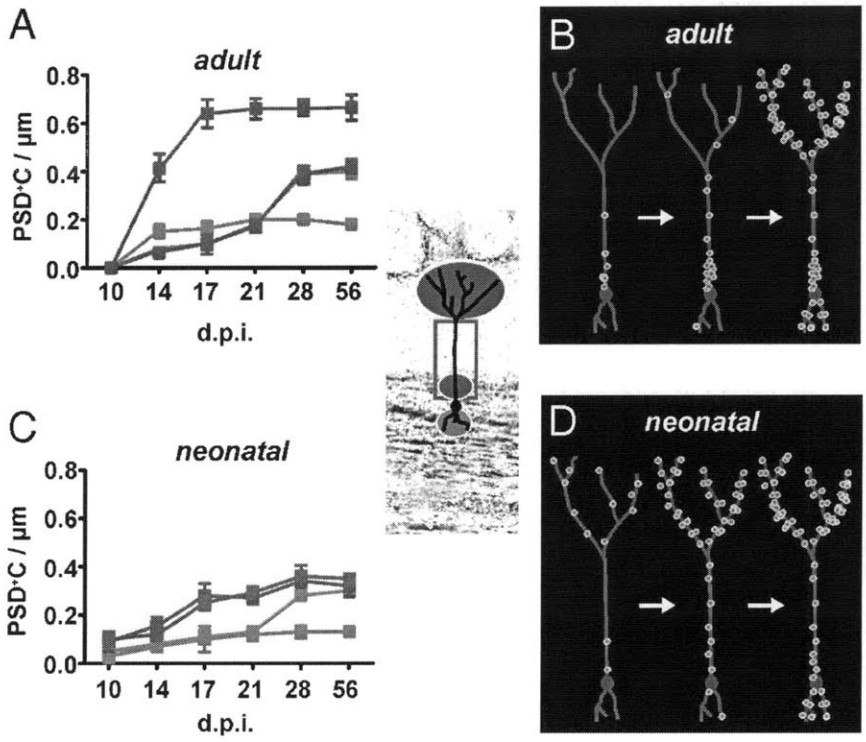

Fig. 3. Domain-specific development of $PSD^{+}Cs$ during maturation of adult- and neonatal-generated GCs (with branching in the superficial external plexiform layer). (A) Mean $PSD^{+}C$ density at different stages (d.p.i.) during the maturation of new GCs generated in adult animals. The dendritic domains are indicated in the graph: basal (blue), proximal (green), and distal domain (red line) as well as the entire unbranched apical dendrite (gray). (B) The diagram illustrates the developmental pattern of $PSD^{+}Cs$ during maturation of adult-generated GCs. (C) Mean $PSD^{+}C$ density at different stages (d.p.i.) during the maturation of new GCs generated in newborn animals. (D) The diagram illustrates the developmental pattern of $PSD^{+}Cs$ during maturation of neonatal-generated GCs.

Figure 4

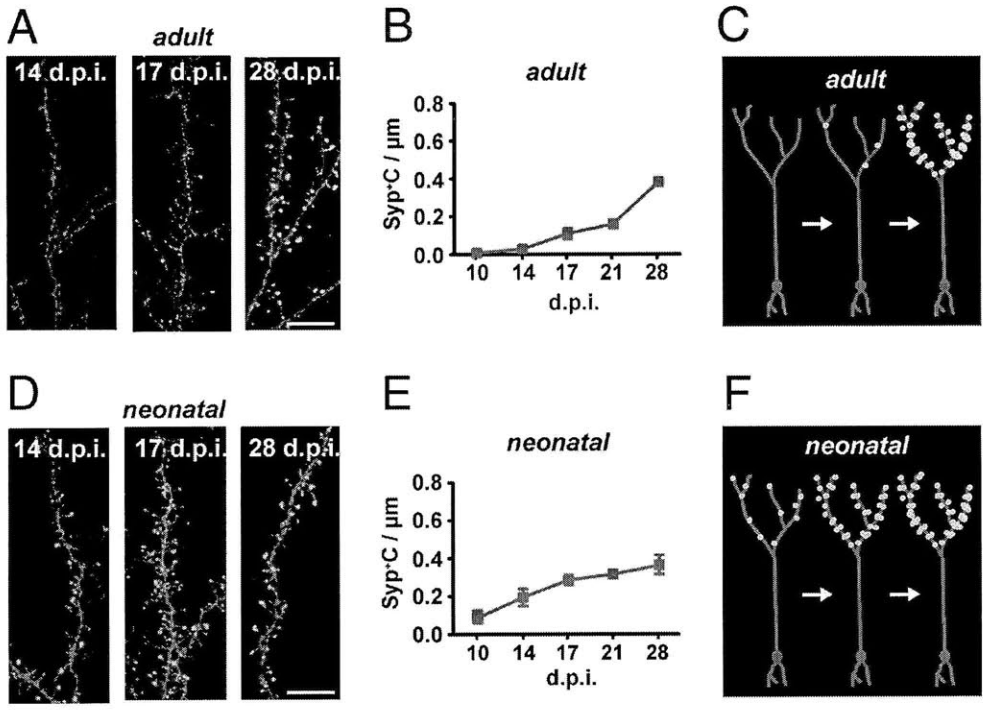

Fig. 4. Development of synaptophysin:GFP-positive clusters (Syp^+Cs) during maturation of adult- and neonatal-generated GCs (with branching in the superficial external plexiform layer). (A) In adult-generated GCs, Syp^+Cs developed during maturation of adult-generated GCs in the distal domain (14, 17, 28 d.p.i.; Scale bar, 10 µm.) (B) Mean Syp^+C density at different stages (d.p.i.) during the maturation of new GCs generated in adult animals. (C) The diagram illustrates the developmental pattern of Syp^+Cs during maturation of adult-generated GCs. (D) In neonatal-generated GCs Syp^+Cs developed earlier than in adult-generated GCs (A) in the distal domain (14, 17, and 28 d.p.i.; Scale bar, 10 µm.) (E) Mean Syp^+C density at different stages (d.p.i.) during the maturation of new GCs generated in neonatal animals. (F) The diagram illustrates the developmental pattern of Syp^+Cs during maturation of neonatal-generated GCs.

Supplementary Figures

S1

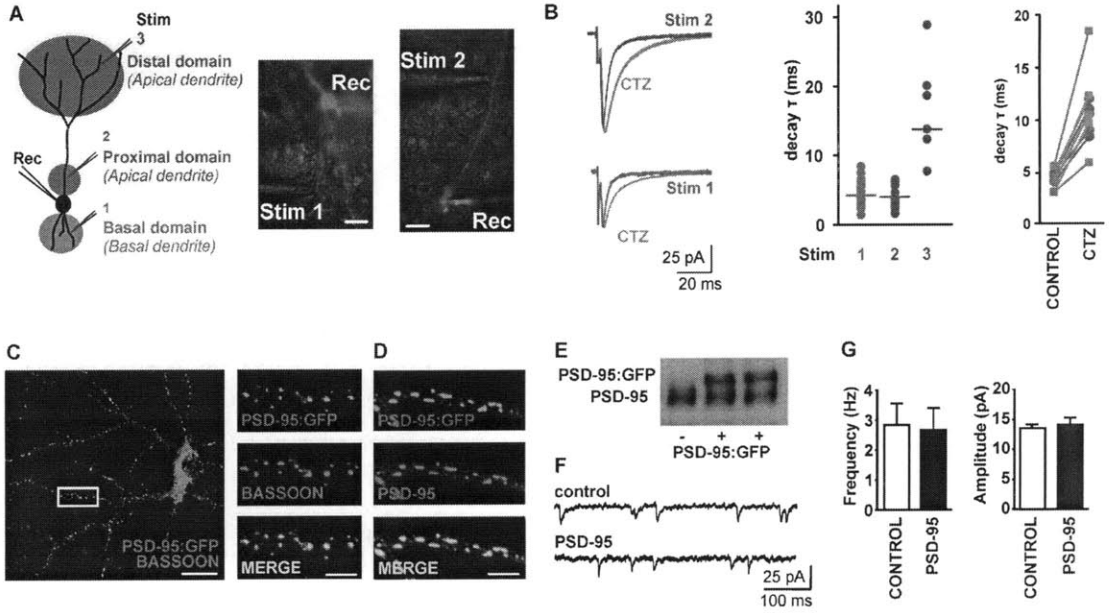

Fig. S1. Glutamatergic input to GCs in brain slices and functional properties of PSD-95:GFP expressed by a retroviral vector in cultured neurons. (A Left) Fluorescence guided focal low amplitude stimulation of one or few fibers terminating either at the basal (1), proximal (2), or distal domain (3). (Right) Sites of stimulation in close proximity to the respective dendritic domain (5 μm) (Scale bar, 10 μm.) (B Left) Fluorescence guided focal low amplitude stimulation to activate one or few fibers terminating either at the basal (1) or proximal (2) domain evoked PSCs that were sensitive to the AMPA-receptor modulator CTZ (10 μM) (V_H = -70; both n = 5). (Center) Evoked PSCs at different dendritic domains (1, 2, or 3) with different 90 –10% decay times recorded at VH =-70 mV (n =18, 13 and 6, respectively). (Right) Graph shows change in 90 –10% decay time in the same GC after application of CTZ for either the basal (blue) or proximal domain (green). (C) A cultured neuron was infected with PSD-95:GFP and labeled with antibody for Bassoon, a presynaptic protein. The confocal image revealed that PSD-95:GFP clusters in dendrites were reliably contacted by a presynaptic terminal. The images on the Right are higher magnification (bar, 3 μm) of the box on the Left image (bar, 10 μm) showing PSD-95:GFP clusters (Top), anti-bassoon immunofluorescence (Middle), and merged image (Bottom). All neurons were examined at 21 days in culture. (D) The PSD-95:GFP clusters (Top) were found in all postsynaptic densities labeled by anti-PSD-95 immunofluorescence (Middle) as seen by the merged image (Bottom) (bar 3 m.) (E) The level of PSD-95 protein (95 kDa) expression was approximately doubled by viral expression of PSD-95:GFP (120 kDa) in cultured neurons 21 d.p.i. compared with the endogenous expression level. In the selected cultures, 90% of neurons expressed PSD-95:GFP. (F) Representative recordings of mEPSCs from two PSD-95:GFP-positive neurons 21 days after infection with a lentiviral vector and uninfected control cells from littermate cultures recorded at the same day (bars indicate 20 pA and 50 ms, respectively). (G) The graphs show the mean mEPSC frequency (P = 0.84) and amplitude (P = 0.47) of neurons infected with a lentiviral vector expressing PSD-95:GFP and uninfected control neurons (n = 8, respectively; all neurons were recorded at 21 d.p.i.).

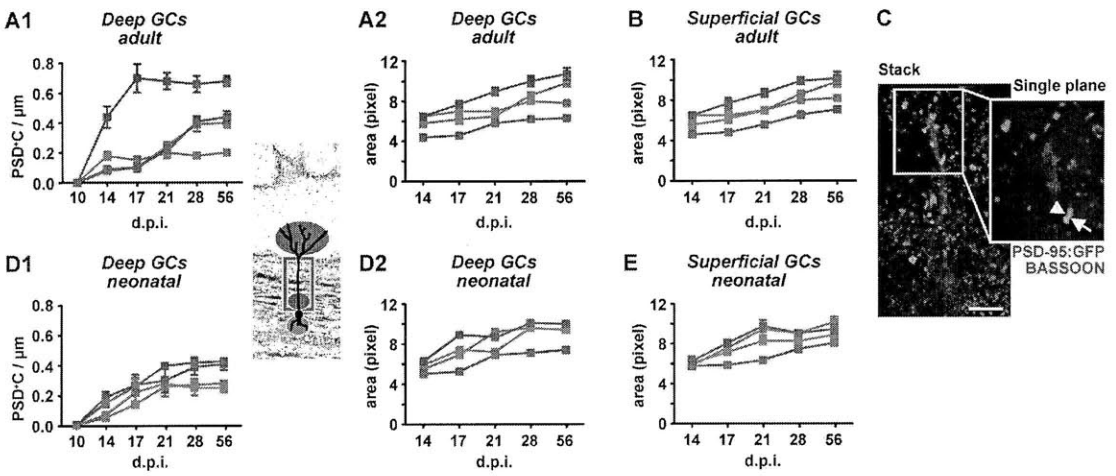

Fig. S2. Domain-specific development of PSD$^+$Cs during maturation of GCs (with branching in the deep or superficial external plexiform layer).

(*A*) Mean PSD$^+$Cdensity (*Left*) and mean PSD$^+$C area (*Right*) at different stages (d.p.i.) during the maturation of deep adult-generated GCs. The dendritic domains are indicatedin the graphs: basal (blue), proximal (green) and distal domain (red) as well as the entire unbranched apical dendrite (gray). (*B*) Mean PSD$^+$C area at differentstages (d.p.i.) during the maturation of superficial adult-generated GCs. (*C*) At 14 d.p.i., PSD$^+$Cs were regularly contacted by a presynaptic marker, bassoon, in adult-generated GCs (Scale bar, 5 µm.) (*D*) Mean PSD$^+$C density (*Left*) and mean PSD$^+$C area (*Right*) at different stages (d.p.i.) during the maturation of deep neonatal-generated GCs. (*E*) Mean PSD$^+$C area at different stages (d.p.i.) during the maturation of superficial neonatal-generated GCs.

Chapter Four

A Critical Period for Activity-Dependent Synaptic Development During Olfactory Bulb Adult Neurogenesis

Wolfgang Kelsch[1, 2], Chia-Wei Lin[1, 2], Colleen P. Mosley[2, 3], Carlos Lois[1, 2, 3]

[1] *Picower Institute for Learning and Memory, Massachusetts Institute of Technology, Cambridge, Massachusetts, United States of America*

[2] *Department of Brain and Cognitive Sciences, Massachusetts Institute of Technology, Cambridge, Massachusetts, United States of America*

[3] *Department of Biology, Massachusetts Institute of Technology, Cambridge, Massachusetts, United States of America*

This paper was published in *Journal of Neuroscience* 29(38): 11852-11858

Note: I characterized the biophysical properties of NaChBac channels and applied this channel to study the effect of enhancing intrinsic membrane excitability on synaptic development of GCs using acute-slice recordings. The result was presented in ***Figure 4.***

Abstract

New neurons integrate in large numbers into the mature olfactory bulb circuit throughout life. The factors controlling the synaptic development of adult-born neurons and their connectivity remain largely unknown. We examined the role of activity-dependent mechanisms in the synaptic development of adult-born neurons by genetic labeling of synapses while manipulating sensory input or cell-intrinsic excitability. Sensory deprivation induced marked changes in the density of input and output synapses during the period when new neurons develop most of their synapses. In

contrast, when sensory deprivation started after synaptic formation was complete, input synapses increased in one domain without detectable changes in the other dendritic domains. We then investigated the effects of genetically raising the intrinsic excitability of new neurons on their synaptic development by delivering a voltage-gated sodium channel that triggers long depolarizations. Surprisingly, genetically increasing excitability did not affect synaptic development, but rescued the changes in glutamatergic input synapses caused by sensory deprivation. These experiments show that during adult neurogenesis in the olfactory bulb synaptic plasticity is largely restricted to an early period during the maturation of new neurons when they are still forming synapses. The addition of cells endowed with such an initial short-lived flexibility and long-term stability may enable the processing of information by the olfactory bulb to be both versatile and reliable in the face of changing behavioral demands.

Introduction

The main olfactory bulb (MOB) in the mammalian brain receives new neurons throughout life (Altman, 1962; Lois and Alvarez-Buylla, 1993; Luskin, 1993). All new neurons added to the adult olfactory bulb are interneurons (Lledo et al., 2008); approximately 95% of these are granule cell neurons (GCs), and the rest are periglomerular neurons. Considerable progress has recently been made in identifying the factors that regulate the specification of the different subtypes of adult-born interneurons in the olfactory bulb (Batista-Brito et al., 2008; Hack et al., 2005; Kelsch et al., 2007; Merkle et al., 2007). In contrast, relatively little is known about the mechanisms that regulate the synaptic development of adult-born neurons and their connectivity within the mature circuit.

Neuronal activity is thought to be an important factor shaping the wiring of new neurons. In neonatal animals sensory deprivation reduces the survival of new GCs (Brunjes, 1994; Saghatelyan et al., 2005), and triggers a decrease in spine density and excitatory inputs (Saghatelyan et al., 2005), whereas pre-existing, mature GCs maintain their spine density (Frazier-Cierpial and Brunjes, 1989; Saghatelyan et al., 2005). Adult-born GCs also have a critical period during their differentiation such that sensory deprivation reduces the survival of new GCs mainly in the third and fourth week after new neurons are born in the subventricular zone (SVZ) (Petreanu and Alvarez-Buylla, 2002; Yamaguchi and Mori, 2005). Before this critical period, the survival and dendritic growth of new GCs is independent of sensory input (Petreanu and Alvarez-Buylla, 2002). Interestingly the beginning of the critical period for survival (approximately 14 days after a new neuron's birth; (Yamaguchi and Mori, 2005)) coincides with the time when glutamatergic input synapses start to develop in adult-born GCs (Kelsch et al., 2008).

Here we investigate whether, in addition to the critical period for survival, there exists a critical period during which the synapses of new neurons are plastic. Towards this goal we used a genetic labelling technique that allowed us to examine how synaptic development is affected by manipulating sensory input and intrinsic excitability of adult-born neurons. To reduce sensory input we performed unilateral naris occlusion and observed that adult-born neurons that developed in a sensory-deprived bulb experienced synaptic losses in their distal and basal dendritic domains, and gain of input sites in the proximal domain. In contrast when sensory deprivation started after their synaptic development was complete, adult-born GCs only gained synapses in the proximal domain, with no changes in the other domains. Next we examined whether synapse development was affected by manipulating the intrinsic

excitability of new GCs. To increase cell-intrinsic neuronal excitability we genetically delivered NaChBac, a bacterial voltage-gated sodium channel (Luan et al., 2006; Nitabach et al., 2006; Ren et al., 2001), into the progenitor cells in the SVZ that give rise to new GCs. Interestingly, this manipulation did not induce detectable synaptic changes in new neurons generated in adult animals under normal conditions, but rescued the changes in glutamatergic input synapses induced by sensory deprivation.

These observations indicate that activity-dependent increases or decreases in synaptic densities are largely restricted to an early period during the maturation of new neurons when they are still forming synapses.

Results

Adult-generated neurons display different synaptic changes in specific dendritic domains in response to sensory deprivation.

To determine how neuronal activity affects the synaptic development of adult-born neurons in the rat olfactory bulb, we blocked sensory input to the bulb by performing unilateral naris occlusion (Fig. 1*A*), and compared the synaptic structure and organization of GCs in the deprived and contralateral control olfactory bulb. We measured the development of glutamatergic input synapses of new adult-born GCs using PSDG, a genetic marker consisting of a fusion protein between PSD-95 and GFP. PSD-95 is a protein localized to the postsynaptic density of glutamatergic input synapses (Sheng, 2001), and PSDG delivered into new neurons with retroviral vectors (M*psdg*) can be used to genetically label these synapses (Gray et al., 2006; Kelsch et al., 2008; Livneh et al., 2009; Niell et al., 2004). We have previously shown that expression of PSDG at the modest levels yielded by retroviral expression does not alter synaptic properties as measured by electrophysiological methods (Kelsch et al., 2008). To analyze the development of output synapses we used SypG, a fusion protein between Synaptophysin and GFP. Synaptophysin is a protein localized to presynaptic neurotransmitter vesicles (Sudhof and Jahn, 1991), and SypG expressed with retroviral vectors (M*sypg*) can be used to genetically label output synapses (Kelsch et al., 2008; Li and Murthy, 2001; Meyer and Smith, 2006). We examined $SypG^{+}$ cluster densitiesat 28 dpi, once GCs had completed their maturation and $SypG^{+}$ clusters were confined to spines of the distal dendritic domain (Supplementary. Fig. 1).

GCs are axonless inhibitory interneurons and their synapses are distributed in three dendritic domains, know as basal, proximal and distal dendritic domains (Fig 1*B*). GCs receive

glutamatergic input synapses through the basal, proximal and distal domains. The distal dendritic domain of GCs contains both input and output synapses, whereas the basal and proximal dendritic domains do not release neurotransmitter (Mori, 1987).

Blocking sensory input during a period in which new neurons are undergoing synaptic development, between 14 and 28 days post infection (d.p.i.) in the SVZ, led to reductions in the density of PSD-95:GFP-positive ($PSDG^+$) input synapses (Fig. 1*C*) in the distal and basal dendritic domains (Fig. 2*A*). Similarly, the density of Synaptophysin:GFP-positive ($SypG^+$) output synapses in the distal dendritic domain decreased significantly under sensory deprivation (Fig. 3). Interestingly, sensory deprivation during synaptic development increased the density of $PSDG^+$ input synapses in the proximal dendritic domain of new GCs (Fig. 2*A*). The changes in synaptic densities became statistically significant at the time when new neurons reached maturity (after 21-28 d.p.i.), and remained so thereafter until the longest time we monitored the new neurons (56 d.p.i.; Fig. 2*A*). For this and the following experiments data from GCs with e.g. different dendritic targeting were pooled as an initial analysis indicated no significant differences between these subpopulations. These observations indicate that sensory deprivation to the bulb triggered up- and down-regulation of the synaptic input and outputs of new GCs. In addition, these activity-dependent synaptic changes were not uniform throughout the cells, but confined to specific dendritic domains.

We next examined whether changes in synaptic organization also occurred when sensory deprivation was started after synaptic development of new GCs was complete. Towards this end, unilateral naris occlusion was started 42 days after a cohort of genetically labeled new neurons had been born in the SVZ (Fig. 1*A*). Adult-born GCs deprived of sensory input for three weeks (between 42 to 63 d.p.i.), starting after completion of synaptic development of a

cohort of labelled neurons, only resulted in an increase in synaptic input in the proximal domain (Fig. 2*B*), with no detectable changes in synaptic input or output densities in the distal and basal domains (Fig. 2*B* and 3). These experiments suggest the existence of a critical period during the synaptic development of new neurons when the organization of synapses throughout the cell can be strongly shaped by sensory experience. In addition, these results indicate that the proximal dendritic domain of new neurons has special properties that enable it to alter its synaptic organization after all other dendritic domains become unresponsive to manipulations of sensory input.

A genetic method to increase cell-intrinsic excitability.

The activity of neurons is primarily regulated by two factors, the synaptic input that they receive and their intrinsic excitability determined by the set of ion channels present in their membranes. To investigate the role of intrinsic excitability in synaptic development, we tested whether increasing cell-intrinsic excitability would change the formation and maintenance of synapses as they integrate into the bulb's circuits. Towards this goal we devised a genetic strategy that would selectively render these new neurons more excitable without significantly altering the properties of the rest of the circuit into which they integrate. To increase the intrinsic excitability of single neurons we used NaChBac, a voltage-gated sodium channel from the hallophilic bacteria *B. halodurans*. Expression of NaChBac increases the intrinsic excitability of neurons because, first, its activation threshold is more negative than that of native sodium channels, and second, NaChBac produces a slowly inactivating depolarizing current that lasts on the order of hundreds of milliseconds (Ren et al., 2001), compared to the approx. 1 ms inactivation time of the endogenous mammalian sodium channels responsible for the fast action potentials (Hille, 2001). To visualize neurons

expressing NaChBac we generated a retroviral vector encoding a fusion protein between GFP and NaChBac (M*nachbacg*). To study the electrical properties of new neurons expressing NaChBac, we delivered M*nachbacg* into GC progenitors in the SVZ. As controls, we co-injected a retroviral vector encoding the red fluorescent protein, mCherry (M*mcherry*) into the same animals, and performed fluorescence-guided whole-cell recordings of either mCherry$^+$ or NaChBac$^+$ cells in acute slices. Unlike control neurons (n=6 GCs), NaChBac$^+$ neurons expressed a TTX-resistant slow-inactivating inward current that activated at -40 mV (n= 5 GCs; Fig. 4*A*). NaChBac expression did not alter other passive membrane properties measured at -70 mV such as membrane time constant, input resistance, and resting membrane potential (data not shown). Whereas a 5 ms pulse of supra-threshold current injection (4 nA), evoked a single spike in mCherry$^+$ control GCs (n=9 GCs), the same current injection reliably caused an additional depolarization lasting on average 566 ± 49 ms in NaChBac$^+$ GCs (n= 8 GCs; Fig. 4*A*). This supra-threshold current injection (4 nA, 5 ms) elicited long depolarizations in NaChBac$^+$ GCs as early as 14-18 d.p.i. (n=8 GCs), which were never observed in control neurons at any of the time points studied. At 28 d.p.i. the activation threshold for spiking in NachBac$^+$ GCs was -41±2.0 mV (n=9 GCs), whereas for mCherry$^+$ control GCs was -30±1.9 mV (n=8 GCs) measured at 26-28 d.p.i. in adult rats. NaChBac expression did not affect the migration of new neurons into the olfactory bulb and increased their survival (Lin, et al, unpublished observations).

Genetically increasing the intrinsic excitability of adult-born neurons does not affect synapse formation.

Having established a method to genetically increase the intrinsic excitability of newly generated neurons, we examined how this manipulation affected the formation of synapses

using a bicistronic construct that expressed both PSDG, the fusion between GFP and PSD-95, and NaChBac (M*psdg:2A:nachbac*; Fig. 4*B*). We measured the density of $PSDG^+$ synapses in new GCs infected with M*psdg:2A:nachbac* and compared them to neurons expressing PSDG either alone (Fig. 4*B*) or with a non-conducting *E*191*K* NaChBac mutant (M*psdg:2A:e191k*) (Supplementary Fig. 1). GCs expressing both PSDG and the non-conducting *E*191*K* NaChBac mutant (M*psdg:2A:e191k*) had the same $PSDG^+$ synapse density as control neurons expressing only PSDG in adult-born GCs (Supplementary Fig. 1), indicating that expression of the non-conducting channel did not change $PSDG^+$ synapse density by itself. To examine whether increased membrane excitability affected output synapses, we generated a bicistronic construct that expressed both Synaptophysin:GFP (*Sypg*), the fusion protein between Synaptophysin and GFP, and NaChBac (M*sypg:2A:nachbac)* (Fig. 6).

Unexpectedly, increasing the intrinsic excitability by NaChBac expression in adult-born GCs did not change the density of $PSDG^+$ synapses in any of their dendritic domains (Fig. 5A), even though NaChBac remained active during synaptic development of adult-born GCs (Fig. 4*A*). Similarly, the density of $SypG^+$ output synapses in adult-generated GCs was not changed by NaChBac expression (M*sypg:2A:nachbac* vs. M*sypg*; Fig. 6). These observations indicate that the formation of synapses is not affected by perturbations in the cell-intrinsic excitability of new neurons.

Increased intrinsic excitability blocks the synaptic changes evoked by sensory deprivation.

The observation that strong synaptic changes were triggered by sensory deprivation, but not by raising the intrinsic excitability of new neurons could be due to the ability of these new neurons to implement mechanisms of plasticity when their synaptic inputs are modified (by sensory deprivation), but not when their intrinsic membrane excitability is perturbed (by NaChBac expression). Alternatively, synaptic changes due to increased excitability of adult-generated neurons may only come into play if their synaptic inputs are perturbed. To test these possibilities we analyzed the distribution of synapses in new $NaChBac^+$ adult-born GCs that had also been deprived of sensory input. As indicated above, sensory deprivation caused a decrease in the number of glutamatergic input synapses in the distal and basal dendritic domains of adult-born neurons and an increase in the proximal domain (Fig. 2). Surprisingly, NaChBac blocked the changes in $PSDG^+$ synapse densities of adult-born neurons triggered by sensory deprivation. In the proximal domain, NaChBac expression completely eliminated the synaptic increases induced by sensory deprivation at all times studied (Fig. 5*B*). In the distal domain, NaChBac expression blocked the decrease in synaptic density induced by naris occlusion partially by 28 d.p.i. and completely by 56 d.p.i. (Fig. 5*B*). These observations indicate that increasing the intrinsic excitability of new neurons in the adult brain can trigger synaptic changes in glutamatergic input synapses but only after their activity is modified by sensory deprivation.

Discussion

The connectivity of neurons within brain circuits is primarily regulated at two levels; first, by determining the identity of the neurons that will become synaptic partners, and second, by controlling the number of synapses formed between these partners. During adult neurogenesis in the OB, the identity of the synaptic partners for new GCs (mitral or tufted cells) appears to be largely determined by genetic factors, such that separate precursors exist in the SVZ which give rise to new GCs apparently committed to make synapses with either mitral or tufted cells (Kelsch et al., 2007). In contrast, the density of synaptic connections can be strongly regulated by neuronal activity (Brunjes, 1994; Saghatelyan et al., 2005). Such a dual control of neuronal connectivity during adult neurogenesis may simultaneously provide stereotypy of the circuit, and flexibility to form novel connections for processing information in response to sensory-driven behavioral demands.

In this study we analyzed how neuronal activity sculpts the synaptic development and connectivity of new GCs added to an adult brain circuit. We observed that new neurons added to the adult olfactory bulb under sensory deprivation experience dramatic changes in their synaptic development. In particular, we focused in this study on how and when neuronal activity can change the density and distribution of synaptic input and output sites of adult-born neurons. These changes are non-uniform in that either increases or decreases in synapse density occurred in different dendritic domains (Fig. *7*). Sensory deprivation caused decreases in synapses in the distal and basal domain, and increases in the proximal domain. Thus, each dendritic domain appears to act as an independent unit of synaptic plasticity.

Interestingly, sensory input-dependent changes in synaptic wiring are largely restricted to the period when the new adult-born neurons develop their synapses. The synapses in the distal and basal domain are modifiable by sensory activity only for a limited time during the maturation of new GCs. After GCs have completed their maturation, the only synapses that appear to retain their modifiability in response to sensory deprivation are located in the proximal dendritic domain. In line with the limited period of activity-dependent synaptic changes that we observed, it has been recently shown that the ability to induce long-term potentiation was also lost after the first month in the life of new adult-born GCs (Nissant et al., 2009).

Given the strong synaptic changes induced by sensory deprivation on new GCs, it is surprising that genetically triggering long depolarizations (approx. 600 msec) in these new neurons throughout their maturation did not interfere with the formation and maintenance of synapses. Despite the strong electrical perturbation induced by NaChBac expression we could not detect any morphological changes in the synapse in any of the dendritic domains of new GCs. Similarly, the frequency and amplitudes of spontaneous EPSC inputs of adult-born GCs expressing NaChBac was not altered as compared to matched controls (unpublished observations). These results were surprising because many neurons have homeostatic mechanisms that regulate their synaptic input so that when their excitability is raised, they reduce the number or strength of their excitatory synapses to prevent runaway activity. Interestingly, although GCs in the OB do not exhibit this compensatory behavior we have recently observed that new neurons in the dentate gyrus with NaChBac-enhanced excitability experience a strong reduction in their excitatory synapses (unpublished results). The observation that increased excitability does not affect the density or distribution of

excitatory synapses in GCs in the OB could be explained by other compensatory mechanisms, such as increased synaptic inhibition or changes in ion channels that could balance the increased intrinsic excitability. However we did not observe any changes in intrinsic membrane or synaptic properties, suggesting either the existence of subtle compensatory mechanisms that escaped our detection methods or, alternatively, that these neurons do not compensate for this form of increased cell-intrinsic excitability.

Adult-born neurons, however, were not completely unresponsive to manipulations of their intrinsic excitability, since NaChBac-enhanced excitability counteracted the changes in glutamatergic input synapses caused by sensory deprivation. These observations also suggest the possibility that there may exist a program regulating the formation and maintenance of synapses in new GCs that requires a minimum threshold of neuronal activity contributed by the combined action of synaptic drive and cell-intrinsic excitability. If neuronal activity falls below that putative threshold due to a reduction in synaptic inputs (as a result of sensory deprivation), new neurons implement changes in the organization of their synapses. If new GCs with reduced synaptic input are simultaneously rendered hyperexcitable (as a result of NaChBac expression), the cells may still be over the threshold so that no synaptic changes occur.

The ability of new neurons to adapt their connectivity to the state of the adult circuit (e.g. sensory deprivation vs. normal environment) may shed light on the contribution of continuous neurogenesis to learning and memory (Aimone et al., 2009; Bischofberger, 2007; Lledo and Saghatelyan, 2005; Nottebohm, 2002). Several studies have demonstrated that the plasticity of adult-born neurons is maximal during their initial development, and that it is

progressively lost as the cells mature (Ge et al., 2007; Nissant et al., 2009; Schmidt-Hieber et al., 2004). Our results extend these observations by demonstrating that the synapses of new neurons have a high degree of structural plasticity during a time window when they are initially added into the circuit. Once they mature, activity-dependent plasticity in new neurons becomes more limited. This window of plasticity may allow the bulb to capture new neurons into stable patterns of connectivity while the circuit is in a certain state and thus generate stable information processing modules, while the next wave of new neurons may capture subsequent 'circuit states'. The addition of cells endowed with such an initial short-lived flexibility and long-term stability may enable the processing of information by the olfactory bulb to be both versatile and reliable in the face of changing behavioral demands.

Methods

Generation of retroviral vectors. Recombinant retroviral vectors under the control of the Rous Sarcoma virus promoter for PSDG and SypG (M*psdg* and M*sypg*), were prepared and stored as described (Kelsch et al., 2008). All constructs described here were generated by inserting the following cDNAs or cassettes downstream from the RSV promoter in the Molar retroviral vector: Mmcherry (mCherry cDNA); Mnachbacg a fusion protein between the N-terminus of NaChBac and the C-terminus of GFP); Mpsdg:2A:nachbac (a bicistronic cassette encoding a fusion between PSD95 and GFP linked by a picornavirus 2A sequence to the NaChBac cDNA); Msypg:2A:nachbac (a bicistronic cassette encoding a fusion between Synaptophysin and GFP linked by a picornavirus 2A sequence to the NaChBac cDNA); Mpsdg:2A:e191k (a bicistronic cassette encoding a fusion between PSD95 and GFP linked by a picornavirus 2A sequence to the non-conducting e191k mutant of NaChBac).

Retroviral labeling *in vivo*. All experiments were performed with 2 month old Sprague Dawley rats. All animal procedures were approved by the local Animal Welfare Committee and NIH guidelines. Retroviral injections were performed as recently described (Kelsch et al., 2008). The stereotaxic coordinates are (anterior; posterior; ventral (in mm in reference to Bregma): +1.2; ±1.6; -3.1). Animals were kept in a 12 h daylight cycle and under the same housing conditions.

Olfactory deprivation. For sensory deprivation experiments, unilateral surgical naris occlusion was performed on the day of intracerebral injection of viruses M*psdg,* M*syp* and M*psdg:2A:nachbac* into the subventricular zone. At the day of surgery adult rats obtained a single i.p. injection of BrdU (100 mg/kg bodyweight) to monitor the success of sensory

deprivation by an external criterion (Yamaguchi and Mori, 2005). Only animals were included into the analysis of early deprivation that displayed a significant decrease in $BrdU^+$ cells in the deprived bulb (see Supplementary Fig. 1). As expected (Yamaguchi and Mori, 2005) after late deprivation no decrease in $BrdU^+$ cells in the deprived bulb (BrdU injection at the day of retroviral infection) was observed (0.98±0.07), but the deprived site displayed a strong reduction in c-fos expression in the granule cell layer and reduction of tyrosine hydroxylase expression in the glomerular layer (see Supplementary Fig. 1). For this selection process immunofluorescence was performed with antibodies against BrdU (Accurate), c-Fos (Oncogene) and tyrosine hydroxylase (Chemicon).

Analysis of synaptic markers. Tissue processing and analysis of $SypG^+$ and $PSDG^+$ clusters was performed as previously described (Kelsch et al., 2008). In brief, 50 μm thick coronal slices were incubated in primary rabbit anti-GFP (1:4.000, Chemicon) and Alexa-555 secondary antibodies (1:750, Molecular Probes). Confocal image stacks were acquired using an Olympus Fluoview confocal microscope (60x oil-immersion lens (NA, 1.4), Olympus, Melville, NY) (pixel size, 0.23x 0.23 μm, 1024x1024 pixel), and with z-step 0.25 μm (80-150 sections). Maximal intensity projections were used to measure the density of $PSDG^+$ or $SypG^+$ clusters of a dendritic segment with the integrated morphometry analysis of MetaMorph software (Universal imaging, West Chester, PA).

Statisitical analysis. Each analyzed data point (e.g. sensory deprivation, basal domain, 17 d.p.i.) contained normally distributed $PSDG^+$ cluster densities from 14 cells. GCs with deep and superficial dendritic targeting in the external plexiform layer (Kelsch et al., 2008) showed the same activity-dependent plasticity in their dendritic domains (data not shown),

therefore presented data were pooled. Statistical significance was determined using a Student' t-test for pair wise comparisons at the same d.p.i..

Electrophysiological recordings. Whole cell recordings were performed as previously described (Kelsch et al., 2008). In brief, 350 μm horizontal acute slices were prepared from adult olfactory bulbs and recovered in recording solution: 125 NaCl, 2.5 KCl, 1.25 NaH_2PO_4, 26 $NaHCO_3$, 1 $MgCl_2$, 2 $CaCl_2$, 20 glucose, 312 mOsm, and pH 7.3. Fluorescence-guided whole-cell patch clamp recordings were performed and analyzed with a MultiClamp 700B amplifier and pClamp9 software (Axon Instruments). The pipette solution contained (in mM): 2 NaCl, 4 KCl, 130 Kgluconate, 10 HEPES, 0.2 EGTA, 4ATP-Mg, 0.3 GTP-Tris, 14 phosphocreatine and pH 7.3 with KOH. Access resistance was <20 MΩ and junction potential was not corrected. To determine the current-voltage relationship of NaChBac expressing GCs, 1 μM tetrodoxin was used. As fluorescence of the fusion protein was too weak to detect constructs containing both NaChBac and a synaptic marker in acute slices, *in vitro* retroviral expression in HEK cell lines was used to confirm that the current was preserved. A slow inactivating inward current was activated by depolarization as previously described (Ren et al., 2001) for M*psdg:2A:nachbac* and M*sypg:2A:nachbac*, but not for mutant M*psdg:2A:e191k* (data not shown).

REFERENCES

Aimone JB, Wiles J, Gage FH (2009) Computational influence of adult neurogenesis on memory encoding. Neuron 61:187-202.

Altman J (1962) Are new neurons formed in the brains of adult mammals? Science 135:1127-1128.

Batista-Brito R, Close J, Machold R, Fishell G (2008) The distinct temporal origins of olfactory bulb interneuron subtypes. J Neurosci 28:3966-3975.

Bischofberger J (2007) Young and excitable: new neurons in memory networks. Nat Neurosci 10:273-275.

Brunjes PC (1994) Unilateral naris closure and olfactory system development. Brain Res Brain Res Rev 19:146-160.

Frazier-Cierpial LL, Brunjes PC (1989) Early postnatal differentiation of granule cell dendrites in the olfactory bulbs of normal and unilaterally odor-deprived rats. Brain Res Dev Brain Res 47:129-136.

Ge S, Yang CH, Hsu KS, Ming GL, Song H (2007) A critical period for enhanced synaptic plasticity in newly generated neurons of the adult brain. Neuron 54:559-566.

Gray NW, Weimer RM, Bureau I, Svoboda K (2006) Rapid redistribution of synaptic PSD-95 in the neocortex in vivo. PLoS Biol 4:e370.

Hack MA, Saghatelyan A, de Chevigny A, Pfeifer A, Ashery-Padan R, Lledo PM, Gotz M (2005) Neuronal fate determinants of adult olfactory bulb neurogenesis. Nat Neurosci 8:865-872.

Llinas RR (1988) The intrinsic electrophysiological properties of mammalian neuons: insights into central nervous system. Science 242:1654-64.

Kelsch W, Lin CW, Lois C (2008) Sequential development of synapses in dendritic domains during adult neurogenesis. Proc Natl Acad Sci U S A 105:16803-16808.

Kelsch W, Mosley CP, Lin CW, Lois C (2007) Distinct mammalian precursors are committed to generate neurons with defined dendritic projection patterns. PLoS Biol 5:e300.

Li Z, Murthy VN (2001) Visualizing postendocytic traffic of synaptic vesicles at hippocampal synapses. Neuron 31:593-605.

Livneh Y, Feinstein N, Klein M, Mizrahi A (2009) Sensory input enhances synaptogenesis of adult-born neurons. J Neurosci 29:86-97.

Lledo PM, Saghatelyan A (2005) Integrating new neurons into the adult olfactory bulb: joining the network, life-death decisions, and the effects of sensory experience. Trends Neurosci 28:248-254.

Lledo PM, Merkle FT, Alvarez-Buylla A (2008) Origin and function of olfactory bulb interneuron diversity. Trends Neurosci 31:392-400.

Lois C, Alvarez-Buylla A (1993) Proliferating subventricular zone cells in the adult mammalian forebrain can differentiate into neurons and glia. Proc Natl Acad Sci U S A 90:2074-2077.

Luan H, Lemon WC, Peabody NC, Pohl JB, Zelensky PK, Wang D, Nitabach MN, Holmes TC, White BH (2006) Functional dissection of a neuronal network required for cuticle tanning and wing expansion in Drosophila. J Neurosci 26:573-584.

Luskin MB (1993) Restricted proliferation and migration of postnatally generated neurons derived from the forebrain subventricular zone. Neuron 11:173-189.

Merkle FT, Mirzadeh Z, Alvarez-Buylla A (2007) Mosaic organization of neural stem cells in the adult brain. Science 317:381-384.

Meyer MP, Smith SJ (2006) Evidence from in vivo imaging that synaptogenesis guides the growth and branching of axonal arbors by two distinct mechanisms. J Neurosci 26:3604-3614.

Mori K (1987) Membrane and synaptic properties of identified neurons in the olfactory bulb. Prog Neurobiol 29:275-320.

Niell CM, Meyer MP, Smith SJ (2004) In vivo imaging of synapse formation on a growing dendritic arbor. Nat Neurosci 7:254-260.

Nissant A, Bardy C, Katagiri H, Murray K, Lledo PM (2009) Adult neurogenesis promotes synaptic plasticity in the olfactory bulb. Nat Neurosci.

Nitabach MN, Wu Y, Sheeba V, Lemon WC, Strumbos J, Zelensky PK, White BH, Holmes TC (2006) Electrical hyperexcitation of lateral ventral pacemaker neurons desynchronizes downstream circadian oscillators in the fly circadian circuit and induces multiple behavioral periods. J Neurosci 26:479-489.

Nottebohm F (2002) Why are some neurons replaced in adult brain? J Neurosci 22:624-628.

Petreanu L, Alvarez-Buylla A (2002) Maturation and death of adult-born olfactory bulb granule neurons: role of olfaction. J Neurosci 22:6106-6113.

Ren D, Navarro B, Xu H, Yue L, Shi Q, Clapham DE (2001) A prokaryotic voltage-gated sodium channel. Science 294:2372-2375.

Saghatelyan A, Roux P, Migliore M, Rochefort C, Desmaisons D, Charneau P, Shepherd GM, Lledo PM (2005) Activity-dependent adjustments of the inhibitory network in the olfactory bulb following early postnatal deprivation. Neuron 46:103-116.

Schmidt-Hieber C, Jonas P, Bischofberger J (2004) Enhanced synaptic plasticity in newly generated granule cells of the adult hippocampus. Nature 429:184-187.

Sheng M (2001) Molecular organization of the postsynaptic specialization. Proc Natl Acad Sci U S A 98:7058-7061.

Sudhof TC, Jahn R (1991) Proteins of synaptic vesicles involved in exocytosis and membrane recycling. Neuron 6:665-677.

Yamaguchi M, Mori K (2005) Critical period for sensory experience-dependent survival of newly generated granule cells in the adult mouse olfactory bulb. Proc Natl Acad Sci U S A 102:9697-9702.

Figure 1

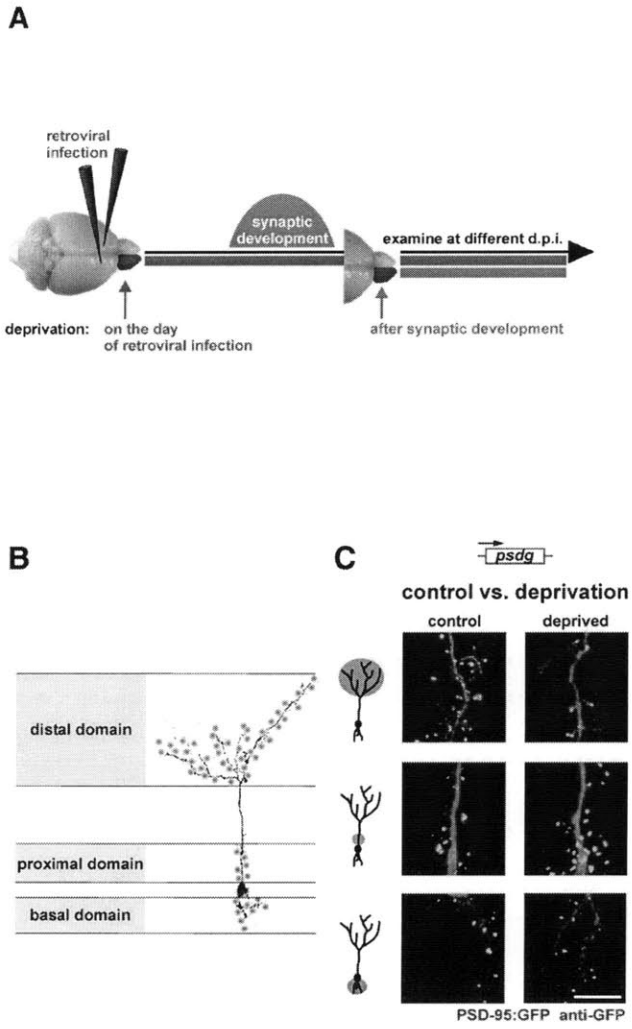

Figure 1. Sensory deprivation changes glutamatergic input synapse development in adult-born GCs. *A*, Progenitor cells were infected with retroviruses in the SVZ in combination with unilateral naris occlusion either at the same day or after synaptic development was complete (starting at 42 dpi). Genetically labeled GCs were examined at different days after infection. *B*, GCs have three main dendritic domains: a basal and a proximal domain that receive glutamatergic input synapses and a distal dendritic domain that contains recurrent input and output synapses. *C*, At 28 dpi, $PSDG^+$ clusters were examined in adult-born GCs in sensory-deprived (starting on the day of retroviral labeling) or contralateral control olfactory bulbs. To attribute $PSDG^+$ clusters (green) to a particular GC, dendritic morphology was visualized by red dye-labeled GFP immunofluorescence against the diffuse PSD-95:GFP present in the cytosol that was otherwise undetectable. The three main dendritic domains were analyzed separately (from top): distal, proximal, or basal domain. Scale bar, 10 μm.

Figure 2

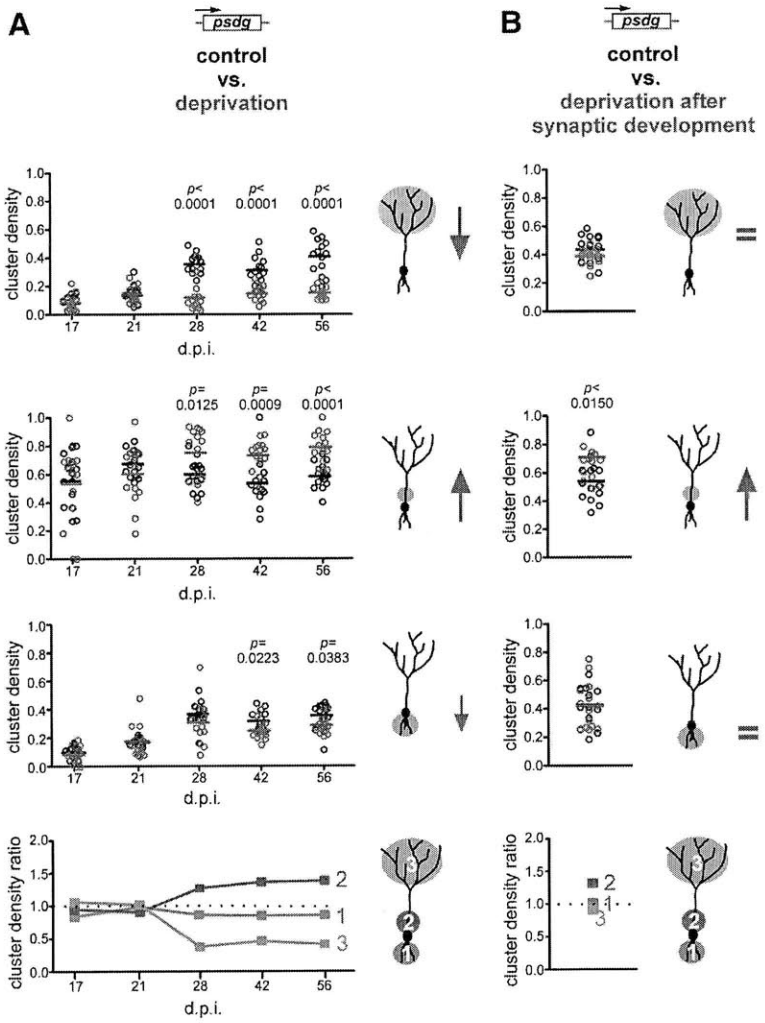

Figure 2. Sensory deprivation changes glutamatergic synapses in specific dendritic domains during a critical period. ***A***, Scatter plot and mean density of $PSDG^+$ clusters (clusters per micrometer) of adult-born GCs in sensory-deprived (starting on the day of retroviral labeling) and contralateral control (red and black circles, respectively) olfactory bulbs at different days after infection. Statistical significance is only indicated if $p < 0.05$ (t test). The bottom graph shows the ratio of the mean cluster density of sensory-deprived over control GCs in a specific domain at a given day after infection. ***B***, When sensory deprivation started after synaptic development was complete, the mean density of $PSDG^+$ clusters (clusters per micrometer) only changed in the proximal domain (unilateral naris occlusion at 42 dpi and examined at 63 dpi).

Figure 3

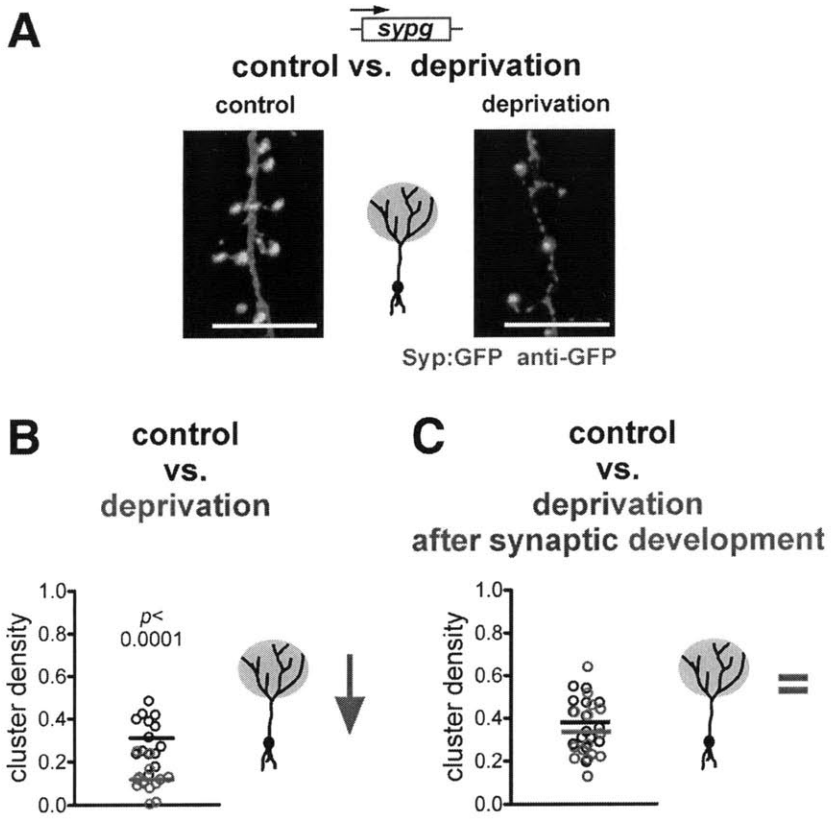

Figure 3. Sensory deprivation during synaptic development reduces output synapse density. ***A***, At 28 dpi, synaptophysin:GFP$^+$ clusters were examined in the distal domain of adult-born GCs from sensory-deprived (starting on the day of retroviral labeling) and contralateral control olfactory bulbs. Scale bars, 10 μm. ***B***, Scatter plot and mean density of SypG$^+$ clusters (clusters per micrometer) of adult-born GCs from sensory-deprived (starting on the day of retroviral labeling) and contralateral control (red and black circles, respectively) olfactory bulbs at 28 dpi (*t* test). ***C***, When sensory deprivation started after synaptic development was complete, there were no changes in the mean density of SypG$^+$ clusters (clusters per micrometer) (unilateral naris occlusion at 42 dpi and examined at 63 dpi).

Figure 4

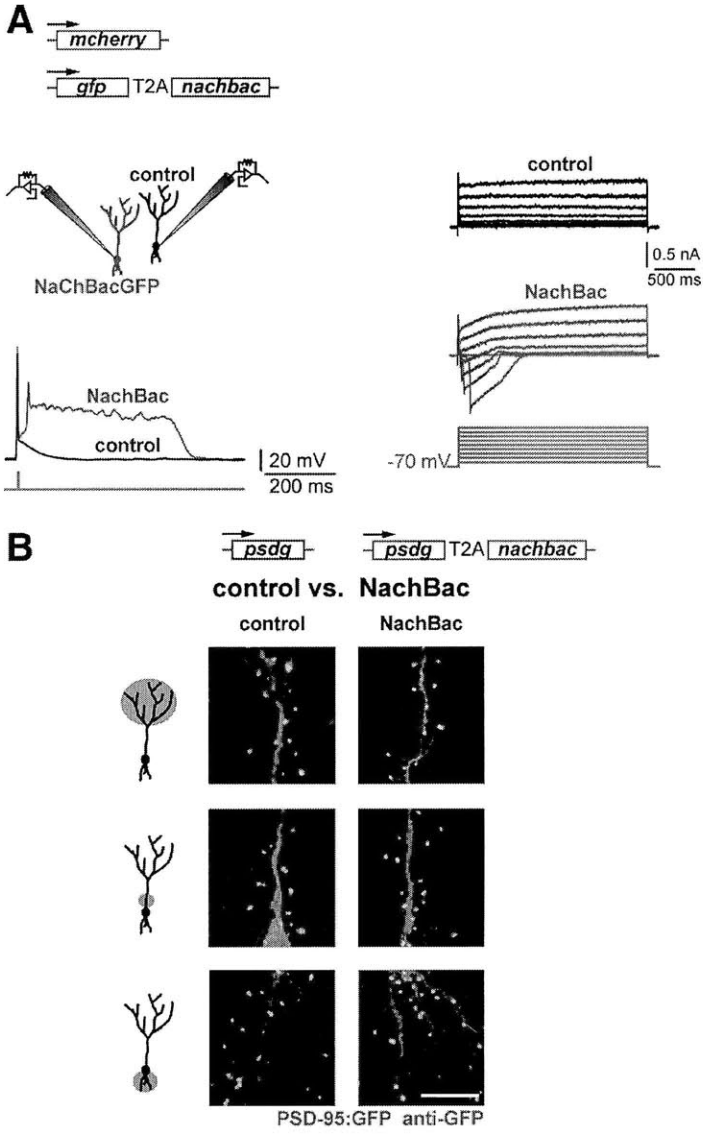

Figure 4. Genetically increased excitability does not change glutamatergic input synapse development. ***A***, Whole-cell recordings were obtained from acute slices containing GCs that either expressed mCherry as control or NaChBac:GFP. Bottom left, At 28 dpi, a short current injection (4 nA, 5 ms) evoked a sustained depolarization in NaChBac expressing GCs but not in controls of adult-born GCs. Right, The current–voltage relationship revealed a voltage-dependent inward current that was only observed in NaChBac-expressing GCs (10 mV steps, V_h = –70 mV, 16 dpi). ***B***, At 28 dpi, $PSDG^+$ clusters were examined in adult-born GCs expressing either the synaptic marker alone or with NaChBac. Scale bar, 10 μm.

Figure 5

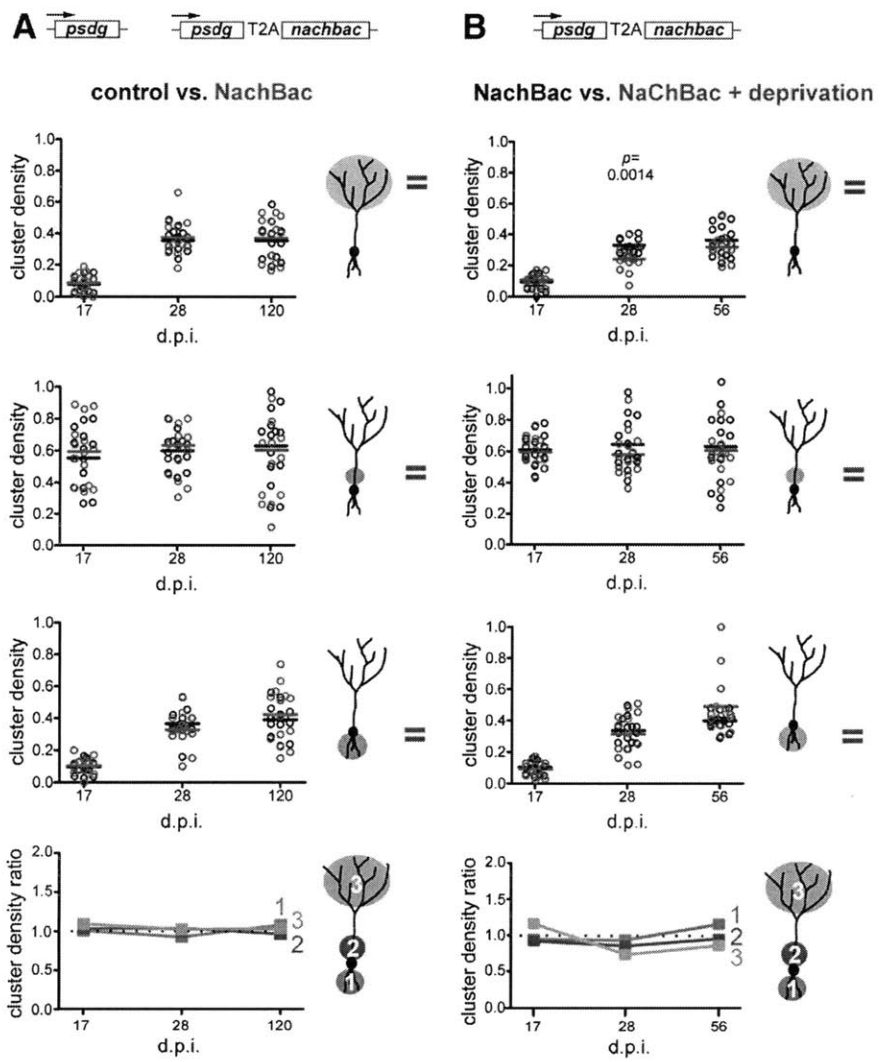

Figure 5. Genetically increased excitability does not change glutamatergic input synapse development and blocks the synaptic changes induced by sensory deprivation. ***A***, Scatter plot and mean density of $PSDG^{+}$ clusters (clusters per micrometer) in a dendritic domain of new control or NaChBac-expressing GCs (black and red circles, respectively) born in the adult and examined at different dpi. Statistical significance is only indicated if $p < 0.05$ (*t* test). The bottom graph shows the ratio of the mean cluster density of NaChBac-expressing over control GCs in a specific dendritic domain at a given day after infection. ***B***, Same as ***A***, but instead, adult-born GCs coexpressed PSD-95:GFP and NaChBac in both the sensory-deprived (starting on the day of retroviral labeling) and contralateral control olfactory bulb. Statistical significance is only indicated if $p < 0.05$ (*t* test).

Figure 6

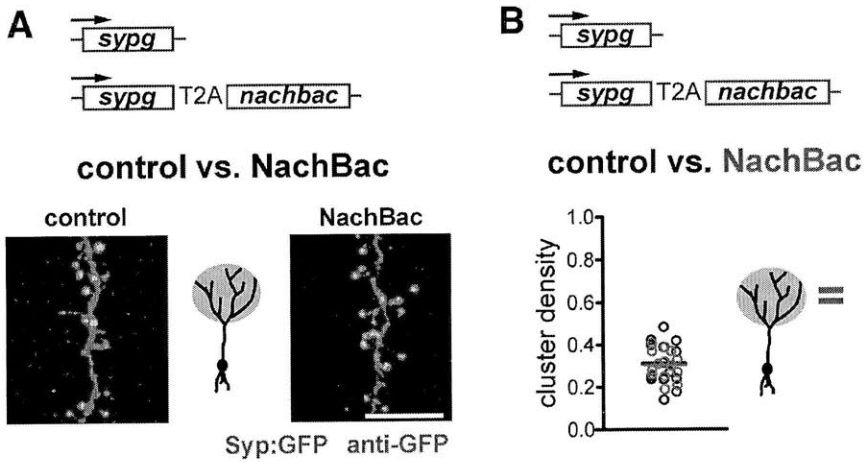

Figure 6. Genetically increased excitability does not change output synapse development. ***A***, At 28 dpi, SypG$^+$ clusters were examined in the distal domain of adult-born GCs expressing either the synaptic marker alone or with NaChBac. Scale bar, 10 μm. ***B***, Scatter plot and mean density of SypG$^+$ clusters (clusters per micrometer) of new control or NaChBac-expressing GCs (black and red circles, respectively) born in the adult at 28 dpi. No significant differences were detected (*t* test).

Figure 7

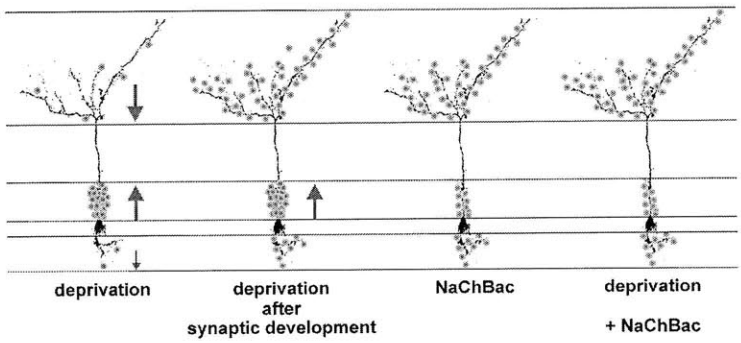

Figure 7. Sensory deprivation and intrinsic excitability differently control synaptic development in the dendritic domains of adult-born neurons. Reduced sensory input during synaptic development changed synaptic densities in all dendritic domains. When sensory deprivation started after the completion of synaptic development, the only detectable changes were increases in the density of glutamatergic input synapses in the proximal domain. Genetically increasing the excitability of new neurons did not affect the synaptic development of cells that matured in a normal sensory stimulation but rescued the synaptic changes triggered by sensory deprivation.

Chapter Five

Genetically Increased Cell-Intrinsic Excitability Enhances Neuronal Integration into Adult Brain Circuits

Chia-Wei Lin[1, 2], Shuyin Sim[1, 3], Alice Ainsworth[1, 2], Masayoshi Okada[1], Wolfgang Kelsch[1] and Carlos Lois[1, 2, 3]

[1] *Picower Institute for Learning and Memory, Massachusetts Institute of Technology, Cambridge, Massachusetts, United States of America*

[2] *Department of Brain and Cognitive Sciences, Massachusetts Institute of Technology, Cambridge, Massachusetts, United States of America*

[3] *Department of Biology, Massachusetts Institute of Technology, Cambridge, Massachusetts, United States of America*

This paper was published in *Neuron* 2010. Jan 14; 65(1)

Note: I contributed to the design, characterization, and execution of whole experiments, except **Figures 4D and 4E** that were completed by Ms. Shuyin Sim. I also have supervised MIT UROP Alice Ainsworth to collect and analyze data that was presented in **Figures 3C to 3G**.

Abstract

New neurons are added to the adult brain throughout life, but only half ultimately integrate into existing circuits. Sensory experience is an important regulator of the selection of new neurons but it remains unknown whether experience provides specific patterns of synaptic input or simply a minimum level of overall membrane depolarization critical for integration. To investigate this issue, we genetically modified

intrinsic electrical properties of adult-generated neurons in the mammalian olfactory bulb. First, we observed that suppressing levels of cell-intrinsic neuronal activity via expression of ESKir2.1 potassium channels decreases, whereas enhancing activity via expression of NaChBac sodium channels increases survival of new neurons. Neither of these modulations affects synaptic formation. Furthermore, even when neurons are induced to fire dramatically altered patterns of action potentials, increased levels of cell-intrinsic activity completely blocks cell death triggered by NMDA receptor deletion. These findings demonstrate that overall levels of cell-intrinsic activity govern survival of new neurons and precise firing patterns are not essential for neuronal integration into existing brain circuits.

Introduction

A striking feature of nervous system development is that many more neurons are produced than are ultimately retained in the mature nervous system (Buss et al., 2006). Neuronal addition persists throughout life in the dentate gyrus of the hippocampus and the olfactory bulb (OB), where there continues to be overproduction and subsequent selection of neurons ([Petreanu and Alvarez-Buylla, 2002], [Winner et al., 2002] and [Yamaguchi and Mori, 2005]). Unlike during embryonic development, neurons born postnatally are added to functionally mature circuits where their integration is believed to be regulated by sensory input or the behavioral state of the animal ([Kee et al., 2007] and [Petreanu and Alvarez-Buylla, 2002]).

It is postulated that the addition of new neurons into the adult brain may be a mechanism for lifelong learning and behavioral adaptation ([Aimone et al., 2006] and [Lledo et al., 2006]).

Since only half of adult-generated neurons ultimately survive and integrate, it has been hypothesized that only new neurons that form relevant connections are incorporated to achieve fine-tuning of existing neuronal circuits ([Aimone et al., 2006], [Alonso et al., 2006], [Kee et al., 2007], [Lledo et al., 2006], [Mouret et al., 2008] and [Wilbrecht et al., 2002]). From experiments involving sensory deprivation in the OB and ablation of the NMDA receptor in the dentate gyrus, it is clear that synaptic input is a key regulator of the integration of adult-born neurons ([Alonso et al., 2006] and [Tashiro et al., 2006a]). This idea is further supported by studies showing a preferential incorporation of adult-generated neurons into active circuits in the dentate gyrus (Kee et al., 2007). In addition, we have recently demonstrated that olfactory deprivation perturbs synaptic development of new neurons in the adult OB and that genetically increasing the intrinsic excitability of individual neurons blocks the changes in synaptic density triggered by sensory deprivation (Kelsch et al., 2009). These observations suggest an interaction between sensory input and intrinsic neuronal activity in synapse formation, and possibly neuronal survival. However, it is still unclear whether the contribution of synaptic input is mainly to provide a precise pattern of neuronal activity to the new neurons or merely a minimum level of membrane depolarization necessary for their selection and integration.

The elucidation of the mechanisms regulating the integration of new neurons has important implications both for understanding how neural circuits are constructed, as well as for successful implementation of stem cell-based replacement therapies for brain repair and neurodegenerative diseases. To evaluate the effect of suppressing or elevating electrical activity on the integration of young neurons into the OB, we used retroviral vectors to

introduce ion channels into neuronal progenitors in the brains of adult rodents. In the current study, we found that overall levels of activity within a new neuron determined its integration into the circuit irrespective of firing patterns. Moreover, increasing intrinsic activity was sufficient to partially overcome cell death induced by sensory deprivation and completely rescued neurons deficient in the NMDA receptor. Our observations reveal a rule of neuronal integration that is reliant on overall levels of membrane depolarization rather than on a specific pattern of firing.

Results

Expression of the Potassium Channel ESKir2.1 Dampens Electrical Activity in Adult-Generated Neurons

The vast majority of new neurons in the OB of adult mammals are granule cells (GCs), inhibitory neurons whose progenitors reside in the subventricular zone (SVZ) (Lois and Alvarez-Buylla, 1994). Neuroblasts generated in the SVZ move along the rostral migratory stream toward the core of the OB and subsequently migrate radially into the granule cell layers. We genetically labeled adult born GCs by injecting retroviral vectors into the SVZ of adult rats. Since retroviral vectors only infect dividing cells, the progenitor cells within the SVZ are labeled but not mature neurons. We later monitored the subsequent integration of new GCs into the OB. The first arriving neuroblasts appeared in the adult rat OB as early as at 5 dpi. By 21 dpi, migrating neuroblasts still in the RMS contributed to 7.4% of the cells in the OB. By 28 dpi, the late arriving neuroblasts contributed to less than two percent of total infected cells inside the OB. The low infectivity rate of the retroviruses in vivo results in the modification of a very small proportion of GCs (less than 0.01% of all GCs), which appear randomly distributed throughout the bulb, thus negligibly perturbing the rest of the circuit

([Kelsch et al., 2007] and [Kelsch et al., 2008]).

To accurately assess neuronal integration, we injected approximate 1:1 titers of mixtures of a virus encoding the channel under study (tagged by GFP) and a virus encoding mCherry, so that mCherry-expressing neurons could be used as age-matched controls. We divided the number of GFP^+ and doubly infected (GFP^+ and $mCherry^+$) neurons by the number of $mCherry^+$-only neurons to derive a survival ratio and used the raw 7 dpi ratio to normalize subsequent time points. Thus, the 7 dpi ratios are 1 and ratios at other time points are relative to the 7 dpi ratio.

To dampen the excitability of adult-born GCs, we expressed a nonrectifying variant of the Kir2.1 potassium channel that contains two mutations, E224S and D172N (Yang et al., 1995), henceforth referred to as ESKir2.1. Expression of ESKir2.1 resulted in a leak current that reduced the cell's input resistance by 2-fold and set a more negative resting membrane potential, thereby reducing the probability of neuronal spiking by increasing the requirement for synaptic input to achieve firing threshold (Figures 1A–1D). Expression of ESKir2.1 hyperpolarized the neuroblasts in the core of the OB as early as at 7 dpi (see Figures S1A–S1H available online) and did not affect the initial stages of development of new GCs, as $ESKir2.1^+$ GCs successfully migrated into the OB and survived as well as control neurons up till 14 dpi (Figures 1E, S2C, and S2D). This observation argues against the possibility that expression of this ion channel results in nonspecific toxic effects in the new neurons.

Dampening Electrical Activity Inhibits Integration of Adult-Generated Neurons into the OB

By 28 dpi, however, the number of $ESKir2.1^+$ neurons integrated into the OB was reduced by

57% ± 8% (***$p < 0.002$; n = 4 bulbs; Figures 1E and S2E). Interestingly, this timing coincides with a critical period for integration of newly generated GCs in the postnatal OB, between 14 and 28 dpi, during which their survival is most sensitive to olfactory deprivation (Yamaguchi and Mori, 2005). These results demonstrate an important role of neuronal activity in regulating the integration of adult-generated neurons in a cell-autonomous manner. Interestingly, spine density and the frequency of spontaneous excitatory postsynaptic current (sEPSC) were indistinguishable between control and ESKir2.1$^+$ neurons, suggesting that suppression of cell-intrinsic neuronal activity has minimal effects on synaptic development (Figures S1I–S1L). However, the amplitude of sEPSC was higher for ESKir2.1$^+$ than controls neurons at 28 dpi (Figure S1J). This increase in sEPSC amplitude may reflect the synaptic scaling previously described in activity-deprived neurons (Turrigiano and Nelson, 2004).

Expression of the Voltage-Gated Sodium Channel NaChBac Elevates Electrical Activity in Adult-Generated Neurons

Recent studies propose that adult neurogenesis serves to facilitate experience-dependent modification of neural circuits for adaptation to environmental changes ([Aimone et al., 2006] and [Wilbrecht et al., 2002]). This hypothesis suggests that the timing of synaptic inputs relative to activity in the rest of the circuit, and their source and strength would all be predicted to participate in regulating the integration of new neurons. Alternatively, integration of new neurons may simply be determined by summing overall levels of activity in a neuron during a specific critical period, regardless of its source or timing, and neurons that meet a minimum threshold are retained. To investigate these possibilities, we increased neuronal activity in individual new GCs in the OB in a manner that reduces their dependency

on synaptic input for firing and evaluated the consequences of this manipulation on neuronal integration into the OB.

To disrupt normal firing patterns and increase the occurrence of neuronal firing, such that neuronal spiking would occur with synaptic inputs that are insufficient to evoke action potentials in control neurons, we used the bacterial voltage-gated sodium channel NaChBac. Two key properties of NaChBac allow for this: first, its activation threshold is approximately 15 mV more negative than that of native sodium channels in granule neurons (Kelsch et al., 2009); second, it inactivates on the order of hundreds of milliseconds, compared to less than 1 ms in mammalian sodium channels ([Bean, 2007] and [Ren et al., 2001]). We have previously observed that NaChBac expression in GCs triggers depolarizations approximately 600 ms long (Kelsch et al., 2009). Such long depolarizations are not uncommon in neurons in the mammalian brain. For instance, cholinergic stimulation has been shown to trigger long depolarizations in several neuronal types (Fraser and MacVicar, 1996). Here, we examined whether this phenomenon also occurs in newly generated GCs. Application of carbachol, a muscarinic agonist mimicking cholinergic input, induced long after-depolarization-potentials (ADPs) in adult-born GCs (Figure 2A). These long depolarizations robustly occurred in adult-born GCs during the early (18 dpi) but not late (28 dpi) phases of their integration into the OB (Figures 2A and 2B). The ADP triggered by carbachol was completely blocked by preapplying atropine, a muscarinic receptor antagonist (Figures 2A and S2F–S2H). These findings suggest that physiological stimuli, such as cholinergic innervation, can trigger long membrane depolarizations in adult-born GCs, similar to those induced by NaChBac expression.

We delivered *NaChBac* to GC precursors in the SVZ using the strategy described for *ESKir2.1*. To assess the ability of NaChBac to enhance the intrinsic excitability of new GCs, we performed whole-cell patch clamp recordings between 14 to 16 dpi, at the beginning of their critical period for survival. At this stage, newly generated GCs expressing NaChBac-EGFP ($NaChBac^+$) have a slow inward current that activates at -41 ± 1.8 mV, which causes neurons to fire spontaneous action potentials significantly more frequently than control neurons and with long plateau potentials lasting on average 608 ± 68 ms (Figures 2D–2F). In addition, we have observed that the electrophysiological effects of NaChBac expression on GCs persist throughout the duration of the critical period (Kelsch et al., 2009). Thus, NaChBac expression is sufficient to increase overall levels of neuronal activity in newly generated GCs.

Increased Intrinsic Electrical Activity Enhances the Integration of Adult-Generated Neurons into the OB

We assessed the effect of increasing electrical excitability via NaChBac expression on the integration of adult-born GCs into the OB, and found that up till 14 dpi, $NaChBac^+$ neurons migrated and integrated into the OB at similar levels to control neurons (Figures 2G, S2A, and S2B). However, beginning at 21 dpi, $NaChBac^+$ neurons integrated into the OB at significantly higher rates than control neurons (21 dpi: $22\% \pm 6\%$; $^{**}p < 0.002$; $n = 4$ bulbs; 28 dpi: $31\% \pm 4\%$; $^{***}p < 0.0001$; $n = 10$ bulbs; Figure 2G). This increase in survival persisted for as long as 2 months after infection (56 dpi; $25\% \pm 3\%$; $^{**}p < 0.0001$; $n = 6$ bulbs). Electrophysiological measurements of sEPSCs in $NaChBac^+$ neurons indicate that they received similar levels of excitatory synaptic input as compared to control neurons,

demonstrating that the enhanced survival of NaChBac$^+$ neurons was accompanied by functional integration into the circuit (Figures 3A and 3B). Furthermore, NaChBac$^+$ neurons were morphologically similar to control neurons, with no changes in the pattern of dendritic arborization or in the linear density of synaptic spines (Figures 3C–3G). This observation is consistent with our previous finding that NaChBac does not affect the density of clusters labeled with the synaptic marker PSD95-GFP in OB GCs (Kelsch et al., 2009). These observations illustrate that NaChBac$^+$ neurons are functional and suggest that strong perturbations of cell-intrinsic neuronal activity via either NaChBac or ESKir2.1 expression have minimal effects on the synaptic development of these neurons.

Our findings suggest that increasing the overall intrinsic level of activity in an adult-born neuron is sufficient to confer a significant survival advantage to that cell but do not allow us to specify whether adult-generated neurons normally have a requirement for patterns of synaptic input specifically driven by sensory experience in order to integrate into the bulb. Multiple studies have demonstrated that sensory input is crucial for the integration of new neurons into the OB ([Alonso et al., 2006] and [Petreanu and Alvarez-Buylla, 2002]), but it remains unclear whether sensory input simply provides a minimum, necessary level of synaptic drive onto new GCs to support survival or if sensory-driven patterns of synaptic input contain information relevant to the selection of the new GC for integration.

NaChBac Rescues Adult-Generated Neurons from Death in a Sensory-Deprived OB

To further explore these questions, we tested whether a NaChBac-mediated increase in neuronal activity can substitute for physiological sensory experience in mediating the integration of adult-born neurons into the OB. We coinjected a mixture of retroviruses bilaterally into the SVZ of animals in which we had unilaterally occluded one nostril, a

procedure that eliminates sensory input to the ipsilateral bulb. Previous works have demonstrated that 50% of new neurons in the adult ultimately integrate into the normal OBs, whereas nostril occlusion further reduces this proportion to 25% ([Winner et al., 2002] and [Yamaguchi and Mori, 2005]). The survival ratio of NaChBac$^+$ neurons compared to control cells in the nonoccluded bulb was approximately 1.33, similar to that described above (Figures 2G and 2H); in contrast, in the occluded bulb this ratio was increased to approximately 1.76 (Figure 2H). Since olfactory deprivation results in approximately 50% decrease in the survival of new GCs, a complete rescue of sensory-dependent GC death by NaChBac in an occluded bulb would result in a survival ratio of 2; thus, a ratio of 1.76 indicates that NaChBac expression provides more than a 75% rescue of GC death resulting from sensory deprivation. This result demonstrates that increased neuronal excitability conferred by NaChBac expression is sufficient to partially substitute for the contribution of sensory-dependent synaptic input in regulating GC integration. This observation parallels our previous data showing that NaChBac expression blocks changes in synaptic density induced by sensory deprivation (Kelsch et al., 2009). Furthermore, this observation suggests that experience-driven synaptic input is not the only mechanism driving the selection of adult-born neurons for integration as corroborated by the finding that 25% of new neurons still survive in sensory deprived bulbs ([Petreanu and Alvarez-Buylla, 2002] and [Yamaguchi and Mori, 2005]).

NMDA Receptor Activity Is Essential for Integration of Adult-Generated Neurons in the OB

Because NaChBac promotes neuronal integration independent of experience-driven synaptic input, it is probable that the mechanism regulating activity-dependent survival is directly

tracking the levels of membrane depolarization. The membrane potential of a neuron is constantly modulated by neurotransmitters acting on synaptic receptors, and in the central nervous system, AMPA- and NMDA-receptors (NMDARs) are the major receptors mediating membrane depolarization. Previous studies have suggested that NMDAR activity regulates the survival of adult-born neurons in the dentate gyrus (Tashiro et al., 2006a). The requirement of NMDAR signaling for neuronal survival may depend on the detection of coincident pre- and postsynaptic activity, such as in spike-timing dependent plasticity (Dan and Poo, 2006), or alternatively, the requirement of NMDAR function for new neuron survival may simply reflect the contribution of NMDAR activity to overall levels of neuronal depolarization in new GCs.

To investigate the contribution of NMDAR to new neuron integration, we first sought to confirm the requirement for NMDAR function in the survival of new GCs in the OB. We genetically ablated the essential NR1 subunit to eliminate all NMDAR-mediated input in individual new GCs by sparsely infecting progenitor cells in the SVZ of *NR1* floxed conditional mice ($NR1^{fl/fl}$) with retroviral vectors encoding the Cre recombinase enzyme ([Kohara et al., 2007] and [Tashiro et al., 2006b]). Cre-mediated ablation of *NR1* successfully eliminated NMDAR expression since application of NMDA failed to induce any currents in Cre^{+} neurons in $NR1^{fl/fl}$ mice (Figures 4A–4C). By 28 dpi, virtually all NMDAR-deficient neurons were eliminated (Figures 4D and 4E). In comparison, no change in the survival of EGFP-Cre^{+} neurons was observed in $NR1^{+/+}$ littermates (Figure 4D). This result demonstrates that the NMDAR, whose ablation decreases the survival of new dentate gyrus neurons by only 50% (Tashiro et al., 2006a), is absolutely required for the integration of adult-born GCs in the OB.

NaChBac Expression Rescues NMDAR-Deficient Adult-Generated Neurons from Death

We next determined whether increasing activity in new GCs via NaChBac expression could substitute for NMDAR function in supporting neuronal integration into the OB. NaChBac and Cre recombinase were simultaneously delivered into $NR1^{fl/fl}$ mice, and GC integration was assessed. We found that increasing the excitability of newly generated NMDAR-deficient GCs via NaChBac expression completely rescued their death (Figures 4D and 4E). The dendritic morphology of NaChBac$^+$ NMDAR-deficient neurons appeared similar to that of control neurons and received AMPAR-mediated synaptic input (Figure S3), indicating that they functionally integrated into the bulb's circuit. These results demonstrate that the requirement for NMDARs in the integration of new GCs most likely reflects the contribution of NMDARs to the overall levels of neuronal activity in the neuron. Furthermore, our data support a model in which activity-dependent integration depends on overall levels of membrane depolarization, irrespective of how this depolarization is achieved.

Discussion

An Activity Threshold for Integration of New Adult-Born Neurons into the OB Circuit

To elucidate whether synaptic input regulates survival by providing new neurons with a precise pattern of neuronal activity, or merely a minimal level of membrane depolarization, we used NaChBac, a bacterial voltage-gated sodium channel, to perturb the spiking pattern of new neurons while simultaneously elevating their activity levels. Our results indicate that the integration of new neurons into the OB circuit predominantly depends on their overall levels of membrane depolarization, regardless of the pattern of action potentials generated.

Interestingly, tonic cholinergic stimulation, which causes sustained depolarizations in adult-born OB neurons during their early integration (Figures 2A–2C and S2), has recently been shown to enhance the survival of new neurons both in the OB and dentate gyrus (Kaneko et al., 2006). Conversely, the removal of cholinergic input into the OB compromises the survival of new neurons (Cooper-Kuhn et al., 2004). Given our findings about depolarization-enhanced integration, the long depolarizations induced by cholinergic stimulation may directly contribute to the improved survival of new neurons observed in previous studies (Kaneko et al., 2006). Interestingly, the long depolarizations induced by cholinergic stimulation occur robustly in young GCs during the critical period of survival at 18 dpi but not after maturation at 28 dpi, indicating a possible role of prolonged cholinergic-induced depolarization specifically in driving survival of new OB granule neurons. General behavioral states, such as running, stress, attentiveness, and depression affect neuronal integration of new neurons into adult brains ([Gould et al., 1997], [Malberg et al., 2000], [Mouret et al., 2008] and [van Praag et al., 1999]). Our results suggest that neuromodulators such as acetylcholine may mediate these effects by acting as significant regulators of the level of depolarization of new neurons.

The notion that general membrane depolarization is a determinant of neuronal integration is further supported by our observation that although NMDAR expression is essential for new neuron integration, NaChBac-mediated depolarization is sufficient to fully rescue NMDAR-deficient neurons from death. Hence, the requirement of NMDAR in new neuron survival may be due to the extended depolarization caused by its slow gating kinetics. Interestingly, recent evidence also indicates that the contribution of NMDAR for synaptic vesicle release in

GCs is not directly through the calcium entry through its pore but indirectly through the influx of calcium through voltage-gated calcium channels, which open as a result of the long depolarization induced by NMDAR activity ([Isaacson, 2001] and [Schoppa et al., 1998]). Together, our data support a model in which activity-dependent integration depends on overall levels of membrane depolarization, determined, for instance, by monitoring calcium influx through L-type voltage-gated calcium channels (Dolmetsch et al., 2001), rather than specifically on neuronal activity mediated by postsynaptic glutamate receptors.

It is not yet known how activity levels could be monitored in order to determine if a particular cell achieves the minimum threshold of neuronal activity required to survive and successfully integrate into the adult brain. New adult-born neurons could act as integrators that measure and summate levels of activity over a critical period, lasting perhaps on the time scale of days, to compute this life or death decision (McCormick, 2001). This critical period spans a time period sometime between 14 to 28 days after the birth of the neuron, when sensory deprivation or ESKir2.1-mediated suppression of activity has the strongest effect on survival (Yamaguchi and Mori, 2005). Alternatively, instantaneous levels of activity may be continuously evaluated such that neurons that never meet the minimum threshold of activity during the critical period are eliminated.

Determinants of Dendritic Morphology of GCs in the OB

When we introduced ESKir2.1 into GCs in the OB, we observed that although the electrical properties of these neurons were altered significantly, their dendritic structures remained unchanged. This is unexpected because overexpression of Kir2.1 in neurons has been

previously shown to alter the morphology of axons, in transfected retinal neurons in zebrafish (Hua and Smith, 2004), as well as dendrites, in transfected rat hippocampal neurons in vitro (Burrone et al., 2002). Two non-mutually-exclusive explanations could account for our findings. First, in previous experiments, Kir2.1 channels were expressed in excitatory neurons ([Burrone et al., 2002] and [Hua and Smith, 2004]), whereas here we specifically target inhibitory interneurons. The plasticity responses of excitatory and inhibitory neurons differ in many respects (Bi and Poo, 1998), and it is plausible that electrical silencing by Kir2.1 channels affects the morphology of excitatory, but not inhibitory neurons. Next, gene delivery methods used in previous work induce much higher levels of Kir2.1 expression than what we report here with oncoretroviral delivery. For instance, calcium-phosphate transfection of Kir2.1 into cultured hippocampal neurons lowers the neurons' input resistance from 166 ± 11 to 63 ± 25 MΩ, which corresponds to a 10,000 pS increase of Kir2.1 conductance (Burrone et al., 2002). In contrast, our oncoretroviral vector delivery of ESKir2.1 results in expression levels that only introduces 600 pS of resting leak conductance and lowers the input resistance of GCs from 1147 ± 59 to 655 ± 76 MΩ, even though neuronal firing is largely eliminated. Thus, it is possible that the changes in neuronal morphology previously reported were not solely due to reduction of neuronal excitability by Kir2.1 activity, but to additional effects resulting from very high levels of expression.

Reduction of sensory input by olfactory deprivation has been shown to modify synaptic structure of GCs (Saghatelyan et al., 2005). We have recently confirmed this observation using genetic labeling of postsynaptic glutamatergic densities with the PSD95-GFP marker (Kelsch et al., 2009). In addition, we observed that whereas NaChBac did not affect the

density of PSD95-GFP synapses in normal conditions, it blocked the synaptic changes triggered by olfactory deprivation (Kelsch et al., 2009). These observations suggest an interaction between sensory input and intrinsic membrane excitability to achieve a minimal level of neuronal activity necessary for the normal development of synapses in GCs. Our current results indicate that this principle also extends to neuronal survival, since there seems to be a minimum threshold of neuronal activity required for the integration of young GCs into the OB. This threshold level of activity can similarly be provided by a combination of synaptic input and intrinsic membrane excitability. Our experiments indicate that the elevation of intrinsic excitability via NaChBac expression is sufficient to counteract the reduction of sensory input. Reaching this minimal level of activity both rescues young GCs from death and allows them to acquire normal synaptic organization in an odor-deprived OB.

Determinants of Overall Activity Level in New Neurons

What drives overall activity levels, and hence survival of new adult-born neurons during the critical period? One feature of the critical period is that it coincides with the onset of synapse formation in GCs, and this has led previous studies to primarily focus on the role of phasic synaptic input, as regulated by sensory experience, in new neuron survival. In addition, during this critical period the intrinsic conductance (e.g., A-type potassium channels, voltage-gated sodium channels) of new neurons undergo major changes as the neurons mature. Our findings show that in addition to synaptic input, membrane conductance, as determined by the repertoire of ion channels expressed by new neurons, may play a pivotal role in regulating integration and survival. Variability in membrane conductance between neurons of the same type has been shown to be significant (Marder and Goaillard, 2006), and

fluctuations in the intrinsic excitability of young neurons could result in differing levels of synaptic input required for their survival. In addition, the intrinsic excitability of OB neurons is strongly modulated by centrifugal innervation originating from other parts of the brain. In particular, cholinergic stimulation induces long-lasting depolarizations in GCs, which facilitate persisting firing modes (Figure S2 and Pressler et al., 2007). These phenomena could account for the observation that cells rendered hyperexcitable by NaChBac expression are able to survive with reduced levels of synaptic input resulting from olfactory deprivation or NMDAR ablation. In this manner, the overall level of activity, as determined by the combination of synaptic inputs received and intrinsic membrane properties, drives integration of new neurons into a circuit.

Methods

Retroviral constructs

The cDNA for NaChBac was obtained from David Clapham (HHMI, Children's Hospital, Harvard Medical School, Boston). NaChBac E191K and Kir2.1 E224S (ESKir2.1) were generated by PCR based on previously published sequences (Taglialatela et al., 1995; Yang et al., 1995; Yue et al., 2002). Retroviral vectors were derived from a Moloney leukemia virus with an internal promoter derived from the Rous sarcoma virus (Molar) (Kelsch et al., 2007). Retroviral particles were produced and stored as previously described (Lois et al., 2002). The viral titers were approximately 106 infectious units/μl. Viral constructs were generated as follows. NaChBac-EGFP: the stop codon of NaChBac was eliminated by PCR and fused in frame to the cDNA of EGFP (Kelsch et al., 2009). NaChBac-Cre: the stop codon of the NaChBac-EGFP fusion was eliminated by PCR, and linked by a foot-and-mouth

disease (FMDV) virus 2A sequence to the cDNA of Cre. ESKir2.1-hrGFP: the cDNA of ESKir2.1 was cloned downstream from the encephalomyelocarditis (EMC) virus internal ribosomal entry site (IRES), and the IRES-ESKir2.1 cassette was subcloned downstream from the humanized recombinant GFP (hrGFP) cDNA. PalmEGFP-NaChBac: the palmitoylation sequence from the GAP43 gene was first added to the N-terminus of EGFP. The stop codon of the palmitoylated version of EGFP was eliminated by PCR and linked by a FMDV 2A picornavirus sequence to the cDNA of NaChBac. PalmEGFPIRESKir2.1: the IRES ESKir2.1 cassette was subcloned downstream from palmitoylated EGFP.

Retroviral injection into animals

8-week old female Sprague-Dawley rats (Charles River and Taconic) and 'floxed' NMDA-receptor subunit 1 mice (Tsien et al., 1996) were stereotaxically injected with 1 μl/hemisphere and 0.5μl/hemisphere of retroviral vectors respectively, after anesthesia with ketamine/xylazine solution. The stereotaxic coordinates were 1.2 mm anterior from bregma, 1.6 mm lateral from the midline, and 3.1 mm ventral from the brain surface in rats (Kelsch et al., 2009), and 1.0 mm anterior, 1.0 mm lateral and 2.3 mm ventral in mice.

Histology

Rats were over-anesthetized with isofluorane (Baxter), while mice were given an overdose of avertin, before they were perfused intracardially, first with phosphate buffer saline (PBS) and then with 3% paraformaldehyde (PFA). The bulbs were incubated with 3% PFA overnight, and cut horizontally with a Leica vibratome into 45 μm sections. For immunocytochemistry, the sections were first blocked with blocking solution containing bovine serum albumin (3 mg/ ml PBS), and 0.25% Triton X-100 in PBS, and incubated overnight with a polyclonal

rabbit anti-GFP antibody (Chemicon; AB3080) diluted 1:3000 in blocking solution. Sections were washed 4 times in PBS, for 15 min each time, before a 2-hour incubation at room temperature with Alexa Fluor® 488 or 555 goat anti-rabbit secondary antibody (Molecular Probes, catalog A11008) diluted 1:700 in blocking solution. The sections were washed 4 times in PBS, for 15 min each time, before mounting on slides with mounting medium (Gel MountTM; Sigma).

Survival ratio analysis

Two viruses were mixed at an approximate 1:1 ratio for survival analysis. One of the viruses carried the construct encoding mCherry, while the other carried one of a range of constructs: hrGFP linked to ESKir2.1 by an EMC IRES, EGFP alone, NaChBac or NaChBac E191K fused to EGFP (NaChBac-EGFP or NaChBacE191K-EGFP), and Cre Recombinase linked with the 2A linker to EGFP, NaChBac-EGFP or NaChBacE191K-EGFP (NaChBac-Cre or NaChBacE191K-Cre). Fluorescently labeled cells were quantified with the aid of the Neurolucida software (MicroBright Field Inc.). The survival ratio is defined as the total number of EGFP-positive cells (including double-labeled cells) divided by of the number of singly labeled mCherry-expressing cells. The ratio of EGFP+ to mCherry+ neurons at 7 days post infection (dpi) was used to normalize all data at subsequent time points for comparison, hence ratios at all subsequent time points were relative to the 7 dpi ratio. Three to 7 entire sections per olfactory bulb were analyzed to collect at least 400 counted cells in each bulb. The mean survival ratio from each bulb was treated as a single sample.

Morphological analysis

Viruses carrying constructs for palmitoylated EGFP connected by a FMDV 2A linker to either NaChBac or NaChBacE191K were injected separately into each SVZ in a single animal. Coronal sections 350 μm-thick were made of each olfactory bulb. The labeled neurons were imaged with a two-photon microscope (Sutter Instruments) with a 60X objective lens. Serial reconstruction and dendrite analysis was performed with the Neurolucida software by a blinded second experimenter. Confocal image stacks were taken with an Olympus Fluoview laser confocal microscope (Olympus) with a 60X objective lens, a zoom of 1.5 and at z-intervals of 0.5μm.

Nostril occlusion

The outer edges of one nostril were cauterized with a high temperature cautery tip (Bovie Aaron Change-A-TipTM) and pinched with forceps to seal together. 500 μl of tissue adhesive (VetbondTM, 3M) was dispensed onto the outer surface of the cauterized nostril as an additional seal. The effectiveness of nostril occlusion was examined 10 days after the surgery after recuperation of the cauterization wound.

Electrophysiological recordings

Animals were given an overdose of ketamine/xylazine then perfused intracardially with ice-cold slicing solution containing (in mM): 212 sucrose, 3 KCl, 1.25 NaH2PO4, 26 NaHCO3, 7 MgCl2, 10 glucose (308 mOsm, and pH 7.3). Bulbs were incubated in ice-cold cutting solution and cut horizontally into 350 μm slices with a Leica microtome at a speed of 0.08 mm/s. Slices were incubated for 30 min at 35°C, for recovery, in carbogenated recording solution containing (in mM): 125 NaCl, 2.5 KCl, 1.25 NaH2PO4, 26 NaHCO3, 1 MgCl2, 2 CaCl2, 20 glucose (312 mOsm, and pH 7.3). Fluorescent-guided whole-cell patch

clamp recordings were performed with a MultiClamp 700B amplifier (Axon Instruments). The pipette solution contained (in mM): 2 NaCl, 4 KCl, 130 K-gluconate, 10 HEPES, 0.2 EGTA, 4 Mg-ATP, 0.3 Tris-GTP, 14 Tris-phosphocreatine (pH 7.3). Successful patching onto the target cell was confirmed by identifying a fragment of fluorescent membrane trapped inside the pipette tip during or after the recording. Pipette resistance ranged from 5 to 8 MΩ, and the pipette access resistance was always less than 16 MΩ after series resistance compensation. The junction potential was not corrected throughout the study. For spontaneous EPSC (sEPSC) recording, the neuron was held at -77 mV and synaptic events were collected at 25°C. sEPSC contributed to the majority of spontaneous events because ~98% of events could be blocked by 100 μM D, L-AP-5 and 20 μM NBQX (Sigma) at the end of the recording. Inhibitory blockers such as bicuculline were not included during sEPSC recording because they triggered frequent EPSC bursting input in granule neurons, which precluded further analysis. NMDAR-mediated current was recorded with pipette solution containing (in mM): 125 Cs-Methanesulfonate, 4 CsCl, 0.2 Cs-EGTA, 2 NaCl, 10 HEPES, 4 Mg-ATP, 0.3 Na-GTP, 10 Tris-phosphocreatine, 5 QX-314, and examined by applying 100 μM NMDA in recording bath solution containing (in μM): 1 TTX, 10 NBQX, 5 Glycine, 20 BMI. It was necessary to record as late as 18 dpi since all control granule cells received NMDAR-mediated current by then. NMDAR elimination by Cre recombinase in NR1fl/fl mice was verified by patch clamp recordings only on neurons expressing both Cre recombinase and NaChBac-EGFP since the number of neurons expressing both Cre recombinase and EGFP was dramatically reduced by 18 dpi and too few surviving neurons remained for recording.

Analysis of electrophysiological data

Data was acquired and analyzed with pClamp9 software (Axon Instruments), and sEPSCs were analyzed with Mini Analysis Program (Synaptosoft Inc.). Only morphologically mature granule neurons with at least 800 pA of TTX-sensitive sodium current measured at -20 mV, and resting membrane potential more negative than -55 mV, were included in the 14 dpi and 28 dpi analyses.

Statistical analysis

The Mann-Whitney test was used for comparing the frequency of spontaneous firing in NaChBac+ and control neurons at resting membrane potential to determine statistical significance (Figure 2C). To analyze survival rates in sensory-deprived versus control bulbs, the paired Student's t-test was used since these were paired bulbs of the same animal (Figure 2E). All other data was analyzed with the two-sample two-tailed Student's t-test in OriginPro 8 (Origin Lab Corporation). Data was reported as mean ± SEM.

References

Aimone et al., 2006 J.B. Aimone, J. Wiles and F.H. Gage, Potential role for adult neurogenesis in the encoding of time in new memories, *Nat. Neurosci.* 9 (2006), pp. 723–727.

Alonso et al., 2006 M. Alonso, C. Viollet, M.M. Gabellec, V. Meas-Yedid, J.C. Olivo-Marin and P.M. Lledo, Olfactory discrimination learning increases the survival of adult-born neurons in the olfactory bulb, *J. Neurosci.* 26 (2006), pp. 10508–10513.

Bean, 2007 B.P. Bean, The action potential in mammalian central neurons, *Nat. Rev. Neurosci.* 8 (2007), pp. 451–465.

Bi and Poo, 1998 G.Q. Bi and M.M. Poo, Synaptic modifications in cultured hippocampal neurons: dependence on spike timing, synaptic strength, and postsynaptic cell type, *J. Neurosci.* 18 (1998), pp. 10464–10472.

Burrone et al., 2002 J. Burrone, M. O'Byrne and V.N. Murthy, Multiple forms of synaptic

plasticity triggered by selective suppression of activity in individual neurons, *Nature* 420 (2002), pp. 414–418.

Buss et al., 2006 R.R. Buss, W. Sun and R.W. Oppenheim, Adaptive roles of programmed cell death during nervous system development, *Annu. Rev. Neurosci.* 29 (2006), pp. 1–35.

Cooper-Kuhn et al., 2004 C.M. Cooper-Kuhn, J. Winkler and H.G. Kuhn, Decreased neurogenesis after cholinergic forebrain lesion in the adult rat, *J. Neurosci. Res.* **77** (2004), pp. 155–165.

Dan and Poo, 2006 Y. Dan and M.M. Poo, Spike timing-dependent plasticity: from synapse to perception, *Physiol. Rev.* **86** (2006), pp. 1033–1048.

Dolmetsch et al., 2001 R.E. Dolmetsch, U. Pajvani, K. Fife, J.M. Spotts and M.E. Greenberg, Signaling to the nucleus by an L-type calcium channel-calmodulin complex through the MAP kinase pathway, *Science* **294** (2001), pp. 333–339.

Fraser and MacVicar, 1996 D.D. Fraser and B.A. MacVicar, Cholinergic-dependent plateau potential in hippocampal CA1 pyramidal neurons, *J. Neurosci.* **16** (1996), pp. 4113–4128.

Gould et al., 1997 E. Gould, B.S. McEwen, P. Tanapat, L.A. Galea and E. Fuchs, Neurogenesis in the dentate gyrus of the adult tree shrew is regulated by psychosocial stress and NMDA receptor activation, *J. Neurosci.* **17** (1997), pp. 2492–2498.

Hua and Smith, 2004 J.Y. Hua and S.J. Smith, Neural activity and the dynamics of central nervous system development, *Nat. Neurosci.* **7** (2004), pp. 327–332.

Isaacson, 2001 J.S. Isaacson, Mechanisms governing dendritic gamma-aminobutyric acid (GABA) release in the rat olfactory bulb, *Proc. Natl. Acad. Sci. USA* **98** (2001), pp. 337–342.

Kaneko et al., 2006 N. Kaneko, H. Okano and K. Sawamoto, Role of the cholinergic system in regulating survival of newborn neurons in the adult mouse dentate gyrus and olfactory bulb, *Genes Cells* **11** (2006), pp. 1145–1159.

Kee et al., 2007 N. Kee, C.M. Teixeira, A.H. Wang and P.W. Frankland, Preferential incorporation of adult-generated granule cells into spatial memory networks in the dentate gyrus, *Nat. Neurosci.* **10** (2007), pp. 355–362.

Kelsch et al., 2007 W. Kelsch, C.P. Mosley, C.W. Lin and C. Lois, Distinct mammalian precursors are committed to generate neurons with defined dendritic projection patterns, *PLoS Biol.* **5** (2007), p. e300

Kelsch et al., 2008 W. Kelsch, C.W. Lin and C. Lois, Sequential development of synapses in dendritic domains during adult neurogenesis, *Proc. Natl. Acad. Sci. USA* **105** (2008), pp. 16803–16808.

Kelsch et al., 2009 W. Kelsch, C.W. Lin, C.P. Mosley and C. Lois, A critical period for activity-dependent synaptic development during olfactory bulb adult neurogenesis, *J. Neurosci.* **29** (2009), pp. 11852–11858.

Kohara et al., 2007 K. Kohara, H. Yasuda, Y. Huang, N. Adachi, K. Sohya and T. Tsumoto, A local reduction in cortical GABAergic synapses after a loss of endogenous brain-derived neurotrophic factor, as revealed by single-cell gene knock-out method, *J. Neurosci.* **27** (2007), pp. 7234–7244.

Lledo et al., 2006 P.M. Lledo, M. Alonso and M.S. Grubb, Adult neurogenesis and functional plasticity in neuronal circuits, *Nat. Rev. Neurosci.* 7 (2006), pp. 179–193.

Lois and Alvarez-Buylla, 1994 C. Lois and A. Alvarez-Buylla, Long-distance neuronal migration in the adult mammalian brain, *Science* 264 (1994), pp. 1145–1148.

Malberg et al., 2000 J.E. Malberg, A.J. Eisch, E.J. Nestler and R.S. Duman, Chronic antidepressant treatment increases neurogenesis in adult rat hippocampus, *J. Neurosci.* **20** (2000), pp. 9104–9110.

Marder and Goaillard, 2006 E. Marder and J.M. Goaillard, Variability, compensation and homeostasis in neuron and network function, *Nat. Rev. Neurosci.* **7** (2006), pp. 563–574.

McCormick, 2001 D.A. McCormick, Brain calculus: neural integration and persistent activity, *Nat. Neurosci.* **4** (2001), pp. 113–114.

Mouret et al., 2008 A. Mouret, G. Gheusi, M.M. Gabellec, F. de Chaumont, J.C. Olivo-Marin and P.M. Lledo, Learning and survival of newly generated neurons: when time matters, *J. Neurosci.* **28** (2008), pp. 11511–11516.

Petreanu and Alvarez-Buylla, 2002 L. Petreanu and A. Alvarez-Buylla, Maturation and death of adult-born olfactory bulb granule neurons: role of olfaction, *J. Neurosci.* **22** (2002), pp. 6106–6113.

Pressler et al., 2007 R.T. Pressler, T. Inoue and B.W. Strowbridge, Muscarinic receptor activation modulates granule cell excitability and potentiates inhibition onto mitral cells in the rat olfactory bulb, *J. Neurosci.* **27** (2007), pp. 10969–10981.

Ren et al., 2001 D. Ren, B. Navarro, H. Xu, L. Yue, Q. Shi and D.E. Clapham, A prokaryotic voltage-gated sodium channel, *Science* **294** (2001), pp. 2372–2375.

Saghatelyan et al., 2005 A. Saghatelyan, P. Roux, M. Migliore, C. Rochefort, D. Desmaisons, P. Charneau, G.M. Shepherd and P.M. Lledo, Activity-dependent adjustments of the inhibitory network in the olfactory bulb following early postnatal deprivation, *Neuron* **46** (2005), pp. 103–116.

Schoppa et al., 1998 N.E. Schoppa, J.M. Kinzie, Y. Sahara, T.P. Segerson and G.L.

Westbrook, Dendrodendritic inhibition in the olfactory bulb is driven by NMDA receptors, *J. Neurosci.* **18** (1998), pp. 6790–6802.

Tashiro et al., 2006a A. Tashiro, V.M. Sandler, N. Toni, C. Zhao and F.H. Gage, NMDA-receptor-mediated, cell-specific integration of new neurons in adult dentate gyrus, *Nature* **442** (2006), pp. 929–933.

Tashiro et al., 2006b A. Tashiro, C. Zhao and F.H. Gage, Retrovirus-mediated single-cell gene knockout technique in adult newborn neurons in vivo, *Nat. Protoc.* **1** (2006), pp. 3049–3055.

Turrigiano and Nelson, 2004 G.G. Turrigiano and S.B. Nelson, Homeostatic plasticity in the developing nervous system, *Nat. Rev. Neurosci.* **5** (2004), pp. 97–107.

van Praag et al., 1999 H. van Praag, G. Kempermann and F.H. Gage, Running increases cell proliferation and neurogenesis in the adult mouse dentate gyrus, *Nat. Neurosci.* **2** (1999), pp. 266–270.

Wilbrecht et al., 2002 L. Wilbrecht, A. Crionas and F. Nottebohm, Experience affects recruitment of new neurons but not adult neuron number, *J. Neurosci.* **22** (2002), pp. 825–831.

Winner et al., 2002 B. Winner, C.M. Cooper-Kuhn, R. Aigner, J. Winkler and H.G. Kuhn, Long-term survival and cell death of newly generated neurons in the adult rat olfactory bulb, *Eur. J. Neurosci.* **16** (2002), pp. 1681–1689.

Yamaguchi and Mori, 2005 M. Yamaguchi and K. Mori, Critical period for sensory experience-dependent survival of newly generated granule cells in the adult mouse olfactory bulb, *Proc. Natl. Acad. Sci. USA* **102** (2005), pp. 9697–9702.

Yang et al., 1995 J. Yang, Y.N. Jan and L.Y. Jan, Control of rectification and permeation by residues in two distinct domains in an inward rectifier K^+ channel, *Neuron* **14** (1995), pp. 1047–1054.

Figure 1

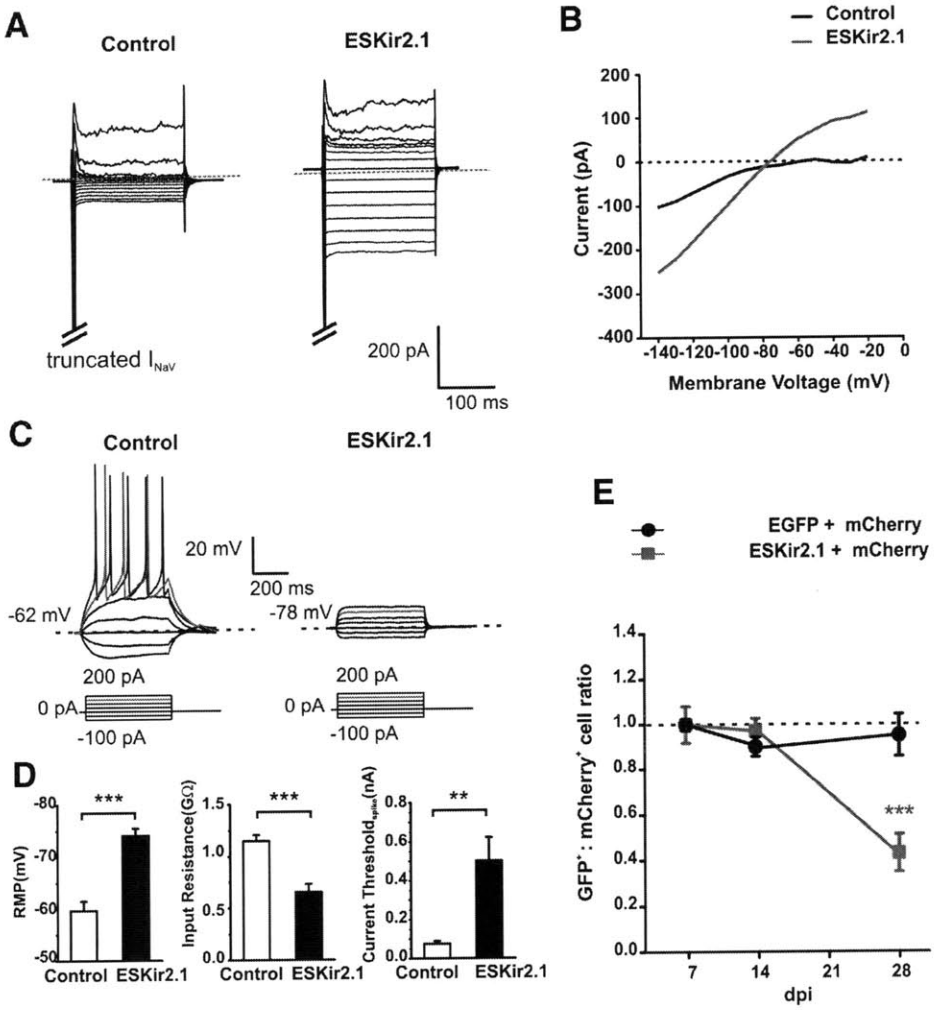

Figure 1. Decreased Intrinsic Neuronal Activity via ESKir2.1 Expression Compromises the Survival and Integration of Adult-Generated Neurons

(A) Current-voltage relationship in control (mCherry$^+$) and ESKir2.1$^+$ neurons. Neurons were clamped at −70 mV and stepwise voltage was applied from −140 to 0 mV.

(B) ESKir2.1$^+$ neurons displayed larger steady-state leak currents than control neurons.

(C) The amount of current sufficient to trigger action potentials in control neurons (left) was below the threshold necessary to elicit action potentials in new neurons expressing ESKir2.1 (right).

(D) Relative to control neurons at 16-18 dpi, ESKir2.1 expression hyperpolarized neurons by 14 ± 2.4 mV (left, $^{***}p < 0.000003$; n = 13 neurons), decreased their input resistance by 492 ± 100.3 MΩ (center, $^{***}p < 0.0002$; n = 11 neurons) and increased the minimal amount of current required to reach spiking threshold by 0.427 ± 0.13 nA (right, $^{**}p < 0.004$; n = 10 neurons).

(E) Normalized survival ratios (number of $EGFP^+$ cells, including double-labeled cells, divided by the number of singly labeled $mCherry^+$ cells, normalized to the 7 dpi value) of $ESKir2.1/hrGFP^+$ and $EGFP^+$ neurons. By 28 dpi, $ESKir2.1^+$ neurons survived significantly less well than control neurons (red line; $-56\% \pm 12\%$; $n = 4$ bulbs each group; $^{**}p < 0.002$) while EGFP did not have an effect (black line; $p < 0.636$; $n = 4$ bulbs).
Two-tailed t test used for statistical analysis. Error bars represent SEM. See also Figure S1.

Figure 2

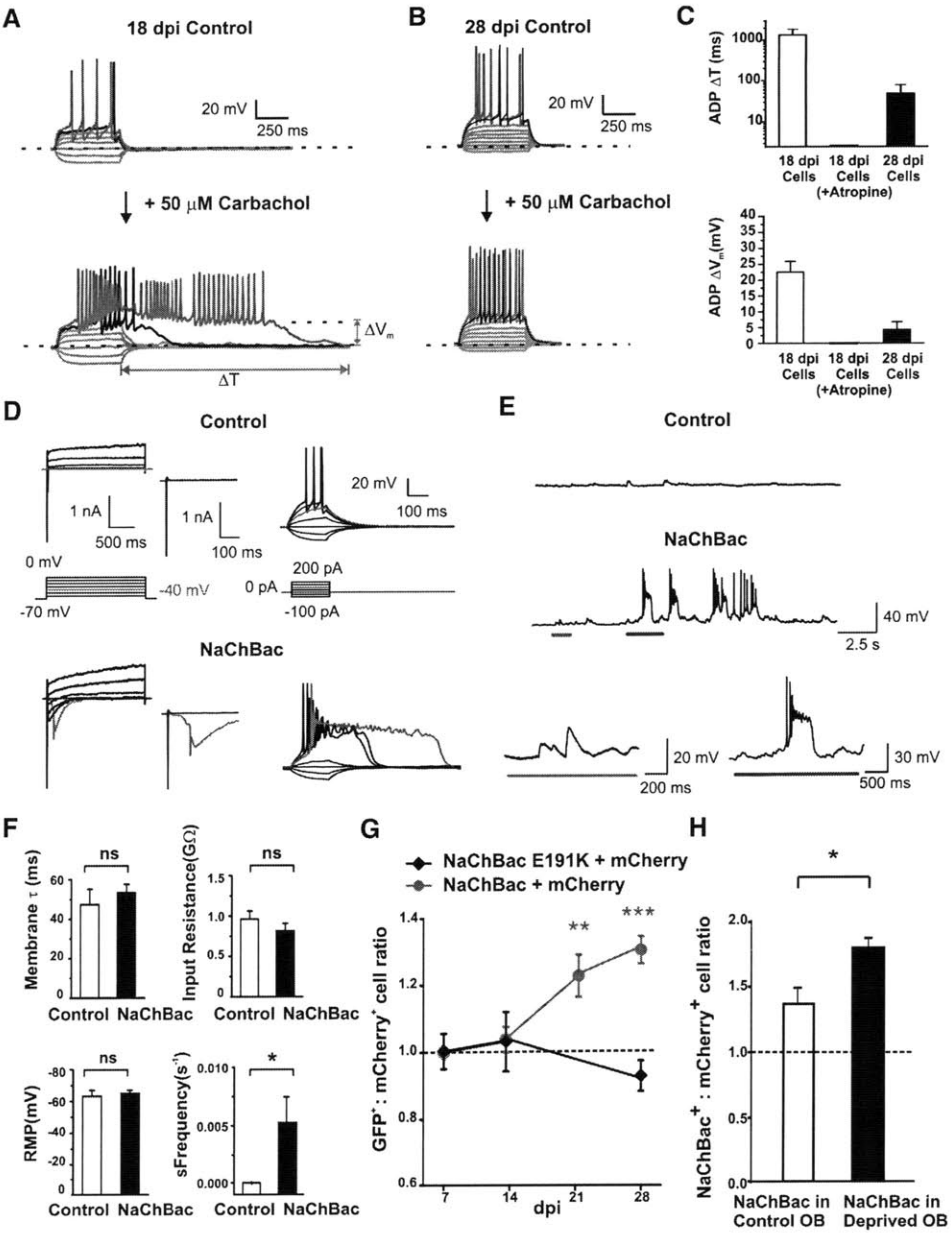

Figure 2. Increased Intrinsic Neuronal Activity via NaChBac Expression Enhances the Survival of Adult-Generated Neurons

(A) Carbachol induced a long-lasting after-depolarization-potential (ADP) in 18 dpi GCs. Additionally, carbachol increased spike numbers upon suprathreshold stimulation.

(B) Carbachol enhanced membrane excitability of 28 dpi GCs by increasing spike numbers upon suprathreshold

stimulation but did not induce the long ADP observed at 18 dpi.

(C) (Upper panel) The after-depolarization-potential (ADP) induced by carbachol was much longer in 18 dpi than in 28 dpi neurons. (Lower panel) The amplitude of ADP induced by carbachol was significantly larger in 18 dpi than in 28 dpi neurons.

(D) (Upper left and center) At 18 dpi, control neurons ($mCherry^+$) recorded in voltage-clamp mode displayed > 2 nA of voltage-sensitive sodium inward current at −20 mV, but none at −40 mV (red trace). In contrast, $NaChBac^+$ neurons (red trace, lower left and center) had a 762 ± 119 pA slow inward current opening at −41 ± 1.8 mV (n = 6 neurons) and >2 nA of inward current at −20 mV. In current-clamp mode (right), a 200 ms pulse of positive 150 pA current injection generated repetitive action potentials in control neurons (upper right), whereas repetitive action potentials with sustained depolarization (608 ± 68 ms, n = 6 neurons) were induced in $NaChBac^+$ neurons (red trace, lower right).

(E) In current-clamp mode, control neurons (top trace) did not fire action potentials, while NaChBac expression resulted in spontaneous, repetitive firing at resting membrane potential (middle trace). A closer look at the NaChBac trace (bottom left) shows that $NaChBac^+$ neurons received functional synaptic inputs as indicated by frequent spontaneous synaptic events. These neurons fired action potentials mediated by endogenous sodium channels riding atop NaChBac-mediated depolarization (bottom right).

(F) All passive electrical properties in $NaChBac^+$ neurons remained similar to control neurons except for a significantly higher rate of spontaneous firing (NaChBac, 0.02 ± 0.007 Hz; control, 0.004 ± 0.004 Hz; $^*p < 0.01$; Mann-Whitney test; n = 6 neurons in each group).

(G) Cell survival ratios of neurons with increased intrinsic excitability. $NaChBac^+$ neurons survived significantly better than control neurons at 21 dpi (red line; 22 ± 6%; n = 4 bulbs; $^{**}p < 0.001$) and 28 dpi (31 ± 4%; n = 10 bulbs; $^{***}p < 0.0001$). The nonconducting mutant NaChBac E191K (black line) did not alter survival.

(H) NaChBac increased the relative survival of adult-generated neurons by a significantly larger factor in the sensory-deprived compared to the nondeprived OB (42% ± 14%; $^*p < 0.05$; n = 4 deprived bulbs, n = 4 control bulbs; paired sample t test).

Two-tailed t test used for statistical analysis. Error bars represent SEM. See also Figure S2.

Figure 3

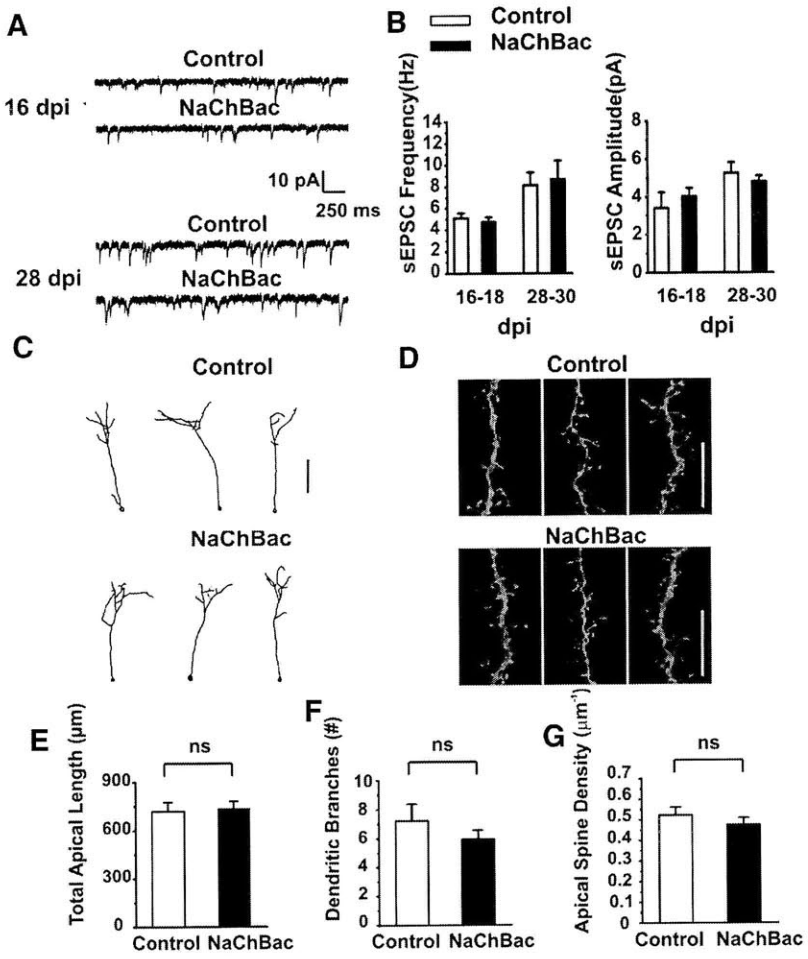

Figure 3. NaChBac$^+$ Neurons Receive Normal Synaptic Input and Display Identical Morphological Characteristics as Wild-Type Neurons

(A) Spontaneous excitatory postsynaptic current (sEPSC) was recorded in NaChBac$^+$ or mCherry$^+$ neurons at 16 and 28 dpi.

(B) NaChBac$^+$ neurons had similar sEPSC frequency and amplitude to control neurons in both the early (16–18 dpi) and late phase (28–30 dpi) of the critical period for survival.

(C) Three-dimensional Neurolucida reconstructions of representative granule neurons. Scale bar represents 100 μm.

(D) Confocal images showing representative dendrite sections. Scale bars represent 20 μm.

(E–G) NaChBac$^+$ neurons in the OB did not display altered apical length ($p < 0.78$; $n = 20–25$ neurons per group) (E), dendritic branching ($p < 0.39$; $n = 14–16$ neurons per group) (F), or apical spine density ($p < 0.33$; $n = 8–10$ neurons per group) (G).
Two-tailed t test used for statistical analysis. Error bars represent SEM.

Figure 4

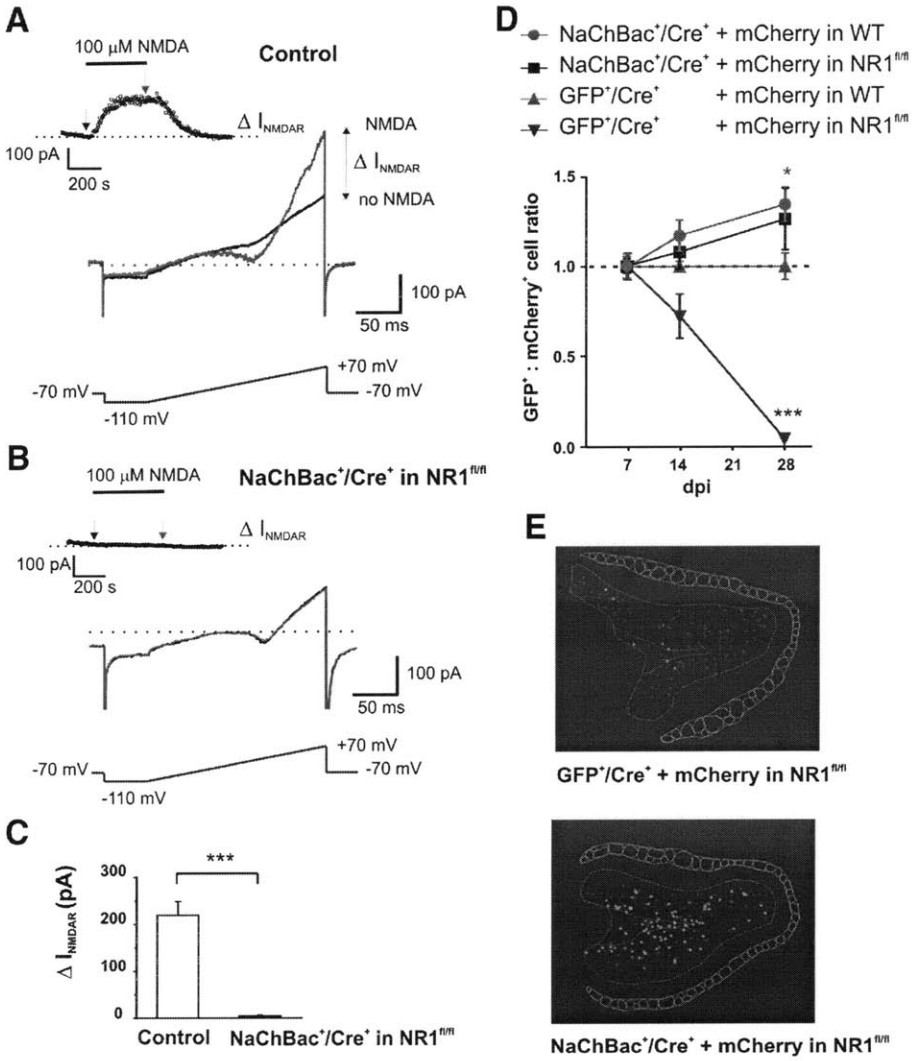

Figure 4. Increased Intrinsic Neuronal Activity Protects NMDAR-Deficient Neurons from Death

(A) Application of 100 μM NMDA activated NMDAR-mediated currents measured at +70 mV in a single control neuron (mCherry$^+$) at 18 dpi (inset). The voltage ramp protocol, from −110 to +70 mV, performed before (black arrow) and during NMDA application (red arrow) showed characteristics of outward-rectifying NMDA currents (red trace) evoked by 1 mM Mg^{2+} present in bath solution.

(B) Expression of the NaChBac-Cre construct completely eliminated NMDAR-mediated currents as examined by application of 100 μM NMDA (inset). The I-V curve remained unchanged before (black trace) and after (red trace) NMDA application.

(C) 100 μM NMDA application elicited 220 ± 29 pA NMDAR-mediated current in 18 dpi control neurons but none in neurons expressing the NaChBac-Cre construct (n = 4 neurons in each group).

(D) Survival rates of control (EGFP/Cre in WT), $NR1^{-/-}$ (EGFP/Cre in $NR1^{fl/fl}$), NaChBac$^+$ (NaChBac/Cre in WT) and $NR1^{-/-}$ NaChBac$^+$ neurons (NaChBac/Cre in $NR1^{fl/fl}$) in the OB. As expected, NaChBac$^+$ neurons survived significantly better than control at 28 dpi in wild-type OBs (red circles; 34.64% ± 12.17%; $^{*}p < 0.05$; n = 5 bulbs). NMDAR-deficient neurons were completely eliminated by 28 dpi (blue triangles; −96.3% ± 0.1%; $^{***}p < 0.0001$; n = 3 bulbs) but survived as well as control neurons when they expressed NaChBac (black squares; $p < 0.1290$; n = 5 bulbs).

(E) Neurolucida trace images showing representative distributions of EGFP$^+$ and mCherry$^+$ cells within representative OB sections at 28 dpi.

Two-tailed t test used for statistical analysis. Error bars represent SEM. See also Figure S3.

Supplemental Figures

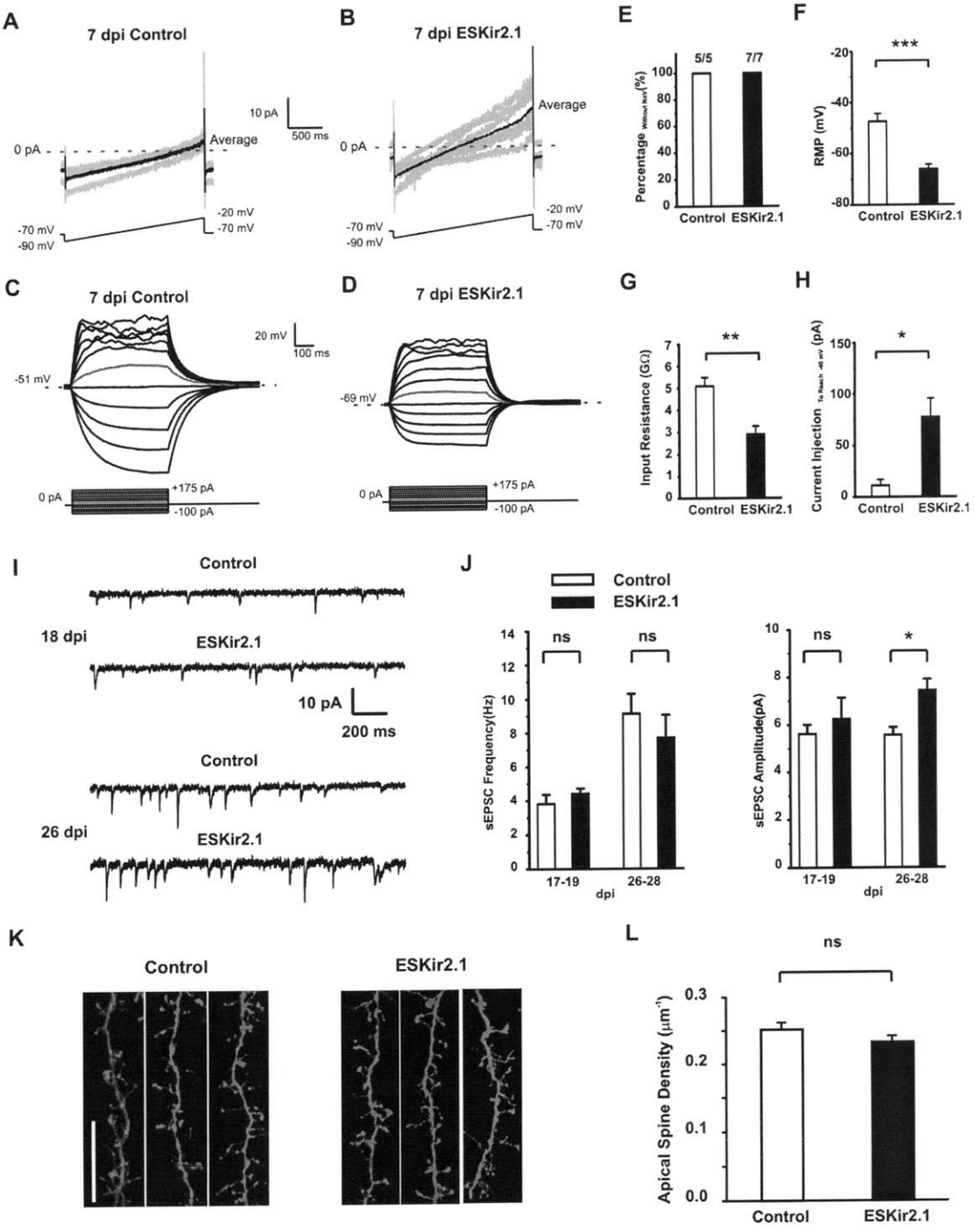

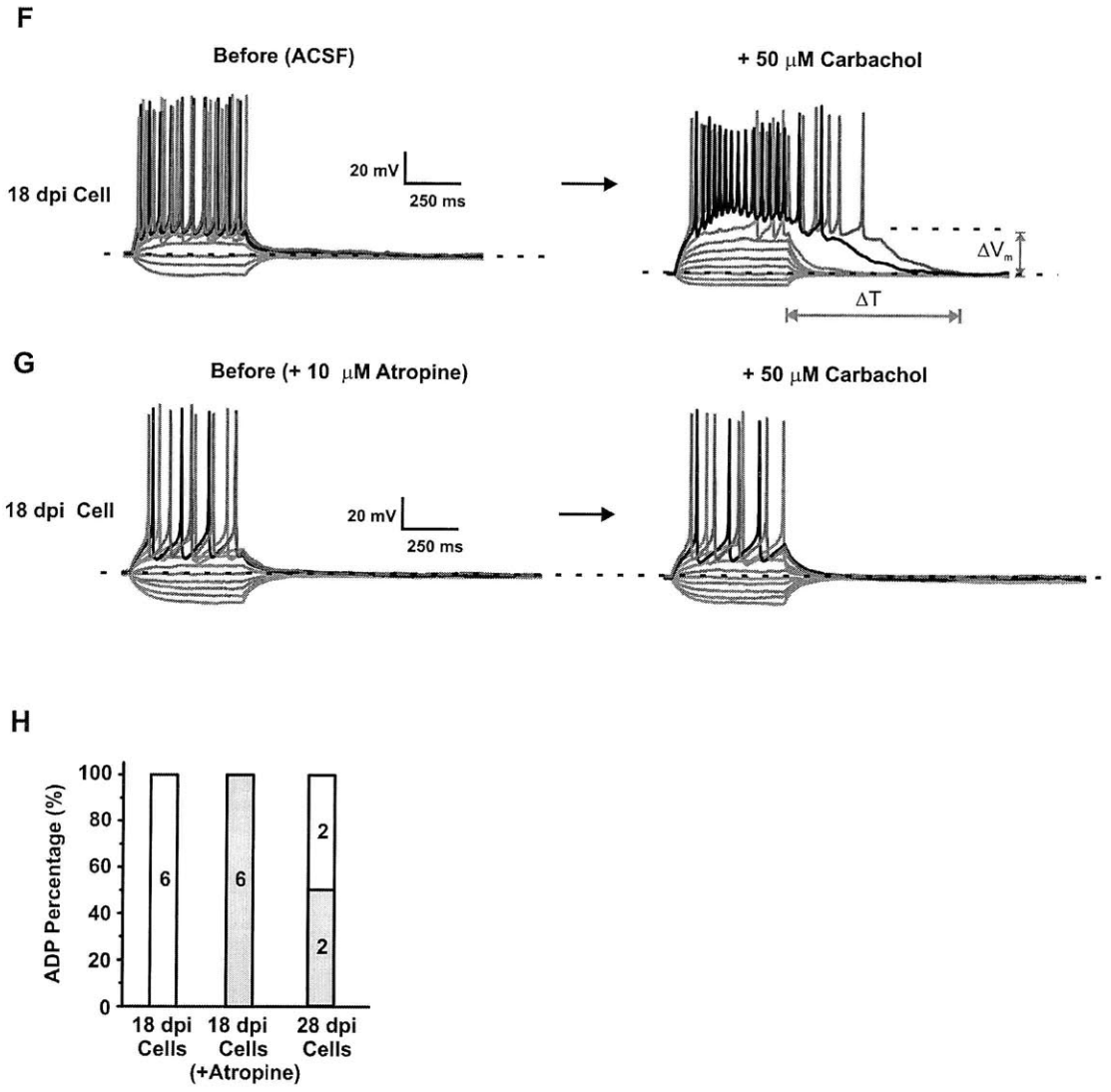

Figure S1. Expression of ESKir2.1 hyperpolarizes 7 dpi neuro blasts in the OB.

(A and B) Leak currents in 7 dpi neuroblasts measured by sweeping the membrane voltage from -90 to -20 mV at a rate of 35 mV/sec. Control neuroblasts (A) had significantly lower levels of linear leak currents than ESKir2.1$^+$ neuroblasts (B). (C and D) Representative traces showing membrane potential changes in response to current injection in control (C) and ESKir2.1$^+$ (D) neuroblasts. ESKir2.1$^+$ neuroblasts were hyperpolarized and required larger current injection to depolarize to levels of membrane potential similar to those of control neuroblasts. (E) At 7 dpi, neither control nor ESKri2.1$^+$ neuroblasts had voltage-gated sodium currents. (F) ESKir2.1$^+$ neuroblasts were more hyperpolarized and (G) had lower input resistances than control neuroblasts. (H) To reach -40 mV, ESKir2.1$^+$ neuroblasts required 70 pA more of current injection than control neuroblasts. Error bars indicate SEM.

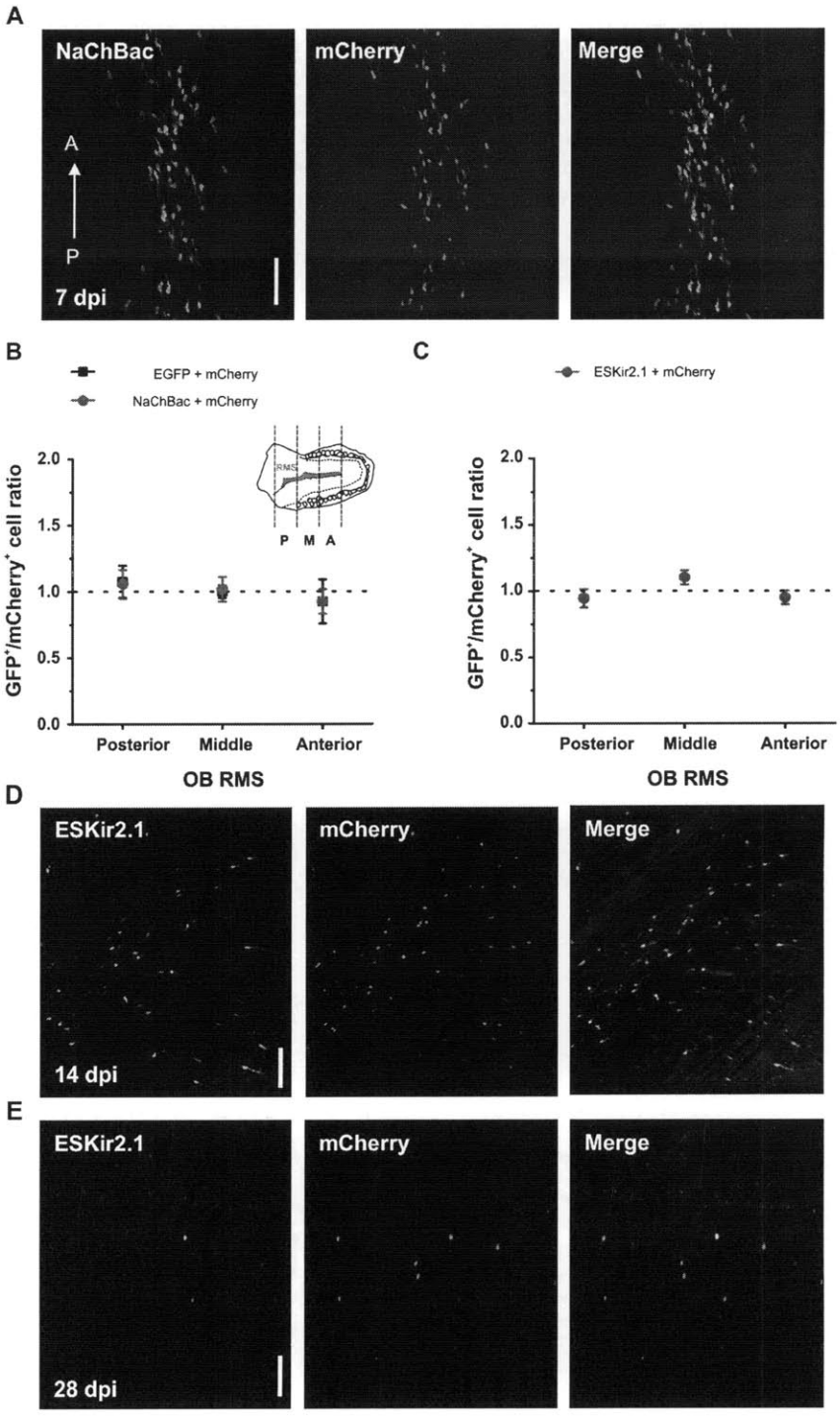

Figure S2. Expression of either ESKir2.1 or NaChBac does not alter the distribution of migrating neuroblasts within the rostral migratory stream (RMS).

(A) Confocal images showing the distribution of migrating NaChBac$^+$ and mCherry$^+$ neuroblasts in the RMS within the OB at 7 dpi. "A" and "P" indicate the anterior and posterior sections of the bulb, respectively. Scale bar represents 100 μm. (B) EGFP$^+$/mCherry$^+$ cell ratios in the posterior, middle, and anterior portions of the RMS remain unchanged by expression of NaChBac at 7 dpi (n = 6-12 bulb sections in each group). "A", "M" and "P" indicate the anterior, middle and posterior regions of the bulb, respectively. The regions are defined as three equal parts that divide the entire population of migrating neuroblasts in horizontal OB sections at 7 dpi when >99% of neuroblasts are located within the RMS (diagram). (C) Expression of ESKir2.1 did not change the migration pattern of neuroblasts at 7 dpi (n = 14 bulb sections). (D) Images showing the distribution of ESKir2.1$^+$ and mCherry$^+$ cells within the OB at 14 dpi. Scale bar represents 100 μm. (E) Images showing the distribution of ESKir2.1$^+$ and mCherry$^+$ cells in the OB at 28 dpi. Scale bar represents 100 μm.

Two-tailed t-test used for statistical analysis. Error bars indicate SEM.

Chapter Six

A Subthreshold Set Point for the Regulation of Excitability in Olfactory Bulb Granule Neurons

Chia-Wei Lin[1, 2], Masayoshi Okada[1], Dimitri Porcelli[2, 3] and Carlos Lois[1, 2]

[1] *Picower Institute for Learning and Memory, Massachusetts Institute of Technology, Cambridge, Massachusetts, United States of America*

[2] *Department of Brain and Cognitive Sciences, Massachusetts Institute of Technology, Cambridge, Massachusetts, United States of America*

[3] *Department of Nuclear Engineering, Massachusetts Institute of Technology, Cambridge, Massachusetts, United States of America*

This paper is under review in *Neuron*

Note: I contributed to the design, characterization, and execution of whole experiments and implementation of simulation. Dr. Masayoshi Okada developed the viral constructs that express different Kir2.1 variants. I also have supervised MIT UROP Dimitri Porcelli to collect and analyze data that was presented in **Figure 7**.

Abstract

How neurons achieve and maintain their characteristic electrical properties remains unknown. Here, we explore this question by altering the resting membrane potential (RMP) of newly generated granule neurons (GCs) during their integration into the olfactory bulb *in vivo*. Genetically depolarizing GCs caused an up-regulation of A-type potassium currents and reduced their excitatory synaptic inputs, thereby restoring their membrane excitability to control levels. In contrast, genetically hyperpolarizing new neurons led to hyperexcitability. Hyperpolarized neurons implemented

compensatory changes in ion channels that restored their membrane excitability near the RMP, although these changes led to increased firing rates. Combined experimental and computational approaches reveal that neurons use compensatory mechanisms to maintain their electrical properties preferentially in the regime of subthreshold voltages. Moreover, our results indicate that in new GCs compensatory changes in intrinsic membrane and synaptic properties correlate with their RMP, regardless of their firing rates.

Introduction

What are the cellular parameters that neurons monitor to achieve their characteristic excitability? It is generally believed that the rate of action potentials is the signal monitored by neurons to regulate their excitability (Burrone and Murthy, 2003; Marder and Goaillard, 2006; Turrigiano, 2008). According to this model, homeostasis in neurons is often compared to a negative feedback electronic design in which the rate of action potentials is constantly compared with a predetermined set point. Neurons can use the difference between both values to adjust their intrinsic membrane and synaptic properties so that the firing rate occurs within an operational range (Davis, 2006). By implementing this negative feedback, neurons could presumably ensure optimal input-output relationships, which is critical to the stability of brain function (Davis, 2006; Marder and Goaillard, 2006; Turrigiano and Nelson, 2004). The models inspired by firing rates as an activity set point for neurons have provided a fruitful framework towards understanding how neurons adjust their excitability upon perturbations of activity (Davis, 2006; Marder and Goaillard, 2006; Turrigiano, 2008).

However, most of these studies have been performed on rhythmically firing neurons, or on neurons with high firing rates (higher that 1 Hz) (Burrone et al., 2002), and it is not known if firing rates are also used as a set point to monitor and adjust the excitability of sparsely firing neurons (Shoham et al., 2006). Furthermore, we have recently observed that genetically enhancing the intrinsic excitability of new granule cells (GCs) in adult rat olfactory bulb (OB) increased their survival (Lin et al., 2010) and, despite having increased spontaneous firing rates, these neurons did not alter their passive membrane and synaptic properties as they integrated into the OB circuit (Lin et al. 2010). This observation suggests that some neurons may monitor parameters other than firing rates to regulate their excitability in the face of activity changes *in vivo*.

Here we investigate the parameters used by GCs, a sparsely spiking neuronal type, to regulate their excitability as they integrate into the circuits of the OB. OB GCs are generated from neuronal progenitor cells residing in the subventricular zone (SVZ). From their origin in the SVZ, young GCs, migrate via the rostral migratory stream (RMS) towards the OB where they mature, form synaptic contacts, and become integrated (Carleton et al., 2003; Lois and Alvarez-Buylla, 1994). In OB GCs, synaptic inputs causes frequent membrane depolarizations in the subthreshold membrane potential range but these depolarizations rarely give rise to spikes. As a result, the firing rates of these neurons are very low (Cang and Isaacson, 2003; Wellis and Scott, 1990). Given their low firing rates, we hypothesized that these neurons may use deviations from their characteristic RMP to monitor changes of membrane excitability.

To test this hypothesis, we genetically depolarized young GCs with a dominant-negative Kir2.1 channel, which suppressed the endogenous inwardly-rectifying potassium

currents that normally regulate the RMP of GCs. Genetically depolarizing neurons caused an increase in their rapidly inactivating A-type potassium current (I_A). Upregulation of I_A in these cells restored their membrane responses in the regime of subthreshold voltages such that the current necessary to elicit action potentials was similar between genetically depolarized and control neurons. In contrast, when we genetically lowered the RMP of GCs by overexpressing Kir2.1, an inwardly rectifying K^+ channel, we observed that despite being chronically hyperpolarized, these genetically modified neurons had high spontaneous firing rates in contrast to the very low firing rates of wild type GCs. This paradoxical hyperactivity arose because genetically hyperpolarized neurons down-regulated their endogenous leak potassium current (I_{Leak}). Downregulation of I_{Leak} in these neurons restored the wild type membrane potential responses in the regime of subthreshold voltages close to the RMP, but strongly reduced the amount of current required to elicit action potentials, which led to markedly elevated spontaneous firing rates. In addition to these compensatory changes of intrinsic potassium conductances, genetically modified neurons also bidirectionally modified their excitatory synaptic inputs, whose amplitude was inversely related to the values of their RMP, regardless of the firing rates of the neurons. These observations indicate that these neurons use compensatory mechanisms to preferentially maintain their properties in the regime of subthreshold voltages, albeit these changes can disrupt their firing rates.

Results

Genetic depolarization of new neurons in the olfactory bulb via expression of DNK, a dominant-negative Kir2.1 channel

To devise a genetic strategy that would allow us to alter the RMP of new GCs, we first surveyed the endogenous ionic conductances that regulate it. By performing fluorescence-guided whole-cell patch clamp recordings of mature GCs (at 28 days post injection (dpi)), we identified an endogenous inwardly rectifying potassium current that contributed to maintaining the RMP of GCs. Low concentrations of Ba^{2+} (100 μM) suppressed this endogenous current and raised the RMP of 28 dpi GCs by 4±0.7 mV (Figure S1). The biophysical properties of this current are consistent with the potassium current mediated by the family of inwardly rectifying Kir2.1, Kir2.2 and Kir2.3 potassium channels (Panama and Lopatin, 2006). Therefore, genetically reducing the levels of Kir2.x current could be used as an effective strategy to depolarize GCs. To test this hypothesis, we expressed a non-conducting mutant Kir2.1 potassium channel (henceforth referred to as DNK) in GCs, which acted as a dominant negative mutant by associating with the native Kir2.x channels, blocking their current, and thereby suppressing the endogenous inwardly rectifying potassium current (Preisig-Muller et al., 2002). We delivered a cDNA encoding both GFP and DNK linked by an internal ribosomal entry site (IRES) sequence into the GC progenitors residing in the SVZ via oncoretroviral vectors. In addition, we co-injected a second virus encoding the red fluorescent protein mCherry to label age-matched control neurons. The bulbs of the injected animals thus contained two populations of neurons, DNK^+ GCs, which also expressed GFP, and $mCherry^+$ cells (Figures 1A and 1B). This strategy allowed for whole-cell recordings of both groups of neurons in the same brain sections to minimize animal-to-animal variability.

By 28 dpi, expression of DNK reduced endogenous Ba^{2+}-sensitive inwardly-rectifying currents by 68±8 percent (n=13; p=0.0004; Figures 1C to 1E) and depolarized

neurons by 5.5±1.2 mV (n=25; p=0.005; Figure 1F), as compared to control neurons. The expression of DNK did not affect the expression level of non-rectifying potassium conductances, such as the background linear leak current (I_{Leak}, red curve), demonstrating the specificity of this genetic manipulation (Figure 1G), and supporting the assumption that the Kir2.x potassium channel family contributes to endogenous inwardly-rectifying currents found in control neurons (Figure 1C).

Neurons increase I_A to oppose genetically induced chronic depolarization

Despite being significantly more depolarized than control neurons, DNK^+ neurons required similar amount of current injection to reach the spike threshold (Figure 1H). This observation suggests that these cells may have up-regulated endogenous outward conductances that cancel out the consequences of chronic depolarization. To explore this possibility, we investigated potassium conductances that can operate at subthreshold voltages (Marder and Goaillard, 2006). Previous studies have found that OB granule cells express A-type Kv4.2 potassium channels, which mediate I_A, a rapidly inactivating potassium current that opens at subthreshold voltages (Kollo et al., 2008; Schoppa and Westbrook, 1999). Given the prominent role of I_A in regulating the subthreshold membrane excitability of many neuronal types (Hoffman et al., 1997) we investigated whether I_A may be used to compensate for the chronic depolarization caused by DNK expression in GCs. We used voltage protocols to isolate I_A while blocking neurotransmitter receptors and other ion channels with a cocktail of antagonists (Figure 2A). These experiments revealed that DNK^+ neurons increased their I_A density by 79±19 percent compared with control neurons (n=16-20; at -40 mV; p=0.004; Figures 2B, 2C and S2A). In contrast, expression of DNK did not change the expression level of I_{DR}, a voltage-gated potassium current that opens above the spike threshold (Figure

S2B). These results indicate that the increase in I_A was a specific response to the genetically induced depolarization mediated by DNK expression.

In addition to the increased amplitude of I_A in DNK^+ neurons, we also found a positive 5 mV shift in inactivation probability of this current (Figure 2D). The combined higher amplitude and the positive shift of the inactivation curve resulted in higher availability of I_A in DNK^+ than in control neurons in the subthreshold regime between -60 and -20 mV (Figure 2E). Therefore, the increased availability of I_A in DNK^+ neurons suggests that this current should have a stronger dampening effect on the genetically modified neurons than in controls. To test this hypothesis, we used 4-aminopyridine (4-AP; 5 mM) to selectively block I_A (Hoffman et al., 1997; Schoppa and Westbrook, 1999) and studied its influence on the excitability of DNK^+ neurons. Before applying 4-AP, control and DNK^+ neurons required similar amount of current injection to reach the first spike threshold (Figures 2F to 2I). However, blocking I_A revealed that DNK cells relied on this current to curb their excitability more strongly than control neurons, because 4-AP reduced the current levels necessary for eliciting spikes by 144±25 pA (n=9) in DNK^+ neurons in contrast with 50±15 pA (n=9) reduction in control neurons (Figures 2G and 2I). These observations indicate that DNK^+ neurons up-regulated I_A, a conductance that operates in the regime of subthreshold voltages, to offset the effects of chronic depolarization caused by expression of DNK.

Overexpression of KIR, a wild type Kir2.1 channel, hyperpolarizes neurons

To further explore the signals monitored by GCs to adjust their excitability, we investigated whether the compensatory changes in the repertoire of ion channels observed in DNK cells was bidirectional. Thus, we genetically hyperpolarized these neurons by over-

expressing the potassium channel Kir2.1 (henceforth referred to as KIR; Figure 3A). Expression of KIR channels in GCs increased inwardly-rectifying potassium current with biophysical properties similar to endogenous Kir2.x current (Figures 3B, S3E, and S3F). In immature GCs at 12 dpi, expression of KIR lowered the RMP of GCs by 18±2 mV (n=9; Figure 3C), lowered their resting input resistance, and reduced their membrane excitability, such that they required 50 pA more positive current than control neurons to trigger first spikes (Figures 3C, S3A, and S3B).

New GCs start forming synapses around 12 dpi, and they complete their maturation after 21 dpi. At 28 dpi, once GCs are fully mature, the RMP was still lower in KIR^+ cells than in control cells (Control: -67±1.3 mV; KIR^+ GCs: -72±0.7 mV; Figure 3D). Surprisingly, 41 percent (17 out of 41 neurons) of mature KIR^+ neurons spiked spontaneously despite being hyperpolarized, which was in stark contrast with control neurons that never spiked spontaneously in slice recordings (25 out of 25 neurons; Figures S4A and S4B). In addition, some KIR^+ neurons (7 out of 17 spontaneously firing neurons; Figure 3F inset and S4C) displayed bursts of sodium spikes on top of a plateau potential, an electrical behavior never observed in control neurons. In some neuronal types, lowering the RMP can de-inactivate cation channels, and this could lead to hyperexcitabily. However, this scenario did not account for the hyperexcitability of KIR^+ neurons because injecting negative current to hyperpolarize control neurons failed to make them more excitable (data not shown).

Hyperpolarization induced by KIR affects synaptic currents

The increased spontaneous spikings observed in KIR^+ neurons suggested that compensatory changes had occurred to counteract the hyperpolarization imposed by KIR

expression. First, we investigated whether increases in the excitatory synaptic input to KIR^+ GCs could account for their enhanced spontaneous firings (Burrone et al., 2002; Davis, 2006; Nelson and Turrigiano, 2008). We measured spontaneous excitatory postsynaptic synaptic currents (sEPSC) and found a small increase (15%) of sEPSC amplitude and no increase of sEPSC frequency in KIR^+ neurons as compared to control neurons (Figures S4D and S4E). However, the amount of positive current required to trigger an action potential in control neurons is 200 pA, which is 28 times larger than the average amplitude of sEPSC (data not shown), indicating that the modest increase in sEPSC amplitude observed in KIR^+ cells cannot account for the spontaneous firings in KIR^+ neurons. Thus, we investigated whether changes in intrinsic membrane properties could explain the paradoxical hyperexcitability of KIR^+ neurons.

Changes in intrinsic membrane properties are responsible for the hyperexcitability of KIR^+ neurons

We examined the intrinsic membrane properties of KIR^+ neurons in the absence of glutamatergic synaptic inputs (by AP-5 and NBQX). Unexpectedly, the current injection necessary to trigger first spikes was reduced by 72±16 pA (n=16; p=0.02) in KIR^+ neurons despite being more hyperpolarized than control neurons (Figure 4A and 4B). Furthermore, subthreshold current injection produced a linear change in the membrane potential of control neurons, but an outwardly rectifying membrane potential response in KIR^+ neurons (Figure 4A). Namely, whereas the electrical responses of KIR^+ and control neurons were similar close to the RMP, current injection induced larger membrane depolarizations in KIR^+ than in control neurons as cells approached their firing threshold. We found that this nonlinear membrane potential response evoked by the subthreshold current injection in KIR^+ neurons

was due to a slowly developing depolarization. Namely, upon positive current injection, the membrane potential of KIR^+ cells did not reach the steady state as quickly as control neurons; instead, it continued to depolarize slowly (gray line; Figure 4A). In addition, KIR^+ neurons also developed an after-depolarization plateau potential (ADP) that decayed slowly back to the RMP after 500 ms of current injection (red line; Figure 4A), which did not occur in control neurons (n=10). This ADP explained why in some KIR^+ neurons had frequent bursts of spikes (Figures 3F and 3G) because once KIR^+ neurons reached the spiking threshold, this ADP would sustain the depolarization phase above the threshold and allowed for multiple spikes to occur. Therefore, hyperpolarizing young neurons by expressing KIR triggered changes in their intrinsic membrane properties such that they required less current to reach threshold, which rendered mature KIR^+ neurons intrinsically more excitable than control neurons (Figures 4A and 4B).

KIR^+ neurons reduce the linear I_{Leak} to restore their membrane responses in the subthreshold regime

Both the slowly developing depolarization and ADP detected in KIR^+ neurons in the absence of synaptic inputs suggest that this genetic manipulation had triggered specific changes in their intrinsic conductances (Figure 4A). The slowly developing depolarization and ADP observed in KIR^+ neurons were likely due to changes in conductances that open at subthreshold voltages, either by increasing depolarizing currents or, alternatively, by decreasing hyperpolarizing currents. To investigate the first possibility, we used specific blockers to test the potential involvement of persistent sodium channels (TTX), calcium-activated nonselective cation channels (niflumic acid), voltage-gated T-type (Ni^+) or L-type calcium channels (Nifedipine) (Egger et al., 2003; Pressler et al., 2007). However, blocking

all of these channels did not prevent either slowly developing depolarization or ADP (data not shown). We next investigated the alternative possibility that the slowly developing depolarization and ADP could result from reduced hyperpolarizing conductances that operate at subthreshold voltages. We studied the background linear leak current (I_{Leak}) because I_{Leak} accounted for the majority of subthreshold outward current at 28 dpi GCs (red trace, Figure 1C), and this leak current was previously found to be subject to homeostatic regulation in cerebellar granule cells *in vivo* (Brickley et al., 2001).

We measured I_{Leak} in the presence of blockers that inhibited synaptic inputs (AP-5, NBQX and picrotoxin), voltage-gated calcium (Nifedipine, Ni^{2+}), and sodium channels (TTX). In the presence of blockers, the remaining measured current mainly consisted of two conductances mediated by I_{Leak} and $I_{Kir2.x}/I_{KIR}$. We used a voltage protocol that swept the membrane voltage from -140 to -20 mV to measure their amplitudes. After blocking synaptic inputs, and voltage-gated calcium and sodium channels, we observed that the inward current was significantly larger in KIR^+ than in control neurons in the voltage range between -140 and -100 mV, consistent with a higher expression level of I_{KIR} (Figure 4C). The current amplitude of KIR^+ neurons was very similar to control neurons at voltages between -100 to -50 mV. Interestingly, this current became much smaller in KIR^+ neurons than in control from -50 to -20 mV (Figures 4C, S3B and S3C). Because inwardly-rectifying channels are mostly closed around -30 mV, the main active conductance around this voltage range is I_{Leak}. This observation suggests that the reduced current observed in KIR^+ neurons between -50 to -20 mV is likely caused by a decrease of endogenous I_{Leak} (Figures 4C and S3C). To examine this possibility, we used 100 μM Ba^{2+} to block Ba^{2+}-sensitive inwardly-rectified currents (mediated both by endogenous Kir2.x and exogenously added KIR) to measure the I_{Leak},

because I_{Leak} is only inhibited by concentrations of Ba^{2+} in the mM range (Goldstein et al., 2001). Indeed, blocking inwardly-rectifying currents by 100 μM Ba^{2+} revealed the Ba^{2+}-insensitive linear current (I_{Leak}) whose amplitude was markedly reduced in KIR^+ GCs compared to control cells (Figure 4D; n=13; 84±9% at -40 mV; p= 0.0007 or 58±7% at -20 mV; p=0.00003).

To gain further insight about the influence of I_{Leak} on the excitability of neurons in the presence of background synaptic input, we blocked inwardly rectifying channels with 200 μM Ba^{2+} (Figure 4E). Upon removing inwardly rectifying current (mediated by both endogenous Kir2.x and exogenous KIR) with 200 μM Ba^{2+}, the resting input resistance of KIR^+ neurons was markedly reduced (579±88 pS), they depolarized by 19.2±2.3 mV, and, as a consequence, their firing rates were dramatically increased (Figures 4E and 4F; n=9-11). By contrast, blocking endogenous inwardly rectifying current by Ba^{2+} in control neurons produced a small depolarization (6.5±0.8 mV; n=7), which triggered spontaneous firings only in one out of 7 neurons (Figure 4F). This result indicates that hyperpolarizing young neurons by KIR overexpression triggered a compensatory reduction of endogenous I_{Leak} in KIR^+ neurons (Figure 4D). I_{Leak} has a strong control on the excitability of normal GCs and because KIR^+ neurons have reduced I_{Leak}, blocking $I_{Kir2.x}/I_{KIR}$ by applying Ba^{2+} strongly raised their RMP and increased their firing rates.

The level of the resting membrane potential bidirectionally regulates A-type potassium channels

Our experiments with KIR demonstrated a significant reduction of I_{Leak} induced by hyperpolarization. However, our observation that depolarizing neurons with DNK triggered a

strong compensatory increase of I_A, suggested that I_A could also be regulated by the status of the RMP. To test this hypothesis, we examined I_A in KIR$^+$ neurons and found that in addition to reducing I_{Leak}, these neurons also reduced their endogenous I_A by approximately 50 percent (Figure S2A). Notably, mature KIR$^+$ neurons were more excitable than control neurons and spontaneously exhibited increased firing rates (Figures 3 and 4). If cells evaluated their probability of spiking to regulate their I_A, one would expect that KIR$^+$ neurons, which required less current than control neurons to reach the spike threshold, would have higher levels of I_A. However, despite the enhanced excitability of KIR$^+$ neurons, I_A was reduced in these cells, suggesting that the regulation of I_A might not be responsive to their higher firing rates. Instead, the values of I_A correlated well with a subthreshold parameter, namely the value of RMP in control, DNK$^+$, and KIR$^+$ neurons (Figure S2). These observations suggest that GCs monitor their subthreshold RMP as a strategy to regulate their I_A.

Reduction of I_{Leak} and I_A restores subthreshold membrane potential responses in KIR$^+$ neurons

Hyperpolarization mediated by KIR expression triggered a reduction of I_{Leak} and I_A currents that accounted for the increased probability of spontaneous firing in these neurons. However, these changes were not consistent with a compensatory mechanism that aims to preserve normal firing rates of GCs, because reducing I_{Leak}, a linear conductance, to compensate for the addition of exogenously added I_{KIR}, anonlinear conductance, led to hyperexcitability (Figures 2C, 2D and S3D). Rather, it seemed more likely that reducing I_{Leak} and I_A was a compensatory mechanism to restore the membrane potential responses of KIR$^+$ neurons in the subthreshold range. To test this hypothesis, we studied the subthreshold membrane responses of KIR$^+$ neurons to current injection in the absence of synaptic inputs,

sodium and calcium spikes. In current-clamp mode, control neurons had a linear membrane response curve to current injection (Figures 5A and 5C), which was expected from the constant conductance slope of I_{Leak} at these voltages (Figure 4C). However, we found that some KIR^+ neurons had a non-linear membrane potential response (58%; n=12; Figures 5B and 5D). This heterogeneous membrane response among KIR^+ neurons likely arose from different expression levels of exogenous KIR between individual neurons, which triggered I_{Leak} compensation to different extents (Figure S3F). Overall, the membrane responses of KIR^+ neurons were sigmoid-like, with values similar to control neurons at voltages between -75 to -55 mV, but dramatically different from control neurons above -55 mV (Figures 5C to 5E). These data suggest that KIR^+ neurons reduced their I_{Leak} and I_A to restore their subthreshold membrane responses to match those of wild-type neurons near the RMP (Figure 5E). However, the responses of KIR^+ neurons deviated greatly from control values towards the voltages approaching the spike threshold, thereby strongly increasing the probability that KIR^+ neurons would spontaneously fire frequent action potentials (Figures 3E to 3H).

Computer simulation supports that reducing I_{Leak} renders KIR^+ neurons hyperexcitable

To quantify to what extent the reduction of I_{Leak} and I_A caused by KIR expression rendered these neurons hyperexcitable we used a computational approach. We modeled individual GCs with two compartments, soma and dendrite, and incorporated species of ion channels identified from previous works and ours into the model (Inoue and Strowbridge, 2008). Because kinetics of both slowly developing depolarization and ADP found in KIR^+ neurons are relatively slow compared to that of I_A, this suggested that it was unlikely that I_A was involved in these membrane responses. Therefore, in our subsequent models, we changed the weight of the two other conductances described in our experiments, I_{Leak} (G_{Leak};

a linear current) and I_{Kir} (G_{Kir}; a non-linear current) that was contributed both by endogenous Kir2.x and exogenous KIR channels. Thus, we studied how decreasing I_{Leak} in KIR^+ model neurons affected their excitability (Figures 6B and 6C). In addition, we set the exogenous G_{Kir} four-fold higher than endogenous G_{Kir}, based on the expression level of exogenous KIR from our experimental measurements (Figure S3F). As expected, without compensatory reduction of G_{Leak}, increasing G_{Kir} enhanced the outward current and dampened the excitability of model granule neurons (Figures 6B and 6C). When G_{Leak} was reduced by 50 % in the model, the total outward current ($G_{Leak} + G_{Kir}$) of KIR^+ model neurons was comparable to that of control neurons between -90 and -60 mV. However, reducing G_{Leak} in KIR^+ model neurons strongly decreased their total outward current ($G_{Leak} + G_{Kir}$) between -60 and -40 mV (Figure 6B). Moreover, once G_{Leak} was reduced by more than 50% in KIR^+ model neurons, the subthreshold membrane response started to become nonlinear, which eventually made KIR^+ model neurons more excitable than control cells (Figure 6C, 6D, and 6E). In KIR^+ model neurons, a 50 to 75 percent reduction of G_{Leak} approximated the excitability of control model neurons at voltages between -70 and -55 mV (Figures 6D and 6E). Because the slope of membrane potential response curve (or gain) increased steeply above -55 mV in KIR^+ model neurons, this nonlinear change rendered these model neurons more excitable than controls (Figure 6E). Taken together, our simulation supports the notion that the paradoxical hyperexcitability of KIR^+ neurons is due to the restoration of membrane responses in the subthreshold regime by reducing G_{Leak}.

This simple model explains several features of our experimental data. First, the behavior of KIR^+ model neurons matched that of KIR^+ neurons when G_{Leak} was reduced by 50 to 75 percent (Figure 6D). This calculated reduction in G_{Leak} matched well with the

observed 54 percent reduction I_{Leak} found in recordings of KIR^+ neurons (Figure 4D). Second, the model accounts for the occurrence of both the slowly developing depolarization and ADP in KIR^+ neurons (Figure 6D), both features that rendered KIR^+ neurons' membrane properties hyperexcitable. In control model neurons, the linear G_{Leak} curbed their excitability in the voltage regimes close to spiking threshold (-55 to -30 mV). However, in model KIR^+ neurons with a reduced G_{Leak}, the slope of membrane potential responses (or gain) abruptly became steeper when passing above -55 mV, as the inwardly rectifying KIR closed towards these voltages (Figure 6B). This computational model supports our experimental results and suggests that KIR^+ neurons attempt to match the intrinsic membrane properties of control neurons in the subthreshold regime that is near the RMP although this leads to runaway hyperexcitability (Figure 3F).

Correlation between RMP and synaptic input amplitude

We observed that genetically modified GCs, in addition to compensatory changes in their intrinsic membrane properties, also displayed synaptic changes, which correlated well with the values of RMP. As mentioned previously, KIR^+ neurons, which were hyperactive albeit hyperpolarized, had increased the amplitude of their sEPSC by 15% (Figures 7A and 7C). These changes can be interpreted as a compensatory mechanism to restore the RMP, since the increase of sEPSC amplitude would tend to raise the RMP in hyperpolarized cells such as KIR^+ neurons. In contrast, DNK^+ neurons, which were depolarized, reduced their sEPSC amplitude and frequency by 19±5% and 61±3%, respectively (Figures 7B and S5A). Thus, in DNK^+ neurons, reducing their excitatory synaptic inputs would counteract the higher RMP imposed by DNK expression. In summary, the changes of sEPSC amplitude seemed to

be consistent with a homeostatic principle that uses the RMP as a set point, but it did not correlate with firing rates.

We also examined whether hyperpolarizing or depolarizing neurons would alter the structure of synaptic spines located in the GC's apical dendrites, their most abundant source of synaptic input (Figure 7D). We classified these apical spines into three groups based on their diameters, as defined previously (Knott 2009). Interestingly, hyperpolarizing or depolarizing neurons with KIR and DNK, respectively, did not change the total spine density of apical dendrites, but changed the ratios of the 3 different classes of spines (Figure 7D to 7H). Neurons hyperpolarized via KIR expression had reduced densities of the smaller (53%), yet increased densities of the larger (96%), class 3 spines. In contrast, in neurons depolarized by DNK had a trend to increase the density of their smaller spines, as compared to control neurons (Figure 7F). Larger spines are believed to contain more synaptic receptors, and interestingly, the morphological changes observed in the dendritic spines of genetically manipulated neurons correlated well with the amplitude of synaptic inputs (Figure 7C and 7H). In summary, these observations suggest that the value of the RMP may determine the size of excitatory synaptic inputs.

Because KIR^+ neurons, although hyperpolarized, were more excitable than control neurons, it remained unclear whether the increase of sEPSC amplitude and density of bigger spines resulted from hyperpolarization or hyperexcitability. To further distinguish these possibilities, we expressed a mutant potassium channel herein named ESK that imparts a prominent linear outward conductance at all membrane potentials, thus strongly hyperpolarizing and dampening the excitability of neurons (Lin et al. 2010; Figure S5).

Like KIR^+ neurons, ESK^+ neurons also reduced their endogenous I_{Leak} (Figure S5). However, because ESK showed no rectification, ESK^+ neurons were always hypoexcitable by requiring 300 pA more positive current to elicit spikes than controls (Figure S5B and S5C). Interestingly, ESK^+ neurons had sEPSC whose amplitude was 40 percent larger than control neurons and increased the density (181%), of bigger, class 3 spines, strongly supporting the hypothesis that the values of RMP regulate synaptic properties such as sEPSC amplitude (Figure 7A and 7C) and spine morphology (Figure 7D to 7H). If the RMP is lowered (as in ESK^+ or KIR^+ neurons), cells increase the amplitude of their sEPSCs and the number of their large synaptic spines. In contrast, if the RMP is raised (as in DNK^+ neurons), cells reduce the amplitude of their sEPSC and increase the number of their small synaptic spines. Thus, these observations indicate that the synaptic changes observed in ESK^+ and KIR^+ neurons is a result of lowering the RMP, because it occurred in neurons that were hyperpolarized regardless of whether their firing rates were increased (KIR^+) or abolished (ESK^+).

Discussion

A subthreshold set point for the regulation of excitability in olfactory bulb granule neurons

By altering the resting membrane potential of olfactory bulb granule neurons, we discovered that the subthreshold membrane properties act as a set point to determine the excitability in this neuronal type. Furthermore, neurons whose electrical properties were genetically manipulated restored their excitability in the range of subthreshold voltages by

changing the repertoire of key potassium conductances, although these changes significantly altered their probability of firing action potentials. This regulation mechanistically differs from previously described forms of homeostatic plasticity in neurons that monitored firing rates as a set point to adjust their excitability (Marder and Goaillard, 2006; Turrigiano and Nelson, 2004).

What could account for the existence of two different modes of homeostatic compensation, one that monitors firing rates and another that monitors subthreshold membrane properties to adjust neuronal excitability? Most previous studies of homeostatic plasticity focused on neurons that either fired rhythmically or had high rates of spontaneous firings (Burrone et al., 2002; Marder and Goaillard, 2006; Turrigiano, 2008). Because these neuronal types constantly generate action potentials, deviation from a set point firing rate can be effectively used to monitor variations in neuronal activity, thus triggering compensatory changes in synaptic or intrinsic membrane properties to restore their characteristic excitability (Hausser and Monsivais, 2003; Nelson et al., 2003). In contrast, mature GCs rarely fire action potentials, and they require approximately 200 pA of current injection to evoke spikes, approximately 10 fold higher than the current injection threshold for cortical pyramidal neurons, a cell type commonly used to investigate mechanisms of homeostatic plasticity (Desai et al., 1999; Maffei and Turrigiano, 2008). Therefore, GCs mostly remain in the regime of subthreshold voltages, fluctuating around their RMP, but rarely firing spontaneous action potentials either in acute slices or *in vivo* (Cang and Isaacson, 2003; Pressler et al., 2007; Wellis and Scott, 1990). Since sparsely spiking neurons mostly fluctuate their membrane potentials below firing threshold, cellular sensors that detect deviations from the RMP could provide error signals for these neurons different from sensors responsive to

firing rates (Alle and Geiger, 2008). Nevertheless, adjusting neuronal excitability based on monitoring the electrical properties in the regime of subthreshold voltages suffers from one major disadvantage as demonstrated by our experiments. Namely, if neurons compensate for their altered electrical properties by modifying conductances that have different properties near the spike threshold (e.g. nonlinear G_{Kir} substituting for linear G_{Leak}), these compensatory changes will lead to hyperexcitability and higher firing rates, as demonstrated in KIR^+ neurons.

Numerous types of neurons, including photoreceptors, retinal bipolar cells, and auditory hair cells, cannot fire action potentials, and instead, use graded potential as their output signals (Copenhagen, 2001). In other neuronal types that fire action potentials, fluctuations of subthreshold membrane potential regulate several key parameters in neuronal function. For instance, graded membrane potentials regulate neurotransmitter release in lobsters (Manor et al., 1997; Marder, 2006), in dendrites from OB periglomerular cells (Murphy et al., 2005), and from axons in some mammalian neurons (Alle and Geiger, 2006; Shu et al., 2006). Our results further extend the function of the subthreshold membrane potential as a set point to regulate the excitability of OB GCs.

Homeostatic regulation of I_{Leak} and I_A in GCs

In OB GCs, we detected a decrease of I_{Leak} in response to hyperpolarization (as in KIR^+ and ESK^+ GCs), but no changes in response to depolarization (as in DNK^+ GCs). By contrast, we observed that altering the resting membrane potential bidirectionally regulates I_A, such that I_A increased in DNK^+ neurons (which were depolarized) and decreased in KIR^+/ESK^+ neurons (which were hyperpolarized) respectively. It is plausible that cells did

not proceed to change I_{Leak} in DNK^+ neurons because increasing I_A was sufficient to restore their subthreshold behavior (Figure 2F to 2I). From the perspective of energy consumption (Alle et al., 2009), up-regulating I_{Leak} will persistently increase outward potassium flow at rest, which would incur a great energy consumption by the Na^+/K^+-ATPase that maintains the physiological ionic gradient. Since I_A is only transiently active when cells are depolarized around -50 mV, neurons may favor the compensatory strategy that use less ATP usage, thus choosing an increase in I_A over I_{Leak}. Indeed, the strong reduction of I_{Leak} triggered by the hyperpolarized KIR^+ and ESK^+ neurons would greatly reduce their outward potassium flow, which also supports the idea that neurons preferentially use the compensatory strategies that minimize the energy expenditure at RMP.

It is worth pointing out that I_A has previously been implicated in the regulation of neuronal excitability in the hippocampus (Bernard et al., 2004). However, in that case, it was reported that an increase in neuronal firing led to a reduction of I_A, suggesting a positive-feedback regulation, an opposite trend to the one we observed here. It is uncertain what accounted for these opposing modes of I_A regulation, positive-feedback versus homeostatic. The previous studies on the regulation of I_A focused on hippocampal neurons in the context of pilocarpine-induced seizures where the excitability of neurons and surrounding circuits were both presumably perturbed. In our study, we selectively manipulated the electrical properties of individual neurons in the context of a normal, unperturbed brain circuit. In addition, it is possible that the regulation of I_A may be different between excitatory hippocampal neurons and inhibitory OB GCs. Nonetheless, both KIR^+ neurons (hyperpolarized but hyperexcitable) and ESK^+ neurons (hyperpolarized and hypoexcitable) had reduced I_A. Thus, the magnitude of I_A correlated well with the RMP of neurons such that

it was increased in depolarized cells (DNK^+ neurons) and reduced in hyperpolarized cells (ESK^+ and KIR^+ neurons), regardless of their firing rates. This observation suggests that the role of I_A may be tailored to restore membrane excitability at subthreshold voltages.

Synaptic plasticity in response to electrical perturbations

In this study, we mainly focused on the homeostatic roles of intrinsic membrane properties (Zhang and Linden, 2003), as changes in intrinsic ion conductances were primarily responsible for the paradoxical hyperexcitability of KIR^+ neurons and for the restoration of membrane excitability of DNK^+ neurons. However, we also observed specific changes of synaptic properties triggered by genetically manipulating the electrical properties of GCs. We found that the value of RMP was inversely correlated with sEPSC amplitude and the thickness of dendritic spines (Figure 7). The rankings of sEPSC amplitude and density of thick spines in neurons followed an order that correlated inversely with the RMP: ESK^+ > KIR^+ > control > DNK^+ (Figure 7). Because larger spines are believed to contain more synaptic receptors, the increased sEPSC amplitude in KIR^+/ESK^+ neurons may be a direct result of their larger size. Alternatively, the increased sEPSC amplitude may result from a scaling of synaptic strength, similar to the compensatory mechanisms observed in cultured hippocampal neurons in which their activity was globally reduced with pharmacological agents (Turrigiano, 2008; Turrigiano et al., 1998). Finally, because the degree of I_A reduction also inversely correlated with the RMP (ESK^+ < KIR^+ < control < DNK^+), reduced I_A in KIR^+ and ESK^+ neurons will likely enhance the cable properties of their dendrites, and this could account for the higher amplitude of sEPSCs recorded in the cell body of these hyperpolarized neurons. Indeed, it has been previously shown that dendritic I_A in OB granule cells can shunt AMPA-mediated synaptic inputs, thereby affecting the amplitude of synaptic

currents measured in the cell body (Schoppa and Westbrook, 1999). Further work will be needed to elucidate whether the changes in synaptic properties in our studies result from synaptic plasticity in the pre and/or postsynaptic cells, or alternatively, from the altered cable properties of dendrites contributed by the different levels of dendritic I_A.

Finally, the different levels of sEPSC amplitude observed in genetically manipulated neurons could result from changes of ionic driving force, such that the driving force in depolarized cells (DNK^+) should be lower than in hyperpolarized cells (ESK^+ and KIR^+). This scenario, however, is unlikely because we measured the amplitude of sEPSC from different neurons by recording them at the same holding potential of -77 mV. Nevertheless, because we cannot completely rule out the possibility that the holding potential of distal dendrites is not well controlled by somatic recordings due to space clamp limitations, it is still possible that changes in ionic driving force could contribute to the observed differences in sEPSCs.

Monitoring subthreshold activity in neurons

What are the cellular sensors that can monitor the electrical properties of neurons in the subthreshold voltages? We propose that the fluctuations around the RMP could act as a feedback signal and that intracellular signaling cascades operating at subthreshold voltages may mediate this process. Indeed, subthreshold depolarization alone, without changing the firing rates, has been shown sufficient to regulate the synaptic strength of cortical neurons cultured *in vitro* (Leslie et al., 2001). The fluctuation in subthreshold membrane potentials also regulates intracellular calcium signaling in the apical dendrites of hippocampal CA1 pyramidal neurons (Magee et al., 1996; Manita and Ross, 2009) and can function as Hebbian

signals for synaptic plasticity in medium-sized spiny neurons (Fino et al., 2009). We have observed that OB GCs use a homeostatic strategy that relies on a subthreshold set point to monitor changes of membrane excitability, rather than their firing rates. A subthreshold set point may also be used to regulate the electrical properties of other types of neurons, and could be a mechanism involved in neuronal diseases such as epilepsy where neurons became pathologically hyperexcitable (Chen et al., 2001).

Methods

Retroviral vectors

Cloning of Kir2.1 variants was performed using standard molecular techniques (Burrone et al., 2002). Retroviral vectors were derived from a Moloney leukemia virus with an internal promoter from the Rous sarcoma virus (Molar). Retroviral particles were produced and stored with approximately 10^6 infectious units/μl, as previously described (Kelsch et al., 2007). To construct hrGFP_IRES_Kir2.1, the cDNA of encephalomyelocarditis (EMC) virus internal ribosomal entry site (IRES) was placed downstream from the humanized recombinant GFP (hrGFP) cDNA and upstream above Kir2.1 cDNA. The variants of Kir2.1, ESKir2.1 (D172N and E224S) and DNKir2.1 (GYG to AAA), were generated by PCR based on previous studies (Taglialatela et al., 1995; Yang et al., 1995; Yue et al., 2002). To quantify the density and morphology of dendritic spines, the PalmGFP_IRES_Kir2.1 was constructed by adding the palmitoylation sequence from the GAP43 gene to the N-terminus of EGFP and the cDNA of PalmGFP was subcloned into the hrGFP_IRES_Kir2.1 cassette to replace hrGFP.

Retroviral labeling *in vivo*

Postnatal days 5 to 6 Sprague-Dawley rat pups (Taconic) were anesthetized by hypothermia and stereotaxically injected with 1 μl of retroviruses bilaterally at a speed of 0.05 μl /sec. The stereotaxic coordinates were (mm from bregma): anterior 0.9, lateral ±2.1, and ventral 2.1.

Histology

Rats were over-anesthetized with isofluorane (Baxter) before they were perfused intracardially, first with phosphate buffer saline (PBS) and then with 3% paraformaldehyde (PFA). The bulbs were incubated in 3% PFA at least overnight, and cut horizontally with a Leica vibratome into 45 μm sections. For immunocytochemistry, the sections were incubated with blocking solution containing bovine serum albumin (3 mg/ ml PBS), and 0.25% Triton X-100 in PBS, and incubated overnight with a polyclonal rabbit anti-GFP antibody (Chemicon; AB3080) diluted 1:3000 in blocking solution. Sections were washed 4 times in PBS, for 15 min each time, before a 2-hour incubation at room temperature with Alexa Fluor® 488 goat anti-rabbit secondary antibody (Molecular Probes, catalog A11008) diluted 1:700 in blocking solution. The sections were washed 4 times in PBS, for 15 min each time, before mounting on slides with mounting medium (Fluoromount^{TM}; Sigma).

Electrophysiology

Animals were given an overdose of ketamine/xylazine and then perfused intracardially with ice-cold slicing solution containing (in mM): 212 sucrose, 3 KCl, 1.25 NaH_2PO_4, 26 $NaHCO_3$, 7 $MgCl_2$, 10 glucose (308 mOsm, and pH 7.3). Bulbs were incubated in ice-cold cutting solution and cut horizontally into 350 μm slices with a Leica microtome at a speed of 0.1 mm/s. Slices were incubated for 30 min at 32°C, for recovery, in carbogenated recording solution containing (in mM): 125 NaCl, 2.5 KCl, 1.25 NaH_2PO_4, 26 $NaHCO_3$, 1 $MgCl_2$, 2

CaCl2, 20 glucose (312 mOsm, and pH 7.3). Fluorescent-guided whole-cell patch clamp recordings were performed with a MultiClamp 700B amplifier (Axon Instruments). The pipette solution contained (in mM): 2 NaCl, 4 KCl, 130 K-gluconate, 10 HEPES, 0.2 EGTA, 4 Mg-ATP, 0.3 Tris-GTP, 14 Tris-phosphocreatine (pH 7.3). Successful patching onto the target cell was confirmed by identifying a fragment of fluorescent membrane trapped inside the pipette tip during or after the recording. Pipette resistance ranged from 5 to 8 MΩ, and the pipette access resistance was always less than 16 MΩ after series resistance compensation. The junction potential was not corrected throughout the study. For recording spontaneous EPSC (sEPSC), the neuron was held at -77 mV and synaptic events were collected at 25°C. The majority spontaneous events came from sEPSC because ~98% of spontaneous events could be blocked by 100 μM D, L-AP-5 and 20 μM NBQX (Sigma) at the end of the recording. Inhibitory blockers such as bicuculline were not included during sEPSC recording because they triggered frequent bursts of EPSC inputs in granule neurons, which precluded further analysis.

I_{Leak} and I_A measurement

The leak current was measured by sweeping voltages from -130 to +20 mV at a speed of 50 mV/sec in the presence of the blockers (in μM): 1 TTX, 20 NBQX, 50 AP-5, 20 Nifedipine, 50 picrotoxin (PTX) and 100 Ni^{2+} to block voltage-sensitive/persistent sodium channels, AMPARs, NMDARs, high-threshold L-type calcium channels, GABA receptors and low-threshold T-type calcium channel, respectively. We used voltage paradigms to isolate I_A from I_{DR} in a neuron because I_A inactivates completely above the voltages about -30 mV. To measure I_A and I_{DR} simultaneously, the cell was pre-pulsed to -120 mV for 200 ms before being clamped at the desired voltages from -60 to +40 mV in a 10 mV increment for 200 ms.

To measure I_{DR} alone, the prepulse voltage was changed to -30 mV, which completely inactivated I_A in 200 ms. I_A can be isolated from digitally subtracting I_{DR} from I_A and I_{DR}.

Computational modeling

To quantify to what extent of I_{Leak} reductions rendered an initially hypoactive KIR^+ neuron more excitable, simulations was performed using custom-made programs written in Matlab. We modeled a granule neuron with a two-compartment model that mimics soma and one dendrite. Six species of ion channels exist in both compartments, including endogenous inwardly rectifying potassium channel ($G_{Kir2.X}$), exogenous inwardly rectifying potassium channel (G_{KIR}), leak potassium channel (G_{Leak}), A-type potassium channel ($G_{K\text{-}A}$), voltage-gated sodium channel (G_{NaV}), delayed rectifying potassium channel ($G_{K\text{-}DR}$). One additional channel, low threshold T-type calcium channel ($G_{Ca\text{-}T}$) was placed in the dendrite but not in the soma according to previous studies (Egger et al., 2003). The somatic (V_s) and dendritic (V_d) membrane potential was updated by solving two sets of differential equations with integration time step 0.2 ms by using Euler method.

Soma: $C_m\, dV_s/dt = -I_{Leak} - I_{Kir2.X} - I_{Kir2.1} - I_{NaV} - I_A - I_{DR} + G_r(V_d - V_s) + I_{inj}$ -----(1)

Dendrite: $C_m\, dV_d/dt = -I_{Leak} - I_{Kir2.X} - I_{Kir2.1} - I_{NaV} - I_A - I_{DR} - I_{Ca\text{-}T} + G_r(V_s - V_d)$ -----(2)

Analysis of electrophysiological data

Data was acquired and analyzed with pClamp9 software (Axon Instruments), and sEPSCs were analyzed with Mini Analysis Program (Synaptosoft Inc.). Only morphologically intact granule neurons with at least 1 nA of TTX-sensitive sodium current measured at -20 mV, and resting membrane potential more negative than -55 mV, were included in the 28 dpi analyses.

Spine analysis

Viruses carrying PalmGFP (control), PalmGFP_IRES_Kir2.1, PalmGFP_IRES_ESKir2.1 or PalmGFP_IRES_DNKir2.1 constructs were injected separately into each SVZ in a single animal. Coronal sections 45 μm-thick were prepared from each olfactory bulb. The labeled neurons were imaged by an Olympus Fluoview laser confocal microscope with a 60X objective lens, a zoom of 1.5 and at z-intervals of 0.2 μm. The spine analysis was performed with the MetaMorph software (Molecular Devices) by a blinded second experimenter.

Statistical analysis

All data was analyzed with the two-sample two-tailed Student's *t*-test in OriginPro 8 (Origin Lab Corporation). Data was reported as box plot or mean ± SEM.

ACKNOWLEDGEMENTS

We thank Garrett Banks for help with engineering of the viral constructs and Weifeng Xu, Benjamin Scott, Matt Anderson, Wolfgang Kelsch and the lab members for comments on the manuscript. This work was supported by an NIDCD RO1 grant to C.L., an M.I.T. Singleton and Chyn Duog Shiah Memorial fellowships to C.W.L.

References

Alle, H., and Geiger, J.R. (2006). Combined analog and action potential coding in hippocampal mossy fibers. Science *311*, 1290-1293.

Alle, H., and Geiger, J.R. (2008). Analog signalling in mammalian cortical axons. Curr Opin Neurobiol *18*, 314-320.

Alle, H., Roth, A., and Geiger, J.R. (2009). Energy-efficient action potentials in hippocampal mossy fibers. Science *325*, 1405-1408.

Bernard, C., Anderson, A., Becker, A., Poolos, N.P., Beck, H., and Johnston, D. (2004). Acquired dendritic channelopathy in temporal lobe epilepsy. Science *305*, 532-535.

Brickley, S.G., Revilla, V., Cull-Candy, S.G., Wisden, W., and Farrant, M. (2001). Adaptive regulation of neuronal excitability by a voltage-independent potassium conductance. Nature *409*, 88-92.

Burrone, J., and Murthy, V.N. (2003). Synaptic gain control and homeostasis. Curr Opin Neurobiol *13*, 560-567.

Burrone, J., O'Byrne, M., and Murthy, V.N. (2002). Multiple forms of synaptic plasticity triggered by selective suppression of activity in individual neurons. Nature *420*, 414-418.

Cang, J., and Isaacson, J.S. (2003). In vivo whole-cell recording of odor-evoked synaptic transmission in the rat olfactory bulb. J Neurosci *23*, 4108-4116.

Carleton, A., Petreanu, L.T., Lansford, R., Alvarez-Buylla, A., and Lledo, P.M. (2003). Becoming a new neuron in the adult olfactory bulb. Nat Neurosci *6*, 507-518.

Chen, K., Aradi, I., Thon, N., Eghbal-Ahmadi, M., Baram, T.Z., and Soltesz, I. (2001). Persistently modified h-channels after complex febrile seizures convert the seizure-induced enhancement of inhibition to hyperexcitability. Nat Med *7*, 331-337.

Copenhagen, D. (2001). Is the retina going digital? Neuron *30*, 303-305.

Davis, G.W. (2006). Homeostatic control of neural activity: from phenomenology to molecular design. Annu Rev Neurosci *29*, 307-323.

Desai, N.S., Rutherford, L.C., and Turrigiano, G.G. (1999). Plasticity in the intrinsic excitability of cortical pyramidal neurons. Nat Neurosci *2*, 515-520.

Egger, V., Svoboda, K., and Mainen, Z.F. (2003). Mechanisms of lateral inhibition in the olfactory bulb: efficiency and modulation of spike-evoked calcium influx into granule cells. J Neurosci *23*, 7551-7558.

Fino, E., Deniau, J.M., and Venance, L. (2009). Brief subthreshold events can act as Hebbian signals for long-term plasticity. PLoS One *4*, e6557.

Goldstein, S.A., Bockenhauer, D., O'Kelly, I., and Zilberberg, N. (2001). Potassium leak channels and the KCNK family of two-P-domain subunits. Nat Rev Neurosci *2*, 175-184.
Hausser, M., and Monsivais, P. (2003). Less means more: inhibition of spontaneous firing triggers persistent increases in excitability. Neuron *40*, 449-451.

Hoffman, D.A., Magee, J.C., Colbert, C.M., and Johnston, D. (1997). K+ channel regulation of signal propagation in dendrites of hippocampal pyramidal neurons. Nature *387*, 869-875.
Inoue, T., and Strowbridge, B.W. (2008). Transient activity induces a long-lasting increase in the excitability of olfactory bulb interneurons. J Neurophysiol *99*, 187-199.

Kelsch, W., Mosley, C.P., Lin, C.W., and Lois, C. (2007). Distinct mammalian precursors are committed to generate neurons with defined dendritic projection patterns. PLoS Biol *5*, e300.

Kollo, M., Holderith, N., Antal, M., and Nusser, Z. (2008). Unique clustering of A-type potassium channels on different cell types of the main olfactory bulb. Eur J Neurosci *27*, 1686-1699.

Leslie, K.R., Nelson, S.B., and Turrigiano, G.G. (2001). Postsynaptic depolarization scales quantal amplitude in cortical pyramidal neurons. J Neurosci *21*, RC170.

Lois, C., and Alvarez-Buylla, A. (1994). Long-distance neuronal migration in the adult mammalian brain. Science *264*, 1145-1148.

Maffei, A., and Turrigiano, G.G. (2008). Multiple modes of network homeostasis in visual cortical layer 2/3. J Neurosci *28*, 4377-4384.

Manor, Y., Nadim, F., Abbott, L.F., and Marder, E. (1997). Temporal dynamics of graded synaptic transmission in the lobster stomatogastric ganglion. J Neurosci *17*, 5610-5621.
Marder, E. (2006). Neurobiology: extending influence. Nature *441*, 702-703.

Marder, E., and Goaillard, J.M. (2006). Variability, compensation and homeostasis in neuron and network function. Nat Rev Neurosci *7*, 563-574.

Murphy, G.J., Darcy, D.P., and Isaacson, J.S. (2005). Intraglomerular inhibition: signaling mechanisms of an olfactory microcircuit. Nat Neurosci *8*, 354-364.

Nelson, A.B., Krispel, C.M., Sekirnjak, C., and du Lac, S. (2003). Long-lasting increases in intrinsic excitability triggered by inhibition. Neuron *40*, 609-620.

Nelson, S.B., and Turrigiano, G.G. (2008). Strength through diversity. Neuron *60*, 477-482.

Panama, B.K., and Lopatin, A.N. (2006). Differential polyamine sensitivity in inwardly rectifying Kir2 potassium channels. J Physiol *571*, 287-302.

Preisig-Muller, R., Schlichthorl, G., Goerge, T., Heinen, S., Bruggemann, A., Rajan, S., Derst, C., Veh, R.W., and Daut, J. (2002). Heteromerization of Kir2.x potassium channels contributes to the phenotype of Andersen's syndrome. Proc Natl Acad Sci U S A *99*, 7774-7779.

Pressler, R.T., Inoue, T., and Strowbridge, B.W. (2007). Muscarinic receptor activation modulates granule cell excitability and potentiates inhibition onto mitral cells in the rat olfactory bulb. J Neurosci *27*, 10969-10981.

Schoppa, N.E., and Westbrook, G.L. (1999). Regulation of synaptic timing in the olfactory bulb by an A-type potassium current. Nat Neurosci *2*, 1106-1113.

Shoham, S., O'Connor, D.H., and Segev, R. (2006). How silent is the brain: is there a "dark matter" problem in neuroscience? J Comp Physiol A Neuroethol Sens Neural Behav Physiol *192*, 777-784.

Shu, Y., Hasenstaub, A., Duque, A., Yu, Y., and McCormick, D.A. (2006). Modulation of intracortical synaptic potentials by presynaptic somatic membrane potential. Nature *441*, 761-765.

Taglialatela, M., Ficker, E., Wible, B.A., and Brown, A.M. (1995). C-terminus determinants for Mg^{2+} and polyamine block of the inward rectifier K+ channel IRK1. EMBO J *14*, 5532-5541.

Turrigiano, G.G. (2008). The self-tuning neuron: synaptic scaling of excitatory synapses. Cell *135*, 422-435.

Turrigiano, G.G., Leslie, K.R., Desai, N.S., Rutherford, L.C., and Nelson, S.B. (1998). Activity-dependent scaling of quantal amplitude in neocortical neurons. Nature *391*, 892-896.

Turrigiano, G.G., and Nelson, S.B. (2004). Homeostatic plasticity in the developing nervous system. Nat Rev Neurosci *5*, 97-107.

Wellis, D.P., and Scott, J.W. (1990). Intracellular responses of identified rat olfactory bulb interneurons to electrical and odor stimulation. J Neurophysiol *64*, 932-947.

Yang, J., Jan, Y.N., and Jan, L.Y. (1995). Control of rectification and permeation by residues in two distinct domains in an inward rectifier K+ channel. Neuron *14*, 1047-1054.

Yue, L., Navarro, B., Ren, D., Ramos, A., and Clapham, D.E. (2002). The cation selectivity filter of the bacterial sodium channel, NaChBac. J Gen Physiol *120*, 845-853.

Zhang, W., and Linden, D.J. (2003). The other side of the engram: experience-driven changes in neuronal intrinsic excitability. Nat Rev Neurosci *4*, 885-900.

Figure 1

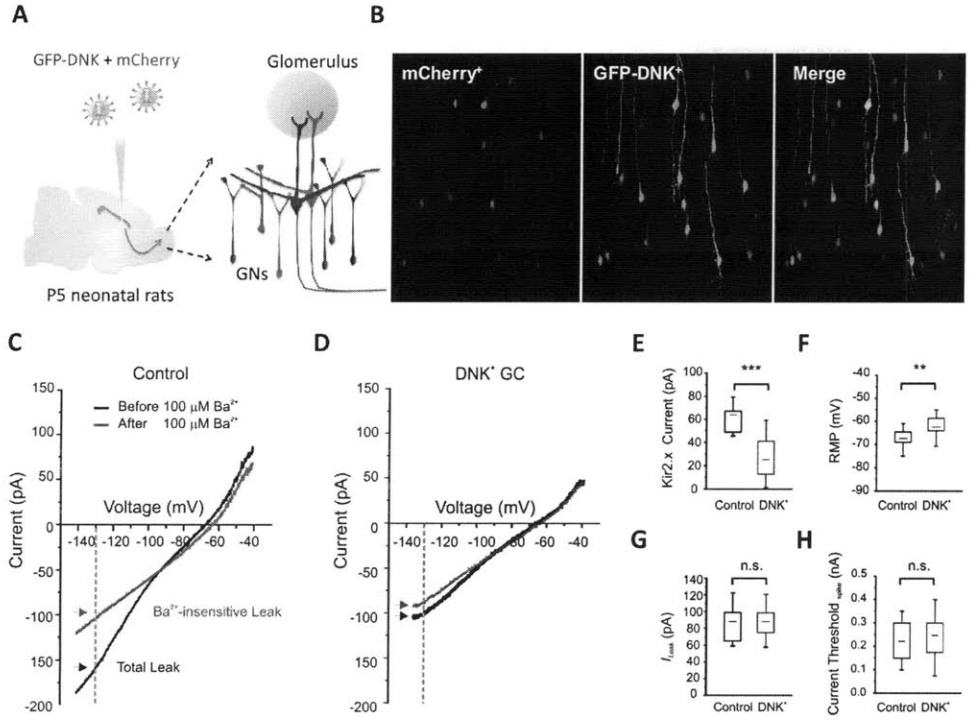

Figure 1. Expression of DNK, a dominant-negative Kir2.1 channel, as a genetic tool to depolarize new GCs *in vivo*

(A) Genetic modification of electrical properties of GCs. A 1:1 mixture of viruses encoding mCherry and a bicistronic vector containing GFP and different variants of Kir2.1 channels (DNK, KIR, and ESK) was injected into the SVZ of P5 rats to label the progenitors that give rise to cells that migrate into the OB and become GCs.

(B) Confocal images showing mCherry$^+$ and GFP-DNK$^+$ GCs, distributed in the same OB slice.

(C) Control neurons had an inwardly-rectifying potassium current that was sensitive to Ba^{2+}.

(D) Expression of DNK markedly reduced the amplitude of the Ba^{2+}-sensitive potassium current.

(E) The amplitude of Ba^{2+}-sensitive potassium current was reduced by 32±4pA in DNK$^+$ neurons (n=13; p=0.00004) .

(F) The resting membrane potential (RMP) of DNK$^+$ neurons was 5±1mV higher than control neurons (n=25; p=0.002).

(G) The amplitude of I_{Leak} was similar between DNK$^+$ and control neurons (n=8-13; p=0.99).

(H) The amount of current required for eliciting first spikes was similar between DNK$^+$ and control neurons (n=9-10; p=0.56).

Figure 2

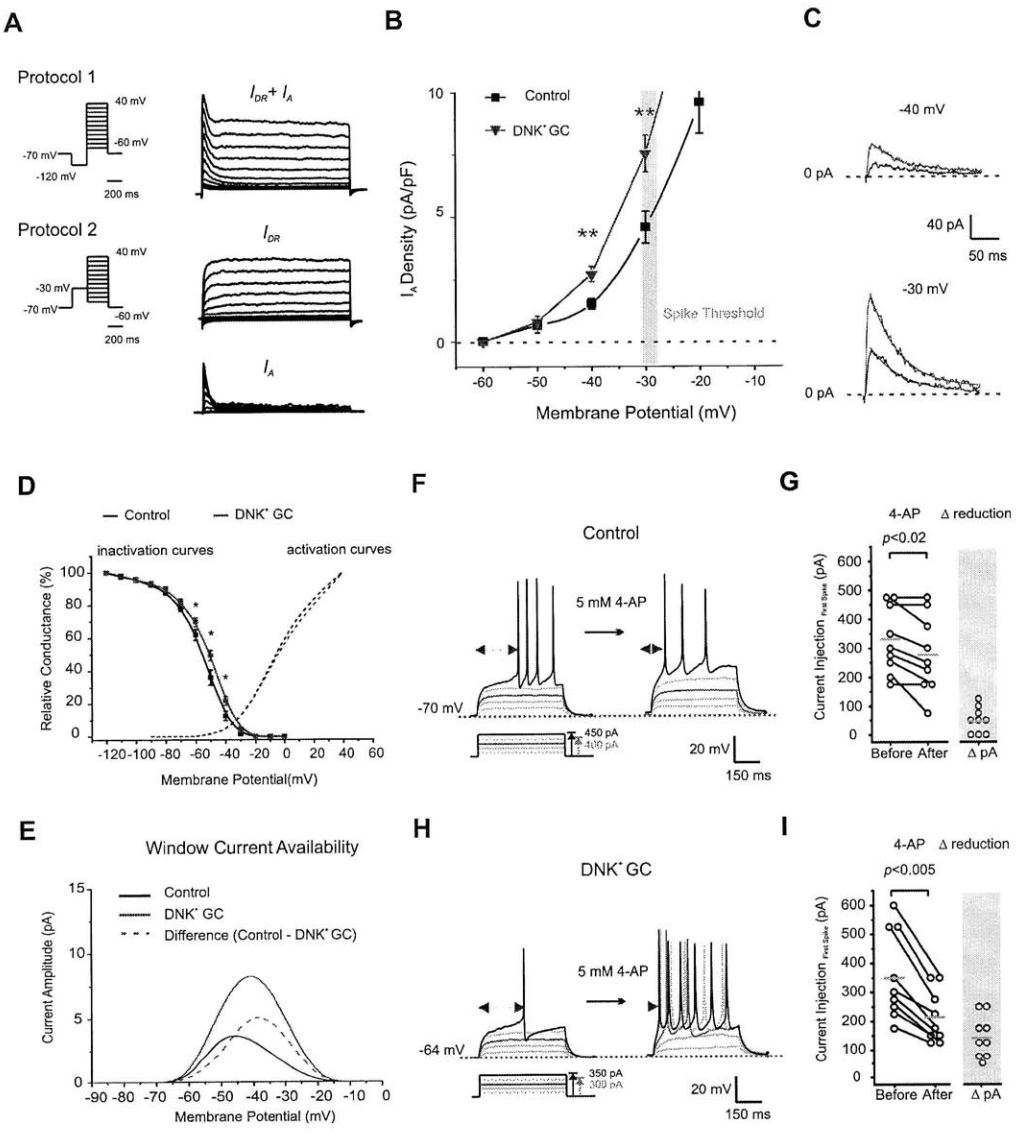

Figure 2. Increases in I_A counteract the depolarization of DNK$^+$ neurons

(A) Using voltage protocols to isolate I_A from I_{DR}. Traces obtained by protocol 1 (top left) revealed both I_A+I_{DR} (prepulse= -120mV for 200ms). Traces obtained by protocol 2 (middle left) only revealed I_{DR} (prepulse= -30mV for 200ms). I_A (bottom right) was derived from digitally subtracting traces obtained by protocol 2 from those by protocol 1.

(B) The peak amplitude of I_A increased in neurons expressing DNK. Notably, increased I_A in DNK^+ neurons could be detected at voltages as low as -40 mV (n=16-20; p=0.004), indicating a higher availability of I_A at subthreshold voltages.

(C) Current traces showed a significant increase of I_A in DNK^+ neurons at -40 mV and -30 mV (n=16-19; p=0.004).

(D) DNK^+ neurons shifted the open probability of the steady-state inactivation curve towards more depolarized voltages, thus allowing for more I_A ready to open at subthreshold voltages.

(E) The window current of subthreshold I_A was higher in DNK^+ neurons than in control neurons, based on the calculation from multiplying activation and inactivation open probability curves.

(F) Inhibiting I_A by 5 mM 4-AP in a control neuron shortened the first spike latency (purple horizontal arrows), and reduced the amount of current required for evoking first spikes by 50±15 pA (n=9; p=0.01)

(G) Inhibiting I_A by 5 mM 4-AP reduced the amount of current required for evoking first spikes in control neurons by 50±15 pA (n=9; p=0.01).

(H) Inhibiting I_A by 5 mM 4-AP in a DNK^+ neuron markedly increased their excitability by reducing the amount of current injection required for evoking first spikes (red line), and shortening the first spike latency (blue arrow).

(I) Inhibiting I_A by 5 mM 4-AP reduced the amount of current required for evoking first spikes in DNK^+ neurons by 144±24 pA (n=9; p=0.0004).

Two-tailed t-test used for statistical analysis in (B) and (D) and pair-sample t-test used for (G) and (I). Error bars represent SEM.

Figure 3

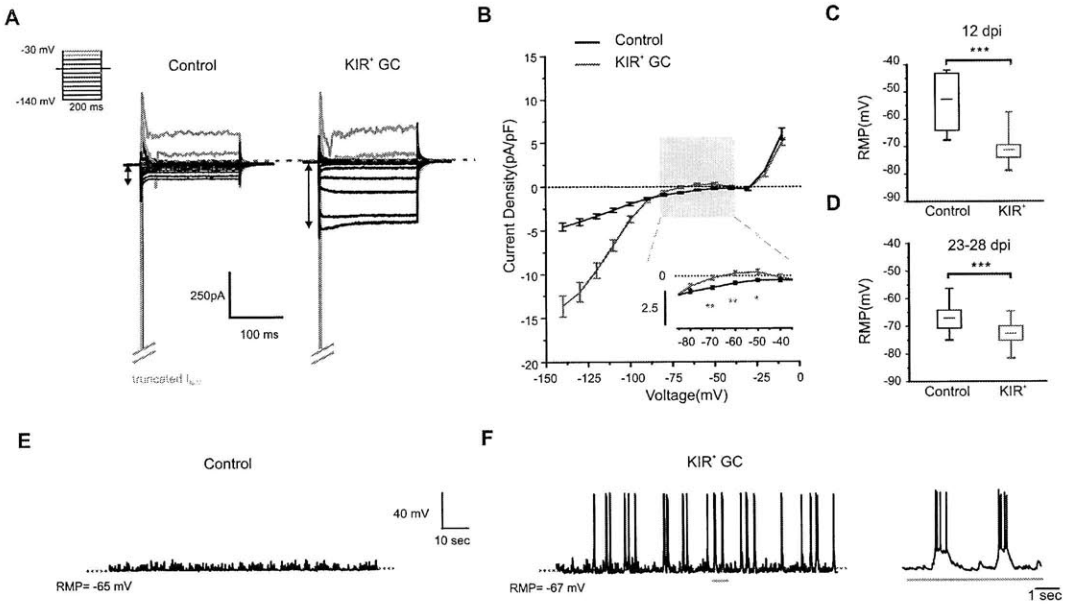

Figure 3. Chronic hyperpolarization triggers paradoxical hyperexcitability in KIR$^+$ neurons

(A) Current-and-voltage traces from control and KIR$^+$ GCs. Inset illustrates the voltage protocol.

(B) Normalized current density (pA/pF) curves showing increased subthreshold current in KIR$^+$ neurons at 12 dpi. Inset shows a high magnification view of the grey area demonstrating the presence of increased outward current in KIR$^+$ neurons between -70 and -50 mV.

(C) Expression of KIR hyperpolarized young GCs at 12 dpi.

(D) The hyperpolarization induced by KIR still persisted in mature, 28 dpi GCs.

(E) Control neurons never spiked spontaneously at rest.

(F) KIR$^+$ neurons displayed spontaneous spiking at RMP. In addition, some spikes occurred as bursts, as demonstrated by the expanded traces shown at the right.

Two-tailed t-test used for statistical analysis. Error bars represent SD in box plots and SEM elsewhere.

Figure 4

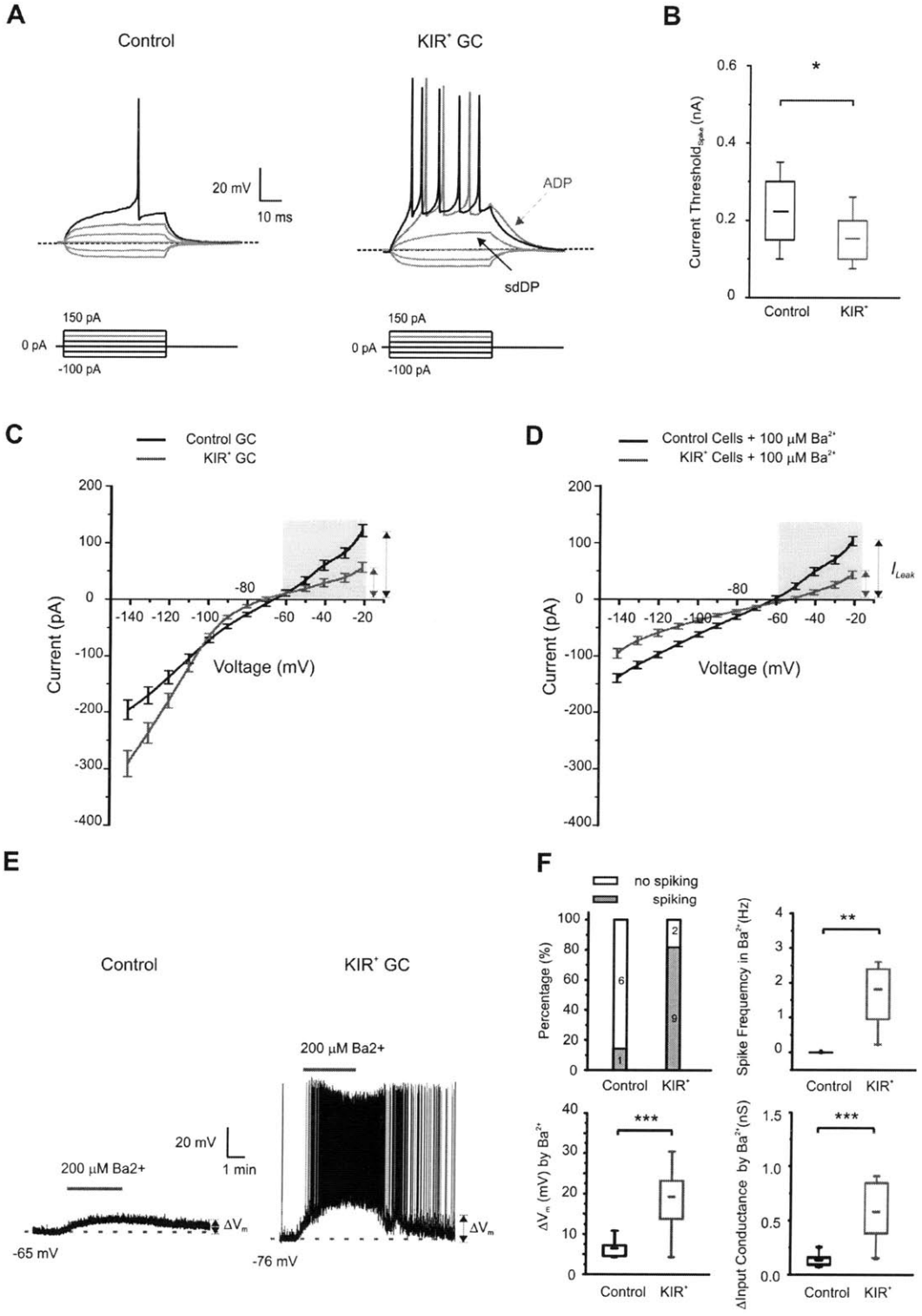
A
Control
KIR+ GC
20 mV
10 ms
ADP
sdDP
150 pA
0 pA
-100 pA
B
Current Threshold (nA)
Control
KIR+
C
Control GC
KIR+ GC
Current (pA)
Voltage (mV)
D
Control Cells + 100 μM Ba2+
KIR+ Cells + 100 μM Ba2+
E
Control
KIR+ GC
200 μM Ba2+
20 mV
1 min
-65 mV
-76 mV
F
no spiking
spiking
Percentage (%)
Spike Frequency in Ba2+ (Hz)
ΔVm (mV) by Ba2+
ΔInput Conductance by Ba2+ (nS)

Figure 4. Hyperpolarization by KIR triggers a down-regulation of I_{Leak}

(A) Stepwise current injection induced membrane potential changes in control and KIR^+ neurons. Notably, KIR^+ neurons fired action potentials with currents that were insufficient to reach threshold in control neurons. KIR^+ neurons displayed a slowly depolarizing potential (sdDP) upon current injection (black arrow) and developed a plateau potential (ADP) after stopping the current injection (red arrow).

(B) KIR^+ neurons required 72±2 pA less current injection than control neurons to trigger their first spikes (n=16; p=0.02).

(C) The current/voltage response of KIR^+ neurons was strongly inwardly rectifying in contrast to the linear response of control neurons. KIR^+ and control neurons shared similar current amplitude between -100 mV and -50 mV but differed significantly above -50 mV, highlighted in the grey square (n=13; 84±9% at -40 mV; p= 0.0007 or 58±7% at -20 mV; p=0.00003).

(D) Applying 100 μM Ba^{2+} revealed that the difference in conductance between control and KIR^+ neurons above -50 mV (grey square) is mediated by the Ba^{2+}-insensitive current I_{Leak} (n=13; 84±9% at -40 mV; p= 0.0007 or 58±7% at -20 mV; p=0.00003).

(E) Blocking of exogenous KIR by Ba^{2+} uncovered the influence of Ba^{2+}-insensitive I_{Leak} on the membrane excitability of neurons. Applying Ba^{2+} depolarized control neurons by approximately 6 mV, but their large I_{Leak} prevented control neurons from firing action potentials at rest. In contrast, application of Ba^{2+} strongly depolarized control neurons by about 20 mV, and they fired APs at a high frequency.

(F) Applying 200 μM Ba^{2+} triggered high frequency of APs in a large percentage of KIR^+ neurons (top left). In the presence of Ba^{2+}, KIR^+ neurons generated more spontaneous firings (top right), became more depolarized (bottom left), and reduced more of their input conductance measured at -77mV (bottom right), than control neurons.

Two-tailed t-test used for statistical analysis. Error bars represent SD in box plots and SEM elsewhere.

Figure 5

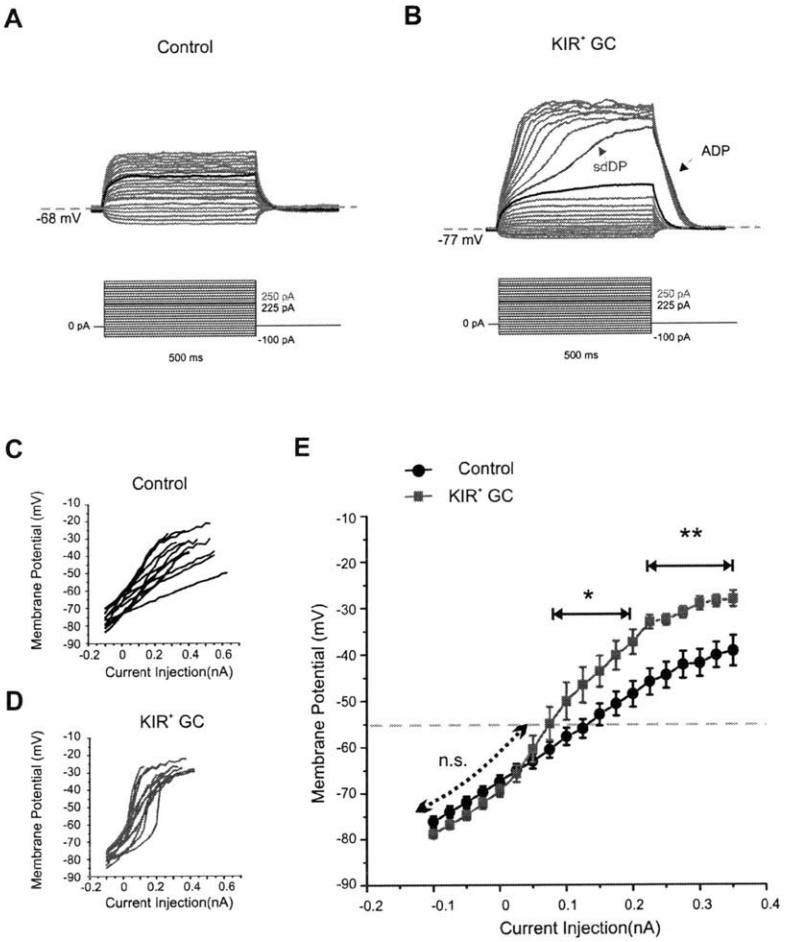

Figure 5. KIR$^+$ neurons have decreased I_{LEAK} and normal membrane potential responses at subthreshold voltages

(A) Membrane potential changes in response to current injection in a control neuron.

(B) Membrane potential changes in response to current injection in a KIR$^+$ neuron. Notice the slowly developing depolarization (sdDP; red arrow) and the ADP (black arrow), which are not present in control neurons.

(C) Individual membrane potential response curves from control neurons (n=13). The curve was derived from plotting the values of membrane potential (y-axis) versus current input (x-axis) at the end of 500 ms of current injection. The control neurons had a roughly linear response curve due to the dominant role of I_{Leak}, a linear conductance, at subthreshold voltages.

(D) Individual membrane potential response curves from KIR$^+$ neurons (n=12).

(E) Averaged membrane potential responses curves revealed that the subthreshold membrane potential responses of KIR$^+$ neurons were similar to control neurons (below grey stippled line) at voltages between -75 and -55 mV. Above -55 mV the membrane responses of KIR$^+$ neurons strongly diverged from those of control neurons.

Two-tailed t-test used for statistical analysis. Error bars represent SEM.

Figure 6

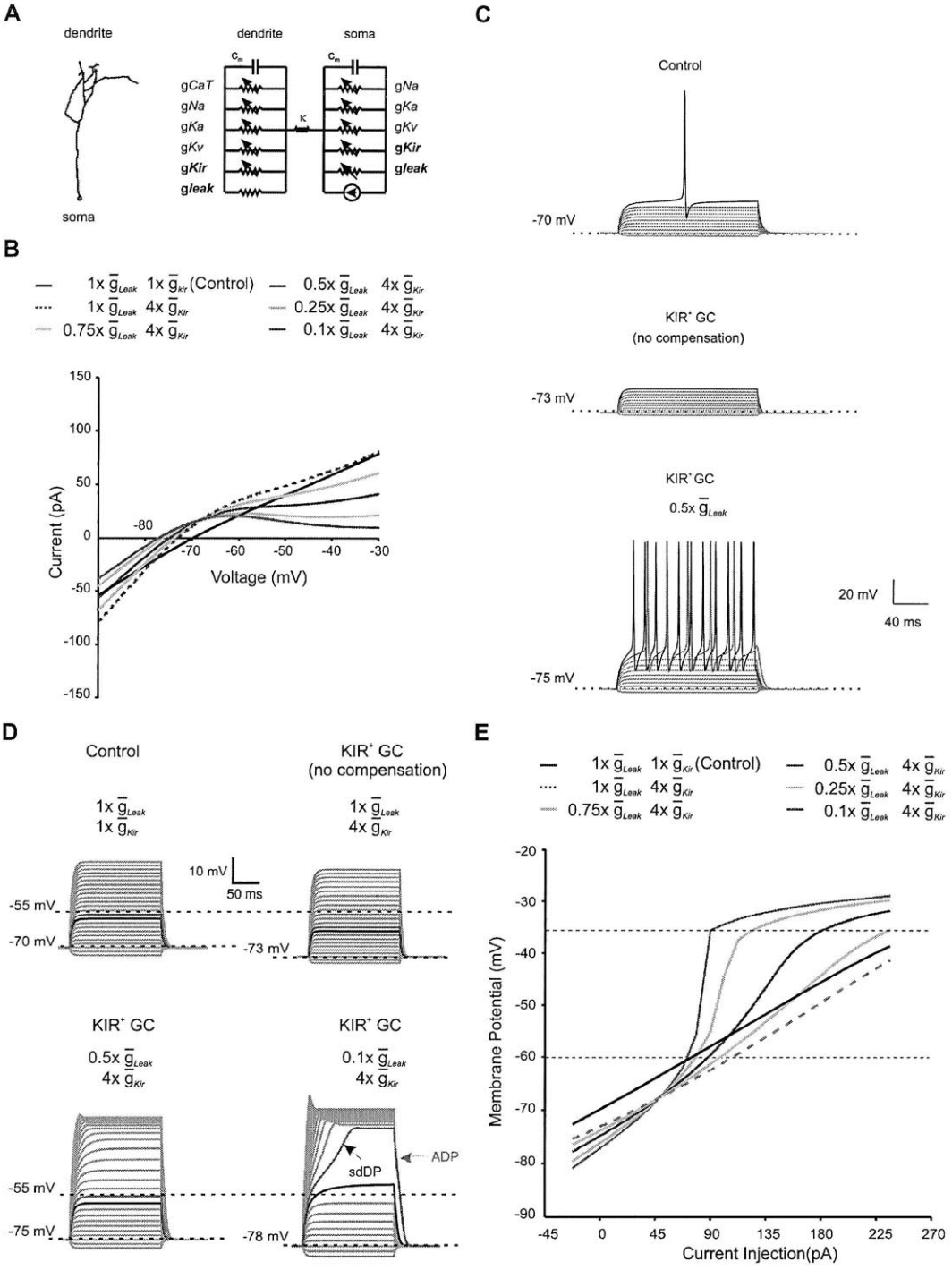
A
dendrite
dendrite
soma
soma
gCaT
gNa
gKa
gKv
gKir
gleak
B
1x $\bar{g}_{Leak}$ 1x $\bar{g}_{Kir}$ (Control)
1x $\bar{g}_{Leak}$ 4x $\bar{g}_{Kir}$
0.75x $\bar{g}_{Leak}$ 4x $\bar{g}_{Kir}$
0.5x $\bar{g}_{Leak}$ 4x $\bar{g}_{Kir}$
0.25x $\bar{g}_{Leak}$ 4x $\bar{g}_{Kir}$
0.1x $\bar{g}_{Leak}$ 4x $\bar{g}_{Kir}$
Current (pA)
Voltage (mV)
C
Control
-70 mV
KIR+ GC
(no compensation)
-73 mV
KIR+ GC
0.5x $\bar{g}_{Leak}$
20 mV
40 ms
-75 mV
D
Control
1x $\bar{g}_{Leak}$
1x $\bar{g}_{Kir}$
KIR+ GC
(no compensation)
1x $\bar{g}_{Leak}$
4x $\bar{g}_{Kir}$
10 mV
50 ms
-55 mV
-70 mV
-73 mV
KIR+ GC
0.5x $\bar{g}_{Leak}$
4x $\bar{g}_{Kir}$
KIR+ GC
0.1x $\bar{g}_{Leak}$
4x $\bar{g}_{Kir}$
sdDP
ADP
-55 mV
-75 mV
-78 mV
E
1x $\bar{g}_{Leak}$ 1x $\bar{g}_{Kir}$ (Control)
1x $\bar{g}_{Leak}$ 4x $\bar{g}_{Kir}$
0.75x $\bar{g}_{Leak}$ 4x $\bar{g}_{Kir}$
0.5x $\bar{g}_{Leak}$ 4x $\bar{g}_{Kir}$
0.25x $\bar{g}_{Leak}$ 4x $\bar{g}_{Kir}$
0.1x $\bar{g}_{Leak}$ 4x $\bar{g}_{Kir}$
Membrane Potential (mV)
Current Injection(pA)

Figure 6. Computer simulations support the existence of a subthreshold set point in GCs.

(A) Diagrams of a two-compartment model of GCs and the distributions of ion channel species in somatic and dendritic compartments.

(B) Current-voltage responses of model neurons with different contributions of G_{Leak} and G_{Kir}. The control model neuron (black solid line) shows a linear current response at all voltages. In the absence of I_{Leak} compensation, addition of exogenous G_{Kir} increased the subthreshold outward current from -60 to -40 mV (black dotted line). Progressive reductions of I_{Leak} scaled down the outward current to various extents. After a 50% reduction of I_{Leak}, the outward subthreshold current above -55 mV became lower in KIR^+ model neurons (blue, orange and purple solid lines) than that in control neurons (black solid line).

(C) Membrane potential changes of a control model neuron in response to stepwise current injection (top). Four-fold increase of G_{Kir} in the absence of G_{Leak} compensation strongly dampened the excitability of the model neuron (middle). A 50% reduction of G_{Leak} rendered a $Kir2.1^+$ model neuron more excitable than a control model neuron (bottom).

(D) Increasing KIR by 4 fold dampened the membrane potential responses of a model neuron upon current injection (top left and right). The slowly developing depolarization (sdDP; black arrow) and ADP (red arrow) emerged when the linear G_{Leak} progressively decreased in a KIR^+ model neuron (bottom left and right). Notably, 50% to 90% reduction of G_{Leak} mimicked the phenotypes of experimental 28 dpi KIR^+ neurons (Figure 5). The G_{Na} and G_{CaT} in the model were set to zero to mimic the experimental conditions that contained TTX and Ni^{2+} to block sodium and calcium channels, respectively (Figure 5).

(E) Responses of membrane potential to current injection in model KIR^+ neurons with various degrees of reduction in G_{Leak}. Reduction of G_{Leak} shifted the membrane response of model KIR^+ neurons towards control neurons at voltages between -70 and -55 mV (area below stippled line). However, this renormalization also steeply changed the slope of response curves above -55 mV and drifted the response curves away from control level near the spike threshold voltages at -30 mV.

Figure 7

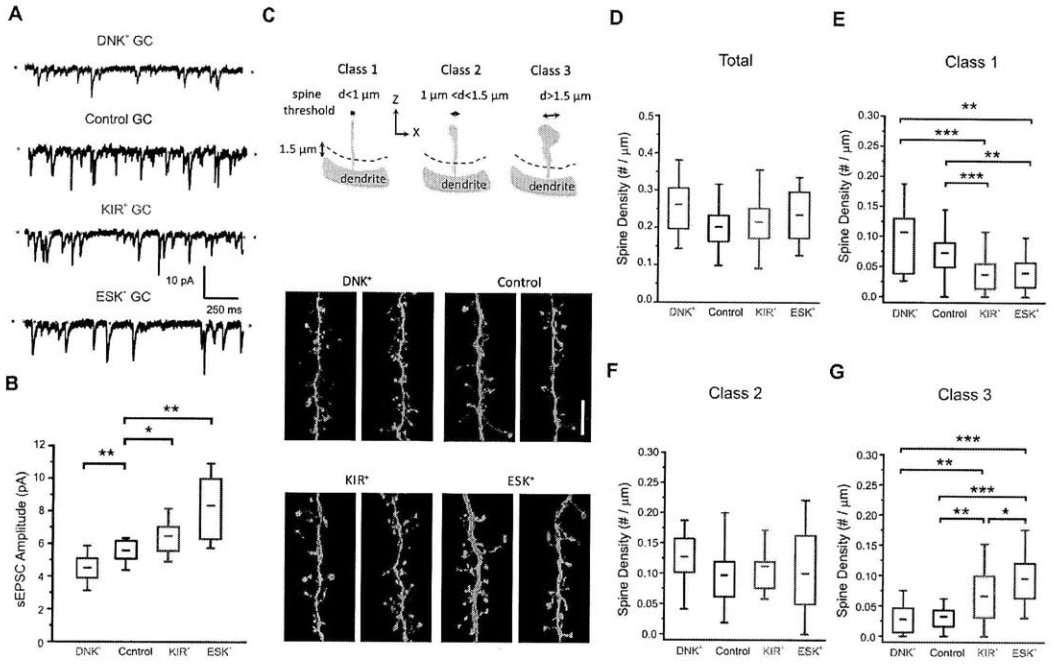

Figure 7. The amplitude of excitatory synaptic input and spine morphology correlate with values of RMP

(A) Traces of sEPSC recorded from neurons expressing different Kir2.1 variants. The holding potential was at -77 mV.

(B) The values of RMP correlated with the amplitude of sEPSC. The more hyperpolarized RMP, the higher sEPSC amplitude. DNK^+ neurons reduced sEPSC amplitude by 19±5% (n=8-10; p=0.01); KIR^+ and ESK^+ neurons increased sEPSC amplitude by 15±5% (n=8-10; p=0.04) and 49±9% (n=8-12; p=0.001), respectively. Note that sEPSC were measured at the same holding potential (-77 mV).

(C) Top: Diagram describing the morphological criteria used for classifying 3 types of spines. Bottom: Confocal images of apical dendrites of control neurons and neurons expressing Kir2.1 variants. Scale bar: 10 µm.

(D) The total spine density was similar among neurons expressing different Kir2.1 variants.

(E) The density of smaller spines (class 1) was significantly lower in KIR^+ (n=25-35 neurons; p=0.0004) and ESK^+ (n=15-35 neurons; p=0.008) neurons, which had a lower RMP than control and DNK^+ neurons.

(F) The number of spines of intermediate size (class 2) was similar among control neurons and neurons expressing different variants of Kir2.1.

(G) The number of large spines (class 3) increased significantly in KIR^+ (n=25-35 neurons; p=0.00035) and ESK^+ (n=15-35 neurons; p=0.00000011) neurons, compared to control and DNK^+ neurons.

Two-tailed t-test used for statistical analysis. Error bars represent SD.

Supplementary Figure 1

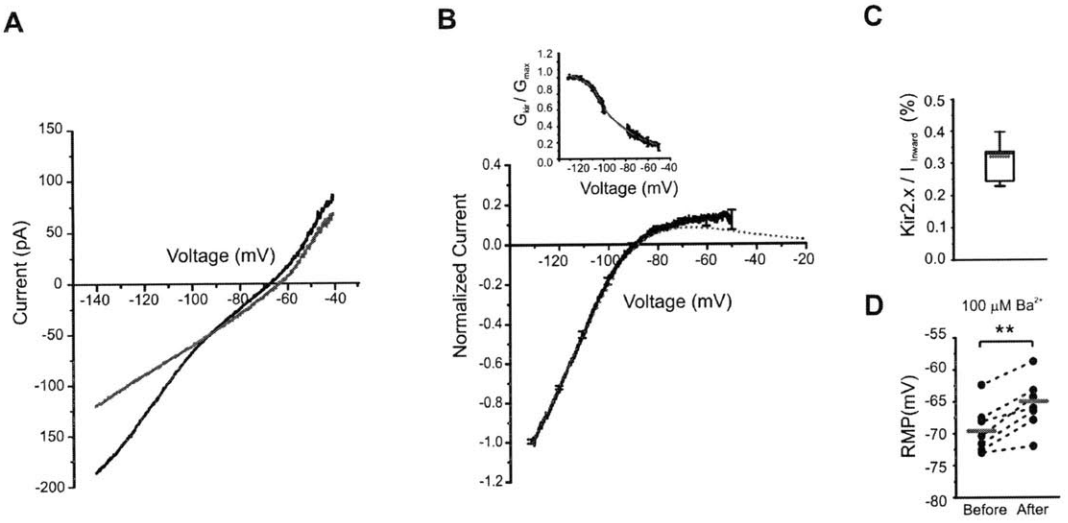

Figure 1. Endogenous Kir2.x contributes to hyperpolarization of RMP

(A) Application of 100 μM Barium (Ba^{2+}) reduced the endogenous Ba^{2+}-sensitive current whose characteristics are comparable to the current mediated by Kir2.x and revealed Ba^{2+}-insensitive background leak current (red trace) in neurons at 28 dpi. Removing Kir2.x current positively shifted the reversal potential.

(B) The current-and-voltage curve of endogenous Ba^{2+}-sensitive current was derived from subtracting the red trace from the black trace in Figure 1C. The current amplitude obtained at -130 mV was used to normalize the current and its voltage dependence was best described by the red dotted curve derived from fitting the normalized conductance curve (inset). Inset shows the normalized conductance curve of Ba^{2+}-sensitive current and its best fitting parameters: A_1=0.12, A_2=0.88, Z_1=3.4, Z_2=14.7, $V_{1/2}$=-107 mV, $V_{1/2}$=-92 mV.

(C) Endogenous Ba^{2+}-sensitive conductance accounted for 32±2% (n=8) of inward conductance measured at -130 mV where open probability of both background leak and Kir2.x conductances is close to 1.

(D) Removing endogenous Ba^{2+}-sensitive depolarized the resting membrane potential of GCs by 4±0.7 mV (n=7; 28 dpi).

Two-tailed t-test used for statistical analysis. Error bars represent SD.

Supplementary Figure 2

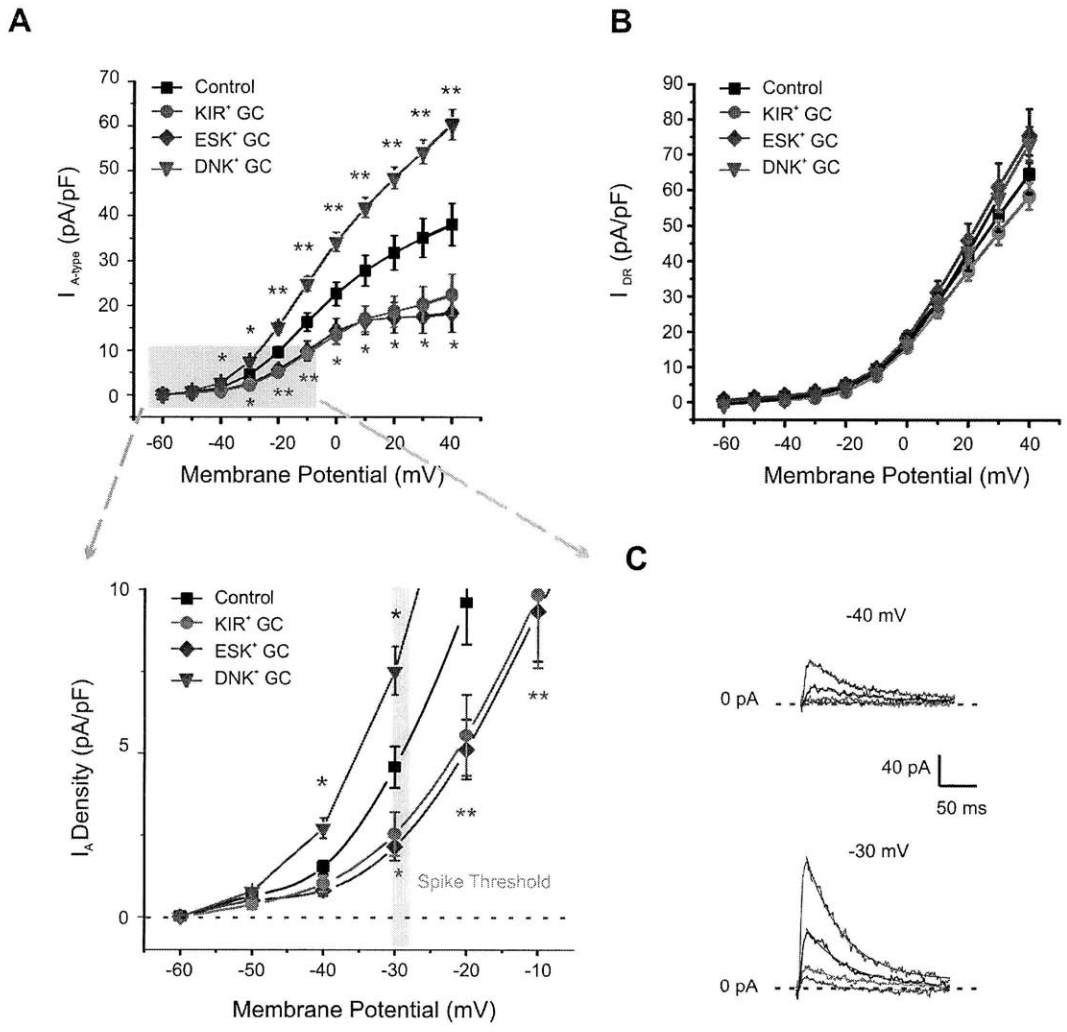

Figure 2. RMP bidirectionally controls the expression level of I_A

(A) Top: The peak amplitude of I_A in neurons expressing different Kir2.1 variants. Expression of DNK increased I_A but expression of KIR (n=13-16; p=0.005) or ESK (n=10-16; p=0.006) decreased I_A at -30 mV and other depolarized voltages. Notably, increased I_A in DNK^+ neurons could be detected at voltages as low as -40 mV, indicating a higher availability of I_A at subthreshold voltages.

Bottom: A close-up window showing I_A current density at voltages between -60 and -10 mV. Note that traces from DNK^+ and control neurons are the same data set used in Figure 2B and 2C.

(B) The peak amplitude of I_{DR} did not show significant difference between neurons expressing different Kir2.1 variants

(C) Current traces showed a significant increase of I_A in DNK^+ neurons but a decrease in KIR^+ and ESK^+ neurons at -40 mV and -30 mV. Note that traces from DNK^+ and control neurons are the same data set used in Figure 2B and 2C.

Two-tailed t-test used for statistical analysis. Error bars represent SEM.

Supplementary Figure 3

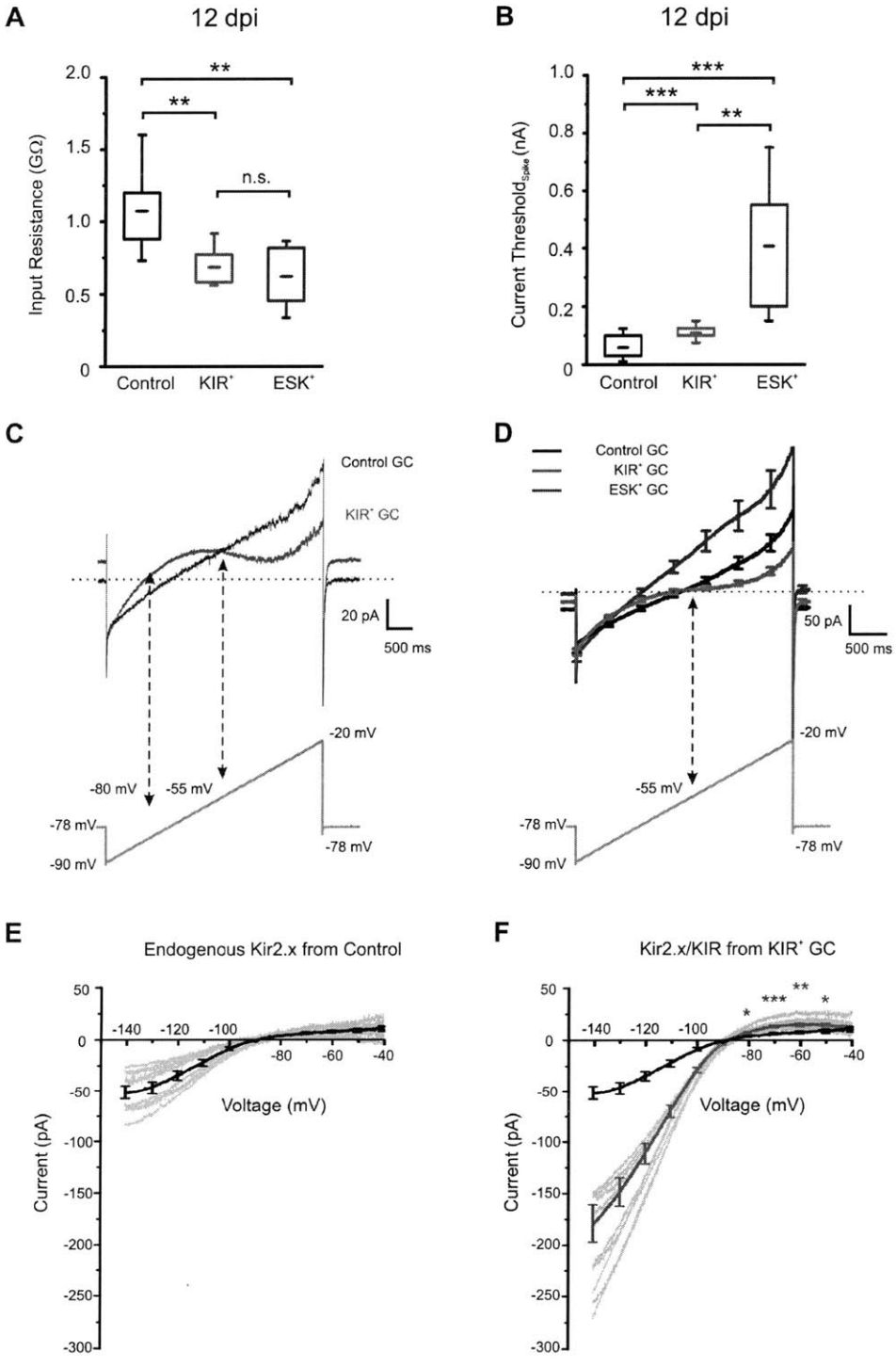

Figure 3. Neurons expressing KIR/ESK dampened their excitability at 12 dpi

(A) Expression of KIR and ESK lowered the input resistance of 12 dpi neurons measured at -77 mV.

(B) Expression of KIR and linear ESK increased the current injection threshold required for first spikes by 51±7pA (n=10) and 348±8pA (n=7), respectively, as compared to control neurons.

(C) Representative current traces elicited by a voltage protocol that swept the holding potential from -90 to -20 mV at a speed of 35 mV/sec. Note that KIR^+ neuron (red line) had a strongly inward rectifying current compared with a control neuron (black line).

(D) Averaged current traces from neurons expressing Kir2.1 variants. KIR^+ neurons (red line) had a lower subthreshold outward current than control neurons (black line) above -50 mV (-60mV, p=0.3; -50mV, p=0.232; -40mV, p=0.012; -30mV, p=0.00796). ESK^+ neurons (blue line) had a higher subthreshold outward current than control neurons (-60mV, p=0.00016; -50mV, p=0.00034; -40mV, p=0.0026; -30mV, p=0.00796).

(E) Mean value (black line) of Ba^{2+}-sensitive (100 μM) inward-rectifying current calculated from individual control $mCherry^+$ neurons (n= 7 neurons; gray lines).

(F) Mean value (red line) of Ba^{2+}-sensitive (100 μM) inward-rectifying current calculated from individual KIR^+ neurons (n= 9 neurons; gray lines). KIR^+ neurons (red line) have a higher inward-rectifying current than control neurons (black line) (-80mV, p=0.013; -70mV, p=0.00045; -60mV, p=0.0059; -50mV, p=0.02).

Two-tailed t-test used for statistical analysis. Error bars represent SD for box plots and represent SEM elsewhere.

Supplementary Figure 4

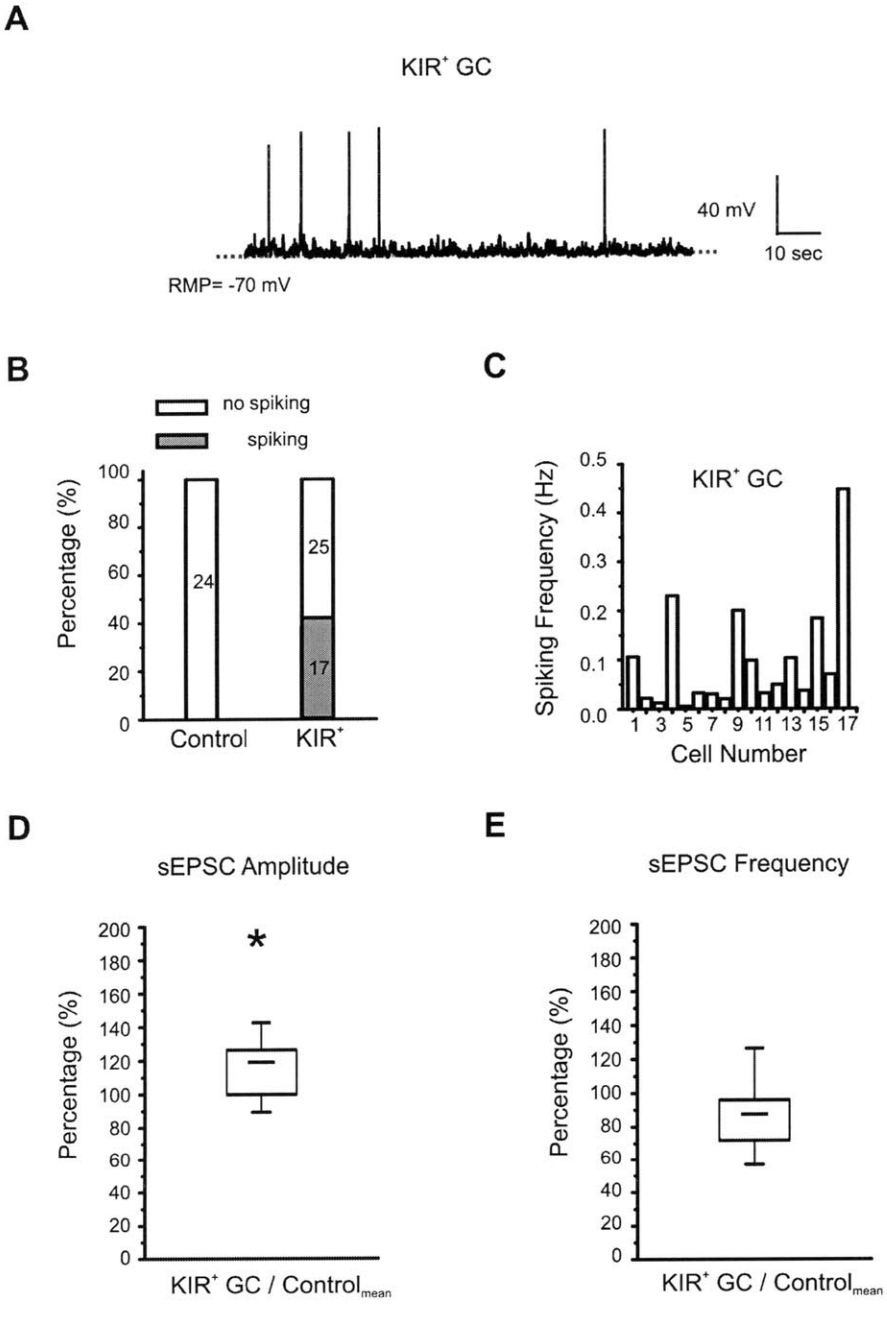

Figure 4. Probability of spontaneous spiking and synaptic properties of KIR^+ neurons

(A) A KIR^+ neuron (26 dpi) spiked spontaneously at RMP.

(B) Statistics showing percentage of spontaneously spiking neurons versus non-spontaneously spiking neurons from control and KIR^+ GCs.

(C) KIR^+ neurons that displayed spontaneously spiking had variable firing rates, ranging from 0.005 to 0.45 Hz in the basal level.

(D) KIR^+ neurons increased the amplitude of sEPSC by 15%. Note that this data set was derived from the same samples used in Figure 7B.

(E) KIR^+ neurons did not change the frequency of sEPSC. Note that this data set was derived from the same samples used in Figure S5A.

Two-tailed t-test used for statistical analysis. Error bars represent SD for box plots

Supplementary Figure 5

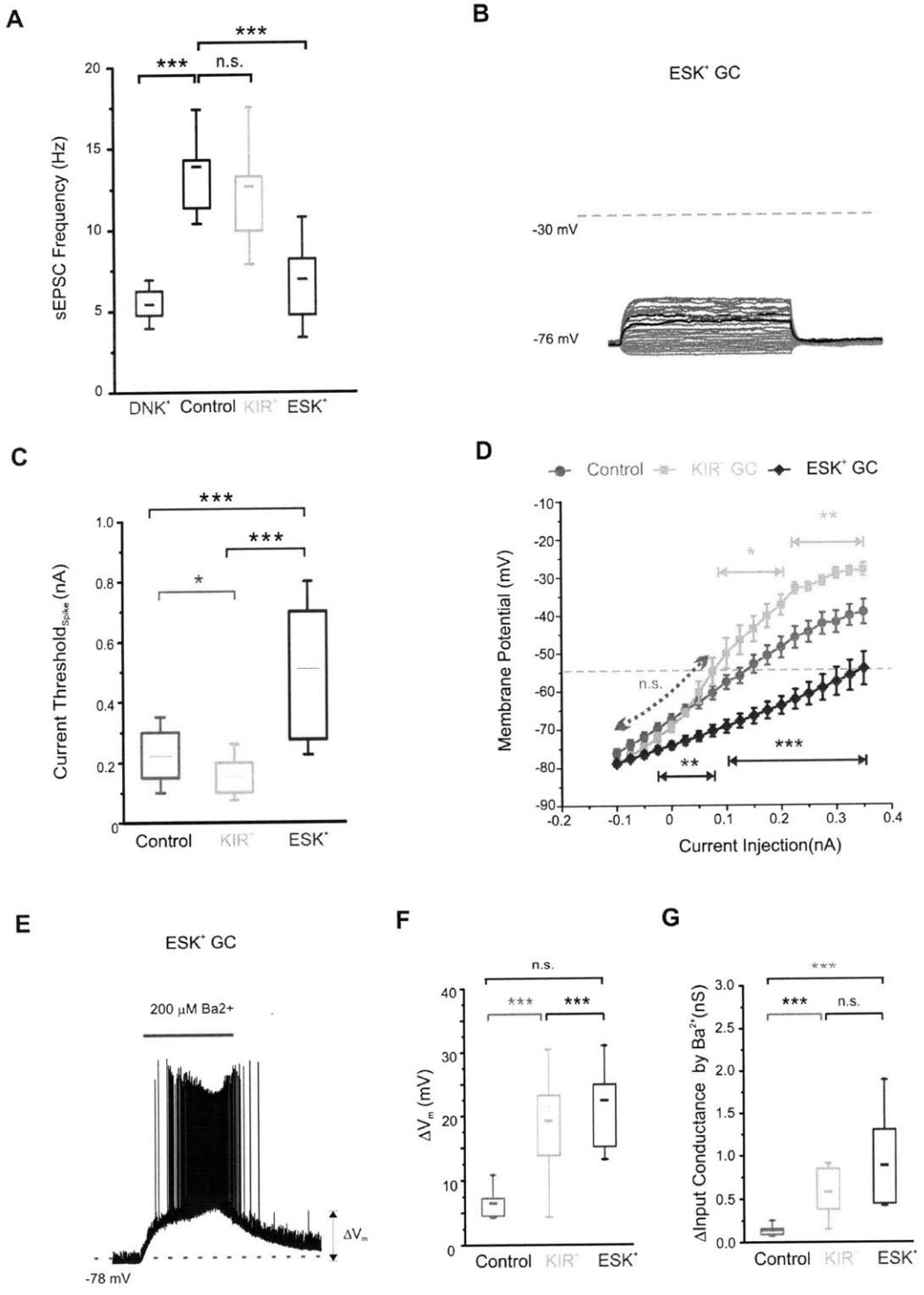

Figure 5. Chronic hyperpolarization and hypoexcitability by expressing ESK also reduce I_{Leak}

(A) Hyperpolarization of neurons by KIR did not significantly affect the frequency of sEPSC measured in GCs' cell bodies (n=8-11; p=0.47). However, weakly chronic depolarization by DNK and strongly chronic hyperpolarization by ESK reduced sEPSC frequency by 61±3% (n=8-9; p=0.00000008) and 50±4% (n=8-12; p=0.0000003), respectively.

(B) Representative membrane potential changes from ESK^+ neurons evoked by current injection.

(C) ESK^+ neurons had decreased excitability as they required 283±78 pA more current than control neurons to elicit first spikes (n=9; p=0.006). Note that box plot from KIR^+ and control neurons are the same data set that appeared in Figure 2B.

(D) Expression of ESK significantly dampened the excitability of neurons because its membrane response curves were lower than those from KIR^+ (light red) and control (light black) $mCherry^+$ neurons. Note that traces from KIR^+ and control neurons are the same data set used in Figure 4E.

(E) Applying 200 μM Ba^{2+} inhibited both endogenous Kir2.x and exogenous ESK and triggered hyperexcitability in ESK^+ neurons, suggesting a significant reduction of I_{Leak}.

(F) Suppressing endogenous Kir2.x and exogenous ESK by 200 μM Ba^{2+} significantly depolarized ESK^+ neurons. Note that box plot from KIR^+ and control neurons are the same data set that appeared in Figure 3F.

(G) Before applying 200 μM Ba^{2+}, endogenous Kir2.x and exogenous ESK accounted for the majority of resting input conductance of ESK^+ neurons. Note that box plot from KIR^+ and control neurons are the same data set that appeared in Figure 3F.

Two-tailed t-test used for statistical analysis. Error bars represent SD for box plots and SEM for membrane potential responses.

Chapter Seven

Future Work

Searching endogenous candidates for regulating neuronal survival

Although membrane depolarization triggered by NaChBac was shown to enhance new neurons' survival, it remains unknown what endogenous candidates capable of altering neuronal excitability can be directly involved in this process (Lin et al., 2010). In ***Chapter 5***, I have demonstrated that cholinergic inputs can have two distinct outcomes in modulating the membrane excitability of new neurons (Page 156). Before the critical period, 14 to 28 dpi, cholinergic inputs produced a long-lasting depolarization after the cell was evoked to have action potentials. After the critical period, cholinergic application only increased spike numbers of neurons without evoking long depolarization (Lin et al., 2010). Therefore, it requires coincident activities, cholinergic inputs and sensory-mediated synaptic membrane depolarization, to elicit a long depolarization in young neurons of 14 dpi. Given the involvement of cholinergic activity in modulating animals' attention, the coincidence of both activities may underlie the enhanced survival of new GCs when animals perform odor-related and attention-required behaviors (Breton-Provencher et al., 2009; Mouret et al., 2009). Furthermore, it may also explain why repeated exposure of odors to mice without olfactory discrimination paradigm did not increase new neurons' survival (Magavi et al., 2005). Interestingly, activation of muscarinic acetylcholine receptors (mAChRs) can induce membrane depolarization, which potentially increases GCs' survival (Kaneko et al., 2006) whereas activation of nicotinic receptors (nAChRs) that produces membrane hyperpolarization has been shown to decrease the GCs' survival (Mechawar et al., 2004).

Because adult-born neurons possess protein machinery necessary for cholinergic modulation as early as at 12 to 14 dpi (Lin et al., 2010), it would be exciting to test the roles of cholinergic inputs on the survival of individual new OB GCs. This will require genetic elimination of either mAChRs or nAChRs in individual new GCs (Mechawar et al., 2004) and systematic alteration of each molecular candidates downstream of the cholinergic receptor activation (Pressler et al., 2007).

Candidates for subthreshold homeostatic regulation

From experimental results presented in ***Chapter 6***, mammalian OB GCs can preferentially use the subthreshold membrane potential response as a set point to control their membrane excitability. What molecular sensors can GCs use in the subthreshold voltages to regulate their activity? One central candidate involved in homeostasis is Ca^{2+}. Two-photon imaging experiments using *Xenopus* frog OB GCs have shown a poor correlation of somatic Ca^{2+} concentration with the spike generation (Lin et al., 2007). Instead, subthreshold membrane depolarization reliably accounted for most of calcium signals as indicated by intracellular Ca^{2+} imaging (Egger, 2007; Lin et al., 2007). Because the low-threshold-activated T-type Ca^{2+} channel operates in the relatively hyperpolarized potentials such as near the RMP, T-type Ca^{2+} channel has been implicated in mediating subthreshold Ca^{2+} influx. Importantly, frog and mammalian OB GCs share very similar electrical and morphological properties; therefore involvement of T-type Ca^{2+} channel in controlling resting Ca^{2+} of mammalian OB GCs is plausible. Indeed, mammalian OB GCs highly express all three members of T-type Ca^{2+} channel, α1G (Cav3.1), α1H (Cav3.2), and α1I (Cav3.3) (Talley et al., 1999), which can mediate subthreshold Ca^{2+} to gate the GABAergic vesicle releases in the dendrodendritic synapses (Egger et al., 2003, 2005). If subthreshold Ca^{2+} functions as a signal for homeostatic

regulation, eliminating T-type Ca^{2+} channels to perturb the resting intracellular Ca^{2+} will reveal further insights about this novel mode of homeostatic regulation (Anderson et al., 2005; Powell et al., 2009).

A-type K^+ channel, as a homeostatic sensor or effector?

GCs regulate the expression level of A-type K^+ channels according to the values of RMP. The more negative RMP, the lower the expression, despite the fact that hyperpolarization by Kir2.1 expression can cause hyperexcitability (***Chapter 6***). Although the pore-forming α subunit Kv4.2 does not confer Ca^{2+} sensitivity to A-type K^+ channels, the auxiliary subunits, K^+ channel-interacting proteins (KChIPs), possess EF-hand domains capable of binding Ca^{2+} (Jerng et al., 2004; Lai and Jan, 2006). Recently, Ca^{2+} has been found to interact with KChIPs, which in turn modulates the inactivation probability of Kv4.2 in cerebellar stellate neurons (Anderson et al., 2010). Moreover, Kv4.2 and KChIPs associate with T-type Ca^{2+} channels (Cav3) to form a signaling complex that may serve to fine-tune the electrical properties of neurons (Anderson et al., 2010). Because this signaling mechanistically agrees with our current findings, it would be interesting to extend the work to OB GCs and examine if this Cav3-Kv4 signaling could be one of bona fide homeostatic effector or sensor in the subthreshold regime.

Why preferentially maintain subthreshold membrane potential responses?

It may look counterintuitive in the first place that OB GCs preferentially maintain their membrane potential responses in the subthreshold regime even at risk of deviating from default firing rates. This principle may seriously perturb the neuronal output. However, the alternative hypothesis suggests that the output of OB GCs, dendrodendrtic neurotransmitter

release, do not correlate with the spike generation. First, OB GCs do not have axons (Shepherd, 2004). Although GCs are able to generate somatic and dendritic action potentials, they do not have a high density of voltage-sensitive sodium channel similar to the subcellular compartments like axon initial segment (Lai and Jan, 2006). Second, cumulative evidence has suggested that release of GABAergic vesicles from GCs' dendrodendritic synapses can be independent of action potentials (Jahr and Nicoll, 1980). This mode of synaptic communication is highly conserved among GCs from different species such as frogs, turtles, and rodents (Jahr and Nicoll, 1980; Schoppa and Urban, 2003). Third, recent experiments have revealed that subthreshold membrane depolarization could trigger reliable GABAergic vesicle release from the dendrites of OB PGCs whose outputs also, in part, rely on dendrodendritic signaling (Murphy et al., 2005). In this study, a single action potential consistently failed to elicit inhibitory outputs but subthreshold long depolarization reliably triggered Ca^{2+} influx for evoking GABAergic vesicle release (Murphy et al., 2005). Therefore, OB GCs' input-output relationship may be biologically meaningful only in the subthreshold regime. To test this hypothesis, future imaging experiments that clarifying the relationship between subthreshold membrane potential and release probability of synaptic vesicle aided by fluorescence-tagged synaptic markers is needed (Li et al., 2005). Moreover, paired-recordings between mitral cell and GCs will offer a variety of experiments for testing the hypothesis and for providing high-resolution mechanistic details. Given the rare opportunity of finding the connected dendrodendrtic pairs in OB slices (Egger and Urban, 2006), genetic tools that can visually reveal connected neurons, mitral cells $\Leftrightarrow$ GCs, will greatly facilitate this future investigation (Gradinaru et al., 2010; Wickersham et al., 2007).

References

Anderson, D., Mehaffey, W.H., Iftinca, M., Rehak, R., Engbers, J.D., Hameed, S., Zamponi, G.W., and Turner, R.W. (2010). Regulation of neuronal activity by Cav3-Kv4 channel signaling complexes. Nat Neurosci *13*, 333-337.

Anderson, M.P., Mochizuki, T., Xie, J., Fischler, W., Manger, J.P., Talley, E.M., Scammell, T.E., and Tonegawa, S. (2005). Thalamic Cav3.1 T-type Ca2+ channel plays a crucial role in stabilizing sleep. Proc Natl Acad Sci U S A *102*, 1743-1748.

Breton-Provencher, V., Lemasson, M., Peralta, M.R., 3rd, and Saghatelyan, A. (2009). Interneurons produced in adulthood are required for the normal functioning of the olfactory bulb network and for the execution of selected olfactory behaviors. J Neurosci *29*, 15245-15257.

Egger, V. (2007). Imaging the activity of neuronal populations: when spikes don't flash and flashes don't spike. J Physiol *582*, 7.

Egger, V., Svoboda, K., and Mainen, Z.F. (2003). Mechanisms of lateral inhibition in the olfactory bulb: efficiency and modulation of spike-evoked calcium influx into granule cells. J Neurosci *23*, 7551-7558.

Egger, V., Svoboda, K., and Mainen, Z.F. (2005). Dendrodendritic synaptic signals in olfactory bulb granule cells: local spine boost and global low-threshold spike. J Neurosci *25*, 3521-3530.

Egger, V., and Urban, N.N. (2006). Dynamic connectivity in the mitral cell-granule cell microcircuit. Semin Cell Dev Biol *17*, 424-432.

Gradinaru, V., Zhang, F., Ramakrishnan, C., Mattis, J., Prakash, R., Diester, I., Goshen, I., Thompson, K.R., and Deisseroth, K. (2010). Molecular and Cellular Approaches for Diversifying and Extending Optogenetics. Cell.

Jahr, C.E., and Nicoll, R.A. (1980). Dendrodendritic inhibition: demonstration with intracellular recording. Science *207*, 1473-1475.

Jerng, H.H., Pfaffinger, P.J., and Covarrubias, M. (2004). Molecular physiology and modulation of somatodendritic A-type potassium channels. Mol Cell Neurosci *27*, 343-369.

Kaneko, N., Okano, H., and Sawamoto, K. (2006). Role of the cholinergic system in regulating survival of newborn neurons in the adult mouse dentate gyrus and olfactory bulb. Genes Cells *11*, 1145-1159.

Lai, H.C., and Jan, L.Y. (2006). The distribution and targeting of neuronal voltage-gated ion channels. Nat Rev Neurosci *7*, 548-562.

Li, Z., Burrone, J., Tyler, W.J., Hartman, K.N., Albeanu, D.F., and Murthy, V.N. (2005). Synaptic vesicle recycling studied in transgenic mice expressing synaptopHluorin. Proc Natl Acad Sci U S A *102*, 6131-6136.

Lin, B.J., Chen, T.W., and Schild, D. (2007). Cell type-specific relationships between spiking and [Ca2+]i in neurons of the Xenopus tadpole olfactory bulb. J Physiol *582*, 163-175.

Lin, C.W., Sim, S., Ainsworth, A., Okada, M., Kelsch, W., and Lois, C. (2010). Genetically increased cell-intrinsic excitability enhances neuronal integration into adult brain circuits. Neuron *65*, 32-39.

Magavi, S.S., Mitchell, B.D., Szentirmai, O., Carter, B.S., and Macklis, J.D. (2005). Adult-born and preexisting olfactory granule neurons undergo distinct experience-dependent modifications of their olfactory responses in vivo. J Neurosci *25*, 10729-10739.

Mechawar, N., Saghatelyan, A., Grailhe, R., Scoriels, L., Gheusi, G., Gabellec, M.M., Lledo, P.M., and Changeux, J.P. (2004). Nicotinic receptors regulate the survival of newborn neurons in the adult olfactory bulb. Proc Natl Acad Sci U S A *101*, 9822-9826.

Mouret, A., Lepousez, G., Gras, J., Gabellec, M.M., and Lledo, P.M. (2009). Turnover of newborn olfactory bulb neurons optimizes olfaction. J Neurosci *29*, 12302-12314.

Murphy, G.J., Darcy, D.P., and Isaacson, J.S. (2005). Intraglomerular inhibition: signaling mechanisms of an olfactory microcircuit. Nat Neurosci *8*, 354-364.

Powell, K.L., Cain, S.M., Ng, C., Sirdesai, S., David, L.S., Kyi, M., Garcia, E., Tyson, J.R., Reid, C.A., Bahlo, M., *et al.* (2009). A Cav3.2 T-type calcium channel point mutation has splice-variant-specific effects on function and segregates with seizure expression in a polygenic rat model of absence epilepsy. J Neurosci *29*, 371-380.

Pressler, R.T., Inoue, T., and Strowbridge, B.W. (2007). Muscarinic receptor activation modulates granule cell excitability and potentiates inhibition onto mitral cells in the rat olfactory bulb. J Neurosci *27*, 10969-10981.

Schoppa, N.E., and Urban, N.N. (2003). Dendritic processing within olfactory bulb circuits. Trends Neurosci *26*, 501-506.

Shepherd, G.M. (2004). The synaptic organization of the brain, 5th ed. edn (Oxford: Oxford University Press).

Talley, E.M., Cribbs, L.L., Lee, J.H., Daud, A., Perez-Reyes, E., and Bayliss, D.A. (1999). Differential distribution of three members of a gene family encoding low voltage-activated (T-type) calcium channels. J Neurosci *19*, 1895-1911.

Wickersham, I.R., Lyon, D.C., Barnard, R.J., Mori, T., Finke, S., Conzelmann, K.K., Young, J.A., and Callaway, E.M. (2007). Monosynaptic restriction of transsynaptic tracing from single, genetically targeted neurons. Neuron *53*, 639-647.